PB97-156681

DEVELOPMENT OF MODELS TO PREDICT OPTIMAL LIFTING MOTION. FINAL PERFORMANCE REPORT

TEXAS TECH UNIV., LUBBOCK

AUG 95

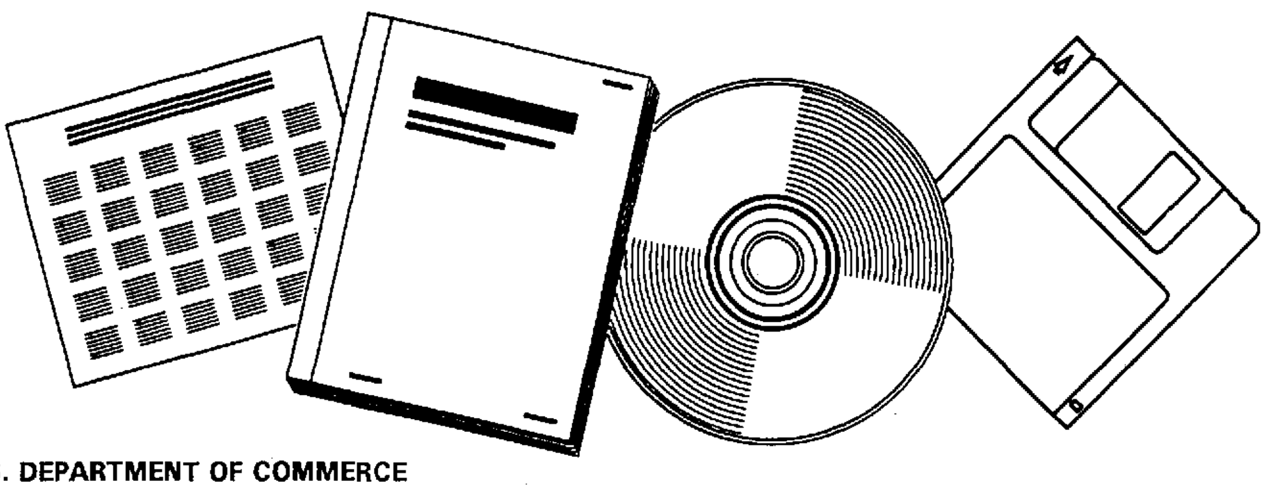

U.S. DEPARTMENT OF COMMERCE
National Technical Information Service

PB97-156681

FINAL PERFORMANCE REPORT

DEVELOPMENT OF MODELS TO PREDICT OPTIMAL LIFTING MOTION

submitted by

M.M. AYOUB

Institute for Ergonomics Research

TEXAS TECH UNIVERSITY
Lubbock, Texas 79409

AUGUST, 1995

50272-101

PB97-156681

REPORT DOCUMENTATION PAGE	1. REPORT NO.	2.	

4. Title and Subtitle Development of Models to Predict Optimal Lifting Motion

5. Report Date 1995/08/00

6.

7. Author(s) Ayoub, M. M.

8. Performing Organization Rept. No.

9. Performing Organization Name and Address Institute for Ergonomics Research, Department of Industrial Engineering, Texas Tech University, Lubbock, Texas

10. Project/Task/Work Unit No.

11. Contract (C) or Grant(G) No.

(C)

(G) R01-OH-02434

12. Sponsoring Organization Name and Address

13. Type of Report & Period Covered

14.

15. Supplementary Notes

16. Abstract (Limit: 200 words) The goal of this study was to continue efforts in the development of a reliable and realistic dynamic lifting simulation model. Specific objectives were to develop a simulation method to predict the sagittal plane lifting motion to validate the simulation method on both male and female subjects, and to perform sensitivity analysis to study the effect of input errors and changes in model parameters on the performance of the simulation method. As developed, the model simulated the dynamic motion of lifting tasks for five body joints: the elbow, shoulder, hip, knee, and ankle. The inputs of the model included initial and final joint postures: sex, weight, and height of the subject; weight load; lifting height; and box dimensions. The angular trajectories of the five joints were predicted on output. The motion of the lift was completely predicted by the model without any video inputs. The simulation model contained three computation units, the dynamics computation, the trajectory formulation and the optimization unit. Study results indicated that the simulation motion followed the actual motion closely. Sensitivity analysis indicated that the optimization constraints had significant effects on the prediction performance of the simulation model.

17. Document Analysis a. Descriptors

b. Identifiers/Open-Ended Terms NIOSH-Publication, NIOSH-Grant, Grant-Number-R01-OH-02434, End-Date-08-31-1995, Musculoskeletal-system-disorders, Humans, Manual-materials-handling, Manual-lifting, Ergonomics, Simulation-methods, Human-factors-engineering, Physical-stress

c. COSATI Field/Group

18. Availability Statement	19. Security Class (This Report)	21. No. of Pages 268
	22. Security Class (This Page)	22. Price

FINAL PERFORMANCE REPORT
(Grant #R01-0H02434)

DEVELOPMENT OF MODELS TO PREDICT OPTIMAL LIFTING MOTION

submitted by

M.M. AYOUB

INSTITUTE FOR ERGONOMICS RESEARCH
TEXAS TECH UNIVERSITY
LUBBOCK, TEXAS

AUGUST, 1995

TABLE OF CONTENTS

LIST OF TABLES

LIST OF FIGURES

ABSTRACT

The biomechanical approach provides estimation of various mechanical stresses acting on the body while a person manually handles an object. Today, photographical motion systems are available for dynamic biomechanical research; however, studies using such systems are mostly performed in the laboratory due to high cost of the equipment and the expertise required in using them. Industrial ergonomists do not have much access to dynamic analyses. To provide ergonomists with a computerized dynamic job analysis tool, a sagittal plane lifting biomechanical simulation model was developed. The model simulates the dynamic motion of lifting tasks for the five body joints: the elbow, shoulder, hip, knee, and ankle. The inputs of the model include initial and final joint postures; subject's sex, weight, and height; weight of load; lifting height; and box dimensions. On output, the angular trajectories of the five joints are predicted. The motion of the lift is completely predicted by the model without any video inputs.

The simulation model contains three computation units, the dynamics computation, the trajectory formation, and the optimization unit. The dynamics unit calculates the kinematics and kinetics. The trajectory formation unit uses numerical techniques to generate smooth joint trajectories. The optimization unit consists of an objective function and several constraints that describe the behavior of the human lifting.

The simulation model was validated using actual lifting data from five male and five female subjects. The lifting tasks included floor-to-knuckle and floor-to-shoulder height lifts. Comparisons were made between the actual lifting motion and predicted motion. The results showed that the simulated motion followed the actual motion closely. Sensitivity analysis showed that the optimization constraints had significant effects on the prediction performance of the simulation model.

SIGNIFICANT FINDINGS

The methodology presented in the study was based on a central thesis, that is, the human motions of lifting are repeatable and consistent under the same task condition. The modeling approach first assumed that the angular trajectories of each joint followed certain consistent patters for the same lifting task. Due to this consistency, a unique polynomial model was derived for each joint based on the trajectory patterns of that joint. The polynomial was controlled by the control points, which were the peaks or troughs of the trajectory. Such polynomials were then used in the lifting optimization model to simulate lifting motions. The optimization model consisted of an objective function and four types of constraints, namely, the joint mobility constraints, the joint moment strength constraints, the collision avoidance constraints, and the postural stability constraints. By varying the values of the control points within the assumed boundaries, the shapes of the polynomials were thus changed, therefore, changing the kinematic properties of the trajectories. The values of the control points were varied until the objective function was minimized and the constraints satisfied. The resulting polynomials were used as the simulated joint trajectories for the lifting motion.

The validation showed that the initial and final velocities and accelerations were usually not zero, indicating that the input of these parameters to the model may be important to the prediction performance. The sensitivity analysis further showed that the input of the initial velocities did improve the prediction in the hip joint trajectories; however, there was no significant improvement in other joints. The validation also showed that the trajectories of each joint followed consistent patterns which allowed for generalization. There was no significant difference between the trajectory patterns of the two sexes. The trajectory patterns were grouped into several different patterns according to lifting conditions and joints. Each pattern was modeled with a Hermite polynomial, characterized by the order of the polynomial and by the locations and bounds of the control points within the trajectories.

The sensitivity analysis for the effects of segment lengths showed that no significant improvement in prediction was found after the measured segment lengths were used in the simulation. This indicated that the use of proportional anthropometric segment lengths was acceptable for the simulation. The sensitivity analysis for the effects of each type of the model constraints showed that none of the constraints were redundant. The removal of any type of constraints from the model degraded the prediction performance in one or more joints.

The prediction performance of the simulation model was shown to be more accurate than the previous model (Ayoub and Hsiang, 1992). Several limitations of the present simulation model must be noted. First, the model should be used with caution in predicting lifting motions performed with extreme squat lifting techniques . There were only two subjects who used squat lifting techniques, providing relatively few samples for the modeling of such lifting styles. The present model is best to be used in predicting sagittal lifting motions for free-style lifting. Second, the validation of the model was accomplished in the kinematic domain, mainly the angular trajectory. The use of the model to predict the kinetics and other important biomechanical parameters such as the compression force at the L5/S1 needs to be validated.

CHAPTER 1
INTRODUCTION

1.1 Motivation

In studies of manual materials handling (MMH), the biomechanical approach provides estimation of various mechanical stresses acting on the human body while a person is performing common manual tasks. For example, the compressive force on the lumbosacral disc (L5/S1), the net muscle moment about a body joint, and the force exertion of a group of muscles are all indicative of body stresses. These parameters, either from direct measurements or often from estimates based on theoretical biomechanical models, are very useful for ergonomists in designing safe and efficient MMH tasks. Since Chaffin (1969) published the use of the "Static Sagittal Plane" model for studying whole-body load lifting, and later popularized it with the Static Strength Prediction Program (The University of Michigan), the software has become a useful tool for industrial ergonomists to analyze, design, and modify jobs. After entering joint postures and the magnitude of the load, the computer program predicts variables such as body strengths, spinal compressions, joint moments, ...etc. One of the concerns in using the results predicted from static biomechanical models is that the imposed body stresses from performing dynamic manual tasks tend to be underestimated and the strength capacities of the body overestimated due to the neglect of inertial forces. Several studies have shown that in estimating stresses on the body, inertial forces can be substantial (for example, Garg et al., 1982; Leskinen, 1985). Therefore, dynamic analyses are usually conducted for more accurate estimation.

The dynamic whole-body lifting model developed by Ayoub and El-Bassoussi (1978) is one of the early works that used dynamic analyses to study stresses on the body during lifting. Since advanced filming techniques were not available, the motion of the body could only be estimated by the Slote and Stone (1963) angular position and time equation. The equation described the angular position of the elbow joint as a function of time and the maximum forearm flexion. Dynamic models were not widely used until the advent of the high-speed computer and cinematographical technology. Today, photographical or optical motion acquisition systems accompanied by fast digital computers are mandatory equipment in biomechanical research laboratories. Studies using the inverse dynamics method, in which the motion of the activity was first filmed and the stresses on the body estimated using dynamic models, can be performed in the laboratory. Unfortunately, the cost of the motion measurement equipment is still high and the operation of the equipment usually requires expertise. Also, the data reduction procedure requires much time and can be very tedious. The major use of such method remains in the laboratory. General industrial ergonomists who recognize the importance of the dynamics of MMH activities do not have much access to dynamic analyses.

Research attempts to provide industry with computerized job analysis tools that do not require filming equipment and take into consideration the dynamics of motion began only recently. Chen and Peacock (1985) developed an interactive dynamic biomechanical lifting model that gives prediction in joint forces and moments from a computer program. No filming is needed to use the model. The angular kinematic variables of lifting were simulated by the Slote and Stone (1963) equation. The validity of the predicted forces and moments from the model was completely dependent on the validity of the Slote and Stone (1963) equation, which was originally developed for the forearm flexion. Applying the equation to the motion of the other body joints is therefore questionable.

Lee (1988) proposed an optimization approach to the determination of lifting motion. The method did not use any equation to represent the angular position and time relationship, such as the Slote and Stone (1963) equation. Instead, the position trajectory was considered to be discrete points in time and the motion was determined by minimizing a function of joint moments. Dynamic programming was used to find the optimal solution. Later Ayoub and Hsiang (1992) developed a similar model using a more efficient solution method based on nonlinear optimization techniques. The position trajectory was described by a polynomial, but the form of the polynomial was not specified. The solution was completely determined by the nonlinear optimization procedure. The model was relatively complex and the formulation contained both nonlinear objective and constraint functions. The solution of complex nonlinear optimization problems with both nonlinear objective and constraint functions is generally intractable (Shanno, 1990). To be of any practical engineering value, the simulation method must provide reliable and realistic solutions. Nevertheless, these previous attempts showed that the motion of manual lifting could be predicted and their results, although validated on relatively few male subjects, appeared promising and encouraging. The goal of the study was to continue the effort in the development of a reliable and realistic dynamic lifting simulation model.

1.2 Objectives

The objectives of the study were:

(1) To develop a simulation method to predict the sagittal plane lifting motion. The method incorporated and refined the optimization lifting models proposed by Lee (1988) and Ayoub and Hsiang (1992). A new polynomial curve generating method was developed to improve the prediction capability of the model. The method aimed at providing realistic and reliable predictions so that it can be practically used.

(2) To validate the simulation method on both male and female subjects. The validity of the method should cover both male and female subjects so that it can be used for both male and female workers. The validation should also show any limitation of the method so that care can be exercised in using the prediction results.

(3) To perform sensitivity analysis to study the effect of input errors and changes in model parameters on the performance of the simulation method.

1.3 Significance

The development of the simulation model aimed at providing industrial ergonomists with a computerized biomechanical model capable of predicting the dynamics of lifting motion. The development of such a model is the first step toward a completely computerized and automated prediction tool for ergonomists. The model can be used to eliminate the need for the motion acquisition equipment and the tedious and time-consuming process of data collection and reduction. In addition, the use of the simulation model promotes a safe method for conducting experiments. Experiments can be carried out on the computer without having to use human subjects. Therefore, the model has significant contribution to ergonomics.

The simulation model is also of great significance to occupational biomechanics. It provides another approach to analyzing the biomechanics of lifting activities. The computer simulation approach in biomechanics has been recognized to possess capabilities to answer what-if questions on the computer (Winter, 1990; Vaughan and Sussman, 1993). The lifting simulation model can be easily used to give new predictions when changes in input variables take place. This gives researchers a new predictive power the experimental approach does not have. Using the simulation model, researchers can explore questions that may be difficult to set up experiments to answer.

CHAPTER 2
LITERATURE REVIEW

The use of the biomechanical approach to study manual materials handling (MMH) tasks has significant implications in ergonomics. The present study aimed at developing a biomechanical simulation model for sagittal plane lifting tasks. It is informative to review the biomechanical models that have been developed in the past for studying human whole-body motion or locomotion.

2.1 General: The Biomechanical Approach

In biomechanics, there are several approaches to studying the mechanical stresses imposed on the human body during work or exercise. Among them, static modeling has been used in places where the work or exercise is static or has slow movements in which inertial forces may be neglected. The human body is treated as a mechanical structure and the forces and moments applied to or generated at particular body parts are estimated using principles of static equilibrium. The "Static Sagittal Plane" model (Chaffin, 1969) was developed for whole-body lifting or push-pull activities. Based on similar models, Park (1973) used optimization schemes to study initial lifting postures. This type of static link-segment models did not consider muscular activities. They could only be used to estimate the net reactions at joints of interest.

Seireg and Arvikar (1973) developed a static model for the lower extremities in which 29 muscles were considered. The model was statically indeterminate because the number of the unknown force variables was greater than that of the equilibrium equations. Several performance criteria were minimized to evaluate the forces applied by these muscles during static postures. Seireg and Arvikar (1975) extended the model to consider 31 muscles in seven segments of the lower extremities to study muscular load sharing during quasi-static walking. Walking was treated as a progression of static postures at successive time frames. The muscular force system was assumed to keep the lower extremities in equilibrium at all times.

Schultz and Andersson (1981) and Schultz et al. (1982) used a trunk model to study the stresses imposed on the lumbar spine. The model incorporated the effect of the ten muscles in the lower trunk area. Optimization techniques were used to determine the force distribution among these muscles for this indeterminate system. Bejjani et al. (1984) used a two-dimensional lifting model to study the relationship of loads on the spine and the knee. The model considered two muscle equivalents at the spine and the knee. Noone and Mazumdar (1992) developed a whole-body lifting model that considered six muscle equivalents acting at the lower back, hip, knee, and ankle. Optimization techniques were used to determine the forces exerted by the six muscle equivalents.

When the body undergoes significant movement, dynamic modeling becomes necessary. The equations of motion of the biomechanical system are often derived from either the Newton-Euler or Lagrangian formulation using principles of dynamics. The equations of motion describe the nonlinear and coupled relationships between the kinematic and kinetic variables of the system. In biomechanics, it is generally accepted that the internal muscle forces are the causes of human movement (Winter, 1990). The muscle forces and the moments resulting from the acting of these forces about each joint are usually viewed as the control variables for human movement.

To study the dynamics of human motion during work or exercise, either the control or the motion of the body segment must be known so that the equations of motion can be solved. When the control is known, equations of motion are integrated to solve for the motion. Given the motion, differentiation is used to derive the control. Based on what parameters are used as inputs to solve the equations of motion, two approaches are available in biomechanics for dynamic studies of human movement. The inverse dynamics approach uses filming techniques to obtain the motion so that equations of motion can be solved using the motion as inputs. The forward or direct dynamics approach uses special forms of control variables to estimate motions resulting from these controls.

Since the inverse approach requires motion inputs, the design of experiments to obtain motion data, the instrumentation, and the data reduction process are usually very involved. The inverse method is sometimes referred to as the analysis or diagnosis approach because one is trying to analyze what happens in the human body based on the observed motion. Due to its motion acquisition nature, only the gross body motion can be obtained and the model tends to stay at the skeletal level. For estimation of muscular stresses, the inverse approach has to rely on static or quasi-static muscular models combined with dynamic estimates of the reactive forces and moments about body joints. Also, the kinematic measurements obtained from filming often cannot detect the subtle movements that may exist and affect the gross motion pattern (Yamaguchi, 1990).

An early effort in the analysis of whole-body lifting motion using the inverse dynamics method was performed by Ayoub and El-Bassoussi (1978). The model was limited to sagittal plane lifting tasks. Röhrle et al. (1984) used a model of the lower body, including the pelvis and the leg, to study the movement of walking. A 42-muscle static model of the lower body was used in conjunction with the dynamic estimates of joint moments to estimate muscle forces using minimization of the muscle forces. Kromodihardjo (1986) developed a three-dimensional model for both symmetrical and asymmetrical lifting tasks. Similarly, the dynamic lifting model developed by Chen and Ayoub (1988) was a three-dimensional whole-body lifting model. The model was used to estimate hip moments. The static trunk muscle model by Schultz and Andersson (1981) was then used to estimate stresses imposed on the lumbar spine. DeVita et al. (1991) used a frontal plane dynamic model of the lower extremities during the stance phase of walking to study asymmetric load carrying. A static model for the trunk and pelvis was used in conjunction with the dynamic model to calculate L5/S1 moments.

The forward approach is usually considered as being able to model what actually happens with human movement. The sequence of events begins with neural stimulation and muscle firing. The forces of muscles acting at each joint create moments and then accelerate body segments (Winter, 1990). The forward method is also referred to as the synthesis or simulation approach because the motion is synthesized or predicted using the specified control functions. The advantage of the forward method over the inverse one is that it can be used to predict continuous controls such as neural functions or muscle forces. Unlike the inverse approach, in which muscle forces can only be estimated statically, dynamics of the control functions can be modeled with the forward approach. However, there are limitations for the forward method (Yamaguchi, 1990). First, the modeling process requires much insight into the neuromuscular and musculoskeletal systems. Assumptions are usually made to simplify the intricate interactions of these two subsystems, resulting in limited predictive power. Second, the forward model is computationally very intensive (Vaughan and Sussman, 1993). Both the integration of equations of motion and optimization of the controls require large computer power. Mathematical consideration in the computational stability sometimes becomes an important issue (Selbie and Chapman, 1987). Such models are therefore more difficult to be developed as reliable and useful engineering tools.

Due to the limitations found with the forward approach, a variation of the inverse dynamics method has been used for motion synthesis. This approach attempts to describe the repeatable and tractable human motion for a particular task group using different forms of kinematic equations. The kinematic equation is usually a generalization of the observed motion data. The kinematic equation can then be used as an input into the equations of motion and the analysis carried out just like the inverse approach. The Slote and Stone (1963) study is one such example. In their study, the forearm position was predicted by a sinusoidal equation. Kinetic analyses were performed based on the predicted kinematics from the equation. The advantage of this approach is that the values of kinematic variables can be obtained economically. There is no need to use expensive and sophisticated filming equipment. Therefore, it has potential to be developed as a useful computerized engineering tool. The disadvantage is that the simulation of kinematics is based on particular tasks. The adaptation of the model to other different tasks is difficult.

In addition to the above approaches, direct measurements of the muscular activities have been used to study the biomechanical system. This approach avoids the complex nature of the forward dynamics method and improves the inability of the inverse dynamics method to predict detailed dynamic muscular activities. Using electromyography (EMG), Marras and Sommerich (1991) and Marras et al. (1991) used direct measurements of muscle activities in the trunk to estimate the dynamic progression of the forces exerted by these muscles. The Schultz and Andersson (1981) static trunk muscle model was then used for the assessment of spinal loading during trunk motion. The direct measurements of muscle activities gave insight into the co-activation nature of the muscular system which was not predicted well by the optimization method proposed in Schultz and Andersson (1981).

The present study was interested in simulating the motion of the body during sagittal plane lifting activities. The following reviews on biomechanical simulation models are presented in detail.

2.2 Simulation Models

2.2.1 Forward Approach

Beckett and Chang (1968) produced the motion of the leg and foot in the swing phase of a step by minimizing the amount of mechanical work done. The leg was treated as a two-link system. The equations of motion were derived using the Lagrangian formulation. The control was the moment generated at the hip joint. The hip moment was assumed to be of constant magnitude and was applied for certain intervals during the leg motion. The magnitude of the hip moment was unknown and determined by the minimization scheme and other constraints.

Huston and Passerello (1971) modeled the human body with 15 segments. The equations of motion for this system were derived using the Newton-Euler formulation. Inputs to the model were external forces and motions of some segments. The input motions of the segments were represented by simple sinusoidal functions. The input forces were derived from documented data in the literature. Integration of the equations of motion was used to produced motions of arm lifting, swimming, and kicking.

Onyshko and Winter (1980) used a seven-link model of the lower body to synthesize the motion of walking. The equations of motion of the system were derived using the Lagrangian formulation. The initial conditions, including limb angles and velocities and joint moment histories obtained from laboratory data, were given to the equations of motion to reproduce kinematics of walking. The moment histories obtained from the experimental data were different from those the human body actually produced, since the calculations of these moments were based on inverse dynamics models. The authors suggested manual adjustments of the moment histories to obtain realistic walking motion.

Hatze (1980,1981) developed a comprehensive computerized human model with 17 segments and 46 muscles. The model not only considered the gross motion of the skeletal system but also simulated the excitation and contraction dynamics of the muscular system. The dynamic equations of motion of the system were developed using the Lagrangian formulation. The equations of motion were coupled with a series of neuromuscular stimulation functions for the 46 muscles. These functions were used as the internal controls of the human model. Once the control functions were specified, muscles then produced moments and the motion of the system was generated by integrating the equations of motion. In addition to simply guessing the form of the neural control functions, the study also used an optimization scheme by maximizing the distance jumped to produce simulated motions of the body in a long jump.

Mena et al. (1981) used a leg model consisting of three segments to synthesize the swing motion of the leg during gait. Equations of motion were derived using the Lagrangian formulation. The actual joint moments derived from filmed kinematics of the leg were used as inputs to the equations of motion. By integrating the equations of motion, simulated kinematics could be reproduced. They used a sinusoidal equation to approximate the hip position trajectory. By varying some parameters in the equation, modified hip trajectories along with actual moments were used as inputs and simulations were performed to study the effects of those parameters. In this study, there was no attempt to generalize the leg motion or control. The synthesis of motion was completely dependent on the actual data on joint moments.

Selbie and Chapman (1987) developed a 15-segment whole-body mechanical model. The Lagrangian formulation was used to derive the equations of motion. Net reactive joint torques derived from inverse analyses of experimental data were used as inputs and the equations of motion were integrated to perform a simulation of running.

Pandy and Berme (1988) synthesized the motion of human walking using a planar lower extremity biomechanical model. They used both three- and five-link models of the leg to study stance knee flexion-extension and foot and knee interaction. The dynamic equations of motion for the model were developed using a special computer algorithm based on the Newton-Euler formulation. The kinematics of walking were generated by integrating the equations of motion using input joint moments. The input joint moments were in the form of either simple step or ramp functions of time. These forms of input moments were not based on any experimental data or analyses. They were used for the special case of walking during the single support phase.

Yamaguchi (1990) performed a dynamic gait simulation using 10 muscles as the control of motion. The mechanical structure of the walking model had 8 degrees of freedom. Dynamic programming was used to determine the optimal control pattern by minimizing cost functions such as the weighted sum of squared deviations from a nominal control trajectory or the weighted sum of cubed muscle stresses. Using the optimal control trajectory, simulated walking motion was performed by integrating the equations of motion of the system.

2.2.2 Inverse Approach

Slote and Stone (1963) used interrupted light photographs to obtain a discrete trajectory of the forearm flexion-extension. The trajectory was then approximated by a continuous sinusoidal function. The complete angular position trajectory of the forearm based on the equation was then used in dynamic equations of motion to derive the power and work for the kinetic analysis.

Townsend and Seireg (1972) synthesized the motion trajectories of the human body during walking. The human body was treated as a single rigid body. The equations of motion were developed using the Newton-Euler formulation. The kinematics simulated were the position of the center of mass and three rotations of the body. A kinematic trajectory equation represented by the sum of a polynomial and a Fourier series was first developed based on the data for normal human walking derived from experiments. The equation was then used in the equations of motion to produce leg forces and hip moments. The solution to the kinematics was generated by minimizing work and footprint size. In order to ensure a feasible starting condition, the actual trajectory of kinematics was used as the input to the optimization process. This approach was a typical example of the combined use of inverse dynamics and optimization to solve the problem of motion synthesis. The unique merit in the study was that the kinematic equation developed from actual walking was used to provide guidance for the synthesized motion, as the authors noted.

Chen and Peacock (1985) used the Slote and Stone (1963) angular position equation in their computerized dynamic biomechanical lifting model. The model was able to perform whole-body kinematic and kinetic analyses without any filmed motion inputs. The Slote and Stone (1963) forearm kinematic equation was used for the motion of every body segment. Their work provided a useful dynamic analysis tool for lifting activities; however, the accuracy of prediction is in question because not every segment follows the kinematic equation developed for the forearm.

Flashner et al. (1987) used a trajectory generator in their model of leg stepping motion. The trajectory generator consisted of a set of cycloidal velocity equations for the knee and hip joints. By minimizing a predetermined performance criterion, the optimal trajectory was chosen and the required controls were computed.

Lee (1988) formulated a lifting task as an optimization problem. The model was intended for the prediction of optimal lifting motion. The biomechanical model used was a five-link whole-body sagittal plane model. The lifting task was described by an objective function of moments and several constraint functions of kinematics and kinetics. The objective function was the minimization of the total physical cost accrued during the lift. The constraints were that the kinematic solution must satisfy the ranges of motion and the kinetic solution must be within the person's strength capability. The optimization model was appealing because the optimal values of kinematic variables were derived based on the performance criteria specified by the objective and constraint functions. However, the method was relatively inefficient. It used dynamic programming to solve the optimization problem. The motion trajectories were discretized. The intermediate and final kinematic solutions were subject to smoothing, which could change the solution that was originally produced. The smoothed solution was then used as an input to the dynamic programming procedure until a reasonable solution was produced. The exhaustive search for an initial solution and the iterative process of smoothing and optimizing required considerable computation time.

Ayoub and Hsiang (1992) and Hsiang (1992) were interested in developing a simulation model for whole-body sagittal plane lifting activities. The optimization model developed by Lee (1988) was reformulated into a nonlinear optimization problem. Eighth-order polynomials were used for the kinematic trajectories. The polynomials were constrained by the initial and final kinematic conditions for the lifting task; however, they were not prescribed by any particular forms. The free-form polynomials were controlled by their coefficients. During the minimization procedure, coefficients were varied until a solution that met the criteria was produced. Unlike the Townsend and Seireg (1972) study in which the actual motion was used as an initial solution to ensure a feasible starting solution, the initial solution to the polynomial coefficients in this lifting motion simulation model was randomly selected. This often resulted in infeasible starting solutions. Also, there was no guidance in the form of the kinematic solution because the polynomial was allowed to be of any form. In general, the nonlinear optimization method was more efficient than the dynamic programming method. The drawback was that the random initial guess in the initial solution and the free-form polynomials sometimes did not provide sufficient guidance to generate a feasible starting solution so that the optimization routine could work reliably.

CHAPTER 3
TECHNICAL BACKGROUND

This chapter describes the technical aspects of the planar dynamic lifting model and the lifting optimization model that were used in the simulation of lifting motion. A brief discussion of the Hermite polynomial is introduced. The planar dynamic lifting model has been widely used in biomechanical studies to estimate forces and moments acting on the body during lifting. The lifting optimization model treats the lifting system as a goal-oriented system subject to various constraints. The Hermite polynomial is a useful numerical technique in engineering applications. All of these played important roles in the present simulation study. Although some of these models and techniques have been documented elsewhere in the literature, the material presented in this chapter serves as a useful background for understanding the methodology used in the entire simulation study. The nomenclature defined in this chapter will be used throughout the subsequent chapters.

3.1 Planar Dynamic Lifting Model

The biomechanical model used in the simulation of lifting motion was a two-dimensional sagittal dynamic five-link lifting model. The detailed discussion of model assumptions and the development of equations of motion can be found in Chaffin and Andersson (1991) and Winter (1990). This section summarizes the model and describes the variables in the context of the simulation study. The following assumptions were made for the planar dynamic lifting model:

(1) The body segment is treated as a rigid body.

(2) The body has a fixed mass.

(3) During the movement, the location of the center of mass of each segment remains fixed in the segment.

(4) The joints are pin-centered joints.

(5) The moment of inertia of each segment about an axis passing through its center of mass, proximal joint, or distal joint, normal to the sagittal plane of motion, is constant throughout the movement.

(6) The length of each segment remains constant throughout the movement.

(7) The joint friction is negligible.

(8) The two-handed lifting motion is symmetrical and confined to the sagittal plane.

(9) The load is a point mass located at the center of the box.

(10) The force of the load passes through the center of mass of the hand.

(11) The hand and the forearm are treated as one rigid link, assuming negligible rotation at the wrist.

(12) The ankle joint is assumed to be stationary throughout the movement.

(13) The trunk is assumed to be one rigid link from the greater trochanter to the glenohumeral joint.

(14) The body consists of five rigid links: the forearm and hand, the upper arm, the trunk, the upper leg, and the lower leg.

(15) The anthropometric data such as segment dimensions, mass, and inertial properties are assumed to conform to those proportions provided in Winter (1990, pp. 56-57).

Figure 3.1 shows the link-segment model of the human body. The five joints under consideration are the elbow, shoulder, hip, knee, and ankle. The angular position of each link is measured between the link and the positive x axis, using the joint as the base point. For example, the angular position of the forearm and hand link, θ_1, is called the angular position of the elbow joint because the elbow is the base point. The angular position is defined between $-\pi$ and π.

Figure 3.2 shows the free-body diagram of two adjacent links in the link-segment model. Using the Newton-Euler formulation, the following equations of motion can be derived with respect to an inertial reference frame:

$$\begin{aligned} &\boldsymbol{R}_j - \boldsymbol{R}_{j-1} + m_j\boldsymbol{g} = m_j\boldsymbol{a}_j \\ &\boldsymbol{M}_j - \boldsymbol{M}_{j-1} - \boldsymbol{r}_{j-1,cmj} \times \boldsymbol{R}_{j-1} + \boldsymbol{r}_{j,cmj} \times \boldsymbol{R}_j = I_j\ddot{\boldsymbol{\theta}}_j \end{aligned} \tag{3.1}$$

where

$\boldsymbol{R}_j$ = force vector acting at joint j to link j

$\boldsymbol{M}_j$ = moment vector acting to link j about joint j

$\boldsymbol{r}_{j,cmj}$ = linear position vector pointing from the center of mass of link j to joint j

$\boldsymbol{a}_j$ = linear acceleration vector of the center of mass of link j

$\ddot{\boldsymbol{\theta}}_j$ = angular acceleration vector of link j

$\boldsymbol{g}$ = gravity vector

m_j = mass of link j

I_j = moment of inertia of link j about an axis passing through the center of mass normal to the sagittal plane of motion

$\times$ = vector (cross) product operator.

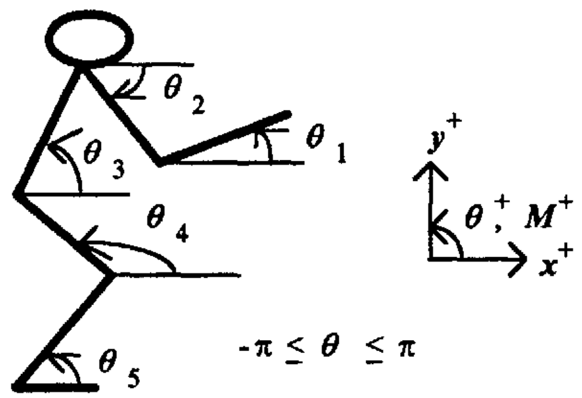

Figure 3.1 The link-segment model of the lifting person

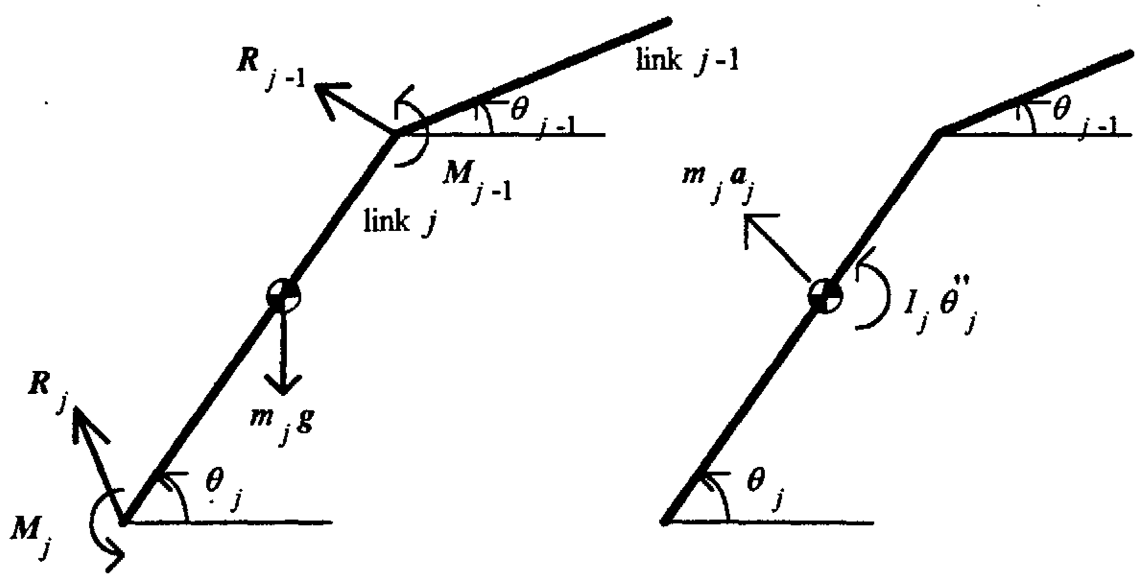

Figure 3.2 The free-body diagram of a body link and its adjacent link

Note that in (3.1) the term $-\boldsymbol{R}_{j-1}$ is the force acting at joint j-1 to link j which is the negative of the force acting at joint j-1 to link j-1, $\boldsymbol{R}_{j-1}$, due to Newton's third law of motion. Similarly, the term $-\boldsymbol{M}_{j-1}$ is the moment acting to link j about joint j-1. For the calculation of kinematics, the following finite difference method was used:

$$\dot{x}_i = \frac{x_{i+1} - x_{i-1}}{2\Delta t} \tag{3.2}$$

$$\ddot{x}_i = \frac{x_{i+1} - 2x_i + x_{i-1}}{\Delta t^2}. \tag{3.3}$$

3.2 Optimization Lifting Model

The optimization lifting model used in the simulation study followed similar formulation approaches proposed by both Lee (1988) and Hsiang (1992). Their models were revised to meet the need of the structure of the present simulation method. A brief discussion of their models has been presented in Chapter 2. This section describes the formulation of the optimization problem in the context of the present simulation study.

In optimization theory, the objective function may be thought of as the cost function of the system and the constraints the available resources of the system. While the cost is being minimized, the resources are usually limited. The optimization lifting model assumes that the human body performs a lifting task according to some criterion such as the minimization of the total muscular effort. While the body is trying to minimize the effort to complete the task, it is subject to various constraints such as the strength capability of the body and the geometrical layout of the work place. With the assumption, the lifting activity is formulated into a mathematical optimization problem with an objective function specifying the minimization of the effort, subject to various constraints.

3.2.1 Objective Function

$$\textit{minimize} \quad \int_{t=0}^{T} \sum_{j=1}^{5} \left(\frac{M_j(t)}{S_j(t)} \right)^2 \tag{3.4}$$

where

S_j = the moment strength of joint j

M_j = the magnitude of the moment vector $\boldsymbol{M}_j$ about joint j

T = total lifting time.

Note that the total lifting time is a model input. Actual lifting time of each lift was recorded from actual experiments. The experiments will be described in the next chapter. The ratio of the joint moment to strength represents the muscular effort exerted at that joint. The ratio is then raised to the second power to increase the penalty for higher deviation of the function from the minimum. The summation of the squared ratio over the 5 joints represents the total muscular effort of the body at one instant during the lift. The time integral of the total muscular effort over the entire period of the lift ensures that the minimization takes into account the complete history of the lift. The same objective function was used by Lee (1988) and Hsiang (1992) and was found to be robust in representing the total lifting effort in their simulation studies. Experimentally, Fogleman (1993) found a decreasing trend in the value of the objective function when subjects performed extended period of lifting tasks.

The static strength prediction equations corrected for population strengths by Stobbe (1982) using the data from Clarke (1966), Schanne (1972), and Burggraaf (1972) were used for the prediction of S_j, as suggested in Hsiang (1992). These equations are estimated regression models of the strength data. The strength capability of each joint is predicted by its joint angle and the angles of the adjacent joints. Since the body configuration is changing during the lift, the strength is posture-dependent and therefore time-variant. These equations can be found in Chaffin and Andersson (1991). Although the prediction equations are for the static strengths, their use in the objective function has been shown to be effective by Hsiang (1992).

3.2.2 Constraints

In optimization problems, constraints are used to control the amount of resources available to the system. Numerically, constraints serve to reduce the feasible solution space while searching for the optimal answer. Both Lee (1988) and Hsiang (1992) used a large number of constraints including kinematic and kinetic constraints. The use of a large number of constraints with more complex forms than simple bounds increases the complexity of the optimization problem dramatically. Furthermore, if many nonlinear constraints are present, the problem is generally intractable, as pointed out by Shanno (1990). To avoid such problems, a new formulation of the constraints for the lifting optimization model was considered as follows:

(1) Joint mobility constraints

$$\alpha_{j,L} \le \alpha_j(t) \le \alpha_{j,U}, \quad j = 1,\ldots,5, \quad 0 \le t \le T \tag{3.5}$$

where

$\alpha_j(t)$ = included angle of joint j at time t

$\alpha_{j,L}$ = minimum included angle of joint j

$\alpha_{j,U}$ = maximum included angle of joint j.

The joint included angle, α, is defined as the relative angle between the two adjacent links connected by that joint. It has a value between -2π and 2π, as shown in Figures 3.3 and 3.4. Since the included angle is a relative angle, the positive sign of the angle follows the arrow head as depicted in Figure 3.4. Note that the angular position θ, however, is an absolute angle and follows the convention depicted in Figure 3.1. The included angle describes the joint rotational mobility in two directions. As shown in Figure 3.3, when one link is fixed, the rotational mobility of the other link in the clockwise direction is usually different from that in the counterclockwise direction. One such example is the shoulder joint. In the standing posture, the entire arm can usually rotate 180° forward in the sagittal plane relative to the trunk; however, backward rotation can only reach about 60°. Equation (3.5) indicates that human movements are constrained by the mobility of each joint. The maximum included angle is the maximum rotational angle in one rotational direction and the minimum included angle the maximum rotational angle in the other direction with a negative sign.

In the literature, the normal ranges of joint mobility are usually defined in terms of joint flexion/extension, abduction/adduction, and medial/lateral rotations. Only joint flexion/extension was considered for the planar sagittal lifting motion. Detailed illustrations and definitions of the classical terminology for human movements can be found in Chaffin and Andersson (1991). According to this terminology, only the shoulder and ankle have both the flexion and extension. The extension angles for the elbow, hip, and knee are all zero. Furthermore, in the standing posture, the ankle cannot extend, that is, its extension is zero, otherwise, the person will fall backwards. Chaffin and Andersson (1991) provided a table of range of joint mobility from the study on young healthy males by Barter et al. (1957) and depicted in Webb Associates (1978). Using these joint mobility data presented in the form of flexion/extension, the boundary information for the joint included angles in (3.5) can be derived. Figure 3.4 shows the relationships between the joint included angles, angles of flexion/extension, and the angular positions defined in the planar lifting model. From the figure, one can find the following:

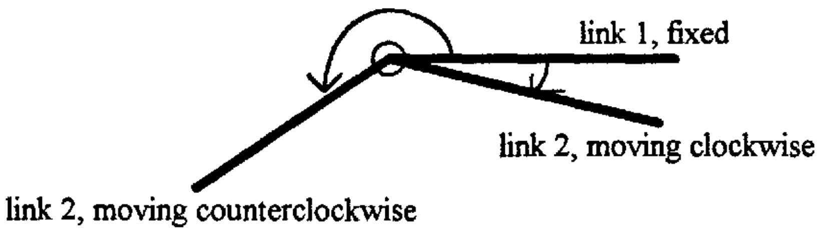

Figure 3.3 Rotational mobility of a joint

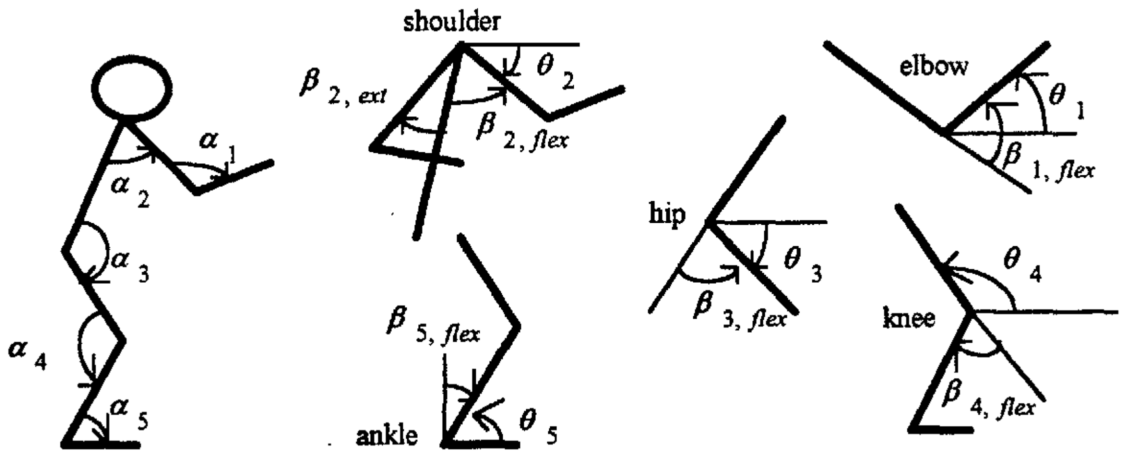

Figure 3.4 Relationships between the joint included angle α, joint flexion/extension angle β, and joint angular position θ

$$\begin{aligned}
\alpha_1 &= \pi - \theta_1 + \theta_2 \\
\alpha_2 &= \pi - \theta_3 + \theta_2 \\
\alpha_3 &= \pi - \theta_4 + \theta_3 \\
\alpha_4 &= \pi - \theta_4 + \theta_5 \\
\alpha_5 &= \theta_5 .
\end{aligned} \tag{3.6}$$

$$\begin{aligned}
\alpha_1 &= \pi - \beta_{1,flex} \\
\alpha_2 &= \beta_{2,flex} \quad or \quad -\beta_{2,ext} \\
\alpha_3 &= \pi - \beta_{3,flex} \\
\alpha_4 &= \pi - \beta_{4,flex} \\
\alpha_5 &= \frac{\pi}{2} - \beta_{5,flex} .
\end{aligned} \tag{3.7}$$

Using (3.7) and the average joint mobility data provided in Chaffin and Andersson (1991), the joint included angle boundaries are listed in Table 3.1. Note that the data in Table 3.1 represents the mean ranges for young healthy males. For the model constraints, these ranges were assumed the same for females.

It is worth noting that both Lee (1988) and Hsiang (1992) used joint angular position constraints. The boundaries for the angular positions were derived from the actual kinematic data collected in their studies. The constraints on the joint angular positions do not truly reflect the limit of motion due to joint mobility. The joint angular position θ is an absolute angle, as mentioned earlier. Joint mobility is a relative angle between two links. Setting limits on θ of each joint independently does not restrict the relationship between the two links. For example, using the boundary data for the shoulder and elbow angular positions provided in Hsiang (1992), we have the following two constraints:

$$-86^\circ \le \theta_{elbow} \le 57^\circ$$
$$-180^\circ \le \theta_{shoulder} \le 0^\circ .$$

Figure 3.5 shows one of the body configurations that satisfy these two constraints but apparently violate the joint range of mobility. The constraints on joint included angles, α, as in equation (3.5), will prevent this situation from occurring.

(2) Joint moment strength constraints

$$M_j(t) \le S_j(t), \quad j = 1,\ldots,5 \tag{3.8}$$

where

S_j = the moment strength of joint j, as predicted by Stobbe's equations

M_j = the magnitude of the moment vector $\boldsymbol{M}_j$ at joint j.

Table 3.1 Ranges of joint included angles, in degrees

joint	lower bound	upper bound
elbow	38	180
shoulder	-61	188
hip	67	180
knee	67	180
ankle	55	90

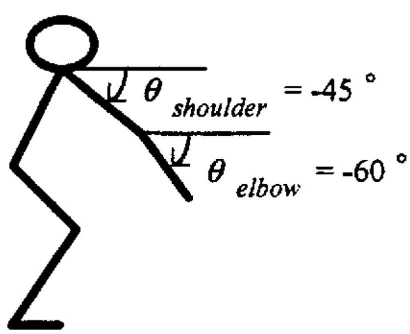

Figure 3.5 Infeasible body configuration that satisfies the joint angular position constraints

The constraints on joint moments describe the strength-limited behavior of human motion. The optimization lifting model is treated at the gross musculoskeletal level. The reactive moment at each joint is assumed to be the net muscular effort exerted by the muscles crossing that joint. This assumption greatly simplifies the model and has the advantage of avoiding the need to model the intricate internal dynamics of the neural and muscular systems.

The joint moment strength constraints were used by both Lee (1988) and Hsiang (1992). In addition, Hsiang (1992) used velocity, acceleration, and jerk (rate of change of acceleration) constraints by specifying simple bounds for these parameters. Similarly, Lee (1988) used a set of acceleration and jerk constraints. The use of the kinematic constraints was not adopted in the present study for two reasons. First, using the kinematic constraints increases the number of constraints dramatically. As mentioned earlier, this tends to make the optimization problem much more complex. Second, it was felt that the joint moment strength should be the dominating limiting factor for the entire motion. In dynamics theory, if we are given the motions of a system, we can deduce the forces and moments acting. Conversely, given the forces and moments, we can solve for the motions (Greenwood, 1988). The kinematics and kinetics are tightly coupled by the equations of motion. For human motion, the kinematics can be viewed as a result of the kinetics, that is, the motion is driven by the forces and moments the body exerts. The constraints specified by the bounds of the kinematic parameters are in theory already governed by the kinetic constraints. Therefore, the kinematic constraints are redundant when the kinetic constraints are present.

(3) Collision avoidance constraints

$$\begin{aligned} &\textit{if} \quad \{ y_{box}(t) \in [\, y_{shelf} - (\frac{h}{2}+\delta),\ y_{shelf} + (\frac{h}{2}+\delta)\,]\} \\ &\textit{then} \quad \{[\, x_{box}(t) + \frac{l}{2} + \delta] - x_{shelf} < 0\} \end{aligned} \tag{3.9}$$

$$\begin{aligned} &\textit{if} \quad \{ y_{knee}(t) \in [\, y_{box}(t) - (\frac{h}{2}+\delta),\ y_{box}(t) + (\frac{h}{2}+\delta)\,]\} \\ &\textit{then} \quad \{[x_{box}(t) - \frac{l}{2}] - [x_{knee}(t) + \delta] > 0\} \end{aligned} \tag{3.10}$$

where

$(x_{box}(t), y_{box}(t))$ = position of the center of box at time t

$(x_{knee}(t), y_{knee}(t))$ = position of the knee joint at time t

(x_{shelf}, y_{shelf}) = position of the edge of shelf

h = height of box in the sagittal plane

l = length of box in the sagittal plane

T = total lifting time

δ = collision tolerance.

These two constraints describe the collision avoidance of the motion. Figure 3.6 shows the geometric relationships between the person, the box, and the shelf. The position of the edge of the shelf, (x_{shelf}, y_{shelf}), was known and was a model input. Equation (3.9) describes the avoidance of collision between the box and the shelf. When there is nothing under the shelf, the box may go under the shelf during the lift; however, when the box is near the shelf, the person will refrain from hitting the shelf. The equation indicates that when the center of the box is at a certain height within the range of $[\, y_{shelf} - (h/2+\delta),\ y_{shelf} + (h/2+\delta)\,]$, the frontal edge of the box, $(x_{box}(t) + l/2)$, must not move beyond the edge of the shelf, x_{shelf}, in order to avoid collision. Note that the collision tolerance, δ, is used to describe the clearance between the box and the shelf that is needed for the person to freely move the box around the edge of the shelf. Similarly, equation (3.10) indicates that when the height of the knee joint is within the upper and lower edges of the box, the horizontal position of the rear edge of the box should be greater than that of the knee plus a tolerance to avoid collision.

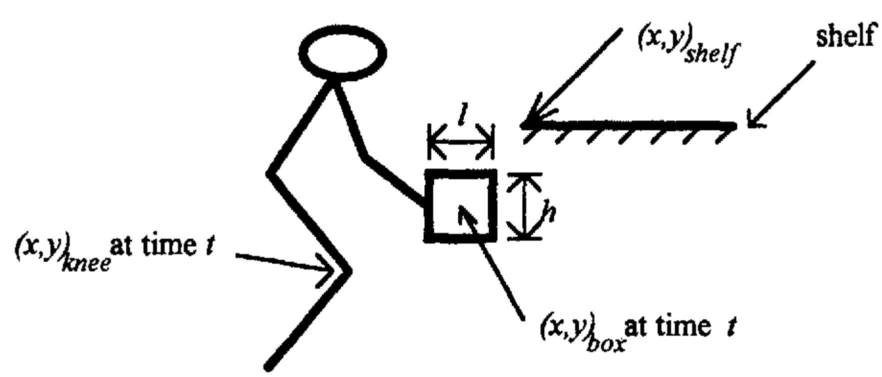

Figure 3.6 Geometric relationships between the person, box, and shelf

(4) Postural stability constraint

$$(x_{heel} + \delta) \le x_{cm} \le (x_{toe} + \delta) \tag{3.11}$$

where

x_{cm} = horizontal position of the system center of mass

x_{heel} = horizontal position of the end of foot

x_{toe} = horizontal position of the tip of foot

δ = allowance for the thickness due to wearing shoes.

The postural stability constraint indicates that the horizontal position of the center of mass of the lifting system, including the person and the box, should not fall outside the foot support area. This constraint assumes a static situation for the lifting system, that is, it merely considers the stability as if the person is holding the box statically at each successive time frame. Furthermore, it assumes that the foot does not actively produce muscle moment to counterbalance the reactive moment acting about the ankle.

3.3 Hermite Polynomial

For various engineering problems, one sometimes needs to represent a true but unknown function $f(t)$, by a polynomial $\theta(t)$, and in addition have the derivatives of $\theta(t)$ represent the derivatives of $f(t)$. It can be shown (Atkinson, 1989) that there exists one polynomial $\theta(t)$, unique among those of degree $\le n$-1, which satisfies

$$\begin{aligned} &\theta^{(i)}(t_1) = y_1^{(i)} \quad i = 0,1,\ldots,\lambda_1 - 1 \\ &\vdots \\ &\theta^{(i)}(t_m) = y_m^{(i)} \quad i = 0,1,\ldots,\lambda_m - 1 \end{aligned} \tag{3.12}$$

where the number of conditions on $\theta(t)$ at t_j is λ_j, $j = 1,2,\ldots,m$, and

$$n = \lambda_1 + \cdots + \lambda_m.$$

The numbers $y_j^{(i)}$ are given data which describe system conditions. The i^{th} derivative of $\theta(t)$ is denoted by $\theta^{(i)}(t)$. In other words, n derivative conditions uniquely determine a polynomial of order $\le n$-1. The numerical solution of the Hermite polynomial $\theta(t)$, given by (3.12), can be found in Atkinson (1989).

CHAPTER 4
METHODS

This chapter describes the simulation method and research procedure for the study. The overall procedure includes three stages. The first stage was the motion data acquisition. Data on the actual lifting motion collected for various lifting conditions using human subjects were digitized and analyzed. These data were used for both the development and validation of the simulation method. The second stage was the development of a reliable simulation method that can generate realistic lifting motions. This stage was the central theme of the study. The development of a good numerical simulation method can greatly facilitate the optimization process for the production of a good solution. In the last stage, the validation of the simulation model by appropriate comparison criteria between the actual and the modeled motions was conducted. Sensitivity analysis was conducted to further understand the behavior of the model in response to changes in model parameters.

4.1 Lifting Motion Data Acquisition

The lifting motion data were collected prior to the development of the simulation method. The major purpose of the data collection was not to study any effects or investigate any causal relationships in the lifting activity; rather, it was a documentation of lifting motion so that the data could be used for the development and validation of the simulation model. The data collection and experimental protocol followed Ayoub (1991) with minor revision. The data collection was in part required by the National Institute of Occupational Safety and Health (NIOSH) grant research project. A lifting/lowering machine with a height-adjustable shelf was used as the working surface for the lifting activity. The Motion Analysis System with VP320 video processor was used for the data acquisition.

The intent of the data acquisition was to cover a wide range of commonly used lifting conditions. Five male and five female subjects were used. The lifting conditions included two ranges of lift, floor-to-knuckle and floor-to-shoulder; three weights of lift, heavy, medium, and light; and two container sizes, large (18"x12"x12") and small (12"x12"x12"). The large box had its length (18") in the sagittal plane. The reason for this arrangement was that the biomechanical lifting model was a planar model. The longer dimension in the sagittal plane allowed for a study of changes in the motion in that plane. The ranges of lift were adjusted to the subject's own knuckle and shoulder heights. For males, the three levels of weights were 25, 35, and 45 lbs. For females, they were 10, 15, and 20 lbs.

Prior to data collection, subjects practiced the lifting activities. The purpose of the training was to familiarize subjects with the activity and reduce the variability in their lifting styles and techniques. Free-style lifts were performed. All twelve combinations of lifting conditions were practiced with one hour per condition, that is, a total of twelve hours of training was performed by each subject. In the training, two minutes were allowed for sufficient rest between lifts. The order of lifts was randomized. The initial location of the box on the floor was controlled. The box was placed on the floor at the same location for every lift, with the frontal edge of the box positioned directly beneath the edge of the shelf. A total of 360 lifts was performed by each subject in the training session.

During data collection, three replications were performed for each condition. The order of lifts was completely randomized within each subject. Reflective markers were attached to the body landmarks at the hand, elbow, shoulder, hip, knee, and ankle as described in Winter (1990). The location of feet was controlled. Subjects selected their preferred locations of feet for the two box sizes and used them throughout the experiments. Prior to each lift, subjects stayed in a motionless static posture with their hands holding the handles of the box without applying any force. They were given an oral signal to start the lift and move the box from the floor to the shelf. Other conditions remained the same as in the training. The collection of twelve conditions on ten subjects with three replications allows for a total of 360 lifts under the simulation study.

The total duration of the filming time was sufficiently longer than the duration of the lift to cover the beginning and end of the lift. For the simulation study, the beginning of the lift was defined as the time at which the box was completely lifted off the floor. The end of the lift was defined as the time at which the box was completely put down on the shelf. Electrical signals initiated instantaneously by the lift-off and landing of the box were sent to the Motion Analysis System and marked in the motion data record. The collected motion data were digitized and smoothed between the two time event marks, using a Butterworth low-pass digital filter at 2 Hz cutoff frequency. Analysis and modeling were based on the smoothed motion data.

4.2 Simulation Method

4.2.1 General Motion Simulation Model

In simulating the motion of a system, the control of the motion must be known in addition to the dynamic equations of motion. The control usually describes the forces or moments that generate the motion of the system. For example, the free fall of a particle has a constant force, the gravitational force, acting on it. The gravitational force can be viewed as a control with constant magnitude and direction. When it is used as an input to the equations of motion, the entire motion of the particle can be predicted given that the initial position is known.

In a more complex system, such as lifting, the control is not constant. The forces and moments at each joint vary during the lift as time proceeds. In the previous chapter, the dynamics of lifting was described by the equations of motion in (3.1). If the entire history of forces and moments were known for a lift, the motion of each joint would be able to be predicted by integrating the equations of motion. Unfortunately, the internal muscle forces acting about the joints are not only time-variant but also difficult to measure or quantify for the lifting activities. Other means have to be used to estimate or predict how humans generate forces and moments in performing a lifting task.

The optimization model introduced in the previous chapter describes how the person performs the lift. It predicts that if the person is going to generate forces and moments to control the motion, he or she will follow the criterion given by the objective function subject to a set of constraints such as avoiding collision between the box and table. With optimization models describing the biomechanical behavior of the motion, we may be able to generate the entire history of the forces or moments and use them as inputs to the dynamic equations of motion to synthesize motion.

So far, the control of a system has been viewed as the forces or moments that generate the motion. The concept of control may also be generalized to apply to any parameters in the equations of motion, for example, the kinematic parameters. Once the entire history of the control parameter is known, one can solve the equations of motion for the other parameters.

Based on the equations of motion and the optimization model, and given a tentative control, the dynamics of the system can be calculated and the behavior of the system can be checked against the optimization model. The tentative control may then be adjusted until the optimal behavior is reached. This process is illustrated in Figure 4.1, the general motion simulation model. The tentative control may be either the system kinematics or

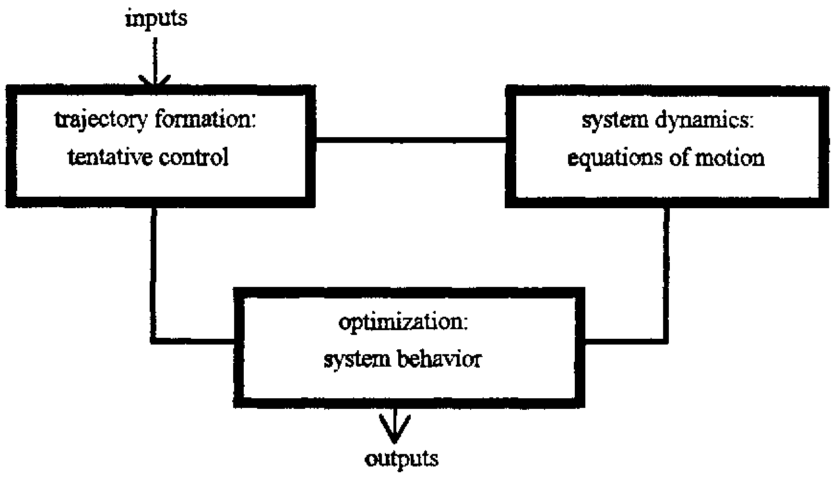

Figure 4.1 General motion simulation model

kinetics. The formation of an entire history of the tentative control requires unique insight into the system kinematics or kinetics under simulation.

4.2.2 Lifting Motion Simulation

The idea of the motion simulation model illustrated in the block diagram in Figure 4.1 was used to simulate the lifting motion. The kinematics, specifically the angular position, was chosen for the trajectory formation because there existed suitable properties that can be modeled. The simulation method consisted of three computation processes: (1) the generation of polynomials which represent the angular position trajectories of the joints, (2) the computation of kinematics and kinetics, and (3) the optimization process.

Figure 4.2 shows the block diagram of the computation flow. The process starts with the generation of an initial hypothetical position trajectory for each joint in the trajectory formation unit. The method that was used to generate these initial trajectories using Hermite polynomial techniques will be discussed in detail in the next section. The position-time data are passed to the dynamics computation unit. Based on these initial position trajectories, kinematics and kinetics are calculated in the system dynamics unit according to the dynamic equations of motion derived in equation (3.1). The kinematics and kinetics are then passed to the optimization unit and the values of the objective and constraint functions are calculated. The optimization unit checks if optimality had been reached and the constraints satisfied. If not, new position trajectories are formed and another loop of computation proceeded until optimality is reached and all the constraints

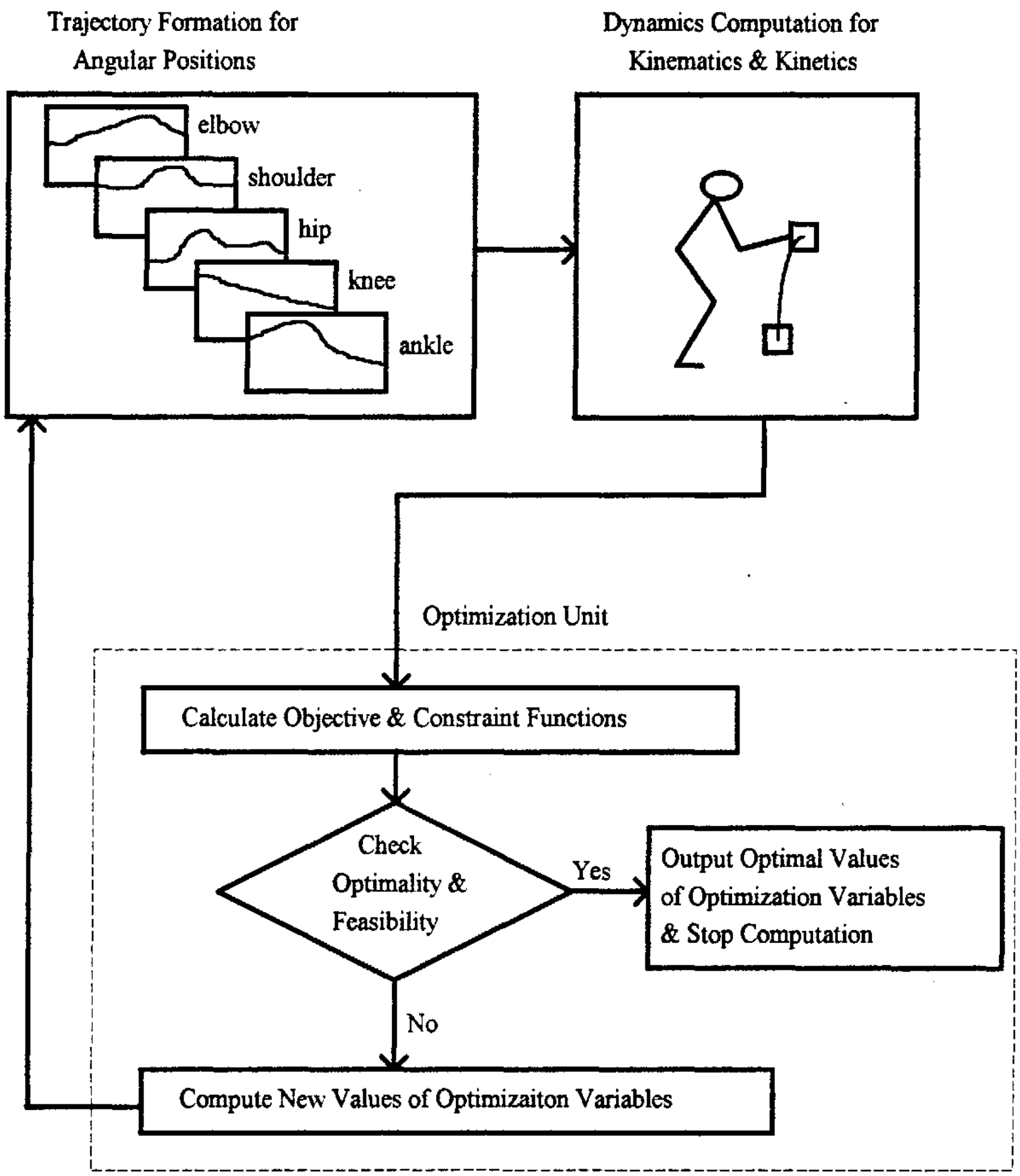

Figure 4.2 Block diagram of the computation flow for the lifting simulation method

satisfied (feasibility). When optimality and feasibility are both reached, the final position trajectories are the outputs of the model.

Note that in the optimization unit, there is a computation of the optimization variables in addition to the computation of the objective and constraint functions. In optimization theory, the term "function" refers to the objective and the constraints. The term "variable" refers to the parameters that are given to the optimization routine to solve for their optimal values. The objective and constraint functions all depend on the optimization variables. During the optimization process, the values of the optimization variables are varied until the objective function is minimized or maximized and constraints satisfied. The optimization variables that are chosen depend on the trajectory formation method. After the initialization of the optimization variables, the position trajectories are generated using these initial variable values. When the computation continues, going through the dynamics computation and the optimization units, new values of the optimization variables are generated by the optimization routine. These new variable values are then given back to the trajectory formation unit and used to generate a new set of joint angular position trajectories. The optimization variables will be described in the next section in more detail when the trajectory formation method is introduced.

The entire approach described above can be characterized as an inverse dynamics plus nonlinear optimization approach. It is inverse dynamics because in this approach, kinetic variables are solved for using kinematics as inputs. It is nonlinear optimization because the objective function and some of the constraints are nonlinear.

The equations of motion unit is a straightforward computation process. The computation only involves differentiation in the inverse dynamics method. Complex numerical integration required by the forward method to solve the equations of motion is avoided. The performance of the optimization unit depends on the software and algorithm used, the nature of the problem, and the way the problem is formulated. In general, large-scale nonlinear optimization problems are computationally intractable, especially if many of the constraints are nonlinear (Shanno, 1990). For engineering applications, the formulation of the problem into a simpler model may help reduce the complexity and avoid the computational intractability. The trajectory formation unit is the beginning of the computation loop. A good numerical trajectory formation method allows sufficient guidance in the generation of a feasible initial solution which may facilitate the optimization process; therefore, it directly influences the performance of the entire simulation model. The trajectory formation method and the implementation of the optimization model are presented below.

4.2.3 Trajectory Formation Using Control Points

To be able to simulate the motion of a complex system, it was assumed that the control of the system followed a certain pattern due to system constraints. Fixed forms or patterns of kinematic or kinetic trajectories have been used by Townsend and Seireg (1972) and Pandy and Berme (1988) to simulate walking motion. In the case of human lifting, the limitations in the body strength and the restrictions in the geometry of the body and workplace make the lifting motion tractable. Although the internal controls such as forces and moments are unknown, the motion in general followed a pattern under the same task condition. It is possible to generate a hypothetical time curve of the angular position for each joint, with the derivatives of the curve following kinematic characteristics of the motion under study. Hermite polynomials were used to generate such curves so that each curve had a particular form following the pattern of the angular position trajectory of each joint. Before we discuss the curve generating method, several assumptions were made about lifting. These assumptions were further examined in the validation stage of the study.

4.2.3.1 Assumptions

The following four assumptions were made for model development:

(1) All the joints are motionless when the lift begins and ends. In performing the lift, the subject started with a static posture (initial posture) and ended at another static posture (final posture). When the lift started, there might be subtle movements of each joint in different orders. It was difficult to define a common beginning and an end for all the joints; however, this assumption was in general true in terms of whole-body action.

(2) The motion undergoes a constant number of acceleration peaks. For the same task condition, the number of peaks (or troughs) is constant in the acceleration trajectory; therefore, the number of peaks is also constant in the velocity and position trajectories. Here, the peaks are defined as the locally highest points in a curve where their derivatives are zero. For a natural lift, the motion is completed without stopping. The kinematic property of the motion can be characterized by these ups and downs in the motion trajectories.

(3) The magnitudes of the acceleration (or velocity, position) peaks are bounded. The peaks in acceleration are bounded in part because of the limit in human strength. The peaks in position are bounded in part because of the geometrical layout of the task, such as the height of the shelf.

(4) The times at which the acceleration (or velocity, position) peaks occurred are bounded. Lifting requires appropriate movement coordination between joints. To smoothly complete a lift, the timing of these peaks plays an important role. Inappropriate timing will result in an unnatural lift and sometimes a failure to complete the lift. The timing of these peaks is in part a result of the body configuration during the lift. For example, at the final stage of the lift, it is difficult to exert a large force to generate a high acceleration because the load is away from the body. A large moment arm is created for the load resulting in a mechanical disadvantage. Also, it is not necessary for a high acceleration to occur at this stage of the lift while one is trying to put the load down.

4.2.3.2 Trajectory Formation

The Hermite polynomial was introduced in section 3.3. When n derivative conditions are given, there is a polynomial $\theta(t)$, unique among those of degree $\leq n$-1, which satisfies all the conditions. The above four assumptions were used to generate a position trajectory for each joint using the Hermite polynomial. The goal in generating a hypothetical position trajectory was to produce a tentative trajectory which can suitably satisfy all the four assumed kinematic properties. In the following, the trajectory formation method for the angular position of a joint is discussed.

The first assumption of a motionless beginning and end for lifting translates into four conditions; that is, the system begins and ends with zero velocity (1st derivative) and acceleration (2nd derivative) :

$$\dot{\theta}(0) = 0 \tag{4.1}$$

$$\dot{\theta}(T) = 0 \tag{4.2}$$

$$\ddot{\theta}(0) = 0 \tag{4.3}$$

$$\ddot{\theta}(T) = 0 \tag{4.4}$$

where

T = total lifting time.

The second assumption of a constant number of peaks in the position trajectory provides additional conditions. For simplicity, assume for now there is only one position peak. The additional condition is a zero velocity at that position peak:

$$\dot{\theta}(t_1) = 0 \tag{4.5}$$

where

t_1 = time at which the peak position occurs.

Note that t_1 is unknown here.

The last two assumptions require that, in this example, the location of the position peak be bounded. Note that the magnitude of the peak is also unknown, but if it is given, this will give another condition:

$$\theta(t_1) = p_1 \tag{4.6}$$

where

p_1 = value of the peak position.

The initial and final angular positions of each joint will be given as model inputs, thus providing two additional conditions:

$$\theta(0) = p_0 \tag{4.7}$$

$$\theta(T) = p_T \tag{4.8}$$

where

p_0 = value of the initial angular position

p_T = value of the final angular position.

Overall, there are eight derivative conditions. A unique polynomial of seventh-order exists satisfying all the conditions. This polynomial was used as the hypothetical angular position trajectory for the simulation model. Figure 4.3 shows the hypothetical trajectory, assuming (p_1, t_1) is known. Note that the location of the peak, although bounded, was actually unknown in the simulation model. The shape of the curve can be varied by moving the location of the peak, thus changing the kinematic properties of the motion represented by the curve. Since one can control the shape of the curve by varying the location of the peak, the peak point is called a control point. It is assumed that there exists one control point in the bounded region so that the corresponding curve passing through the control point possesses fine kinematic properties of the motion under study. By searching for the location of the control points within the bounded region as shown in Figure 4.3, a position trajectory can be found to reasonably simulate the motion under study.

4.2.3.3 Formulation for Each Joint

So far, the discussion of the trajectory formation has been focusing on the trajectory of a single joint. In the planar dynamic lifting model described in section 3.1, there were five joints under study, namely, the elbow, shoulder, hip, knee, and ankle, with a joint angular position $\theta_j(t), j = 1,2,\ldots,5$, defined for each joint, respectively. The lifting motion under study can be completely defined by these five coordinates. The task of simulation was to find a tentative position trajectory for each of the five joints. The

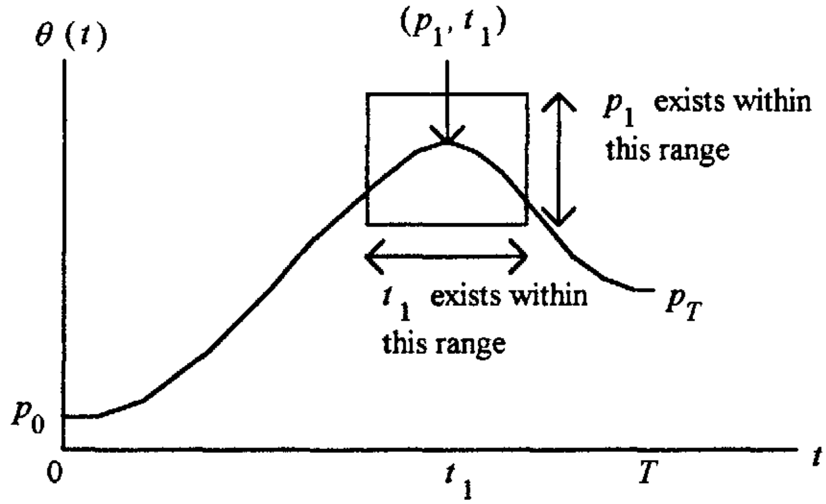

Figure 4.3 Hypothetical trajectory of angular position

kinematic properties, for example, the number of the control points, were different for each joint. Therefore, a unique trajectory formation model was developed for each joint, based on its own kinematic properties. The development of an appropriate trajectory model for each joint was the major objective of the study. The model must consider all the kinematic characteristics of the position, velocity, and acceleration trajectories. The kinematics of the actual data were studied to obtain a generalization of motion patterns for each joint. Specifically, the four assumptions made earlier were examined. The number of the control points and the boundary region of the control points were determined for each joint. Furthermore, the tentative position trajectory must also have its derivatives conforming to the patterns of the velocity and acceleration trajectories.

The general formulation of the trajectory model is presented now. For a given joint j, $j = 1,2,\ldots,5$, there exist control points (p_{ij}, t_{ij}), $i = 1,2,\ldots,m_j$, where m_j is the number of the control points for joint j. The initial and final positions of joint j are given as p_{0j} and p_{Tj}, respectively. The position trajectory is uniquely determined by the polynomial of order $2m_j + 5$, which satisfies:

$$\theta_j(0) = p_{0j} \tag{4.11}$$

$$\theta_j(T) = p_{Tj} \tag{4.12}$$

$$\theta_j(t_i) = p_{ij}, \quad i = 1,2,\ldots,m_j \tag{4.13}$$

$$\dot{\theta}_j(0) = 0 \tag{4.14}$$

$$\dot{\theta}_j(T) = 0 \tag{4.15}$$
$$\dot{\theta}_j(t_i) = 0, \quad i = 1,2,\ldots,m_j \tag{4.16}$$
$$\ddot{\theta}_j(0) = 0 \tag{4.17}$$
$$\ddot{\theta}_j(T) = 0. \tag{4.18}$$

4.2.3.4 Normalization

In the above derivation of a hypothetical trajectory, the initial and final positions, p_0 and p_T, were given as model inputs. They are subject to variation between lifts. The total lifting time, T, of each lift was a given input and subject to variation too. Two lifts may have a different T but their general pattern looks the same. Similarly, two lifts may have the same trajectory differed only by their initial and final positions. Figure 4.4 shows that in one case two similar curves end at different times, and in another case the two are the same but merely separated by their initial and final positions. To facilitate formulation and to compare motion patterns between different lifts, it is convenient to use the following normalization scheme:

$$\lambda = \frac{\theta - p_0}{p_T - p_0} \tag{4.9}$$
$$\tau = \frac{t}{T} \tag{4.10}$$

where

λ = normalized angular position

τ = normalized time, $0 \le \tau \le 1$.

The normalization is a rescaling of the coordinates in both the time and position scales. Using this normalization scheme, the peak position (p_1,t_1) in Figure 4.3, will be transformed into normalized coordinates (λ_1, τ_1), bounded in a normalized rectangle region. If there are more than one peak position, each will be bounded within its own region. The normalized system time always starts at 0 and ends at 1. The use of normalized coordinates allowed for a comparison between different lifts and possibly a generalization of motion patterns among different lifts. It was hypothesized that after normalization, the trajectories of the actual motion from different lifts under the same task condition would look similar. There may also be common locations for the control points after normalization. The normalized control points $(\lambda_{ij}, \tau_{ij})$ for the actual lifts were calculated and their bounds derived, where $i = i^{th}$ control point and $j = j^{th}$ joint.

The normalized control points $(\lambda_{ij}, \tau_{ij})$ are used as the optimization variables mentioned earlier in the previous section. When $(\lambda_{ij}, \tau_{ij})$ are initialized with some value, they are unnormalized into (p_{ij}, t_{ij}). The tentative trajectories are then generated using equations (4.11) to (4.18). After the optimization routine calculates new values of $(\lambda_{ij}, \tau_{ij})$, they are unnormalized and passed to the trajectory formation unit to generate new trajectories using equations (4.11) to (4.18) again. The advantage of using $(\lambda_{ij}, \tau_{ij})$ as the optimization variable is that their values can be initialized using any value within

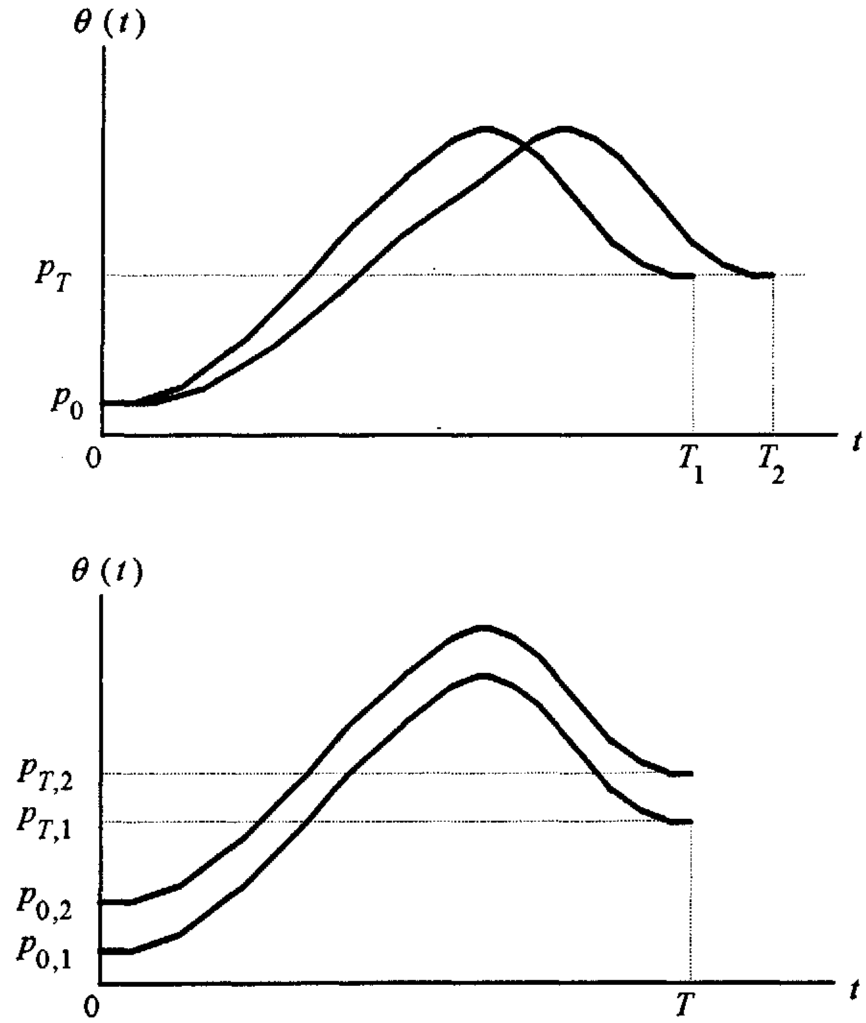

Figure 4.4 Two angular position curves with a similar pattern but different total lifting times and initial and final positions

the bounds derived from the actual data. This bounded region for $(\lambda_{ij}, \tau_{ij})$ represents the common locations of the position peaks among different lifts and subjects. The generated polynomials using $(\lambda_{ij}, \tau_{ij})$ as initial inputs will be of fixed forms which are similar to the patterns of the actual trajectories. This is also likely to ensure a feasible starting solution to facilitate the optimization process.

4.2.4 Optimization Implementation

The goal of the optimization is to search for the optimal values of $(\lambda_{ij}, \tau_{ij})$ so that the objective function is minimized and the constraints satisfied. There are infinite solutions to the values of $(\lambda_{ij}, \tau_{ij})$ within their bounds. The optimization unit serves the purpose for finding the optimal solution within those bounds.

The GRG2 nonlinear optimization software (Lasdon and Waren, 1986) is a widely distributed system and has been shown to be effective to deal with problems where the objective and constraint functions are both nonlinear (Subramanian and Hung, 1993). For the optimization of the model presented in section 3.2, the GRG2 system was used. To use GRG2, it was required to design an interface program in which the values of the optimization variables and the objective and constraint functions were calculated and returned to the main routine in GRG2. The entire problem has the form:

$$\begin{array}{ll} \underset{(\lambda_{ij}, \tau_{ij})}{\textit{minimize}} & \text{objective function (3-4)} \\ \textit{subject to} & \text{constraint functions(3-5)(3-8)(3-9)(3-10)(3-11).} \end{array}$$

The $(\lambda_{ij}, \tau_{ij})$ in the above formulation denotes the optimization variables that are varied until the objective function is minimized and the constraints satisfied.

In summary, the implementation starts with the initialization of the normalized coordinates $(\lambda_{ij}, \tau_{ij})$ within its general bounds. Based on the initial values, original coordinates of the control points (p_{ij}, t_{ij}) are calculated using equations (4.9) and (4.10), noting that the initial and final positions are given inputs. Tentative position trajectories are then generated using equations (4.11) to (4.18). Based on the tentative trajectories, kinematics and kinetics are calculated using equations (3.1) to (3.3). Objective and constraint functions are then calculated using equations (3.4), (3.5), and (3.8) to (3.11). The values of the variables and functions are passed to the GRG2 system and new values of the normalized coordinates are provided by GRG2 and the process continues until

GRG2 reaches optimality. The final values of $(\lambda_{ij}, \tau_{ij})$ given by GRG2 are then used to generate the final solution for the angular position trajectory of each joint.

4.3 Validation and Analysis

As with any model development, assumptions are usually made to facilitate the modeling process. The success of the model depends on how close the assumptions are to the actual behavior of the system being modeled. In section 4.2.2, four fundamental assumptions were made about the motion of lifting. The formation of a hypothetical position trajectory was completely built upon these assumptions. Therefore, it is important to examine the reality of these assumptions. Since these assumptions are concerned with the general pattern of the motion, the validation is in fact a test of the generalization capability of the trajectory formation method. The actual motion patterns of the data, regarding the number of the control points and where they are located in the normalized coordinate space, were examined.

The ultimate goal of the lifting simulation is to allow one to predict realistic motions of lifting. Comparisons between the actual and modeled motions were performed to provide information about how good the model is in predicting the actual motion.

Finally, sensitivity analysis was performed to further understand the behavior of the model. Sensitivity analysis is concerned with the changes in the performance of the model in response to any input errors or changes in model parameters. The effects of several model parameters were examined in the analysis.

4.3.1 Distribution of Normalized Trajectory

The first assumption made about the motion of lifting was that the initial and final velocities and accelerations for each joint were zero when the lift began and ended. As mentioned earlier, it was difficult to define a common beginning and an end for all the joints under consideration. In general, the whole-body motion started and ended with static postures. In the experimental setup, the beginning and end of the motion were defined as the lift-off and landing of the box, respectively. For each joint, the velocities and accelerations occurring at the lift-off and landing of the box were examined to verify this assumption.

The second assumption was that the number of peaks was constant in the trajectories of the angular position, velocity, or acceleration. The number of peaks (including troughs) in the position, velocity, and acceleration trajectories was examined.

The third and fourth assumptions were examined together. The locations of the control points (position peaks) were assumed to be bounded. For comparison and generalization purposes, the locations of the normalized control points $(\lambda_{ij}, \tau_{ij})$ were examined.

4.3.2 Comparison between Actual and Modeled

Graphs of the actual trajectory and the predicted trajectory allow for direct visual comparisons. The time plot of the angular position trajectory of each joint gives useful information about the difference in the general pattern between the actual and the modeled motions. Another useful graph is the stick diagram of the lift which gives information about the relationship between the lifting person and the workplace at successive time frames.

Comparisons based on pre-determined performance criteria were made. Since the position trajectory is a time series, the typical evaluation criterion, mean square error (MSE), was used as the first performance criterion (Aczel, 1989), where

$$MSE = \frac{\sum_{i=1}^{n}[\theta(i) - \hat{\theta}(i)]^2}{n} \tag{4.19}$$

where

$\theta(i)$ = actual position at time frame i

$\hat{\theta}(i)$ = predicted position at time frame i.

Note that there is a drawback in using MSE as the only criterion. Figure 4.5 shows two predicted curves and the actual curve. The two predicted curves may have the same MSE but the first curve follows the trend of the actual curve more closely. The patterns in the velocity and acceleration of the second curve will be completely opposite to those of the actual curve. To amend the deficiency in using MSE, Hsiang (1992) used the number of disconcordant pairs, which measures the disagreement of the trend in the movement of the two curves. From time frame i to $i + 1$, if one curve is moving up and the other is moving down, then we have a disconcordant pair. When the two curves follow the same trend, the number of disconcordant pairs will be small. The mean number of disconcordant pairs (MNDP) was used as the second performance criterion, where

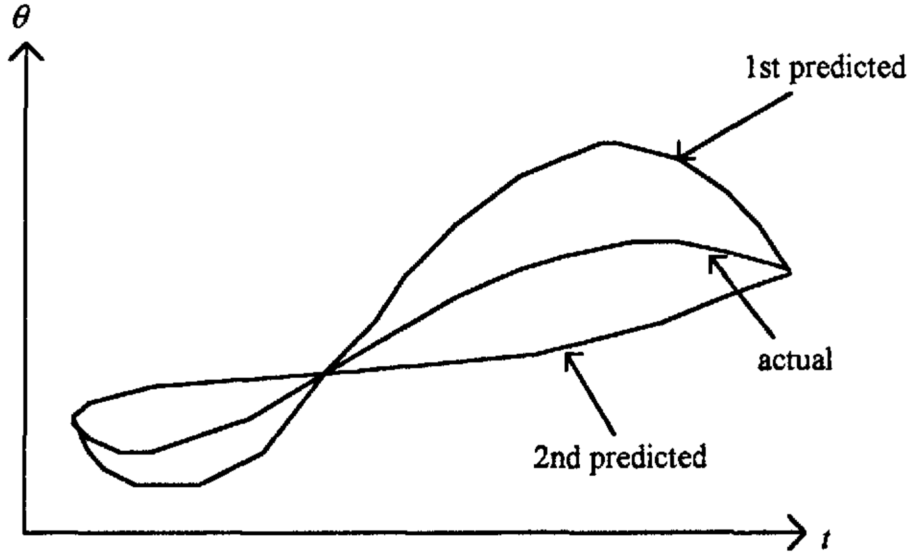

Figure 4.5 Example trajectories with similar MSE but different patterns

$$MNDP = \frac{\sum_{i=1}^{n-1} f\{[\theta(i+1)-\theta(i)][\hat{\theta}(i+1)-\hat{\theta}(i)]\}}{n-1} \tag{4.20}$$

where

$f\{x\} = 1, \quad x < 0$

$\quad = 0, \quad$ otherwise.

4.3.3 Sensitivity Analysis

The goal of the sensitivity analysis is to study the effects of the model parameters on the general performance of the model. The sensitivity of the model can be viewed as the effect of a specific input error on the model prediction error (Park, 1973). To carry out the sensitivity analysis, repeated computer experiments of the simulation model based on different parameter inputs other than those used in the original model are often necessary.

4.3.3.1 Effects of Segment Lengths

The simulation model has assumed the standard anthropometric data as summarized in Winter (1990). The parameters used for segment lengths were assumed to be proportional to the body stature. For each subject, the actual proportions of the segment lengths in the body stature may not conform to those as listed in Winter (1990). It is of interest to examine the effects of the segment length parameters. The simulation was conducted using the actual segment lengths measured from each subject. The model performance criteria resulting from the use of the actual segment lengths were compared to those from the original model using the standard proportional segment lengths.

4.3.3.2 Effects of Initial Joint Velocities

The simulation model has assumed a motionless beginning and end for all the five joints. Specifically, the velocities were assumed to be zero for all the joints at the defined beginning and end. The effects of different initial velocities at different joints which reflected the movement coordination between the joints prior to the lift-off of the box may have important implications to the model performance. To examine their effects, actual initial joint velocities were used as inputs to the simulation model. The performance criteria resulting from the use of the actual initial velocities were compared to those from the original model.

4.3.3.3 Effects of Optimization Model Constraints

In section 3.2, four types of constraints were developed to describe the limitation in lifting motion. They were the joint mobility constraints, the joint moment strength constraints, the collision avoidance constraints, and the postural stability constraints. The effects of the constraints were examined. If certain constraints were found to have little effects on the overall prediction performance, they can be removed from the model to increase the efficiency of the optimization process. The effects of the constraints were examined by removing each type of constraint individually from the model while keeping all the other constraints in the model. The performance criteria resulting from the removal of each type of constraint were compared to those from the original model.

CHAPTER 5
VALIDATION AND DISCUSSION

The methodology presented in the previous chapter was based on a central thesis, that is, the human motions of lifting are repeatable and consistent under the same task condition. The modeling approach first assumed that the angular trajectories of each joint followed certain consistent patters for the same lifting task. Due to this consistency, a unique polynomial model was derived for each joint based on the trajectory patterns of that joint. The polynomial was controlled by the control points, which were the peaks or troughs of the trajectory. Such polynomials were then used in the lifting optimization model to simulate lifting motions. The optimization model consisted of an objective function and four types of constraints, namely, the joint mobility constraints, the joint moment strength constraints, the collision avoidance constraints, and the postural stability constraints. By varying the values of the control points within the assumed boundaries, the shapes of the polynomials were thus changed, therefore, changing the kinematic properties of the trajectories. The values of the control points were varied until the objective function was minimized and the constraints satisfied. The resulting polynomials were used as the simulated joint trajectories for the lifting motion.

This chapter describes the results of the simulation study including the validation and sensitivity analysis. In section 5.1, the actual patterns of the joint trajectories of the ten subjects are first examined. Based on the actual patterns, polynomials were derived for each joint. The bounds of the control points for the polynomials were derived from the actual lifts. Using these polynomials and the boundary information, the simulation for each actual lift was performed and the results are presented in section 5.2. Comparisons between the actual and the simulated motions were made using previously defined criteria, MSE (mean squared error) and MNDP (mean number of disconcordant pairs). Finally, changes to the entire simulation model were made and simulations corresponding to each change were performed. The results of the sensitivity analyses are presented in section 5.3. A final discussion regarding the general performance of the present simulation model is presented in section 5.4.

5.1 Joint Trajectory Patterns

In order to model the trajectory of each joint using the polynomial presented in section 4.2.3, it was assumed that the trajectory followed consistent patterns. Specifically, four assumptions were made about the patterns of the trajectory. First, the initial and final velocities and accelerations were assumed as zero. Second, the angular trajectory of each joint has a constant number of peaks or troughs. Third, the magnitudes of these peaks or troughs were bounded. Finally, the times at which these peaks and troughs occurred were also bounded. These assumptions were verified and the results are presented below.

5.1.1 Initial and Final Joint Velocities and Accelerations

Initial and final joint velocities and accelerations were assumed as zero in the simulation model. To verify this assumption, initial and final joint velocities and accelerations were calculated for the 360 actual lifts. The histograms of the initial and final joint velocities and accelerations are presented in Figures 5.1 to 5.4. For initial velocities, the elbow, shoulder, and knee had the highest number of lifts at zero rad/sec. The hip and ankle had the highest count at 0.2 rad/sec. For final velocities, the elbow and hip had the highest count at 0 rad/sec. For initial accelerations, the elbow had the highest count at zero rad/sec/sec. For final accelerations, the shoulder and knee had the highest count at zero rad/sec/sec.

Table 5.1 shows the 95% confidence intervals from a student t-distribution for the means of the initial and final velocities and accelerations. The statistical package Minitab was used. Note that since the sample size was 360, t distribution approaches normal distribution. Except the initial velocity at the shoulder, the 95% confidence intervals for the means of initial and final velocities and accelerations do not contain zero, indicating that for most joints, the initial and final velocities and accelerations were not zero. It must be noted that although the tests failed to show that the means of the initial velocities and accelerations were zero, their values were relatively close to zero when compared to the maximum velocities and accelerations in each lift. In general, the forms of a polynomial will not be completely altered by the use of some small initial or final velocities and accelerations. In the simulation model, zero initial and final velocities and accelerations were used, assuming that the actual initial and final velocities and accelerations were not available. Given the actual initial velocities, the effects of the non-zero initial velocities were further studied in the sensitivity analysis and will be presented in section 5.3.

5.1.2 Normalized Trajectories

In section 4.2.3, a normalization scheme was presented to study the patterns of the trajectories across different lifts. The magnitude of the angular position was rescaled by

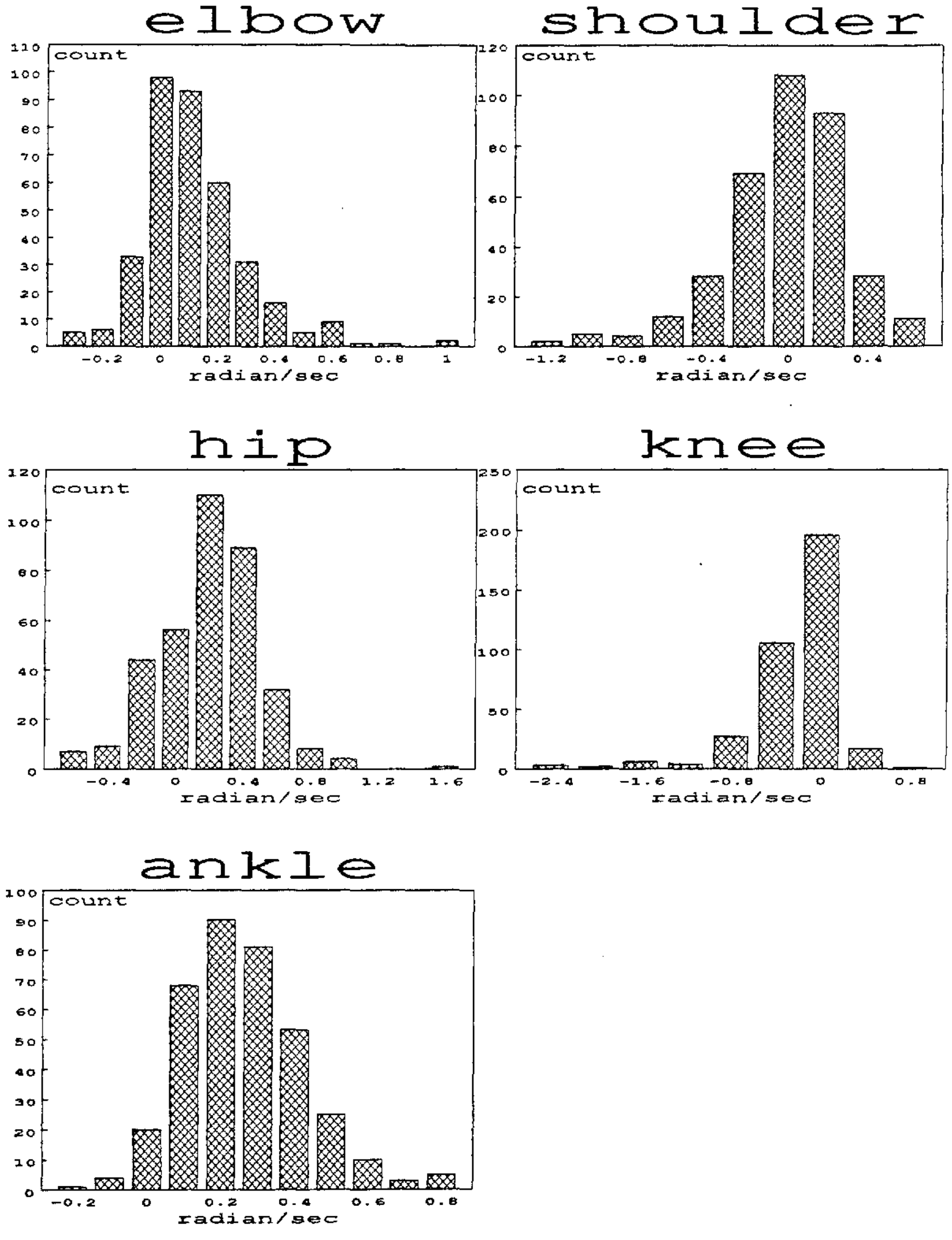

Figure 5.1 Histograms for initial joint velocities

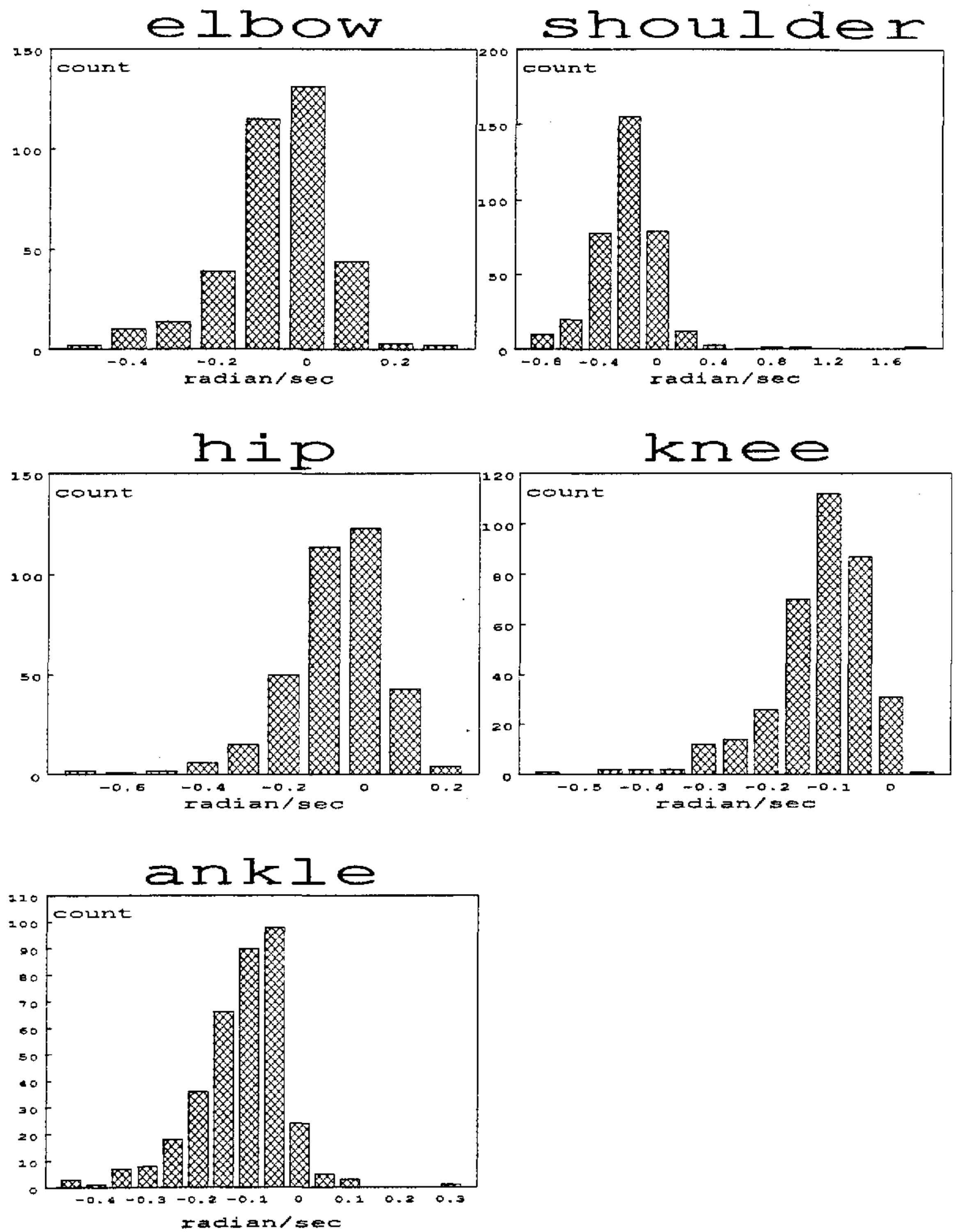

Figure 5.2 Histograms for final joint velocities

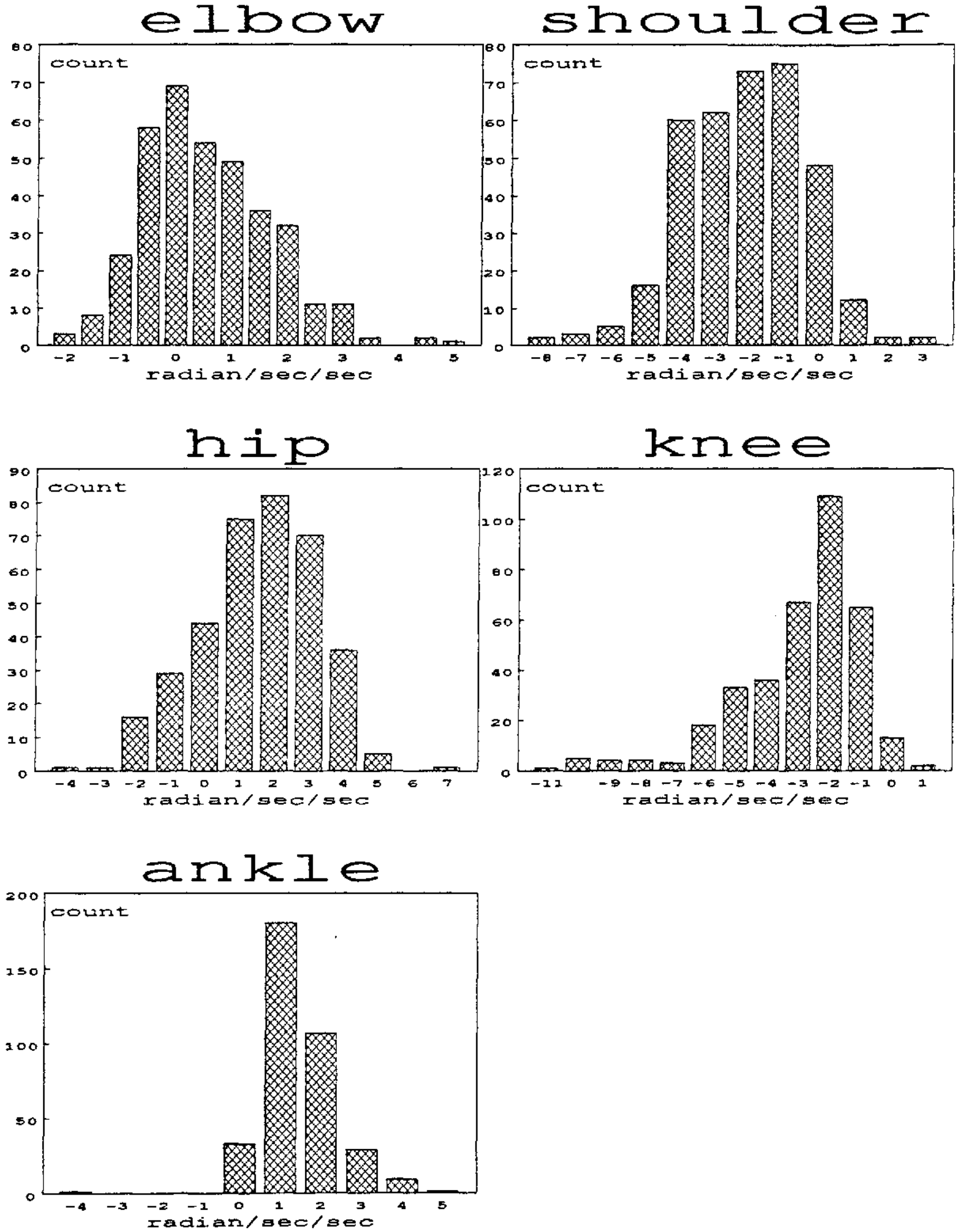

Figure 5.3 Histograms for initial joint accelerations

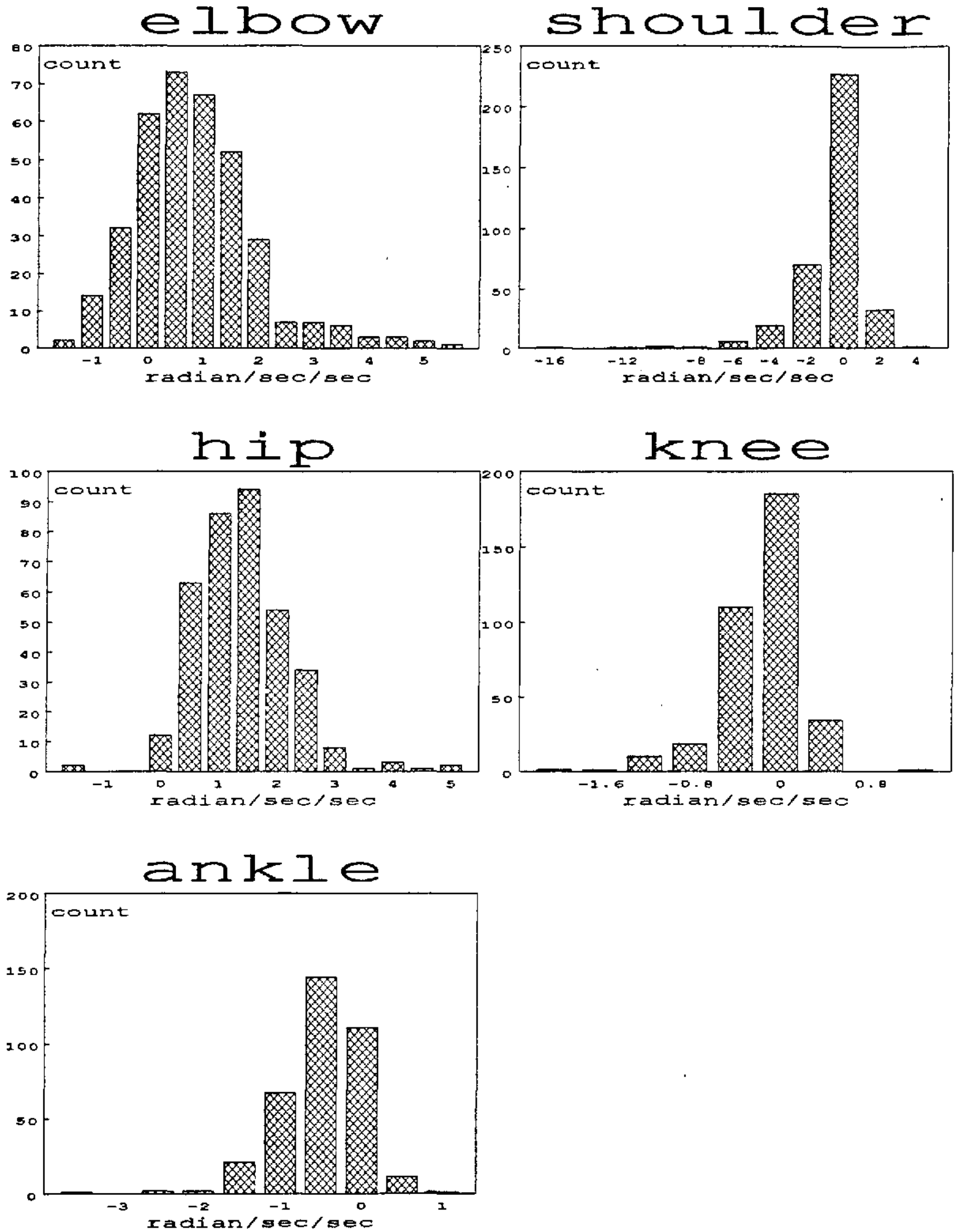

Figure 5.4 Histograms for final joint accelerations

Table 5.1 Confidence intervals for the means of initial and final velocities and accelerations (N=360)

	initial velocity (rad/sec)			final velocity (rad/sec)		
joint	mean	stdev	95% C.I.	mean	stdev	95% C.I.
elbow	0.118	0.010	(0.099,0.137)	-0.063	0.006	(-0.075,-0.51)
shoulder	-0.018	0.016	(-0.045,0.014)	-0.209	0.013	(-0.234,-0.184)
hip	0.200	0.016	(0.169,0.232)	-0.074	0.007	(-0.087,-0.061)
knee	-0.225	0.021	(-0.266,-0.183)	-0.115	0.004	(-0.124,-0.107)
ankle	0.261	0.009	(0.245,0.278)	-0.114	0.005	(-0.123,-0.104)

	initial acceleration (rad/sec/sec)			final acceleration (rad/sec/sec)		
joint	mean	stdev	95% C.I.	mean	stdev	95% C.I.
elbow	0.566	0.061	(0.446,0.685)	0.860	0.059	(0.744,0.977)
shoulder	-2.160	0.092	(-2.341,-1.978)	-0.735	0.103	(-0.938,-0.531)
hip	1.545	0.090	(1.370,1.721)	1.415	0.044	(1.329,1.501)
knee	-2.894	0.103	(-3.097,-2.692)	-0.171	0.018	(-0.206,-0.136)
ankle	1.447	0.047	(1.355,1.539)	-0.502	0.027	(-0.555,-0.448)

constant and the locations of the peaks or troughs are bounded, the normalized trajectories will look similar across different lifts. Figures 5.5 to 5.9 show the trajectories of each joint for all twelve lifting conditions for subject 1. It can be seen that a common pattern exists for each joint across different conditions. The purpose of the trajectory formation method presented earlier in section 4.2.3 was to generate a polynomial of a fixed form representing the common pattern of the trajectories across different lifts. The task here is to determine the structure of the polynomial, i.e., the order of the polynomial and the common locations of the control points. To accomplish this task, the normalized trajectories were reviewed across the ten subjects and the twelve lifting conditions. Appendix A presents the normalized trajectories for the remainder of the subjects. The determination of the polynomial model for each joint is presented in the following.

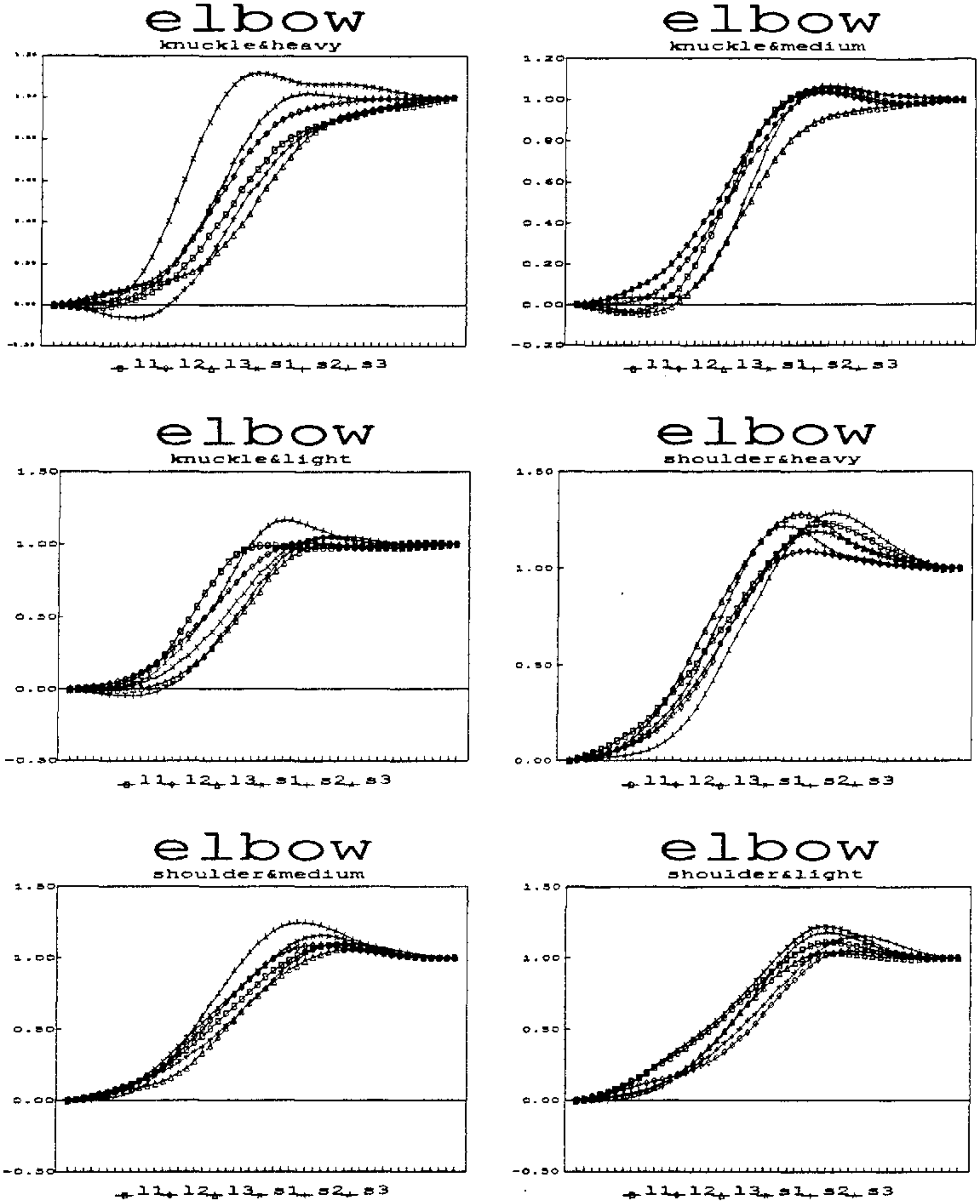

Figure 5.5 Normalized elbow trajectories of subject 1. The 6 graphs present combinations of 2 lifting heights (knuckle, shoulder) and 3 weights (heavy, medium, light). Three large container lifts (l1,l2,l3) and small container lifts (s1,s2,s3) are plotted in the same graph.

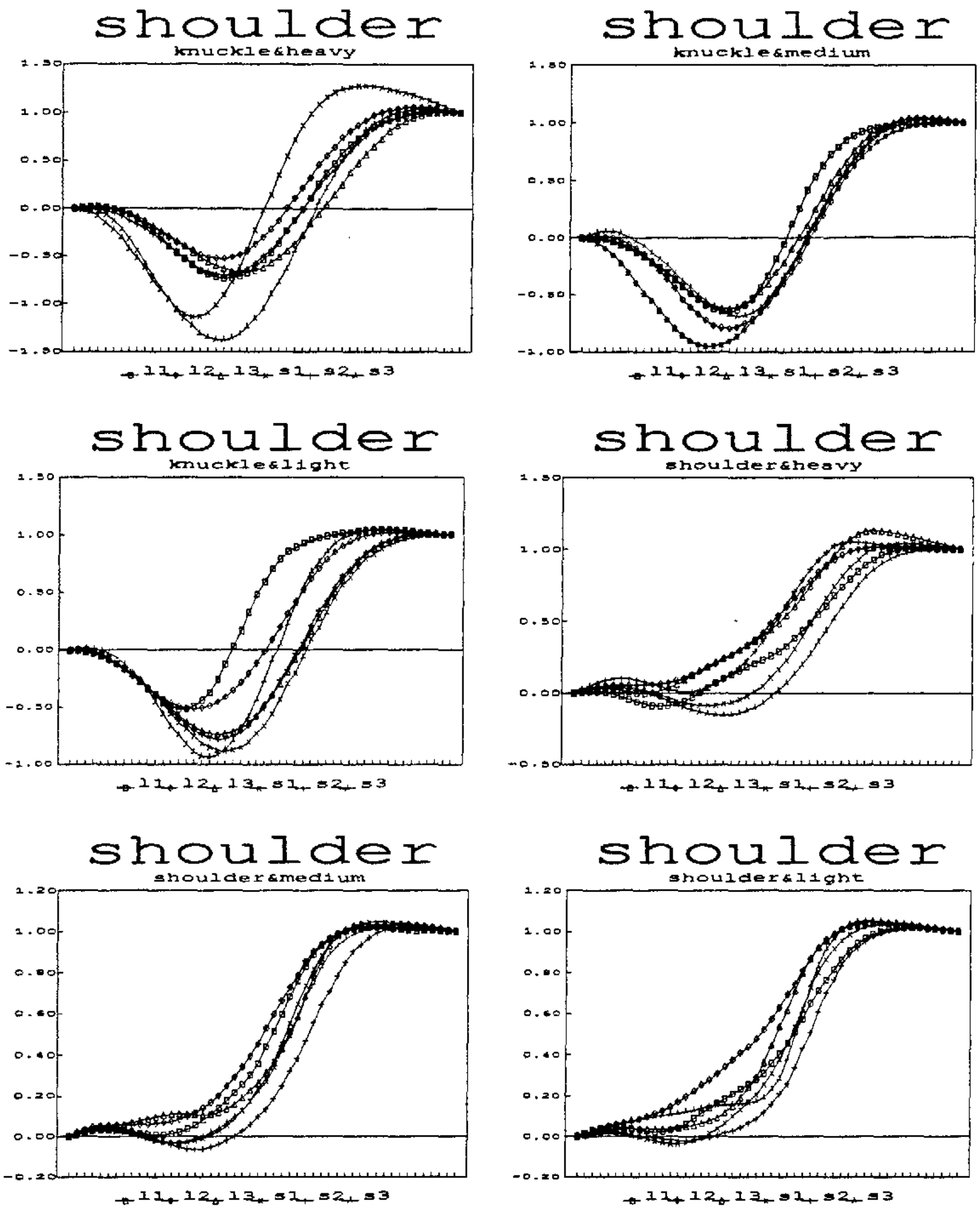

Figure 5.6 Normalized shoulder trajectories of subject 1. The 6 graphs present combinations of 2 lifting heights (knuckle, shoulder) and 3 weights (heavy, medium, light). Three large container lifts (l1,l2,l3) and small container lifts (s1,s2,s3) are plotted in the same graph.

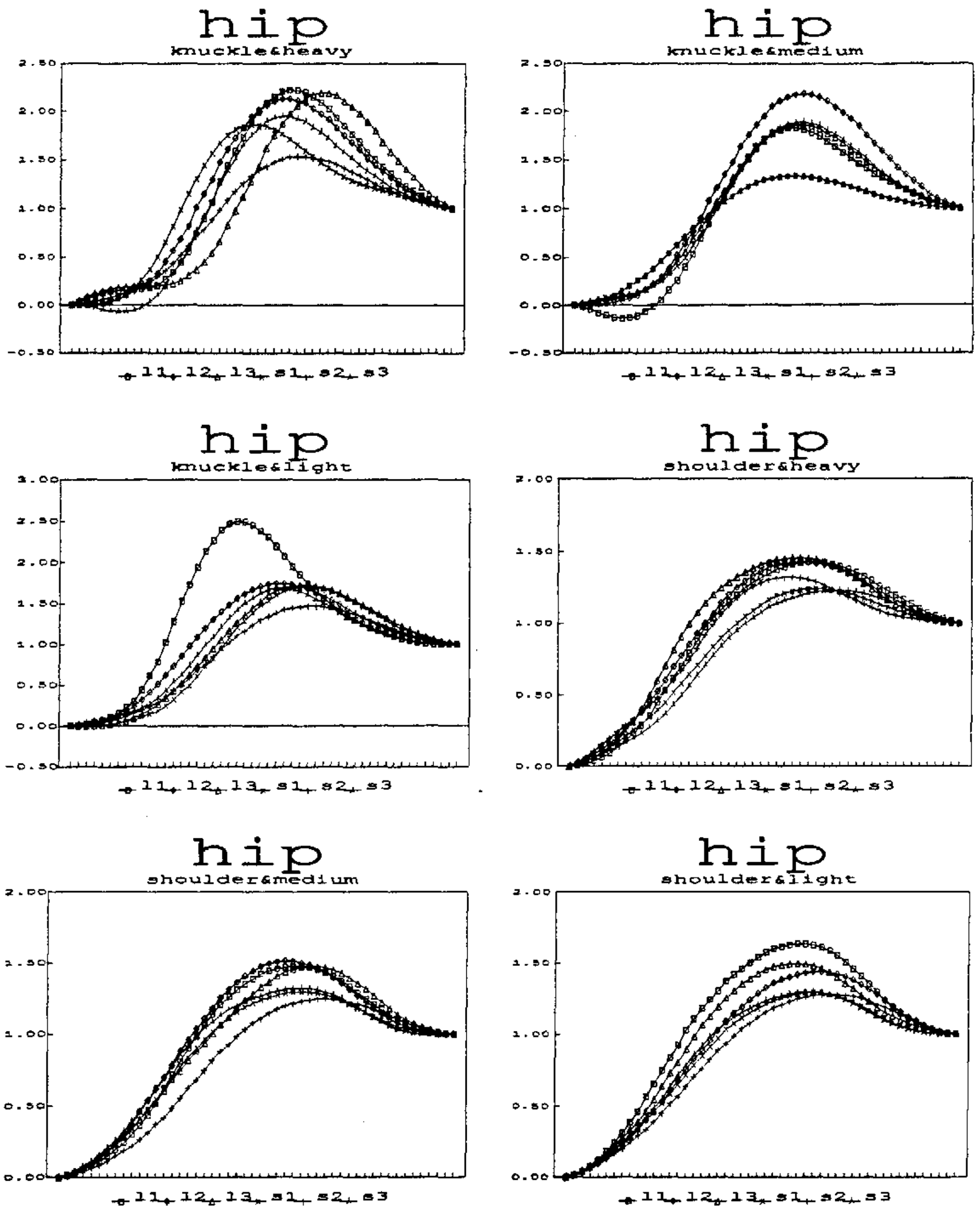

Figure 5.7 Normalized hip trajectories of subject 1. The 6 graphs present combinations of 2 lifting heights (knuckle, shoulder) and 3 weights (heavy, medium, light). Three large container lifts (l1,l2,l3) and small container lifts (s1,s2,s3) are plotted in the same graph.

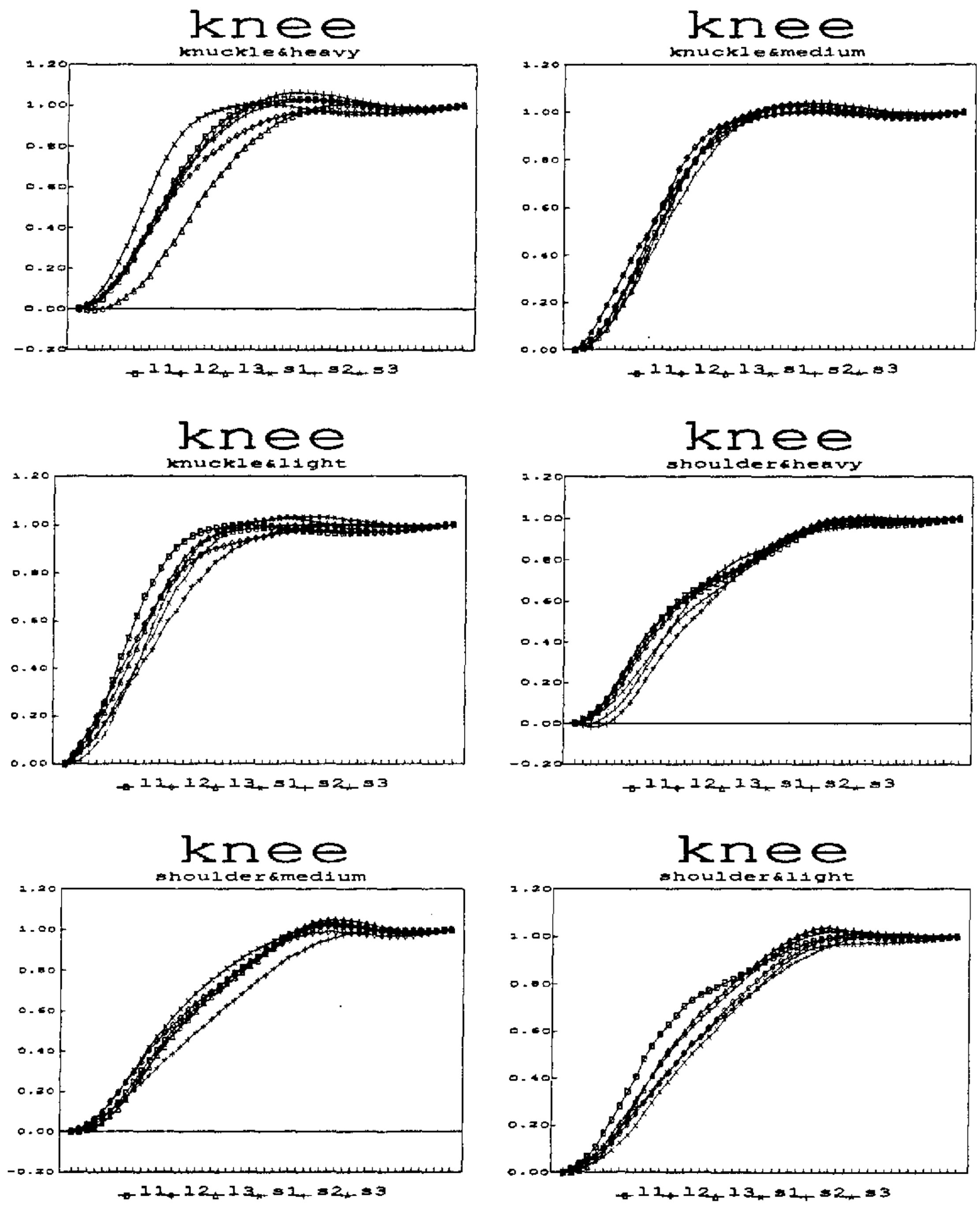

Figure 5.8 Normalized knee trajectories of subject 1. The 6 graphs present combinations of 2 lifting heights (knuckle, shoulder) and 3 weights (heavy, medium, light). Three large container lifts (l1,l2,l3) and small container lifts (s1,s2,s3) are plotted in the same graph.

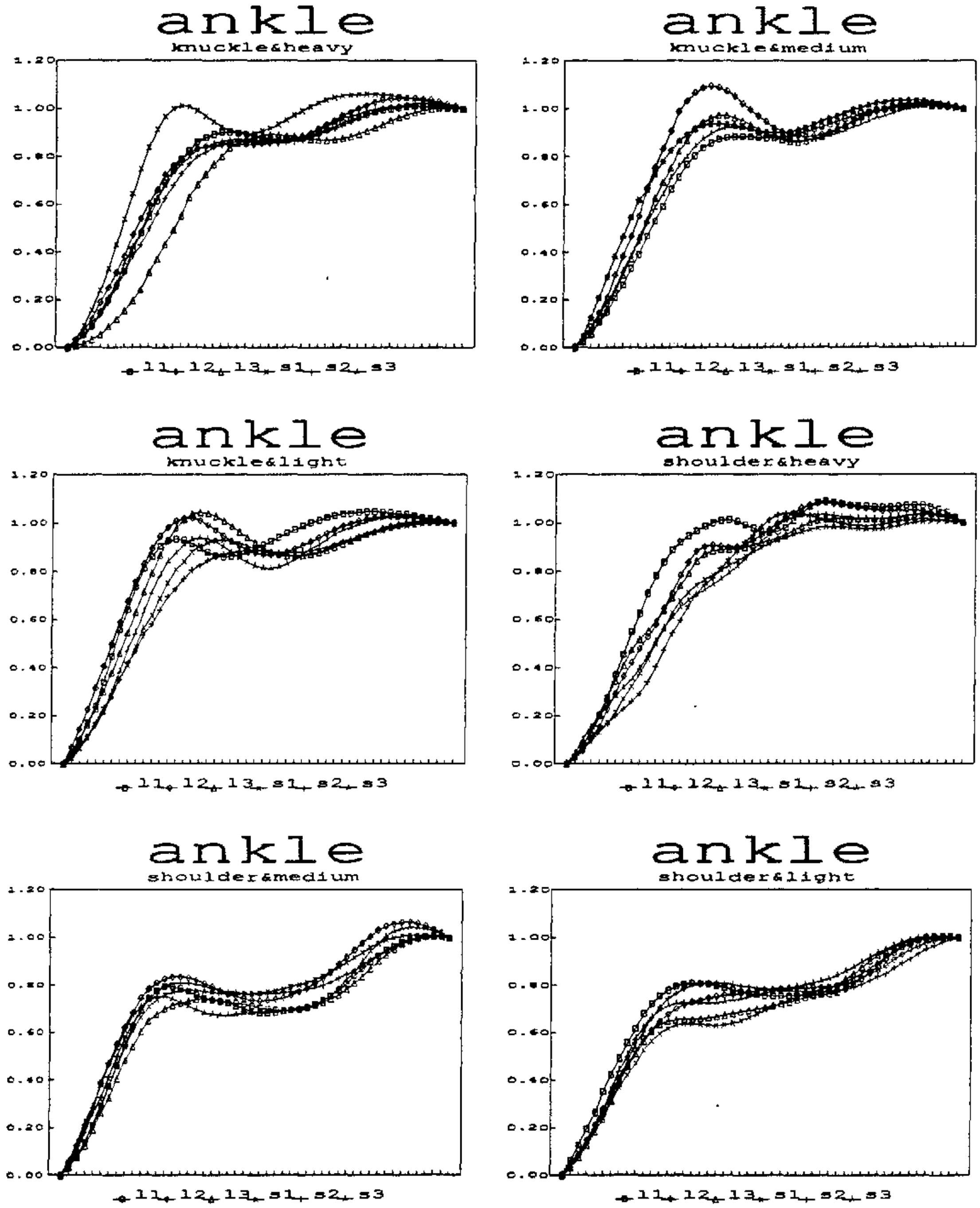

Figure 5.9 Normalized ankle trajectories of subject 1. The 6 graphs present combinations of 2 lifting heights (knuckle, shoulder) and 3 weights (heavy, medium, light). Three large container lifts (l1,l2,l3) and small container lifts (s1,s2,s3) are plotted in the same graph.

5.1.2.1 Elbow Pattern

After reviewing the normalized trajectories of the elbow joint across the twelve lifting conditions and ten subjects, a common pattern was found and the polynomial structure was determined. Figure 5.10 shows the elbow trajectory pattern and the corresponding Hermite polynomial. There was one peak point, $(\lambda_{elbow}, \tau_{elbow})$, towards the end of the lift. The peak point was designated as the control point for the elbow trajectory. Since there were eight derivative conditions, a seventh-order Hermite polynomial was used as the elbow trajectory model. Note that the polynomial model is presented in terms of the unnormalized coordinates.

5.1.2.2 Shoulder Pattern

The joint trajectory pattern for the shoulder is shown in Figure 5.11, with its corresponding Hermite polynomial model. The shoulder trajectory had one trough point towards the beginning of the lift, $(\lambda_{shoulder1}, \tau_{shoulder1})$, and one peak point towards the end of the lift, $(\lambda_{shoulder2}, \tau_{shoulder2})$. The trough was designated as the first control point and the peak the second control point for the shoulder trajectory. Since there were ten derivative conditions, a ninth-order Hermite polynomial was used as the shoulder trajectory model.

5.1.2.3 Hip Pattern

Examining the hip trajectories across the ten subjects, it was found that unlike the elbow and shoulder, where one common pattern was found across the subjects and conditions, the hip patterns need to be handled differently. For the floor-to-shoulder lifts, the hip had a common pattern across the ten subjects. The pattern and its corresponding Hermite polynomial model are shown in Figure 5.12. There was one peak, $(\lambda_{hip}, \tau_{hip})$, towards the end of the lift and it was designated as the control point for the hip trajectory. Thus, eight derivative conditions determined a seventh-order polynomial for the hip in the floor-to-shoulder lifts.

For the floor-to-knuckle lifts, two patterns existed for the hip trajectory. Eight subjects had a hip pattern similar to the pattern shown in Figure 5.12. However, the other two subjects had an entirely different pattern. Figure 5.13 presents the normalized hip trajectories of subject 10 for the floor-to-knuckle lifts. Apparently, the pattern in Figure 5.13 is quite different from the one as shown in Figure 5.12. It is necessary to develop a different model for the pattern shown in Figure 5.13. It was found that the two subjects having the different hip pattern for the floor-to-knuckle lifts actually performed the lifts

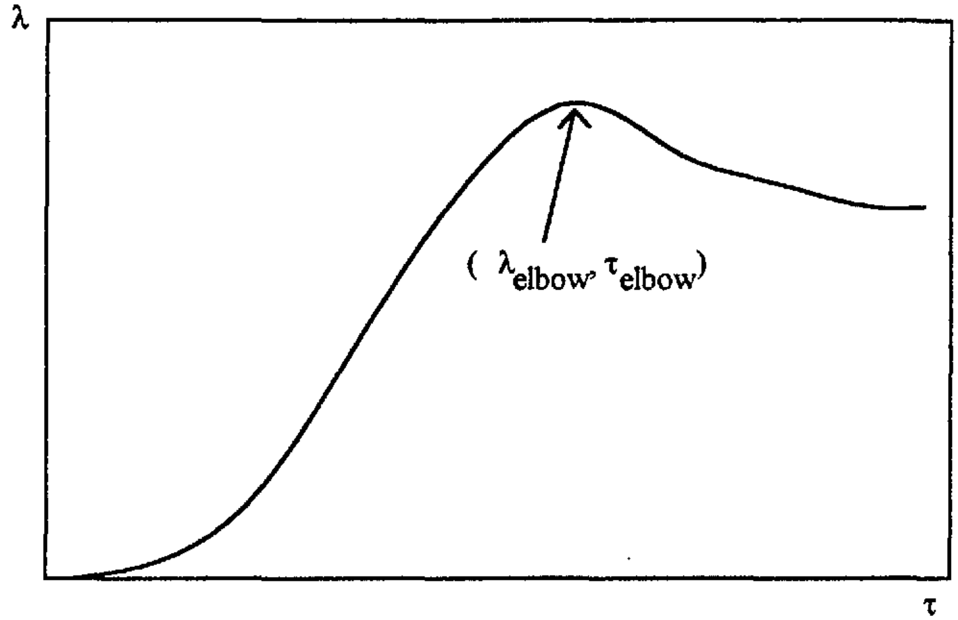

The Hermite polynomial in terms of the unnormalized coordinates for the above pattern is consisted of the following equations:

$$\dot{\theta}(0)=0; \quad \dot{\theta}(T)=0; \quad \ddot{\theta}(0)=0; \quad \ddot{\theta}(T)=0;$$
$$\dot{\theta}(t_1)=0; \quad \theta(t_1)=p_1; \quad \theta(0)=p_0; \quad \theta(T)=p_T$$

where

T = total lifting time
p_0 = initial position
p_T = final position
p_1 = control point position
t_1 = time at which p_1 occurs.

Figure 5.10 The elbow trajectory pattern and its Hermite polynomial model

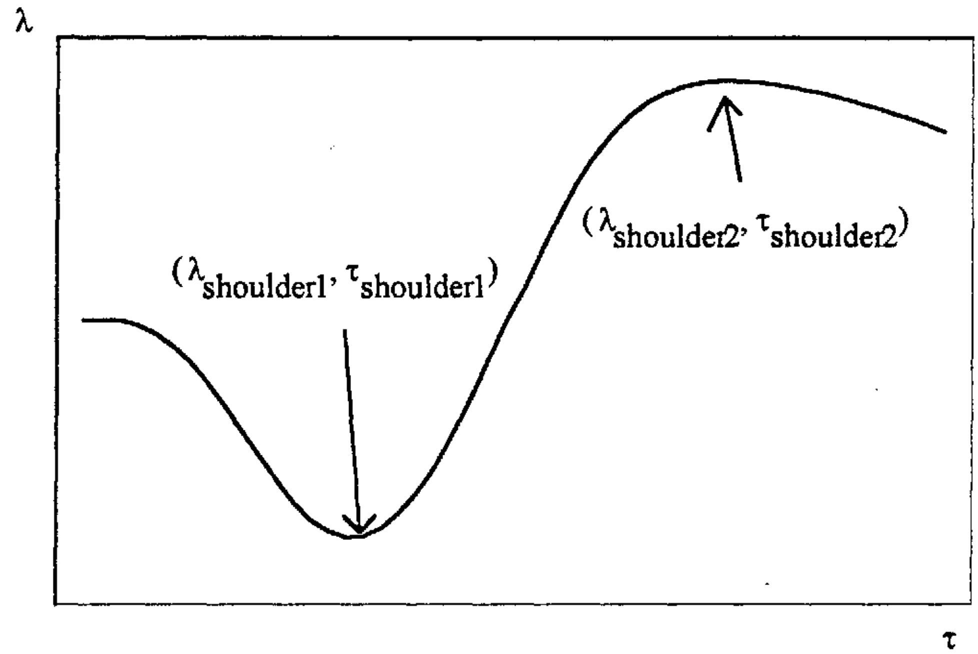

The Hermite polynomial in terms of the unnormalized coordinates for the above pattern is consisted of the following equations:

$$\dot{\theta}(0)=0;\quad \dot{\theta}(T)=0;\quad \ddot{\theta}(0)=0;\quad \ddot{\theta}(T)=0;\quad \dot{\theta}(t_1)=0;$$
$$\theta(t_1)=p_1;\quad \dot{\theta}(t_2)=0;\quad \theta(t_2)=p_2;\quad \theta(0)=p_0;\quad \theta(T)=p_T$$

where

T = total lifting time
p_0 = initial position
p_T = final position
p_1 = 1st control point position
t_1 = time at which p_1 occurs
p_2 = 2nd control point position
t_2 = time at which p_2 occurs.

Figure 5.11 The shoulder trajectory pattern and its Hermite polynomial model

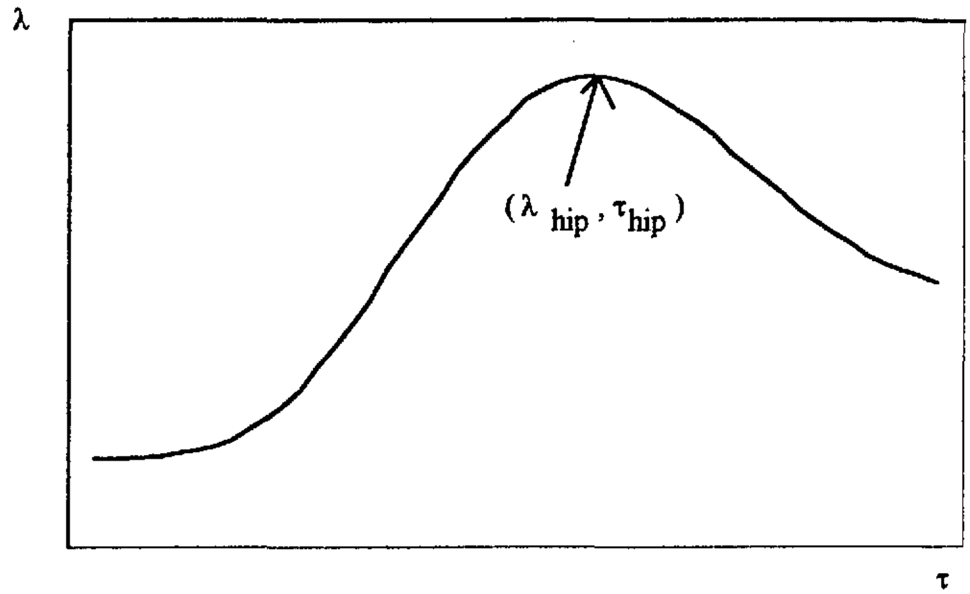

The Hermite polynomial in terms of the unnormalized coordinates for the above pattern is consisted of the following equations:

$$\dot{\theta}(0) = 0; \quad \dot{\theta}(T) = 0; \quad \ddot{\theta}(0) = 0; \quad \ddot{\theta}(T) = 0;$$
$$\dot{\theta}(t_1) = 0; \quad \theta(t_1) = p_1; \quad \theta(0) = p_0; \quad \theta(T) = p_T$$

where

T = total lifting time
p_0 = initial position
p_T = final position
p_1 = control point position
t_1 = time at which p_1 occurs.

Figure 5.12 The hip trajectory pattern and its Hermite polynomial model for floor-to-shoulder lifts

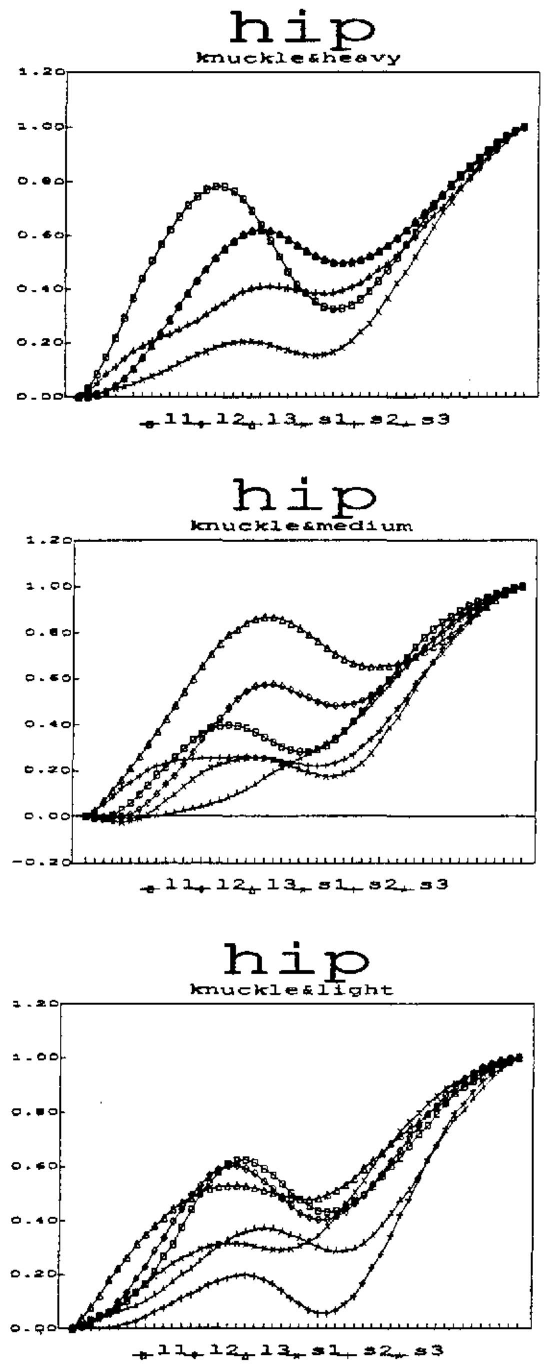

Figure 5.13 Normalized hip trajectories for the floor-to-knuckle lifts performed by subject 10, who used the squat lifting style. The 3 graphs are for the heavy, medium, and light lifting weights. Three large container lifts (l1,l2,l3) and three small (s1,s2,s3) container lifts are plotted in the same graph.

using an extreme squat lifting technique. Their back was straight and the knee was bent during the initial lift-off. The other eight subjects performed the lifts using a free-style technique closer to the back lift, in which the back was stooped during the initial lift-off. Due to the difference in lifting styles, the hip trajectory was modeled differently for the floor-to-knuckle lifts. For the free-style lifts, the Hermite polynomial model as shown in Figure 5.12 was used. For the squat-style lifts, the pattern found from the two subjects (subjects 9 and 10 as shown in Figures A.38 and A.43) and its corresponding Hermite polynomial are shown in Figure 5.14. Two control points were used, one for the peak, $(\lambda_{hip1}, \tau_{hip1})$, and one for the trough, $(\lambda_{hip2}, \tau_{hip2})$. A ninth-order Hermite polynomial was used as the trajectory model.

5.1.2.4 Knee Pattern

Similar to the elbow, one control point, $(\lambda_{knee}, \tau_{knee})$, was used for the knee. A seventh-order Hermite polynomial was used as its trajectory model. Figure 5.15 shows the pattern and its polynomial model.

5.1.2.5 Ankle Pattern

Although Figure 5.9 shows a common pattern for subject 1, the ankle trajectories in fact had a variety of patterns from different subjects. The patterns were so different to be classified according to lifting conditions. The variation in the ankle trajectory patterns was mostly due to individual subject effects. The change in the ankle trajectory in the actual radian scale was very small. In general, the ankle increased gradually and then flattened out. A seventh-order Hermite polynomial with one control point, $(\lambda_{ankle}, \tau_{ankle})$, was used to model the ankle trajectory. Figure 5.16 presents the pattern and its polynomial model.

5.1.3 Control Point Locations

After the polynomial model was determined for each joint, the locations of the control points of each trajectory model were derived from actual lifts. As described earlier, the bounds on the locations of the control points were to be used by the optimization model. The shape of the polynomial could be greatly affected by the location of the control points. The location of each control point was determined by the values of λ and τ, as appeared in Figures 5.10, 11, 12, 14, 15, and 16, for each joint. Correlations between λ and τ were calculated for each control point. There was no

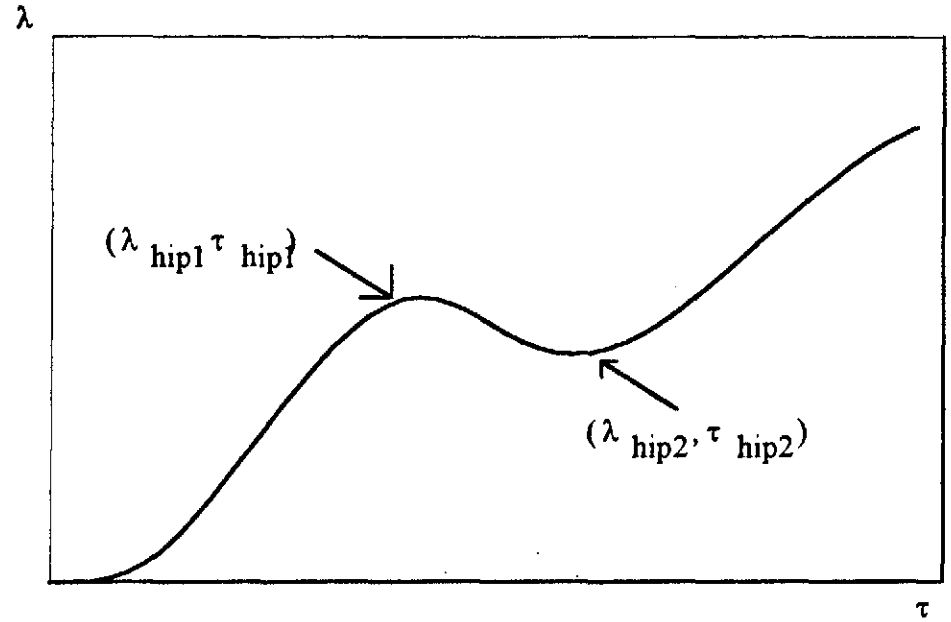

The Hermite polynomial in terms of the unnormalized coordinates for the above pattern is consisted of the following equations:

$$\dot{\theta}(0) = 0; \quad \dot{\theta}(T) = 0; \quad \ddot{\theta}(0) = 0; \quad \ddot{\theta}(T) = 0; \quad \dot{\theta}(t_1) = 0;$$
$$\theta(t_1) = p_1; \quad \dot{\theta}(t_2) = 0; \quad \theta(t_2) = p_2; \quad \theta(0) = p_0; \quad \theta(T) = p_T$$

where

T = total lifting time
p_0 = initial position
p_T = final position
p_1 = 1st control point position
t_1 = time at which p_1 occurs
p_2 = 2nd control point position
t_2 = time at which p_2 occurs.

Figure 5.14 The hip trajectory pattern and its Hermite polynomial model for the floor-to-knuckle lifts performed with the squat lifting technique

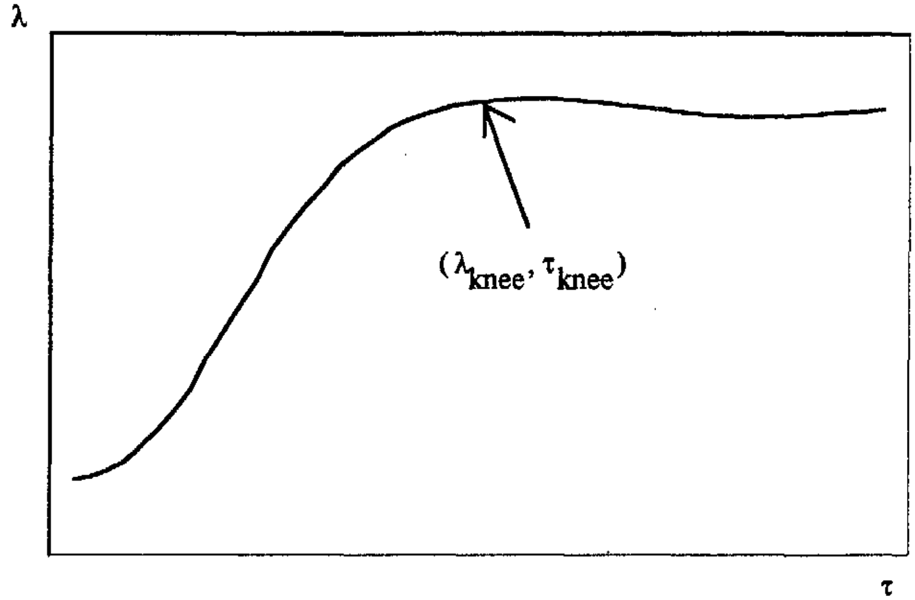

The Hermite polynomial in terms of the unnormalized coordinates for the above pattern is consisted of the following equations:

$$\dot{\theta}(0)=0; \quad \dot{\theta}(T)=0; \quad \ddot{\theta}(0)=0; \quad \ddot{\theta}(T)=0;$$

$$\dot{\theta}(t_1)=0; \quad \theta(t_1)=p_1; \quad \theta(0)=p_0; \quad \theta(T)=p_T$$

where

T = total lifting time
p_0 = initial position
p_T = final position
p_1 = control point position
t_1 = time at which p_1 occurs.

Figure 5.15 The knee trajectory pattern and its Hermite polynomial model

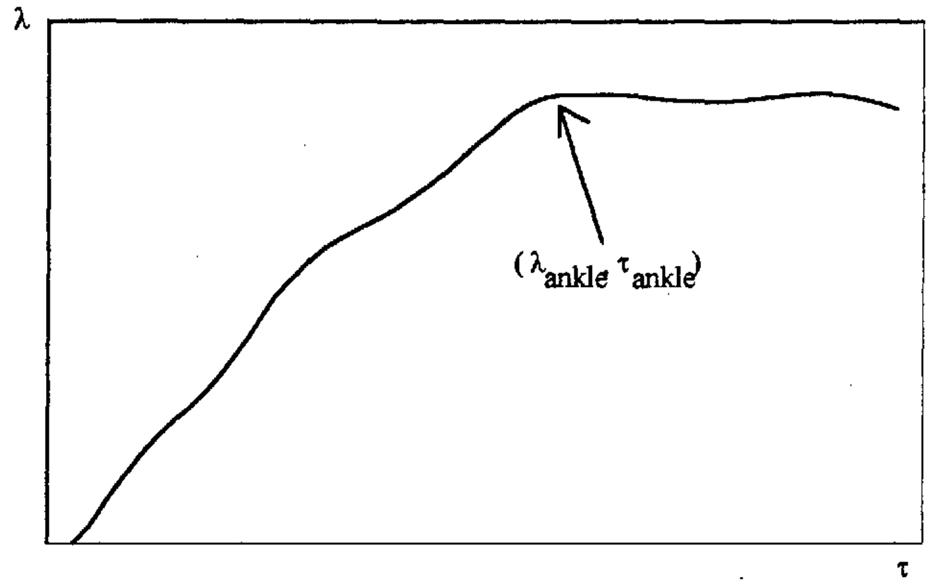

The Hermite polynomial in terms of the unnormalized coordinates for the above pattern is consisted of the following equations:

$$\dot{\theta}(0) = 0; \quad \dot{\theta}(T) = 0; \quad \ddot{\theta}(0) = 0; \quad \ddot{\theta}(T) = 0;$$
$$\dot{\theta}(t_1) = 0; \quad \theta(t_1) = p_1; \quad \theta(0) = p_0; \quad \theta(T) = p_T$$

where

T = total lifting time
p_0 = initial position
p_T = final position
p_1 = control point position
t_1 = time at which p_1 occurs.

Figure 5.16 The ankle trajectory pattern and its Hermite polynomial model substantial correlation between λ and τ; therefore, λ and τ were treated individually and their bounds derived separately. The bounds of λ and τ were derived in the following manner. First, analysis of variance was conducted for each λ and τ against the lifting conditions. If for a certain condition, the values of λ (or τ) were significantly different from those of λ (or τ) for other conditions, the bounds were derived separately for each significantly different condition. If the values of λ (or τ) were not significantly different from those of λ (or τ) for other conditions, the bounds were derived jointly for all the conditions.

Analysis of variance showed no difference in the values of λ and τ between sexes; therefore, both females and males used the same bounds. For the elbow trajectory, $\lambda$was different between the two lifting heights ($p<.001$) and between the two container sizes ($p<.001$). The bounds of λ for the elbow, λ_{elbow}, were determined using the maximum and minimum values of λ in each of the two lifting heights and two container sizes. The means of λ within each of the two lifting heights and two container sizes were used as the initial solutions for the control points in the optimization routine. The normalized time τ for the elbow was different between the two lifting heights ($p<.001$). The bounds of τ for the elbow, τ_{elbow}, were determined using the maximum and minimum values of τ in each of the two lifting heights. The means of τ within each of the two lifting heights were used as the initial solutions for the optimization. Similar analysis was performed for the control points in other joints. Table 5.2 summarizes the significant factors that affected the values of λ and τ for each control point. Table 5.3 presents the means and bounds of λ and τ for each control point under various conditions that were found to be significantly different. The values presented in Table 5.3 for λ and τ were used later for the optimization.

5.2 Comparison between Actual and Modeled

Given the information provided in Table 5.3, simulation was performed for each of the 360 lifts. For each lift, a tentative trajectory was generated using the Hermite polynomial model for each joint. The control points of the polynomial were initialized at the mean values as shown in Table 5.3. Based on the tentative trajectories, kinematics and kinetics were calculated using the dynamic biomechanical lifting model. The objective function and constraints were then calculated. The values of the control points were then varied within the bounds provided in Table 5.3 to minimize the objective function. The minimization process was carried out using the nonlinear optimization routine, the GRG2 system.

Table 5.2 Factors affected the values of λ and τ for each control point

control point coordinates	significant factors
λ_{elbow}	lifting height (p<.001), container size (p<.001)
τ_{elbow}	lifting height (p<.001)
$\lambda_{shoulder1}$	lifting height (p<.001), container size (p<.001)
$\tau_{shoulder1}$	lifting height (p<.001), container size (p<.001)
$\lambda_{shoulder2}$	lifting height (p<.001), lifting weight (p<.001)
$\tau_{shoulder2}$	lifting height (p<.001)
λ_{hip}	lifting height (p<.001), container size (p<.001)
τ_{hip}	none
λ_{knee}	lifting height (p<.001), container size (p<.05)
τ_{knee}	lifting height (p<.001)
λ_{ankle}	none
τ_{ankle}	lifting height (p<.001), container size (p<.001)

For floor-to-knuckle height in squat lifts:

control point coordinates	significant factors
λ_{hip1}	container size (p<.05)
τ_{hip1}	none
λ_{hip2}	container size (p<.05)
τ_{hip2}	none

Table 5.3 Means and bounds for each control point under various lifting conditions

variables	lifting conditions	mean	stdev	minimum	maximum
λ_{elbow}	knuckle height & large box	1.11	0.16	0.7	1.52
	knuckle height & small box	1.17	0.19	0.87	1.84
	shoulder height & large box	1.29	0.16	0.95	1.56
	shoulder height & small box	1.31	0.16	1.01	1.65
τ_{elbow}	knuckle height	0.72	0.09	0.50	0.90
	shoulder height	0.66	0.09	0.50	0.90
$\lambda_{shoulder1}$	knuckle height & large box	-0.64	0.33	-1.49	-0.02
	knuckle height & small box	-0.82	0.49	-2.45	-0.02
	shoulder height & large box	-0.10	0.15	-0.52	0.15
	shoulder height & small box	-0.18	0.16	-0.64	0.15
$\tau_{shoulder1}$	knuckle height & large box	0.40	0.07	0.26	0.64
	knuckle height & small box	0.41	0.06	0.20	0.56
	shoulder height & large box	0.26	0.07	0.02	0.60
	shoulder height & small box	0.29	0.07	0.02	0.42
$\lambda_{shoulder2}$	knuckle height & heavy weight	1.15	0.33	1.00	2.74
	knuckle height & medium weight	1.09	0.2	1.00	2.21
	knuckle height & light weight	1.05	0.16	1.00	2.2
	shoulder height & heavy weight	1.08	0.06	1.00	1.27
	shoulder height & medium weight	1.06	0.05	1.00	1.20
	shoulder height & light weight	1.06	0.05	1.00	1.24
$\tau_{shoulder2}$	knuckle height	0.91	0.06	0.70	1.00
	shoulder height	0.84	0.08	0.68	0.96
λ_{hip}	knuckle height & large box	1.54	0.42	1.02	2.77
	knuckle height & small box	1.31	0.23	1.06	1.95
	shoulder height & large box	1.45	0.31	1.08	2.73
	shoulder height & small box	1.26	0.23	1.04	2.55
τ_{hip}	overall	0.63	0.07	0.44	0.94

Table 5.3 (continued)

variables	lifting conditions	mean	stdev	minimum	maximum
λ_{knee}	knuckle height & large box	1.02	0.15	0.70	1.50
	knuckle height & small box	1.05	0.13	0.85	1.45
	shoulder height & large box	0.84	0.19	0.32	1.05
	shoulder height & small box	0.89	0.17	0.20	1.05
τ_{knee}	knuckle height	0.53	0.08	0.36	0.88
	shoulder height	0.61	0.14	0.16	0.88
λ_{ankle}	overall	0.99	0.39	0.04	2.86
τ_{ankle}	knuckle height & large box	0.49	0.21	0.24	0.92
	knuckle height & small box	0.55	0.24	0.24	0.96
	shoulder height & large box	0.32	0.19	0.10	0.96
	shoulder height & small box	0.43	0.27	0.12	0.94
For floor-to-knuckle height in squat lifts:					
λ_{hip1}	large box	0.44	0.29	-0.25	0.90
	small box	0.23	0.15	-0.05	0.42
τ_{hip1}	overall	0.31	0.09	0.10	0.42
λ_{hip2}	large box	0.29	0.29	-0.50	0.65
	small box	0.05	0.38	-1.00	0.38
τ_{hip2}	overall	0.49	0.09	0.28	0.64

5.2.1 Graphical Comparison

Graphical presentations of the actual lifts and the simulated lifts are shown in Figures 5.17 to 5.28 for subject 1. For each of the twelve lifting conditions, the three actual trajectories and the corresponding three predicted trajectories were plotted together for each joint. In general, the simulated trajectories followed the patterns of the actual trajectories closely. Appendix B presents the graphical comparison for the remainder of the subjects.

There are several points worth noting with regard to the graphical comparison. First, the general pattern of the actual trajectory was predicted very well. This was due to the use of the specific Hermite polynomial designed for each joint based on the patterns generalized from the ten subjects. Such fixed-form polynomials were able to warrant, to a degree, the final outcome of the prediction with regard to the shapes and forms of the trajectory pattern. However, there were rare occasions in which the polynomials oscillated too much, creating extra peaks or troughs that were not needed. The shoulder prediction in Figure 5.22 presents an example. Two predicted trials had oscillations around the trough. The extra peaks or troughs in the position trajectory will create false velocities and accelerations. Unfortunately, this problem is inherent with the use of the polynomial techniques to approximate actual functions (Atkinson, 1989).

Second, there were cases in which the predicted trajectory lagged behind the actual or vice versa. For example, in Figure 5.19, the first actual elbow trajectory (a1) and the predicted (p1) are in a phase shift. Usually, this happened for only one or two joints. Such phase difference could be caused by the inaccurate estimation of the beginning and ending of the lift for each joint. In fact, each joint started the motion at slightly different times. However, for modeling purposes, the lift-off and landing of the container have been used as the beginning and ending of the motions of the five joints simultaneously.

Third, in some predictions, the peaks of the trajectories did not seem to be high enough as in the actual trajectories. The hip predictions in Figure 5.17 were an example. The peaks of the predicted hip trajectories in all three trials were lower than those of the actual. Recalling that in initializing the control points of each trajectory, the means from the actual lifts were used. Some subjects might have higher locations of the control points than the means. As a result, the GRG2 tried to minimize the objective function in the vicinity of the initial solutions. Since GRG2 is a gradient-based optimization system, it is subject to local optimum problem, that is, the final solution may be dependent on the initialization. If the control points were initialized with larger values, it was possible that the final solutions have higher peaks. The purpose of the simulation was to provide a

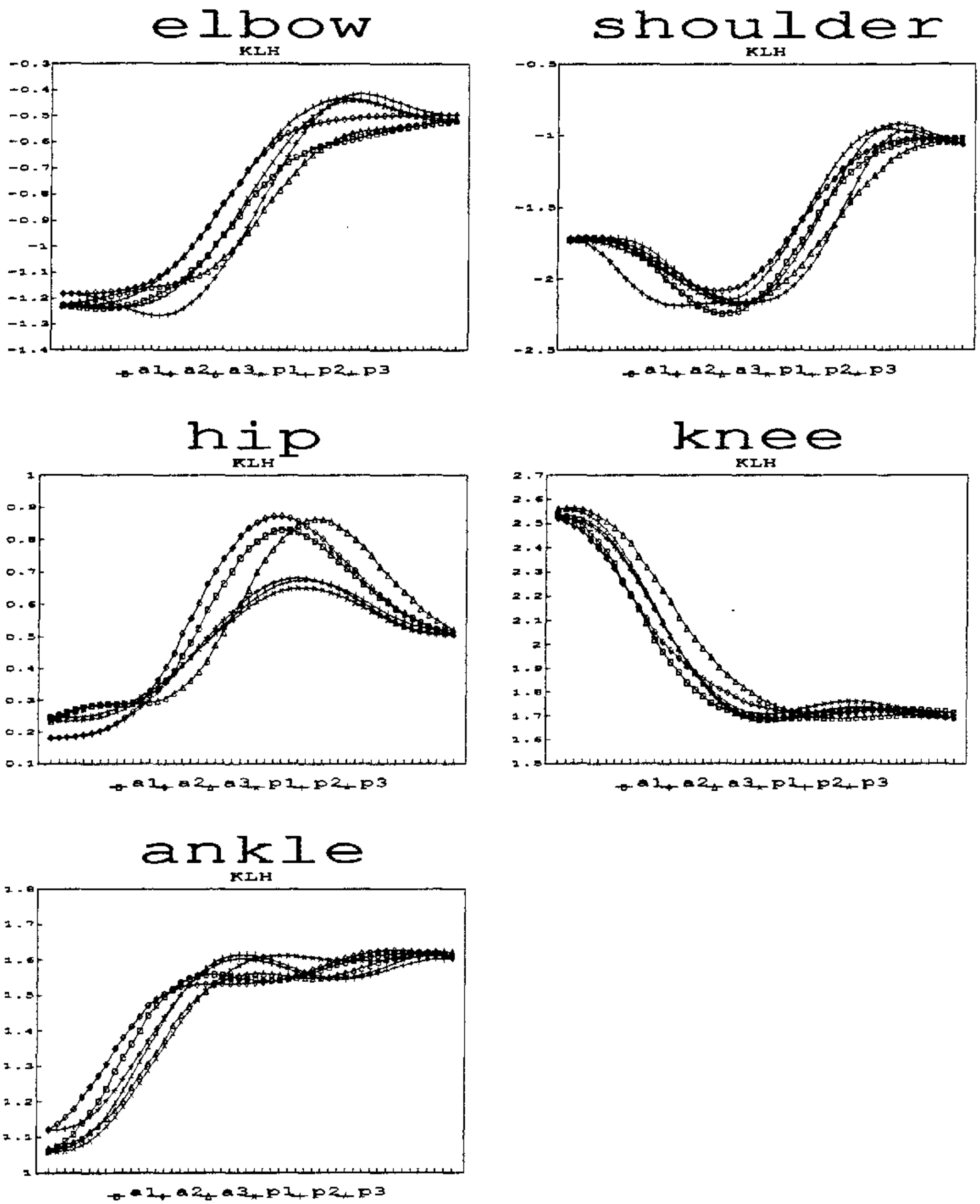

Figure 5.17 Actual (a1,a2,a3) joint trajectories versus simulated (p1,p2,p3) trajectories for floor-to-knuckle, large container, and heavy weight (KLH) condition for subject 1.

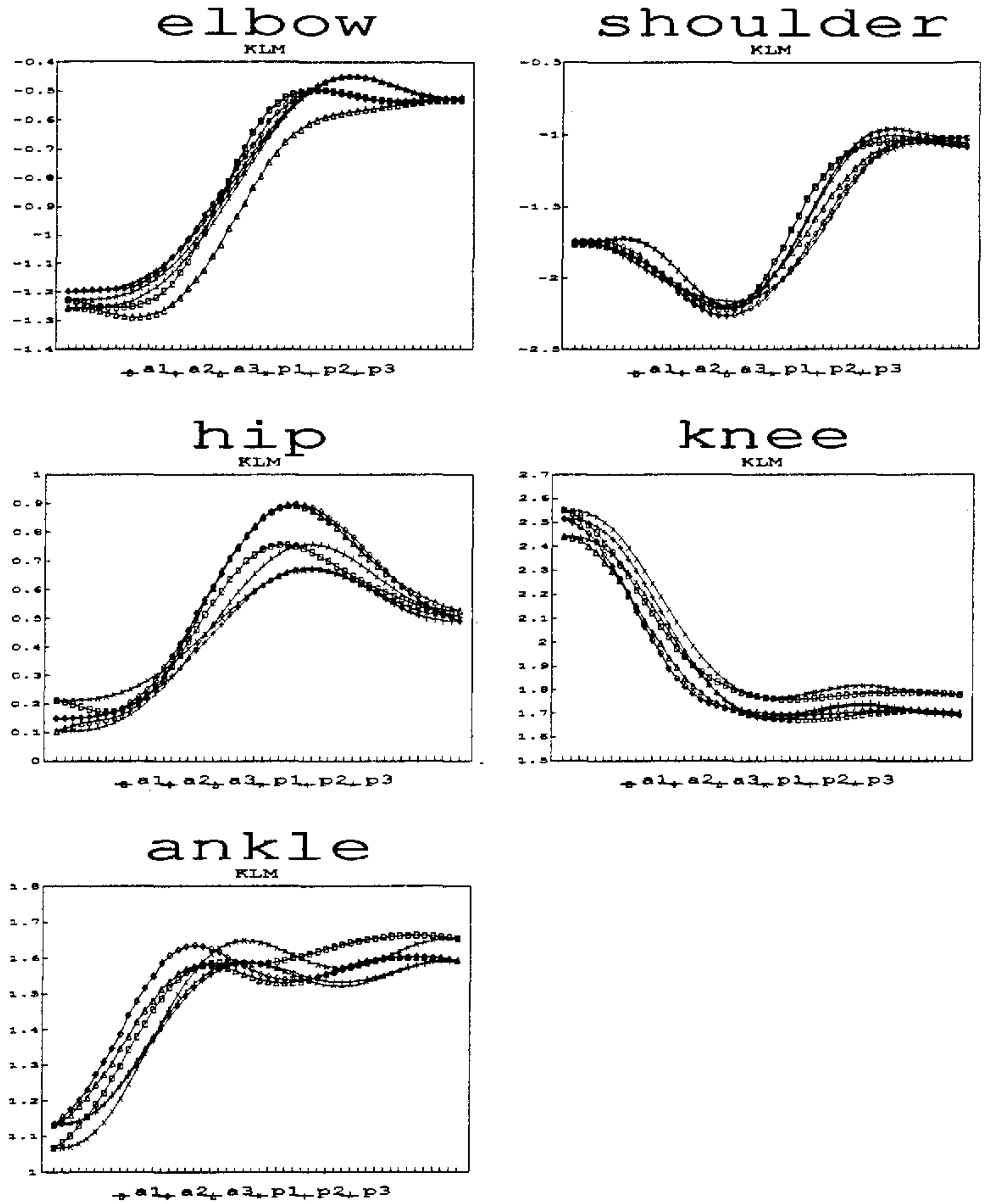

Figure 5.18 Actual (a1,a2,a3) joint trajectories versus simulated (p1,p2,p3) trajectories for floor-to-knuckle, large container, and medium weight (KLM) condition for subject 1.

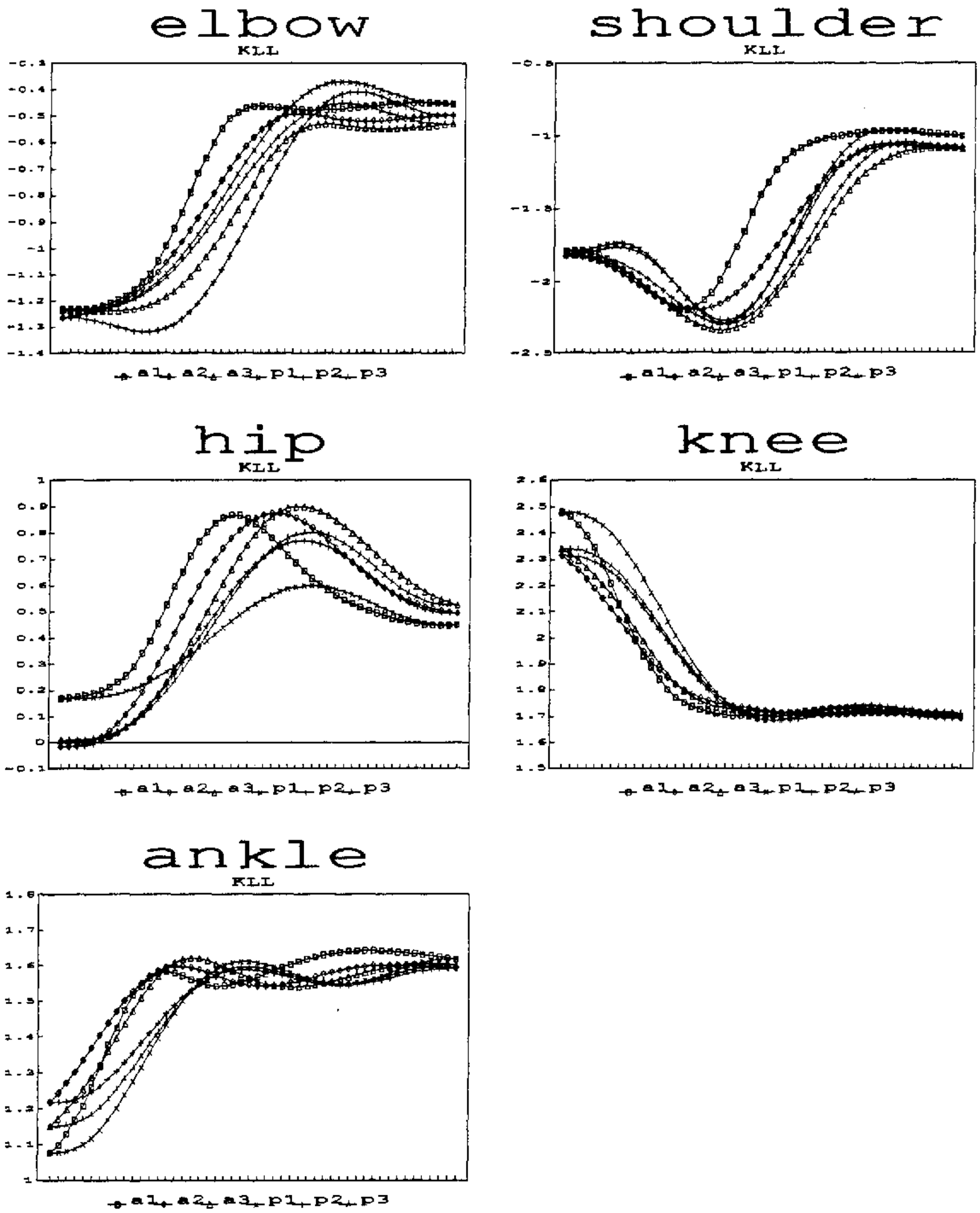

Figure 5.19 Actual (a1,a2,a3) joint trajectories versus simulated (p1,p2,p3) trajectories for floor-to-knuckle, large container, and light weight (KLL) condition for subject 1.

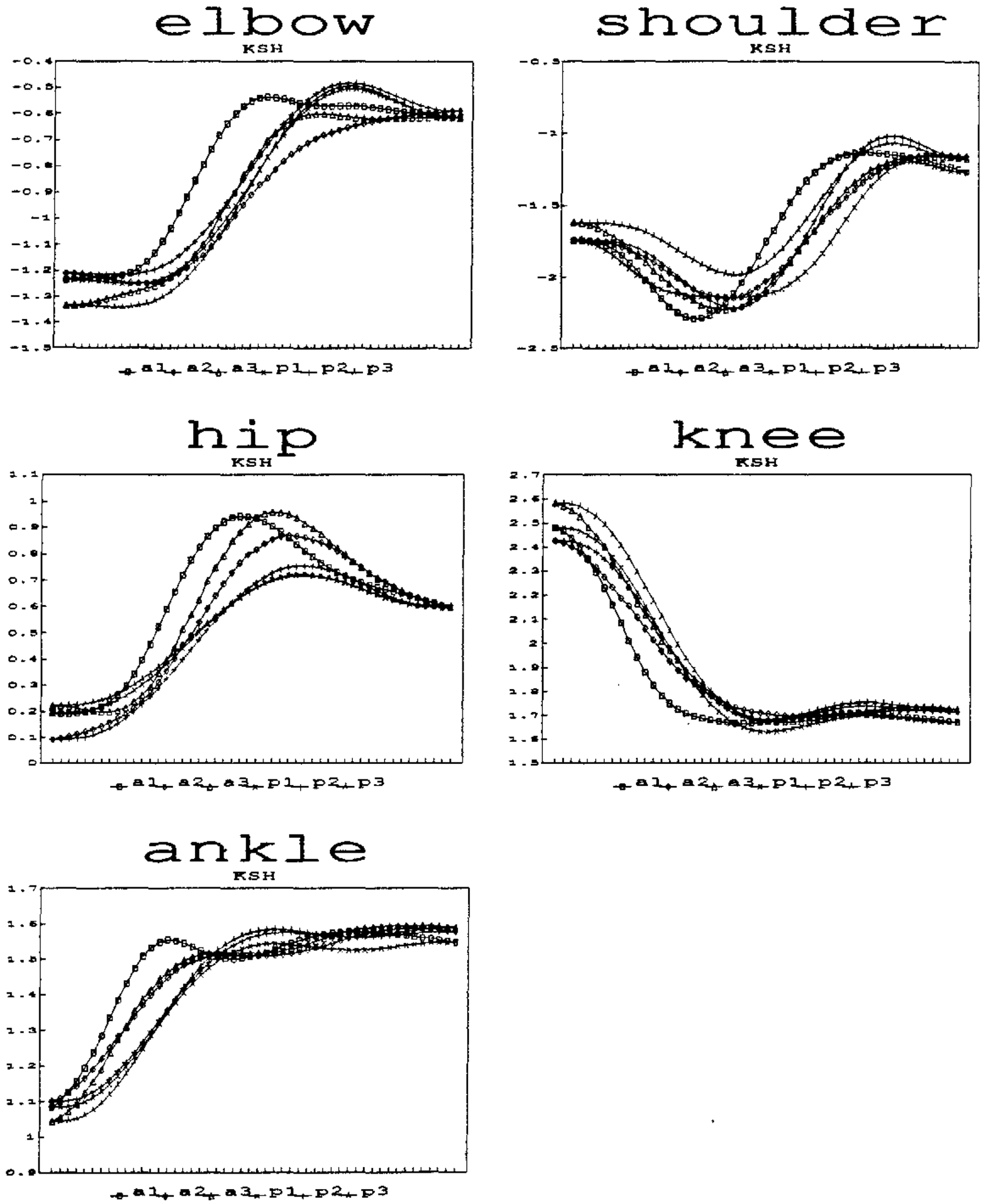

Figure 5.20 Actual (a1,a2,a3) joint trajectories versus simulated (p1,p2,p3) trajectories for floor-to-knuckle, small container, and heavy weight (KSH) condition for subject 1.

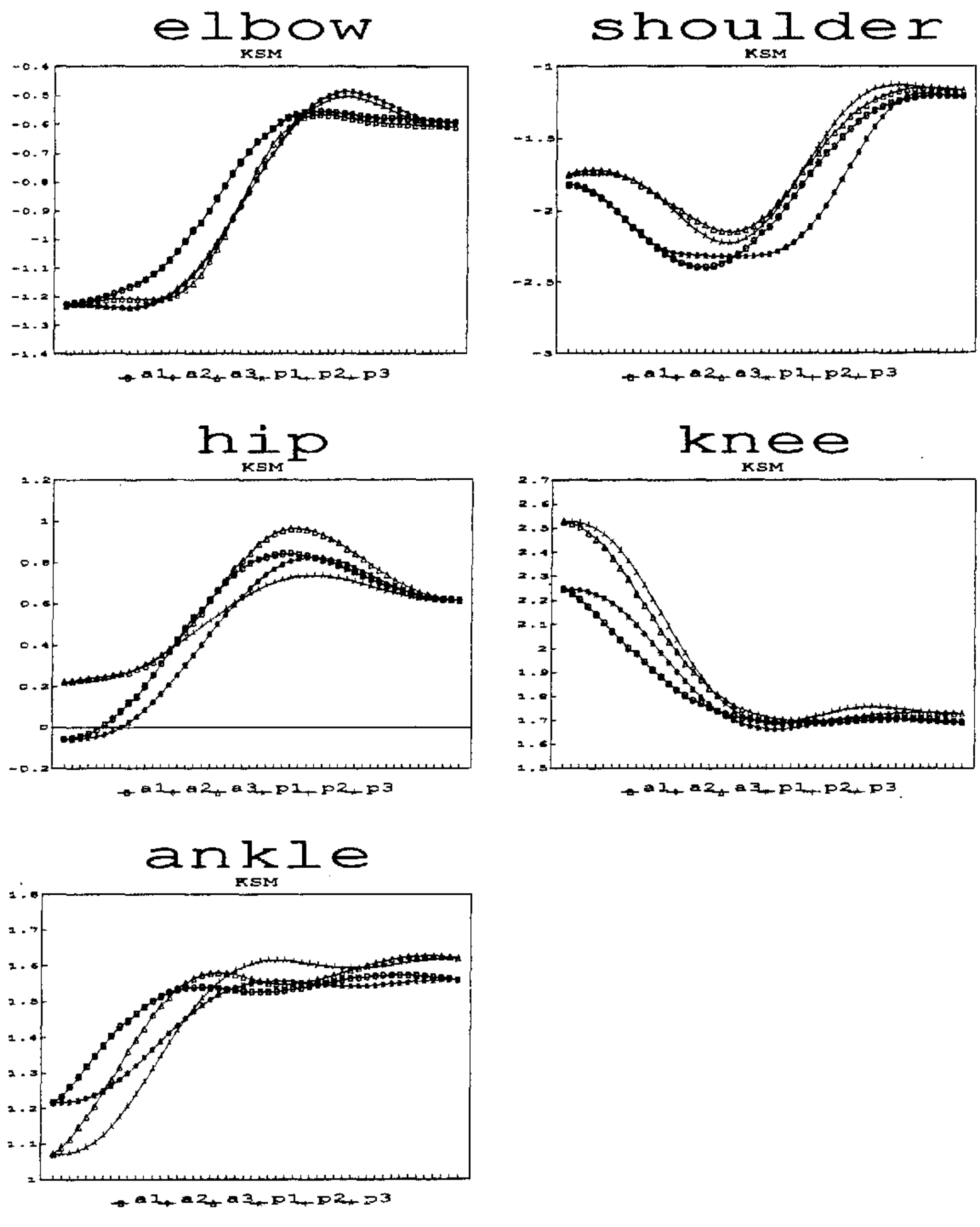

Figure 5.21 Actual (a1,a2,a3) joint trajectories versus simulated (p1,p2,p3) trajectories for floor-to-knuckle, small container, and medium weight (KSM) condition for subject 1.

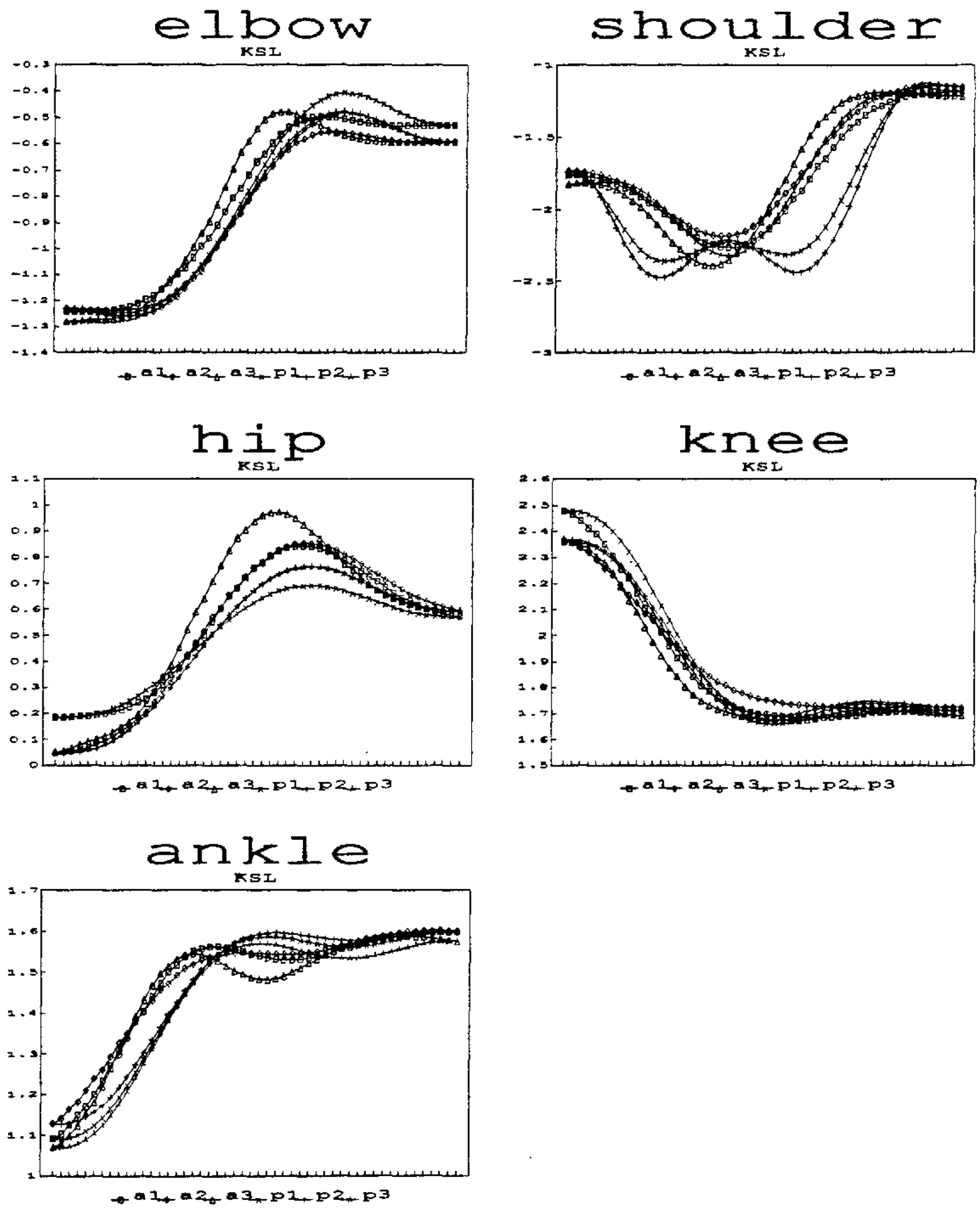

Figure 5.22 Actual (a1,a2,a3) joint trajectories versus simulated (p1,p2,p3) trajectories for floor-to-knuckle, small container, and light weight (KSL) condition for subject 1.

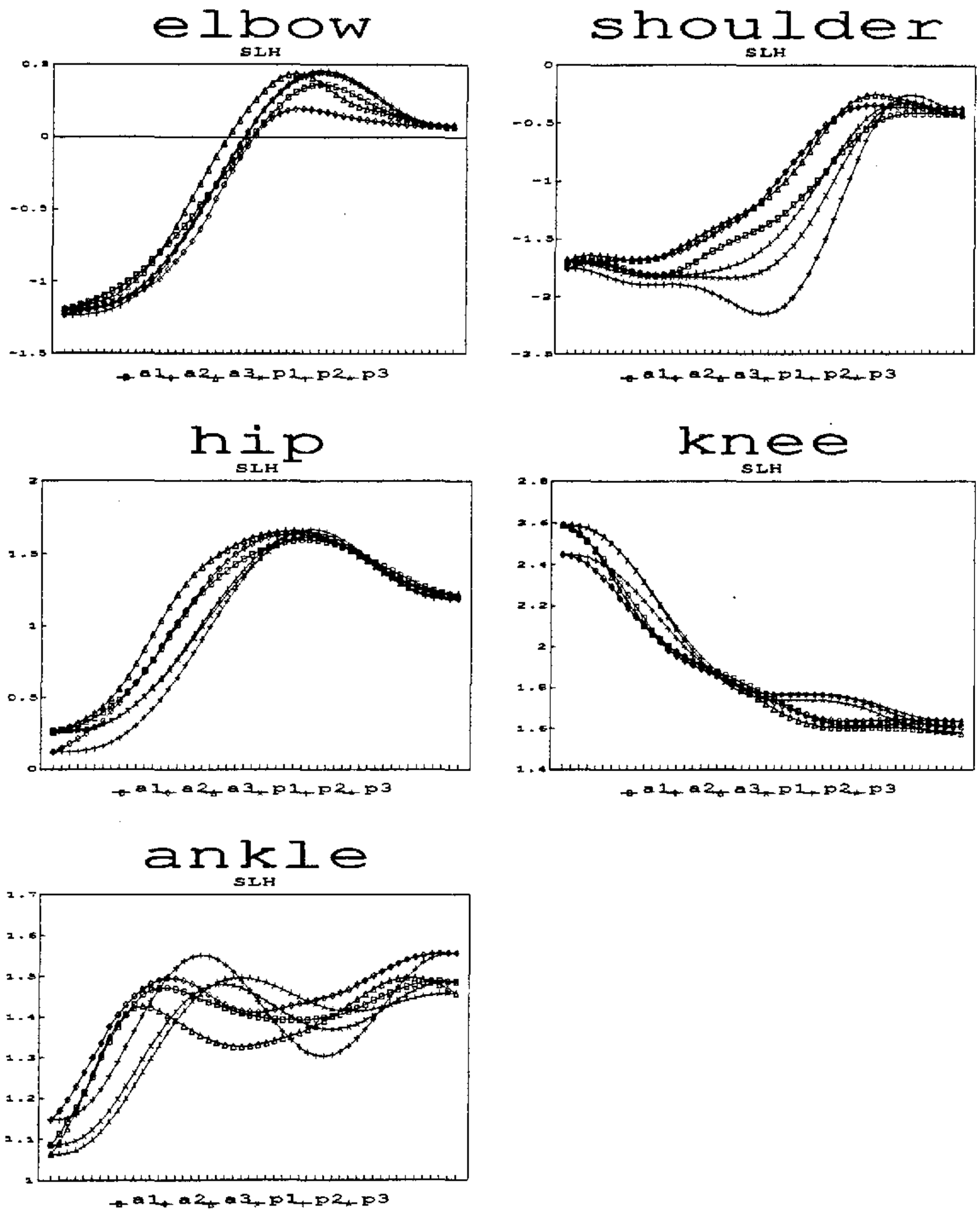

Figure 5.23 Actual (a1,a2,a3) joint trajectories versus simulated (p1,p2,p3) trajectories for floor-to-shoulder, large container, and heavy weight (SLH) condition for subject 1.

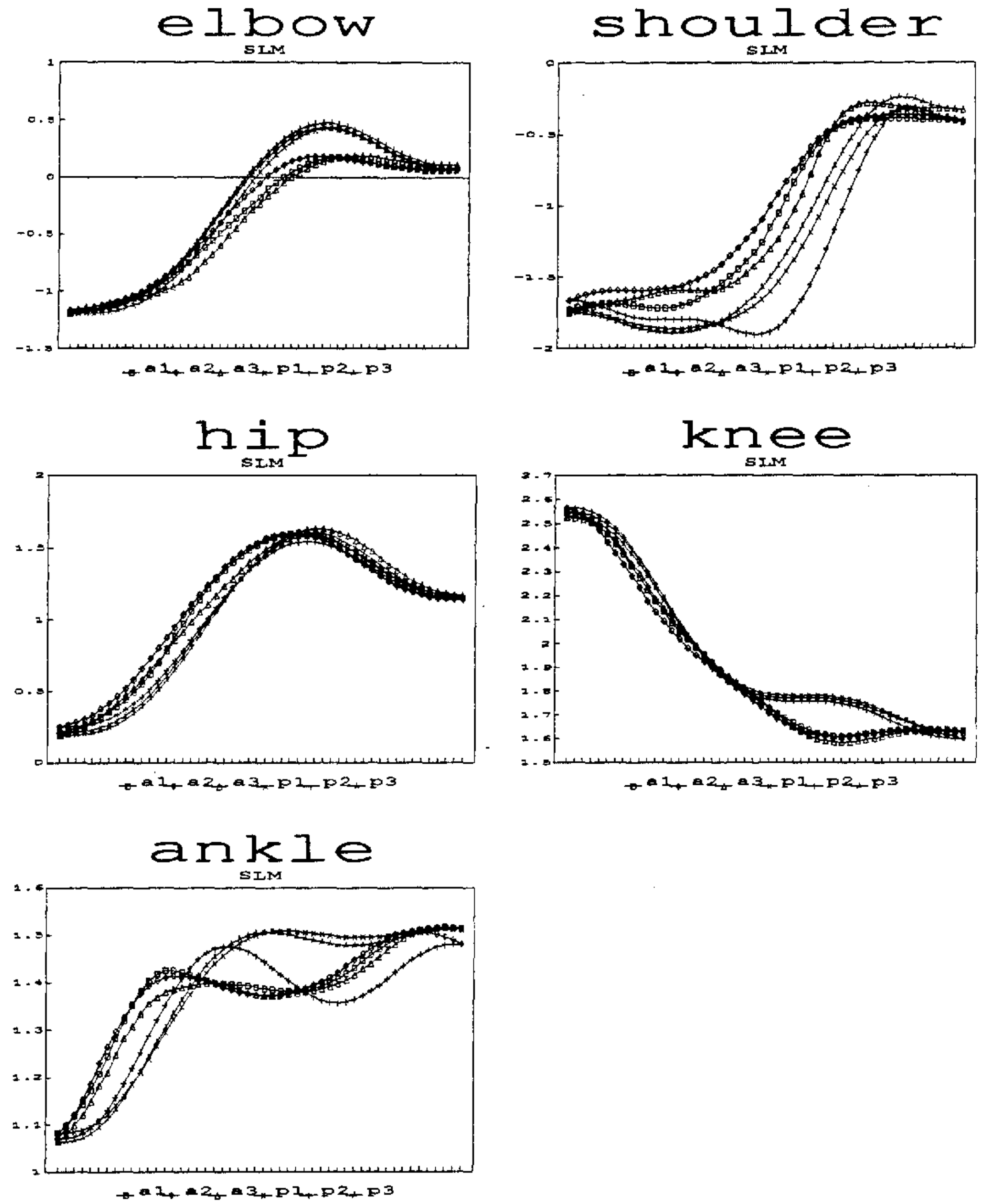

Figure 5.24 Actual (a1,a2,a3) joint trajectories versus simulated (p1,p2,p3) trajectories for floor-to-shoulder, large container, and medium weight (SLM) condition for subject 1.

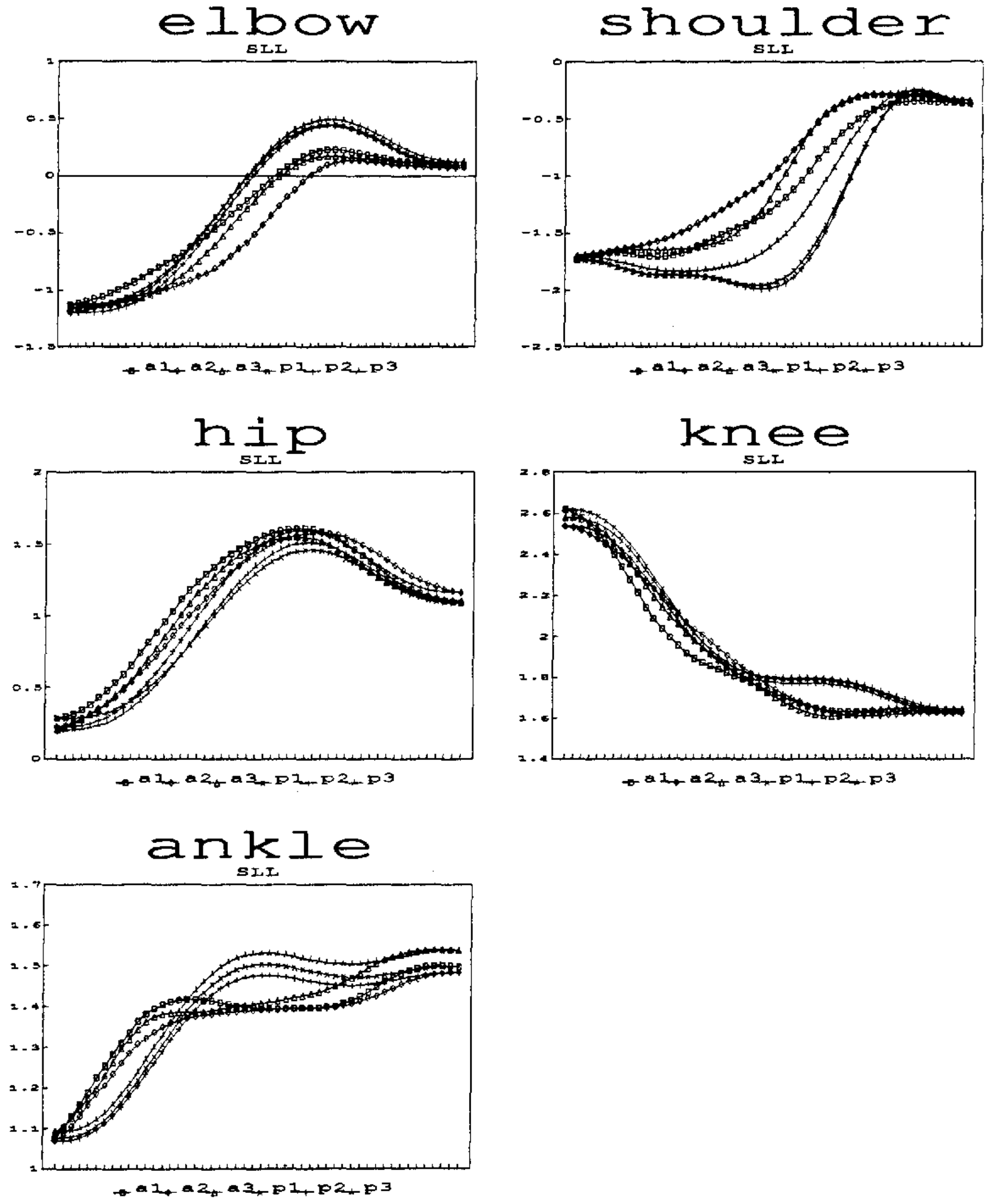

Figure 5.25 Actual (a1,a2,a3) joint trajectories versus simulated (p1,p2,p3) trajectories for floor-to-shoulder, large container, and light weight (SLL) condition for subject 1.

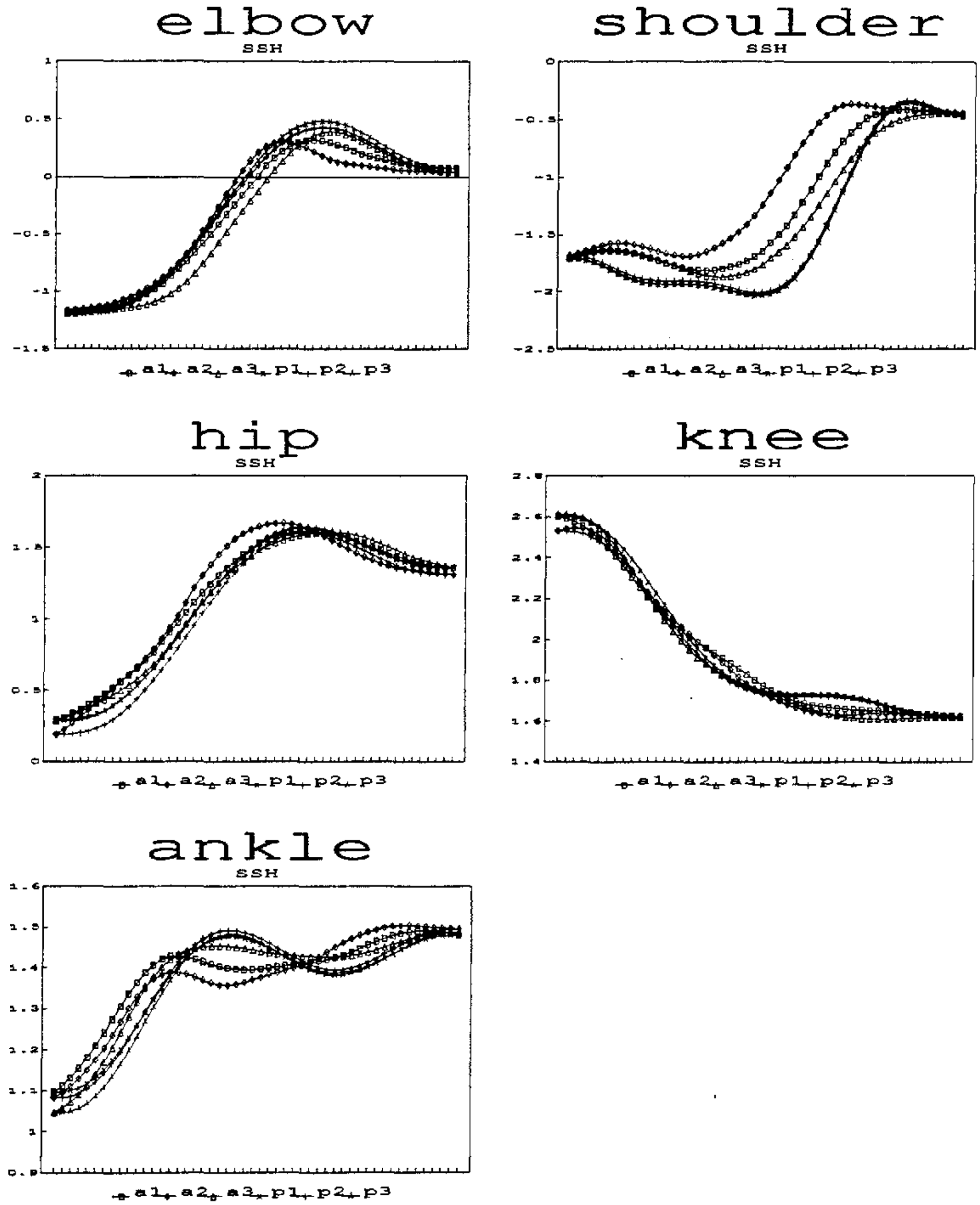

Figure 5.26 Actual (a1,a2,a3) joint trajectories versus simulated (p1,p2,p3) trajectories for floor-to-shoulder, small container, and heavy weight (SSH) condition for subject 1.

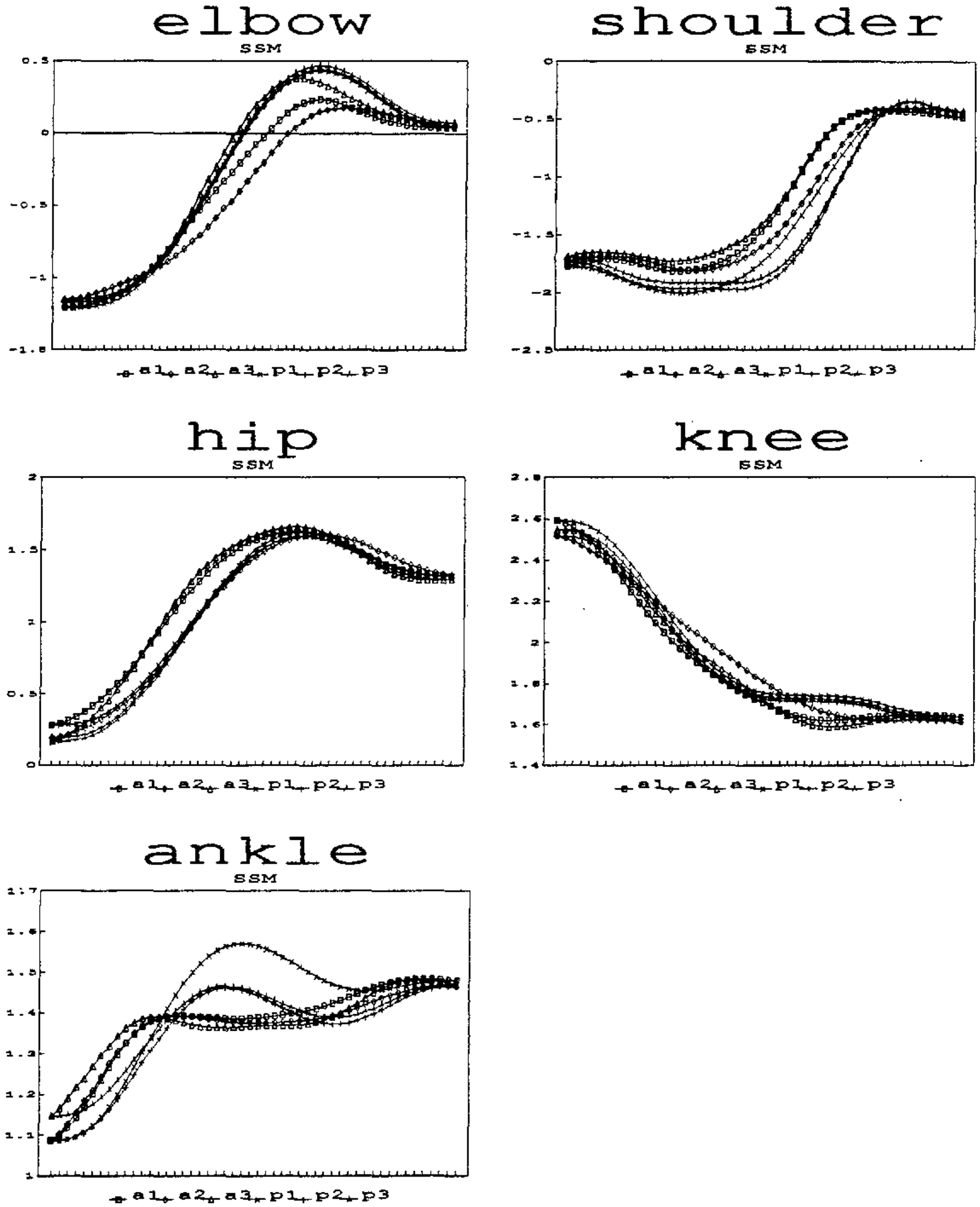

Figure 5.27 Actual (a1,a2,a3) joint trajectories versus simulated (p1,p2,p3) trajectories for floor-to-shoulder, small container, and medium weight (SSM) condition for subject 1.

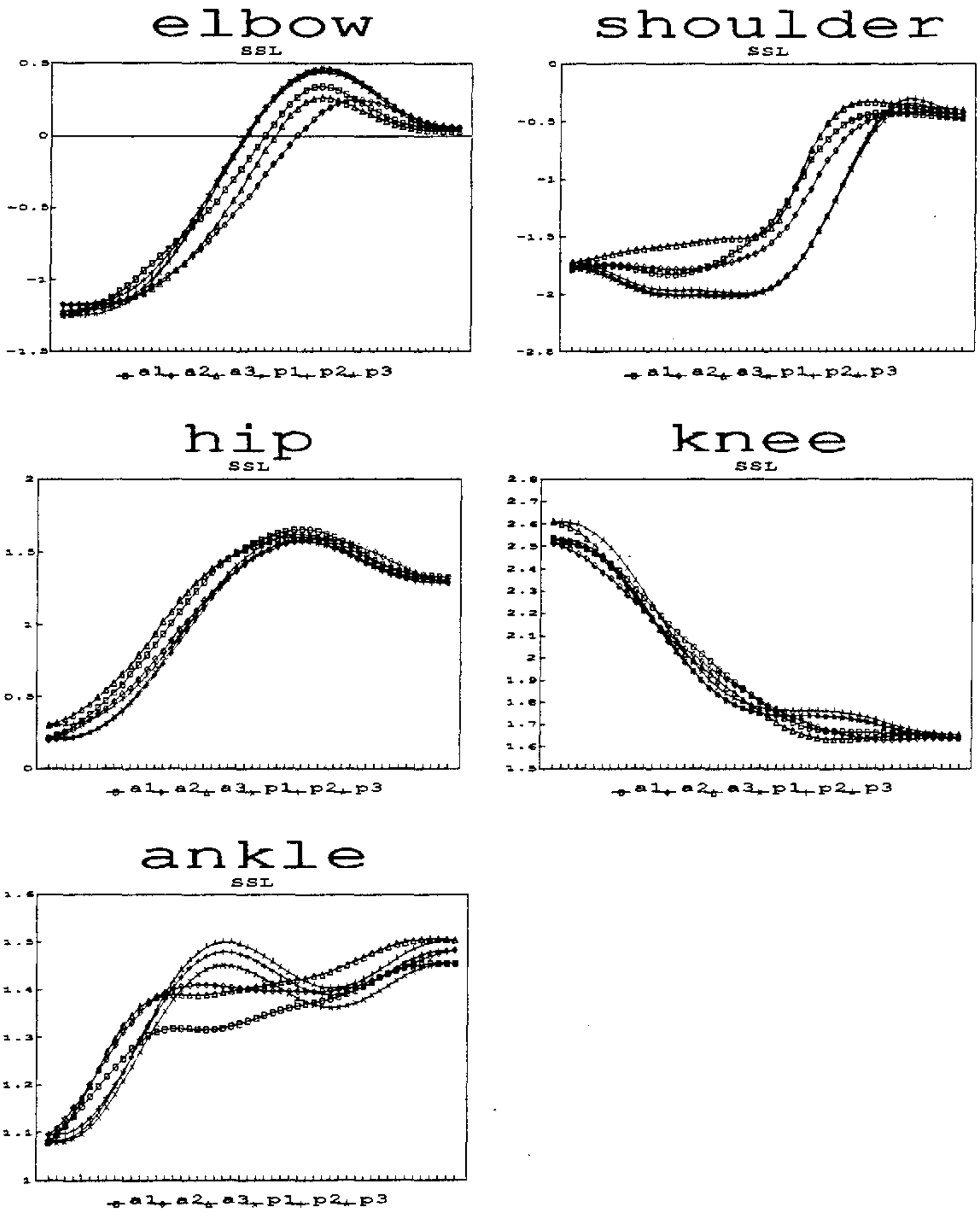

Figure 5.28 Actual (a1,a2,a3) joint trajectories versus simulated (p1,p2,p3) trajectories for floor-to-shoulder, small container, and light weight (SSL) condition for subject 1.

method to approximate the motion for a population. If the global optimum is desired, search algorithms will have to be used. Since the problem was relatively large and complex, search methods will be much more inefficient.

5.2.2 MSE and MNDP

The above graphical comparison provides qualitative descriptions for the general prediction performance of the simulation model. A more systematic evaluation was conducted using the two criteria proposed in Chapter 4. MSE is the mean squared error between the predicted and the actual trajectories. MNDP is the mean number of disconcordant pairs between the predicted and the actual trajectories. MSE measures the closeness of the two trajectories and MNDP measures the agreement in the moving trends of the two trajectories.

MSE and MNDP of each simulation lift were calculated using equations (4.19) and (4.20). Mean MSE and MNDP were then calculated. Table 5.4 presents the mean MSE for each joint for the two lifting heights, two container sizes, and three lifting weights. Comparing the two lifting heights, the floor-to-knuckle lifts had significantly smaller MSE's than the floor-to-shoulder lifts for the elbow, shoulder, hip, and ankle ($p<.001$, .01, .001, .001, respectively); however, for the knee, the floor-to-knuckle lifts had a significantly greater MSE than the floor-to-shoulder lifts ($p<.001$). Comparing the two container sizes, the small container lifts had significantly smaller MSE's than the large container lifts for the hip and ankle ($p<.001$, .05, respectively). For the knee, the large container lifts had significantly smaller MSE's than the small container lifts ($p<.05$). For the elbow and shoulder, no differences in MSE were found between the two container sizes. Finally, there was no significant difference in MSE between the lifting weights. The statistical evaluation presented here shows the prediction performance of each individual joint with regard to the lifting conditions. From the results, there was no indication that, for all five joints, the model predicted better in one condition than the other .

Table 5.5 presents the mean MNDP for the two lifting heights, two container sizes, and three lifting weights for each joint. Comparing the two lifting heights, the floor-to-shoulder lifts had significantly smaller MNDP's than the floor-to-knuckle lifts for the elbow, shoulder, and knee ($p<.001$, .05, .001, respectively). No significant difference in MNDP was found for the hip. For the ankle, the floor-to-knuckle lifts had a smaller MNDP than the floor-to-shoulder lifts ($p<.01$). Comparing the two container sizes, the

Table 5.4 Mean MSE for the two lifting heights, two container sizes, and three lifting weights for each joint. The unit is rad^2.

height	N	elbow	shoulder	hip	knee	ankle
knuckle	180	0.016871	0.069770	0.016614	0.078842	0.0045651
shoulder	180	0.047039	0.094682	0.031114	0.011587	0.0081531

container	N	elbow	shoulder	hip	knee	ankle
large	180	0.032051	0.086003	0.031144	0.035391	0.0069476
small	180	0.031859	0.078449	0.016584	0.055038	0.0057707

weight	N	elbow	shoulder	hip	knee	ankle
heavy	120	0.037135	0.086020	0.021367	0.043981	0.0069642
medium	120	0.031210	0.076891	0.022495	0.043341	0.0060834
light	120	0.027520	0.083767	0.027731	0.048321	0.0060298

Table 5.5 Mean MNDP for the two lifting heights, two container sizes, and three lifting weights for each joint.

height	N	elbow	shoulder	hip	knee	ankle
knuckle	180	0.25159	0.24717	0.11077	0.18798	0.36191
shoulder	180	0.11032	0.22166	0.09592	0.13401	0.39580

container	N	elbow	shoulder	hip	knee	ankle
large	180	0.17857	0.24433	0.09932	0.17313	0.36463
small	180	0.18333	0.22449	0.10737	0.14887	0.39308

weight	N	elbow	shoulder	hip	knee	ankle
heavy	120	0.19303	0.23912	0.10833	0.15085	0.37381
medium	120	0.18707	0.22177	0.10000	0.15816	0.38282
light	120	0.16276	0.24235	0.10170	0.17398	0.37993

small container lifts had a significantly smaller MNDP than the large container lifts for the knee ($p<.01$); however, for the ankle, the large container lifts had a smaller MNDP ($p<.05$). No significant differences in MNDP were found for the elbow, shoulder, and hip between the two container sizes. Finally, there was no significant difference in MNDP between the different lifting weights.

MSE measures the closeness between the actual trajectory and the simulated trajectory. MNDP measures the moving trend of the two trajectories. Although there was disagreement between the results from the two criteria, the results from MNDP should be interpreted with care. One reason for this was that MNDP was greatly affected by the smoothness of the trajectories. The simulated trajectory was smooth because it was a polynomial; however, the smoothness of the actual trajectory varied from lift to lift, even if they were smoothed using the same smoothing constant.

5.3 Sensitivity Analysis

So far, the simulation for the 360 lifts was performed using the model presented earlier in Chapter 4. The model has assumed standard proportional segment lengths for every subject. The model used zero initial velocities for the Hermite polynomials to generate the joint trajectories. Also, the model used all four types of constraints in the optimization procedure, namely, the joint mobility constraints, the joint moment strength constraints, the collision avoidance constraints, and the postural stability constraint. The simulation performed under these conditions will be called the "original" simulation hereafter. For each condition described above, sensitivity analysis was performed by changing the condition or removing it from the model and performing the simulation for the 360 lifts again. The simulation performed under the new condition will be called the "new" simulation. The results for each of the "new" simulations are presented below.

5.3.1 Effects of Segment Lengths

The original simulation used standard proportional segment lengths. New simulation was performed for the 360 lifts using the measured segment lengths from each subject. Appendix C provides the subject characteristics including the measured segment lengths. The resulting MSE and MNDP were calculated for each lift. For these two criteria, smaller values indicate better prediction. For the same lift, if the criterion from the new simulation is smaller than that from the original simulation, the new simulation has a better prediction due to the use of actual segment lengths. The difference in MSE between the new simulation and the original simulation was calculated for each of the 360 lifts. A paired t-test was conducted for this difference in MSE. Similarly, a paired t-test was conducted for the difference in MNDP. Since it was expected that the use of actual segment lengths would improve the simulation results, the testing hypothesis was

$$\mu = 0 \text{ vs. } \mu < 0$$

where

$\mu = (MSE_{new} - MSE_{original})$ or $(MNDP_{new} - MNDP_{original})$, for each joint.

Table 5.6 shows the test results. For the ankle, the new simulation had a smaller MNDP than the original simulation ($p<.001$); however, in most cases, the null hypothesis was not rejected for both criteria, indicating that there was no significant improvement in the simulation due to the use of actual segment lengths.

5.3.2 Effects of Initial Joint Velocities

The original simulation assumed zero initial velocities for each lift. New simulation was performed using the actual initial joint velocities from each lift. Paired t-tests were conducted for the differences in MSE and MNDP between the new simulation and the

Table 5.6 T-tests results for the use of actual segment lengths versus proportional lengths. N=360.

MSE tests:

μ (difference in)	mean	stdev	t	p value
MSE_{elbow}	0.00355	0.02417	2.79	1.00
$MSE_{shoulder}$	-0.00236	0.09587	-0.47	0.32
MSE_{hip}	0.00065	0.01434	0.86	0.81
MSE_{knee}	-0.00239	0.04196	-1.08	0.14
MSE_{ankle}	0.00218	0.00943	4.39	1.00

MNDP tests:

μ (difference in)	mean	stdev	t	p value
$MNDP_{elbow}$	0.00703	0.09188	1.45	0.93
$MNDP_{shoulder}$	0.00170	0.11965	0.27	0.61
$MNDP_{hip}$	-0.00363	0.04810	- 1.43	0.077
$MNDP_{knee}$	0.02863	0.11088	4.90	1.00
$MNDP_{ankle}$	-0.02387	0.09350	-4.84	0.0000

original simulation. It was expected that the use of actual initial joint velocities would improve the simulation; therefore, the following hypothesis was tested:

$$\mu = 0 \text{ vs. } \mu < 0$$

where

$\mu = (MSE_{new} - MSE_{original})$ or $(MNDP_{new} - MNDP_{original})$.

Table 5.7 shows the test results. The difference in MSE was significantly smaller than zero for the hip ($p<.001$), indicating a significant improvement in hip simulation by using actual initial joint velocities. For other joints, no significant improvement in MSE was found due to the use of initial velocities. The MNDP was significantly smaller in the new simulation than in the original simulation for the elbow, hip, and ankle (p<001, .005, .001., respectively). Both MSE and MNDP indicate that the hip trajectories were predicted better when actual initial joint velocities were used.

5.3.3 Effects of Optimization Model Constraints

The original simulation used four types of constraints. New simulation was performed by removing each type of constraints from the optimization model while

Table 5.7 T-tests results for the use of actual initial velocities versus zero velocities. N=360.

MSE tests:				
μ (difference in)	mean	stdev	t	p value
MSE_{elbow}	0.00151	0.02637	1.09	0.86
$MSE_{shoulder}$	0.02159	0.10477	3.91	1.00
MSE_{hip}	-0.00504	0.01539	-6.21	0.0000
MSE_{knee}	-0.00115	0.05282	-0.41	0.34
MSE_{ankle}	0.00127	0.00921	2.61	1.00
MNDP tests:				
μ (difference in).	mean	stdev	t	p value
$MNDP_{elbow}$	-0.01491	0.08624	-3.28	0.0006
$MNDP_{shoulder}$	0.01315	0.11874	2.10	0.98
$MNDP_{hip}$	-0.00760	0.05301	-2.72	0.0034
$MNDP_{knee}$	0.03679	0.11047	6.32	1.00
$MNDP_{ankle}$	-0.03560	0.11651	-5.80	0.0000

keeping the other three types of constraints in the model. It was expected that when a type of constraints was removed from the model, the prediction would be worse, increasing the values of MSE and MNDP. Paired t-tests were performed for the differences in MSE and MNDP between the new simulation and the original simulation. The hypothesis was

$$\mu = 0 \text{ vs. } \mu > 0$$

where

$\mu = (MSE_{new} - MSE_{original})$ or $(MNDP_{new} - MNDP_{original})$.

Table 5.8 shows the test results for the case where the new simulation was performed without the joint mobility constraints. Except for the differences in MSE for the knee and MNDP for the ankle, the null hypothesis was rejected at 5% significance level, indicating that MSE and MNDP increased in the new simulation. In most cases, the prediction was worse when the joint mobility constraints were removed from the model. This confirms the importance of the joint mobility constraints in the entire simulation model.

Table 5.8 T-tests results for the simulation without the use of the joint mobility constraints versus the original simulation. N=360.

MSE tests:				
μ (difference in)	mean	stdev	t	p value
MSE_{elbow}	0.00603	0.03297	3.47	0.0003
$MSE_{shoulder}$	0.06377	0.16848	7.18	0.0000
MSE_{hip}	0.00653	0.02395	5.17	0.0000
MSE_{knee}	-0.00056	0.04095	-0.26	0.60
MSE_{ankle}	0.00406	0.01575	4.89	0.0000
MNDP tests:				
μ (difference in)	mean	stdev	t	p value
$MNDP_{elbow}$	0.02307	0.10280	4.26	0.0000
$MNDP_{shoulder}$	0.05981	0.12506	9.07	0.0000
$MNDP_{hip}$	0.00913	0.07221	2.40	0.0085
$MNDP_{knee}$	0.01451	0.12134	2.27	0.012
$MNDP_{ankle}$	-0.00765	0.09506	-1.53	0.94

Table 5.9 shows the test results for the case where the new simulation was performed without the joint moment strength constraints. The null hypothesis was rejected for the differences in MSE for the shoulder and ankle, and in MNDP for the shoulder, hip, and knee ($p<.001$, .001, .001, .005, .001, respectively), indicating that for these criteria, the removal of the joint moment strength constraints worsened the prediction.

Table 5.10 shows the test results for the case where the new simulation was performed without the collision avoidance constraints. The null hypothesis was rejected for the differences in MSE for the elbow, hip, and ankle, and in MNDP for the hip and knee (all $p<.001$), indicating that for these criteria, the removal of the collision avoidance constraints worsened the prediction.

Table 5.11 shows the test results for the case where the new simulation was performed without the postural stability constraints. The null hypothesis was rejected for the differences in MSE for the elbow, shoulder, and ankle, and in MNDP for the elbow,

Table 5.9 T-tests results for the simulation without the use of the joint strength constraints versus the original simulation. N=360.

MSE tests:

μ (difference in)	mean	stdev	t	p value
MSE_{elbow}	-0.00045	0.02361	-0.36	0.64
$MSE_{shoulder}$	0.04325	0.12288	6.68	0.0000
MSE_{hip}	0.00009	0.01366	0.13	0.45
MSE_{knee}	-0.00143	0.02871	-0.94	0.83
MSE_{ankle}	0.00181	0.01002	3.43	0.0003

MNDP tests:

μ (difference in)	mean	stdev	t	p value
$MNDP_{elbow}$	0.00720	0.09336	1.46	0.072
$MNDP_{shoulder}$	0.04756	0.10402	8.68	0.0000
$MNDP_{hip}$	0.00856	0.05879	2.76	0.0030
$MNDP_{knee}$	0.03934	0.10649	7.01	0.0000
$MNDP_{ankle}$	-0.02619	0.08905	-5.58	1.00

Table 5.10 T-tests results for the simulation without the use of the collision avoidance constraints versus the original simulation. N=360.

MSE tests:

μ (difference in)	mean	stdev	t	p value
MSE_{elbow}	0.00858	0.03655	4.45	0.0000
$MSE_{shoulder}$	-0.00491	0.10565	-0.88	0.81
MSE_{hip}	0.00332	0.01716	3.68	0.0001
MSE_{knee}	0.00113	0.02731	0.78	0.22
MSE_{ankle}	0.00299	0.01169	4.85	0.0000

MNDP tests:

μ (difference in)	mean	stdev	t	p value
$MNDP_{elbow}$	0.00482	0.11787	0.78	0.22
$MNDP_{shoulder}$	0.00062	0.12592	0.09	0.46
$MNDP_{hip}$	0.01593	0.07238	4.18	0.0000
$MNDP_{knee}$	0.02902	0.10386	5.30	0.0000
$MNDP_{ankle}$	-0.01927	0.09368	-3.90	1.00

shoulder, hip and knee ($p<.001$, .01, .001, .005, .001, .001, .001, respectively), indicating that for these criteria, the removal of the postural stability constraints worsened the prediction.

5.4 Final Discussion

The sensitivity analysis has shown that the removal of any of the four types of constraints from the optimization unit would in general degrade the prediction performance of the simulation model in one or more joints, suggesting that it is necessary to keep these constraints in the model. The one-at-a-time approach was adopted in the analysis of the constraint effects for two reasons. First, it was not the intent of the study to investigate the joint effects of these constraints on the performance of the simulation. The interaction between different types of constraints is usually complex and difficult to explain. Second, the one-at-a-time method required a total of 1440 simulations (360 lifts x 4 types of constraints), an enormous task for the study. The investigation of interaction

Table 5.11 T-tests results for the simulation without the use of the postural stability constraints versus the original simulation. N=360.

MSE tests:

μ (difference in)	mean	stdev	t	p value
MSE_{elbow}	0.00298	0.02398	2.36	0.0095
$MSE_{shoulder}$	0.02303	0.10185	4.29	0.0000
MSE_{hip}	0.00036	0.01335	0.51	0.30
MSE_{knee}	0.00208	0.03938	1.00	0.16
MSE_{ankle}	0.00354	0.01143	5.88	0.0000

MNDP tests:

μ (difference in)	mean	stdev	t	p value
$MNDP_{elbow}$	0.01548	0.09713	3.02	0.0013
$MNDP_{shoulder}$	0.03112	0.10505	5.62	0.0000
$MNDP_{hip}$	0.01077	0.06150	3.32	0.0005
$MNDP_{knee}$	0.03226	0.10792	5.67	0.0000
$MNDP_{ankle}$	-0.02098	0.08503	-4.68	1.00

would have required more experiments for the simulation, which is practically impermissible for the study. At least, the one-at-a-time constraint analysis has shown that the current optimization model does not contain any redundant constraints.

The use of actual segment lengths showed no significant improvement in the prediction performance for most of the joints. This indicates that the use of standard proportional segment anthropometric data is generally acceptable for the gross body motion simulation purpose. The segment lengths were not a major source of simulation error.

The input of actual initial joint velocities provided more information for the forms and shapes of the polynomial. The initial velocity tells the trajectory how to move its first step; therefore, it might affect the shape of the polynomial. However, these effects might be minimal. More importantly, the initial velocity reflects how each joint moved in relation to each other at the initial moment of the lift. As mentioned earlier, the joints did not start the motion simultaneously. The use of a common beginning and ending for all five joints was a practical consideration because technically it was difficult to measure the beginning and ending of the motion for each joint. In the sensitivity analysis, the hip joint had significant improvement in its prediction due to the input of actual initial velocities. The other joints, however, did not have such improvement. It is interesting that the mean initial velocity of the hip was higher than that of the elbow and shoulder, as shown in Table 5.1. In general, the lower body joints had higher initial velocities than the upper body joints. Perhaps, for a particular joint, the magnitude of the initial velocity must be large enough to affect the shape of the polynomial. The improvement in the hip prediction encourages future study to look into the coordination of the joints at the moment of the initial lift-off.

The major objective of the study was to develop a more accurate simulation model for lifting activities. A cross-study comparison may reveal whether or not this mission has been accomplished. Table 5.12 compares the simulation results of the present study with the results from Ayoub and Hsiang (1992) and Hsiang (1992). The table shows the mean MSE for the 360 lifts conducted in the present study and those resulted from the 1992 simulation study consisted of 64 lifts. Although the lifting tasks may not be identical, the MSE results of the present simulation are much smaller.

The earlier work of optimization lifting model by Lee (1988) and biomechanical simulation of manual materials handling by Ayoub and Hsiang (1992) and Hsiang (1992) have contributed much to the optimization theory and foundation for the lifting simulation study. Their work focused on the formulation of the optimization lifting model and the optimization solution methods. By examining the motions of a large number of subjects, the present study was able to find the repeated common patterns across subjects. These patterns were then generalized by the Hermite polynomials.

The improvement in the prediction capability of the present simulation over the previous models can be attributed to several factors. First, the phase difference between the actual and predicted trajectories has been reduced considerably. Phase relationships between the predicted and actual trajectories have been pointed out in Hsiang (1992) as one of the major causes responsible for the large MSE. Even if two trajectories are of similar patterns, if one lags behind the other, the MSE would be large. Although the phase difference still existed, the present study has minimized such phase difference by using Hermit polynomials controlled by the peak or trough in the trajectory. The bounds on the location of the control point generalized from the large set of actual data essentially provide sufficient guidance for the polynomial as to where these points should be located.

Table 5.12 Mean MSE for the two lifting heights and two container sizes from the simulation studies conducted by Ayoub and Hsiang (1992) and Hsiang (1992), and the present study (1995). The unit is rad^2.

study in Ayoub and Hsiang (1992) and Hsiang (1992) :

height	N	elbow	shoulder	hip	knee	ankle
knuckle	32	0.28	2.31	0.58	0.21	0.18
shoulder	32	1.21	3.20	0.23	0.24	0.15

current study:

height	N	elbow	shoulder	hip	knee	ankle
knuckle	180	0.016871	0.069770	0.016614	0.078842	0.0045651
shoulder	180	0.047039	0.094682	0.031114	0.011587	0.0081531

study in Ayoub and Hsiang (1992) and Hsiang (1992):

container	N	elbow	shoulder	hip	knee	ankle
large	32	0.6	2.78	0.38	0.33	0.19
small	32	0.87	2.72	0.43	0.12	0.14

current study:

container	N	elbow	shoulder	hip	knee	ankle
large	180	0.032051	0.086003	0.031144	0.035391	0.0069476
small	180	0.031859	0.078449	0.016584	0.055038	0.0057707

Second, the present study used fixed-form polynomials which warranted that the predicted trajectory followed the kinematic characteristics of each joint. Based on the characteristics of each joint trajectory, a polynomial model was developed for that joint. Each polynomial trajectory model was a result of the generalization of the joint patterns over the 360 lifts.

Third, the normalization scheme used in the study helped the formation of these consistent patterns across subjects and lifting tasks. Without the normalization, the control points would have scattered widely and these patterns would not emerge.

Finally, the use of joint mobility constraints may have contributed to the improved simulation results. The previous optimization models by Lee (1988) and Hsiang (1992) both used joint kinematic constraints in which the ranges of the absolute joint angles were specified. As discussed in Chapter 3, the present study proposed the use of ranges for the joint included angles, which truly constrains the mobility between the adjacent segments.

The present simulation model has its limitations. The study aimed at the simulation for sagittal plane lifting activities, especially for free-style lifting. Two of the subjects (subjects 9 and 10) in the study used the extreme squat lifting technique. Although the different pattern in their hip trajectories for the floor-to-knuckle lifts was identified and was modeled differently, the applicability of the present simulation model to squat lifts must be reserved. One problem was that there was not enough samples for the modeling of squat lifting. Another problem was that in squat lifting, the optimization model may be different from the present one. The squat lifting may require a different objective function in which some joints may be weighted higher than the others, for example, the knee may be weighted higher than the hip. The consideration of different styles of lifting is suggested for future research.

The validation process was accomplished in the kinematic domain, mainly the joint position trajectory. It is not clear whether the prediction of kinetics and compression forces at the spine will be reasonable or not, when the simulated joint positions of the study are used. The computation of the kinetics and other useful biomechanical parameters is beyond the scope of the present study. Future research is recommended to compare the kinetic performance of the simulation model with other models in the literature.

CHAPTER 6
CONCLUSIONS AND RECOMMENDATIONS

The present study has accomplished the three objectives of the study: (1) to develop a more accurate simulation method for the prediction of the motion of the sagittal plane lifting activities; (2) to validate the simulation model on both males and females; and (3) to perform sensitivity analysis to understand the effects of the changes in model inputs on the prediction performance of the simulation model. This chapter summarizes the simulation model. Conclusions from the study and recommendations for future development are presented.

6.1 Summary and Conclusions

The simulation model consisted of three computation units. The first unit was the trajectory formation unit, in which the angular trajectories of the joints were generated. The generated trajectories were based on a set of polynomials controlled by the peaks and troughs of the trajectories. A unique polynomial trajectory model was developed for each joint. This method had advantages in providing enough guidance as to the forms and shapes of the simulated trajectories. The second unit was the dynamic biomechanical lifting model unit, in which the kinematics and kinetics of lifting were calculated. The third unit was the optimization unit. The earlier optimization models of lifting proposed by Lee (1988) and Ayoub and Hsiang (1992) were adapted. The constraint set was revised to be used with the trajectory formation method.

The validation showed that the initial and final velocities and accelerations were usually not zero, indicating that the input of these parameters to the model may be important to the prediction performance. The sensitivity analysis further showed that the input of the initial velocities did improve the prediction in the hip joint trajectories; however, there was no significant improvement in other joints. The validation also showed that the trajectories of each joint followed consistent patterns which allowed for generalization. There was no significant difference between the trajectory patterns of the two sexes. The trajectory patterns were grouped into several different patterns according to lifting conditions and joints. Each pattern was modeled with a Hermite polynomial, characterized by the order of the polynomial and by the locations and bounds of the control points within the trajectories.

The sensitivity analysis for the effects of segment lengths showed that no significant improvement in prediction was found after the measured segment lengths were used in the simulation. This indicated that the use of proportional anthropometric segment lengths was acceptable for the simulation. The sensitivity analysis for the effects of each type of the model constraints showed that none of the constraints were redundant. The removal of any type of constraints from the model degraded the prediction performance in one or more joints.

The prediction performance of the simulation model was shown to be more accurate than the previous model (Ayoub and Hsiang, 1992). Several limitations of the present simulation model must be noted. First, the model should be used with caution in predicting lifting motions performed with extreme squat lifting techniques . There were only two subjects who used squat lifting techniques, providing relatively few samples for the modeling of such lifting styles. The present model is best to be used in predicting sagittal lifting motions for free-style lifting. Second, the validation of the model was accomplished in the kinematic domain, mainly the angular trajectory. The use of the model to predict the kinetics and other important biomechanical parameters such as the compression force at the L5/S1 needs to be validated.

6.2 Recommendations for Future Study

The scope of the current simulation study has been limited to the kinematic domain. The prediction accuracy is not known if the kinematic outputs of the model are used for further calculations to obtain kinetics. For example, how is the L5/S1 compression force resulting from the simulation model compared to the one calculated from the dynamic biomechanical lifting model using actual motion inputs? Further validation of the model in kinetics is recommended for future study.

The current study found that the initial velocity had important effects on the prediction of the hip trajectory. The initial velocity of each joint reflects how the joint moves in relation to each other at the moment of the lift-off. At the present, the coordination of the joints at the initial lift-off is not considered in the simulation model. Future study is recommended to investigate the effects of the initial joint coordination on the performance of the simulation model.

As pointed out earlier, the present simulation model was developed for free-style lifting. The lifting technique, squat or stoop lift, seemed to affect the motion trajectory significantly. Further, the objective function in the present study was used to predict the motion of free-style lifting. It is not known whether or not the objective function will be different from the current one when lifting style changes. In the current objective function, the joint loading ratio, moment/strength, has an equal weight for every joint.

Since the squat lift uses the knee more than the back at the initial lift-off, the weight of the joint loading ratio may have to be adjusted. Future study is recommended to evaluate the effects of the weights of the joint loading ratio in the objective function for different lifting styles.

In the long-term, two important areas are recommended for further development of the simulation model. First, a computer system with animation capability of human motions needs to be developed. Ultimately, the development of a fully animated human motion simulation system will be useful for ergonomists to visualize the human-task environment. Second, three-dimensional human motion simulation modeling for lifting tasks is recommended. Many industrial manual materials handling tasks consist of twisting and rotation of the trunk during lifting. Three-dimensional simulation models are necessary in these situations.

REFERENCES

Aczel, A.D., 1989. Complete Business Statistics, Irwin, Homewood, IL, Chapter 11: Time Series and Forecasting, pp595-691.

Atkinson, K.E., 1989. An Introduction to Numerical Analysis, 2nd Edition, John Wiley & Sons, New York, pp159-163.

Ayoub, M.M., 1991. Development of Models to Predict Optimal Lifting Motion, A NIOSH (National Institute of Occupational Safety and Health) grant research proposal, Texas Tech University.

Ayoub, M.M. and El-Bassoussi, M.M., 1978. Dynamic Biomechanical Model for Sagittal Plane Lifting Activities. In: Safety in Manual Materials Handling, Edited by Drury, C.G., Department of Health, Education, and Welfare, Publication No. NIOSH 78-185, Cincinnati, Ohio, pp88-95.

Ayoub, M.M. and Hsiang, M.S., 1992, Biomechanical Simulation of a Lifting Task. Advances in Industrial Ergonomics and Safety IV, Taylor & Francis, Bristol, PA, pp831-838.

Barter, J.T., Emanuel, I., and Truett, B., 1957. A Statistical Evaluation of Joint Range Data, WADC-TR-57-311, Wright-Patterson Air Force Base, Ohio.

Beckett, R. and Chang, K., 1968. An Evaluation of the Kinematics of Gait by Minimum Energy. Journal of Biomechanics, 1, pp147-159.

Bejjani, F.J., Gross, C.M., and Pugh, J.W., 1984. Model for Static Lifting: Relationship of Loads on The Spine and The Knee. Journal of Biomechanics, 17(4), pp281-286.

Burggraaf, J.D., 1972. An Isometric Biomechanical Model for Sagittal Plane Leg Extension, M.S. Thesis, The University of Michigan.

Chaffin, D.B., 1969. A Computerized Biomechanical Model - Development of and Use in Studying Gross Body Actions. Journal of Biomechanics, 2, pp429-441.

Chaffin, D.B. and Andersson, G.B.J., 1991. Occupational Biomechanics, 2nd Edition, John Wiley & Sons, New York.

Chen, H.C. and Ayoub, M.M., 1988. Dynamic Biomechanical Model for Asymmetrical Lifting. Trends in Ergonomics/Human Factors V, Edited by Aghazadeh, F., Elsevier Science Publishers B.V., North-Holland, pp879-886.

Chen, J.G. and Peacock, B., 1985. An Interactive Biomechanical Lifting Model. Trends in Ergonomics/Human Factors II, Edited by Eberts R.E. and Eberts C.G., Elsevier Science Publishers B.V., North-Holland, pp527-542.

Clarke, H.H., 1966. Muscle Strength and Endurance in Man, Prentice-Hall, Englewood Cliffs, NJ, pp39-51.

Flashner, H., Beuter, A., and Arabyan, A., 1987. Modeling of Control and Learning in a Stepping Motion. Biological Cybernetics, 55, pp387-396.

DeVita, P., Hong, D., and Hamill, J., 1991. Effects of Asymmetrical Load Carrying on the Biomechanics of Walking. Journal of Biomechanics, 24(12), pp1119-1129.

Fogleman, M.T., 1993. An Investigation of Changes in Biomechanical Strategies Over Extended Lifting Periods, Ph.D. Dissertation, Texas Tech University.

Garg, A., Chaffin, D.B., and Freivalds, A., 1982. Biomechanical Stresses from Manual Load Lifting: A Static vs. Dynamic Evaluation. IIE Transactions, 14(4), pp272-281.

Greenwood, D.T., 1988. Principles of Dynamics, 2nd Edition, Prentice-Hall, Englewood Cliffs, NJ.

Hatze, H., 1980. Neuromusculoskeletal Control Systems Modeling - A Critical Survey of Recent Developments. IEEE Transactions on Automatic Control, AC-25(3), pp375-385.

Hatze, H., 1981. A Comprehensive Model for Human Motion Simulation and its Application to the Take-Off Phase of the Long Jump. Journal of Biomechanics, 14(3), pp135-142.

Hsiang, M.S., 1992. Simulation of Manual Materials Handling, Ph.D. Dissertation, Texas Tech University.

Huston, R.L. and Passerello, C.E., 1971. On the Dynamics of A Human Body Model. Journal of Biomechanics, 4, pp369-378.

Kromodihardjo, S., 1986. A 3-D Kinetic Biomechanical Model of Symmetrical and Asymmetrical Lifting Tasks. Ph.D. Dissertation, University of Cincinnati.

Lasdon, L.S. and Waren, A.D., 1986. GRG2 User's Guide, School of Business Administration, University of Texas at Austin.

Lee, Y-H. T., 1988. An Optimization Approach to Determine Manual Lifting Motion, Ph.D. Dissertation, Texas Tech University.

Leskinen, T.P.J., 1985. Comparison of Static and Dynamic Biomechanical Models. Ergonomics, 28(1), pp285-291.

Marras, W.S. and Sommerich, C.M., 1991. A Three-Dimensional Motion Model of Loads on the Lumbar Spine: I. Model Structure. Human Factors, 33(2), pp123-137.

Marras, W.S., Sommerich, C.M., and Granata, K.P., 1991. A Three-Dimensional Motion Model and Validation of Loads on the Lumbar Spine. Proceedings of the Human Factors Society 35th Annual Meeting, pp795-799.

Mena, D., Mansour, J.M., and Simon, S.R., 1981. Analysis and Synthesis of Human Swing Leg Motion During Gait and its Clinical Applications. Journal of Biomechanics, 14(12), pp823-832.

Noone, G and Mazumdar, J., 1992. Lifting Low-lying Loads in the Sagittal Plane. Ergonomics, 35(1), pp65-92.

Onyshko, S. and Winter, D.A., 1980. A Mathematical Model for the Dynamics of Human Locomotion. Journal of Biomechanics, 13, pp361-368.

Pandy, M.G. and Berme, N., 1988. Synthesis of Human Walking: A Planar Model for Single Support. Journal of Biomechanics, 21(12), pp1053-1060.

Park, K.S., 1973. A Computerized Simulation Model of Postures During Manual Materials Handling, Ph.D. Dissertation, The University of Michigan.

Röhrle, H., Scholten, R., Sigolotto, C., and Sollbach, W., 1984. Joint Forces in the Human Pelvis-Leg Skeleton During Walking. Journal of Biomechanics, 17(6), pp409-424.

Schanne, F.A., 1972. A Three-Dimensional Hand Force Capability Model for the Seated Operator, Ph.D. Dissertation, The University of Michigan.

Schultz, A.B. and Andersson, G.B.J., 1981. Analysis of Loads on the Lumbar Spine. Spine, 6(1), pp76-82.

Schultz, A.B, Andersson, G.B.J., Haserspeck, K., Örtengren, R., Nordin, M., and Björk, R., 1982. Analysis and Measurement of Lumbar Trunk Loads in Tasks Involving Bends and Twists. Journal of Biomechanics, 15(9), pp669-675.

Schultz, A.B, Andersson, G., Örtengren, R., Haserspeck, K., and Nachemson, A., 1982. Loads on the Lumbar Spine, Validation of a Biomechanical Analysis by Measurements of Intradiscal Pressures and Myoelectric Signals. The Journal of Bone and Joint Surgery, 64-A(5), pp713-720.

Seireg, A. and Arvikar, R.J., 1973. A Mathematical Model for Evaluation of Forces in Lower Extremities of the Musculoskeletal System. Journal of Biomechanics, 6, pp311-326.

Seireg, A. and Arvikar, R.J., 1975. The Prediction of Muscular Load Sharing and Joint Forces in the Lower Extremities During Walking. Journal of Biomechanics, 8, pp89-102.

Selbie, W.S. and Chapman, A.E., 1987. A Mathematical Simulation of Running. In: Biomechanics X-B, Edited by Jonsson, B, Human Kinetics Publishers, Champaign, IL, pp831-836.

Shanno, D.F., 1990. Recent Advances in Numerical Techniques for Large-Scale Optimization, In: Neural Networks for Control, Edited by W. Thomas Miller, III, Richard S. Sutton, and Paul J. Werbos, MIT Press, Cambridge, MA, pp171-178.

Slote, L. and Stone, G., 1963. Biomechanical Power Generated by Forearm Flexion. Human Factors, 5, pp443-452.

Stobbe, T.J., 1982. The Development of A Practical Strength Testing Program for Industry. Ph.D. Dissertation, The University of Michigan.

Subramanian, V. and Hung, M.S., 1993. A GRG2-Based System for Training Neural Networks: Design and Computational Experience. ORSA Journal on Computing, 5(4), pp386-394.

The University of Michigan. 2D Static Strength Prediction Program, information from catalogue materials.

Townsend, M.A. and Seireg, A., 1972. The Synthesis of Bipedal Locomotion. Journal of Biomechanics, 5, pp71-83.

Vaughan, C.L. and Sussman, M.D., 1993. Human Gait: From Clinical Interpretation to Computer Simulation. Current Issues in Biomechanics, Edited by Grabiner, M.D. Human Kinetics Publishers, Champaign, IL. Chapter 3, pp53-68.

Webb Associates, 1978. Anthropometric Source Book, Vol. I, NASA Ref. 1024, National Aeronautics and Space Administration, Washington, DC, Chapters VI and VII.

Winter, D.A., 1990. Biomechanics and Motor Control of Human Movement, 2nd Edition, John Wiley & Sons, New York.

Yamaguchi, G.T., 1990. Performing Whole-Body Simulations of Gait with 3-D, Dynamic Musculoskeletal Models. In: Multiple Muscle Systems, Biomechanics and Movement Organization. Edited by Winters, J.M. and Woo, S.L.Y., Springer-Verlag, Secaucus, NJ, pp663-679.

APPENDIX A
NORMALIZED JOINT TRAJECTORIES
FOR ADDITIONAL SUBJECTS

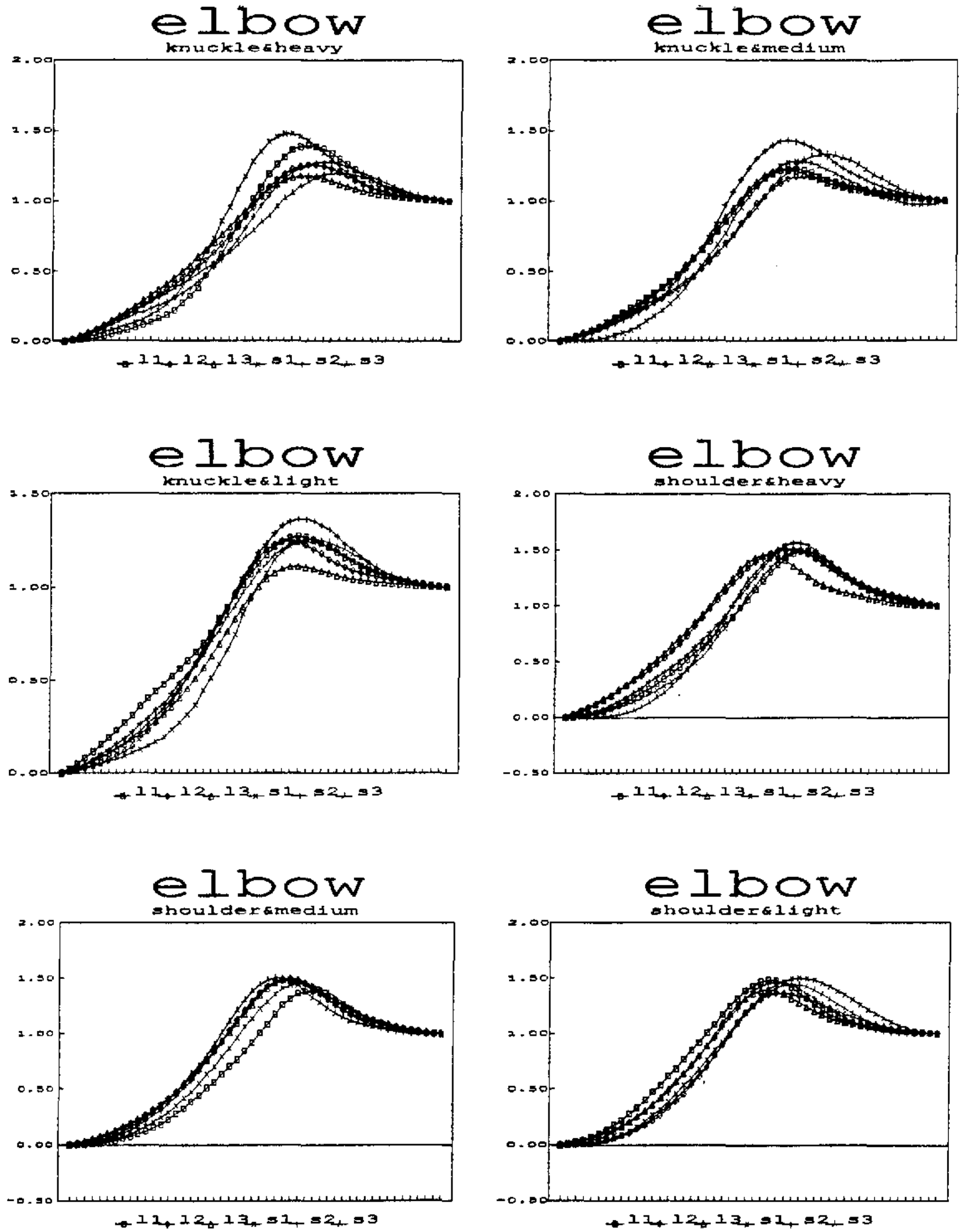

a. elbow

Figure A.1 Normalized trajectories of subject 2

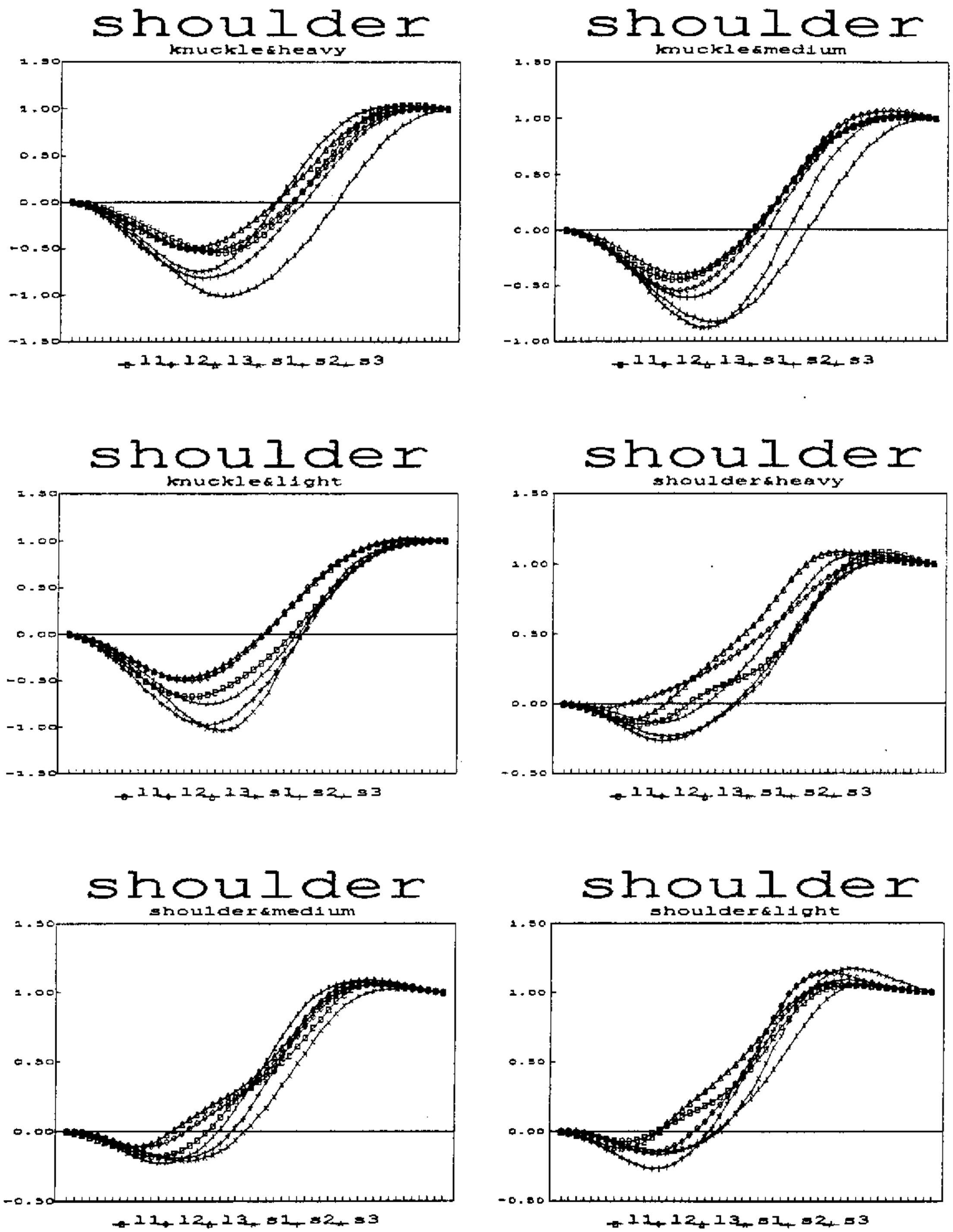

b. shoulder

Figure A.1 Continued

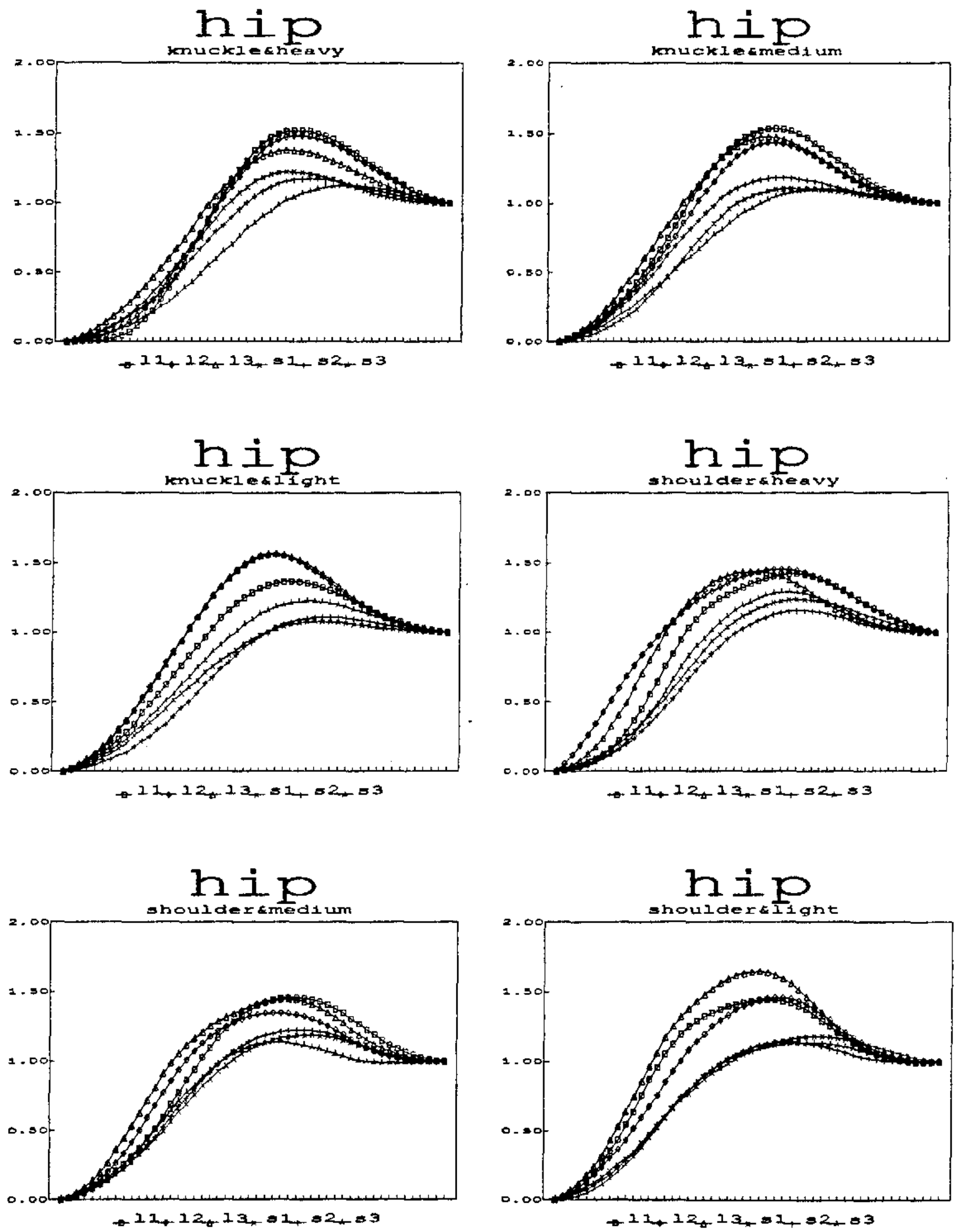

c. hip

Figure A.1 Continued

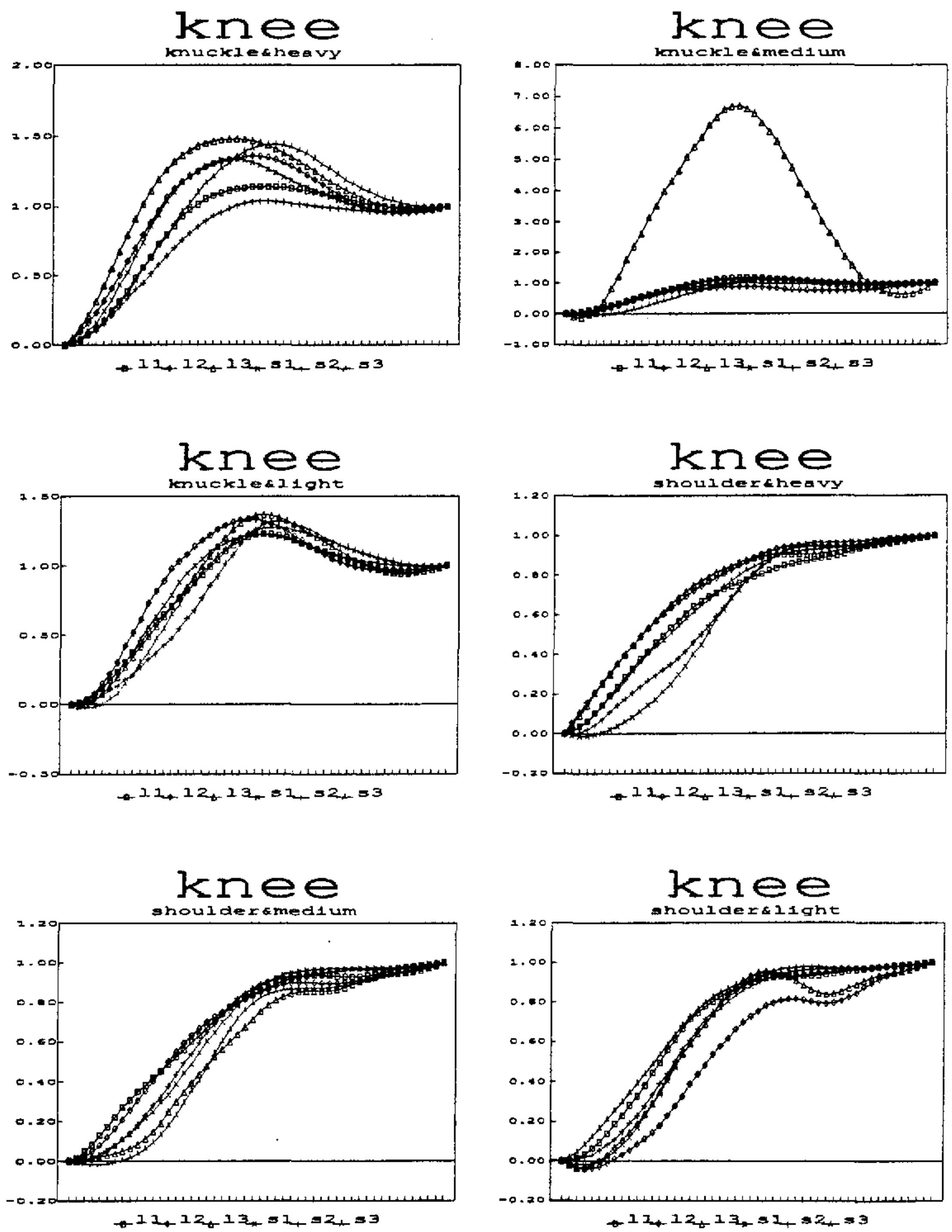

d. knee

Figure A.1 Continued

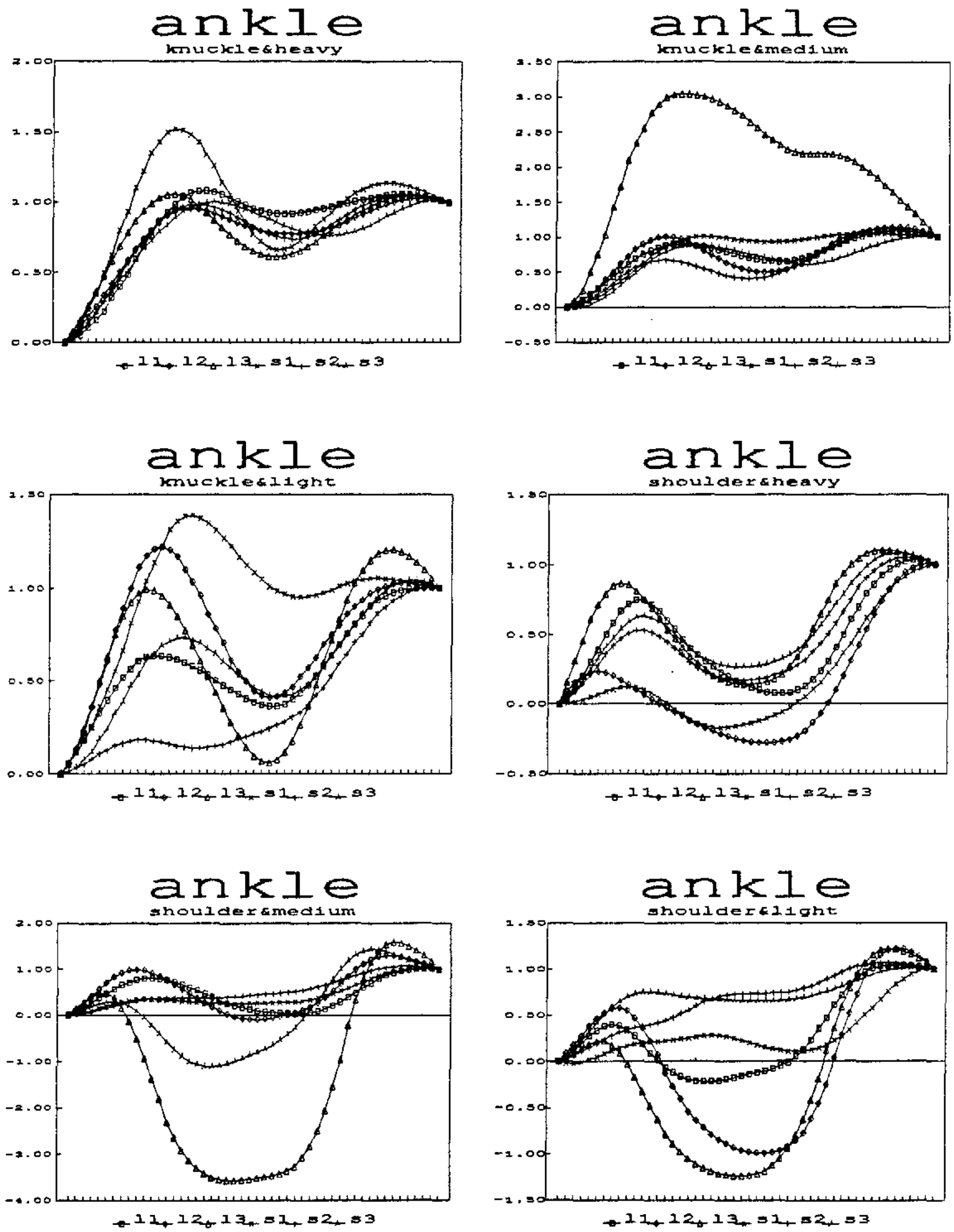

e. ankle

Figure A.1 Continued

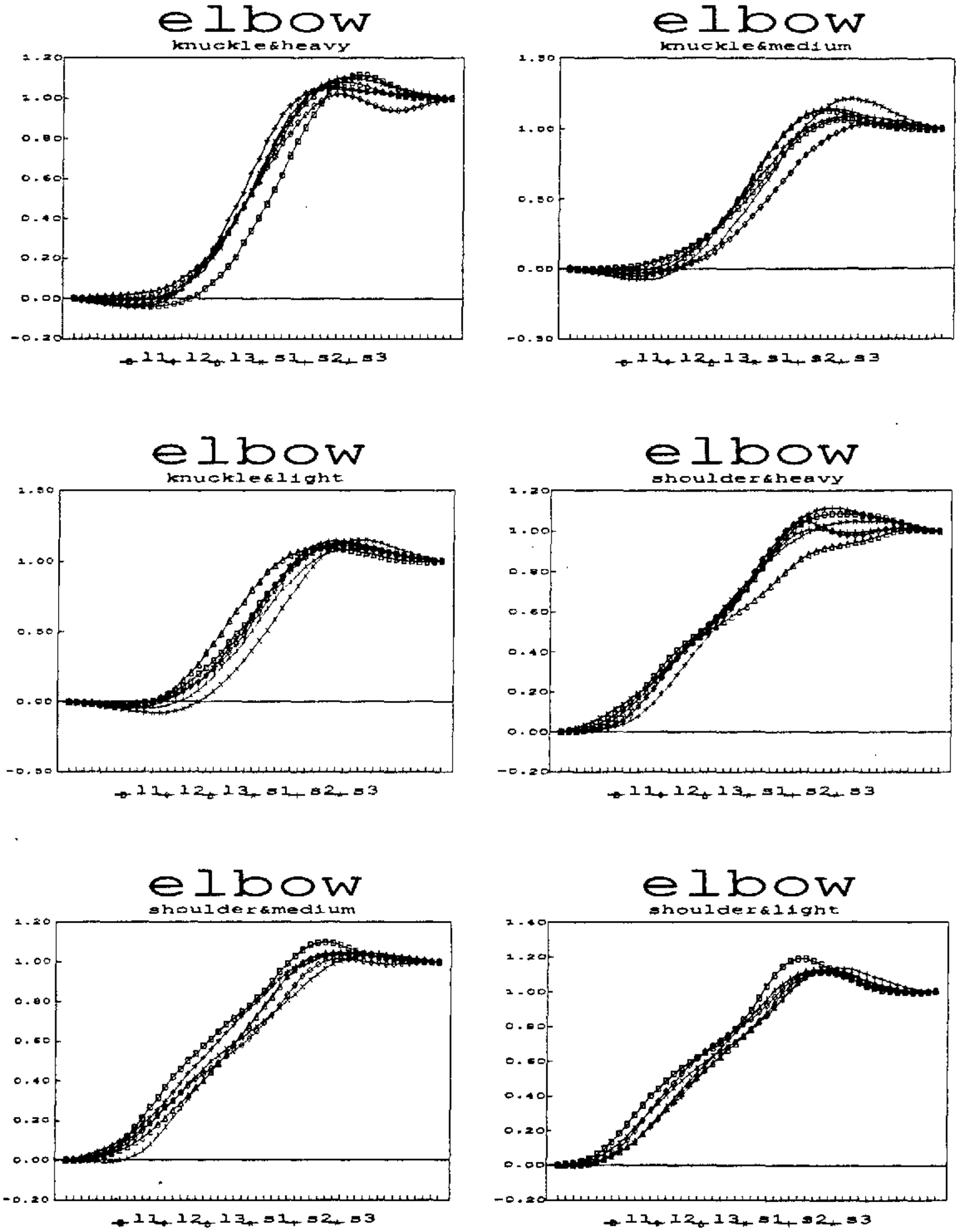

a. elbow

Figure A.2 Normalized trajectories of subject 3

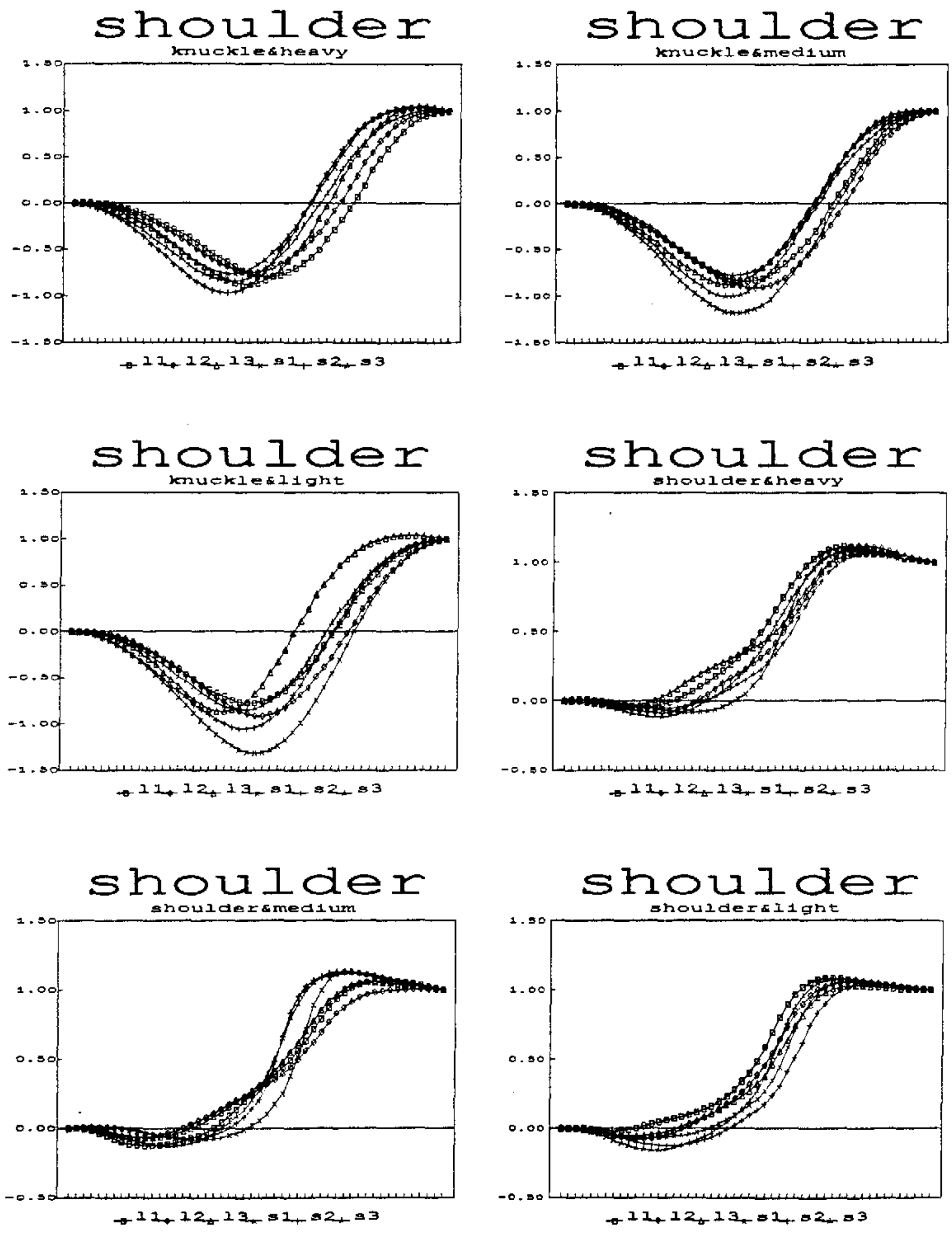

b. shoulder

Figure A.2 Continued

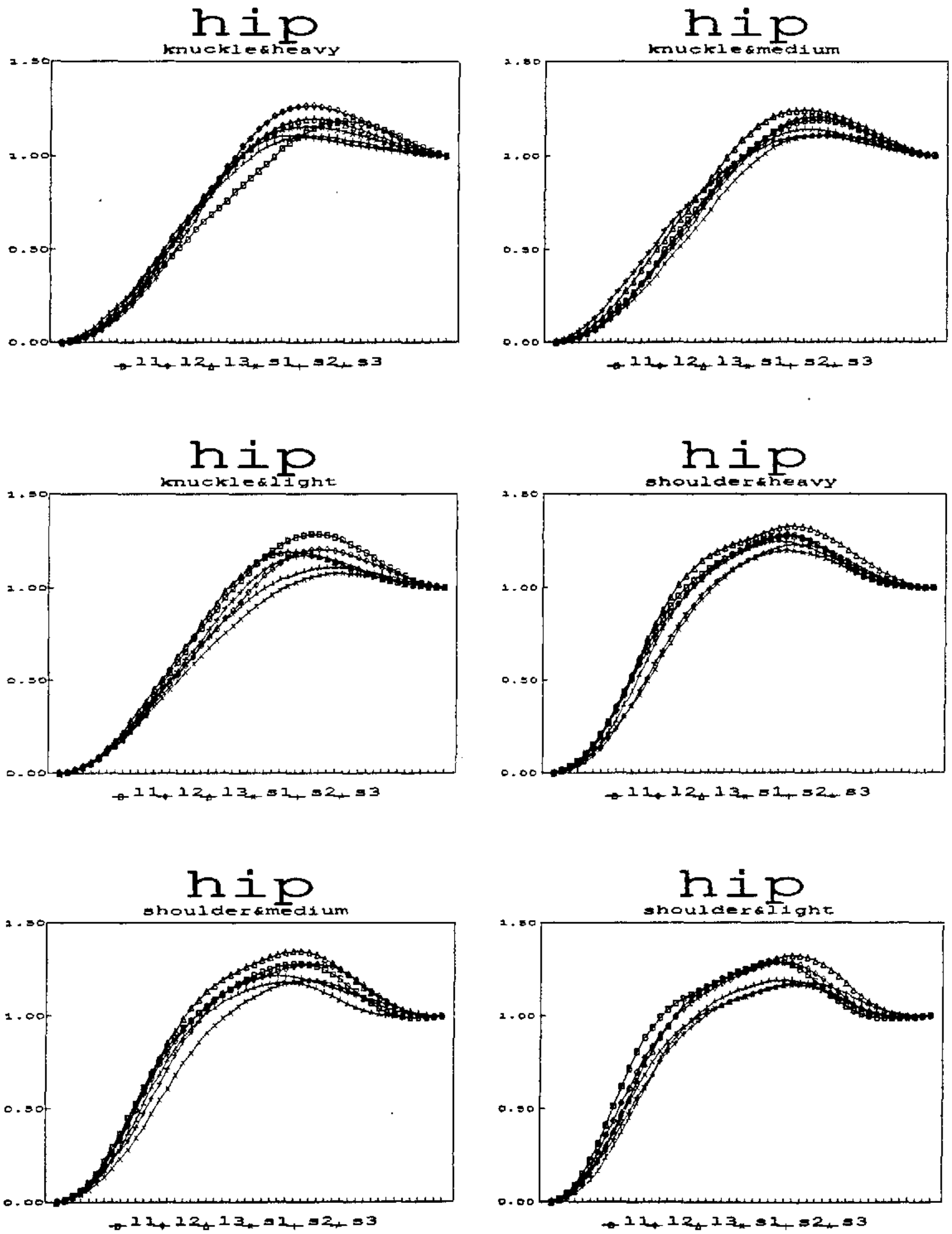

c. hip

Figure A.2 Continued

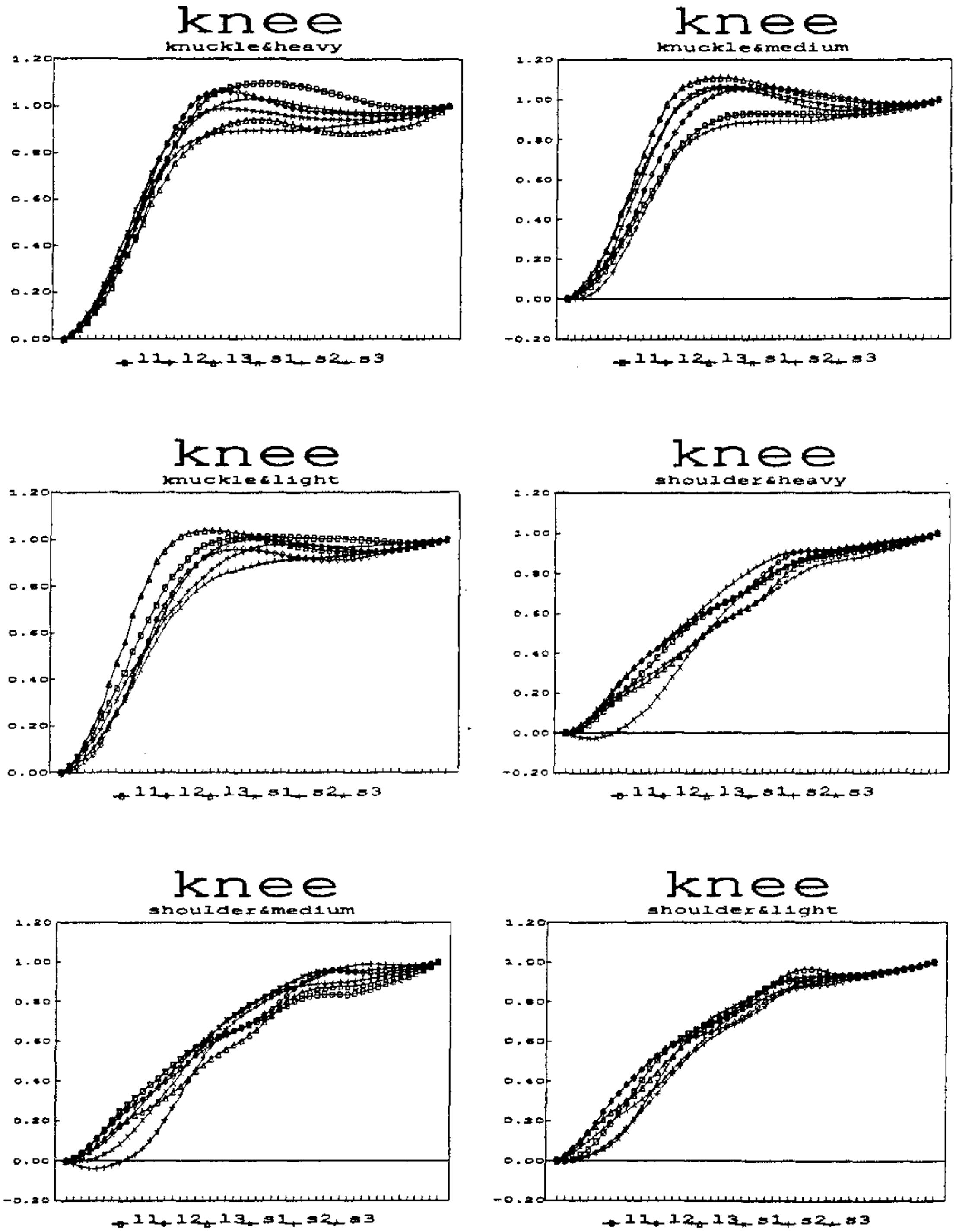

d. knee

Figure A.2 Continued

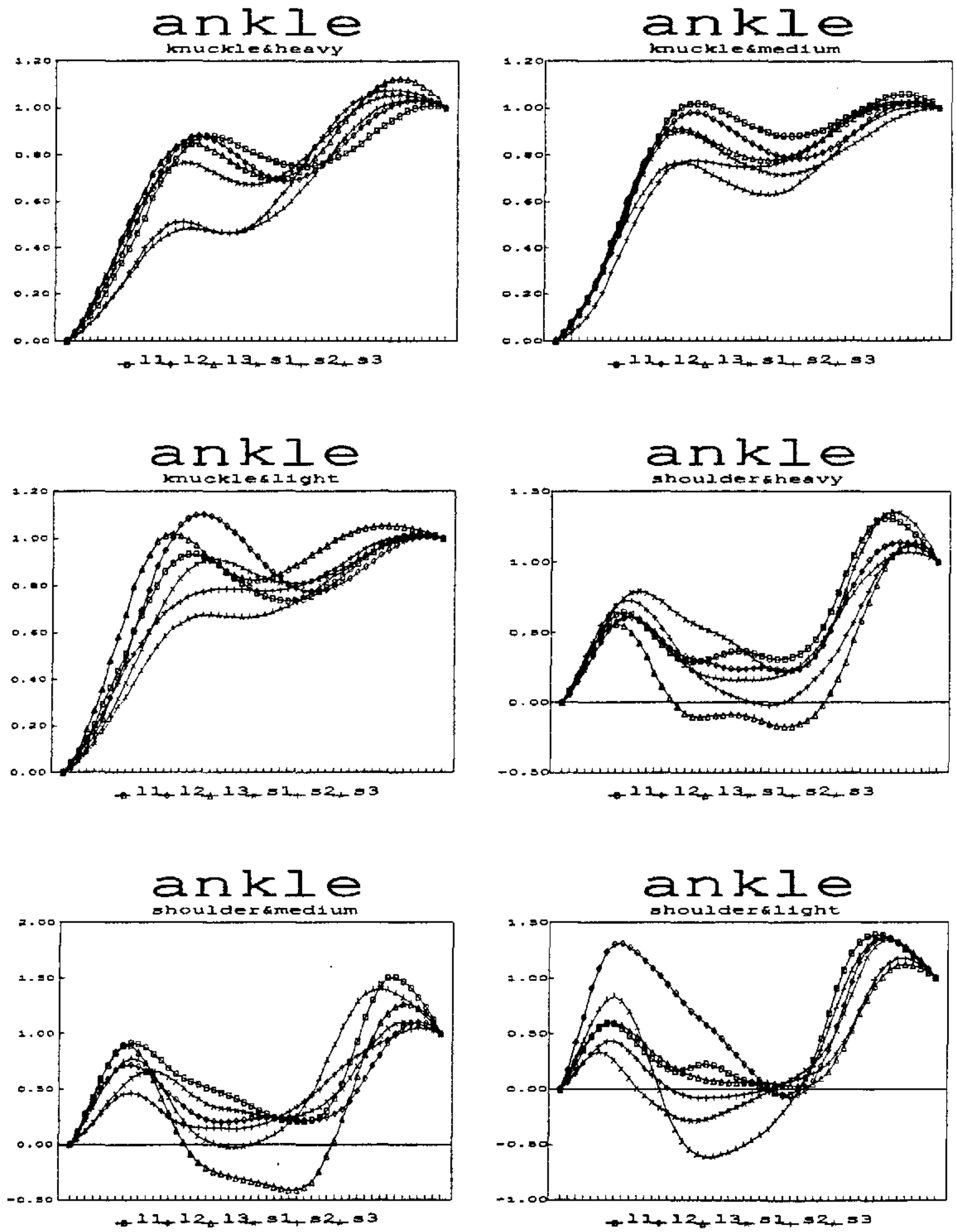

e. ankle

Figure A.2 Continued

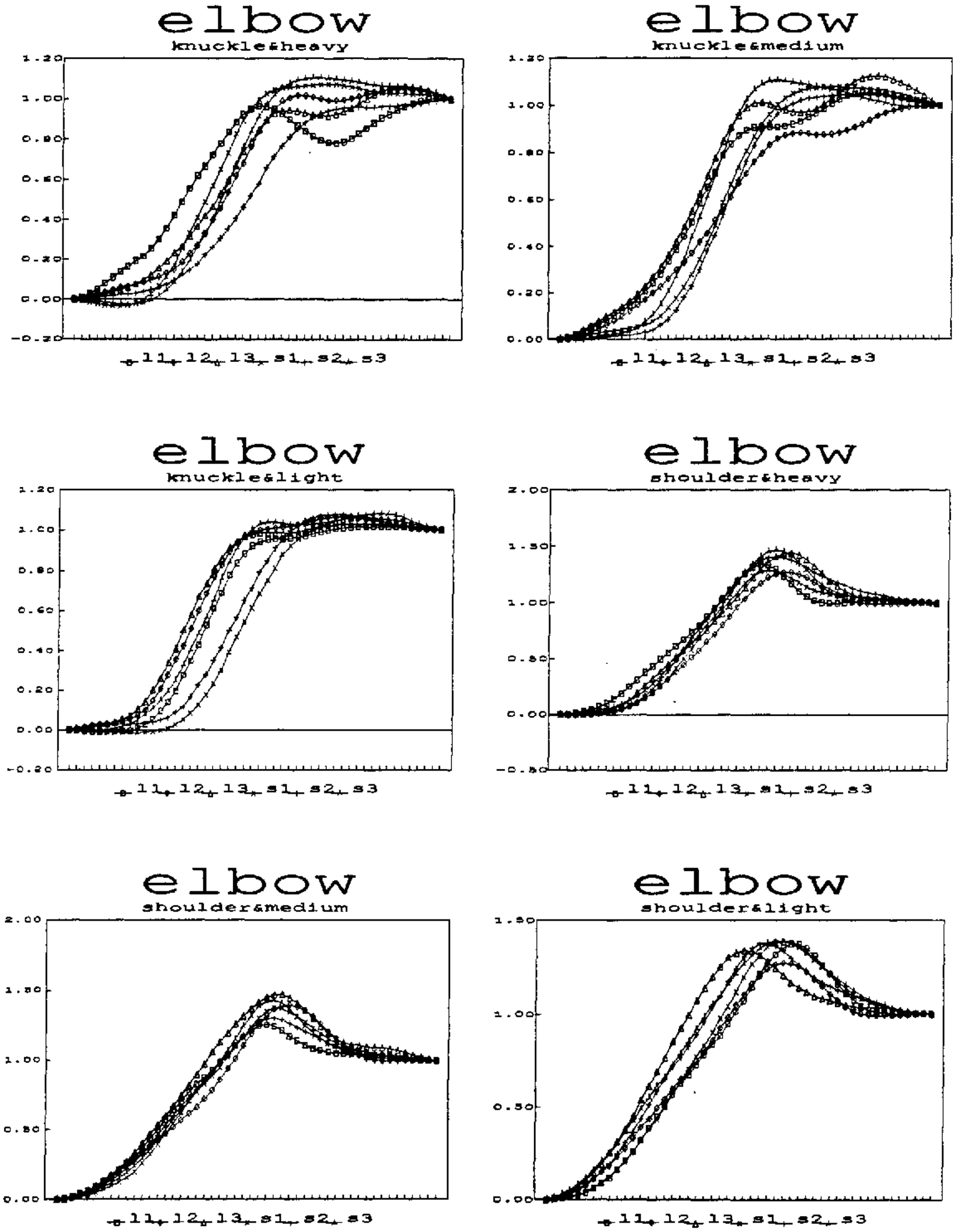

a. elbow

Figure A.3 Normalized trajectories of subject 4

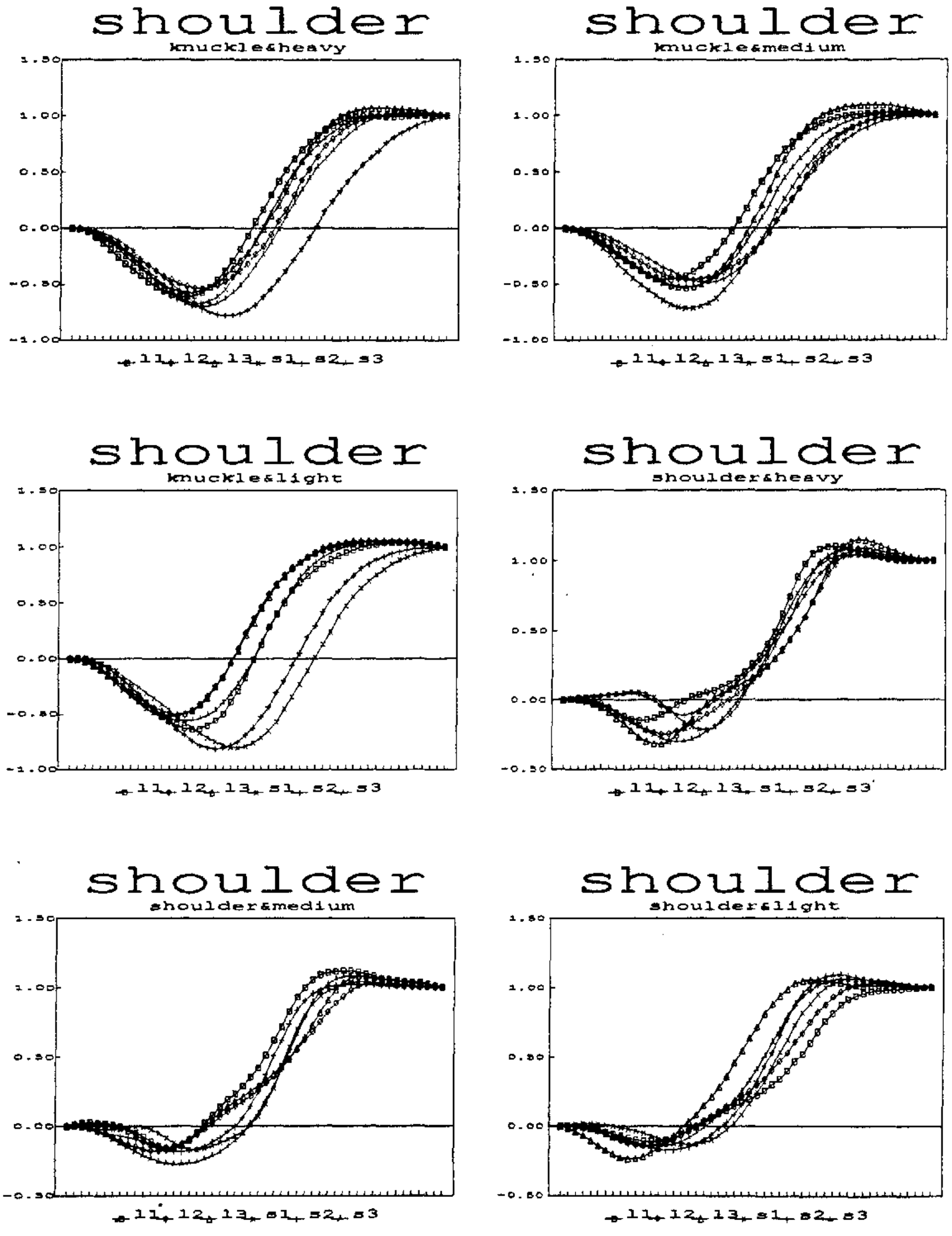

b. shoulder

Figure A.3 Continued

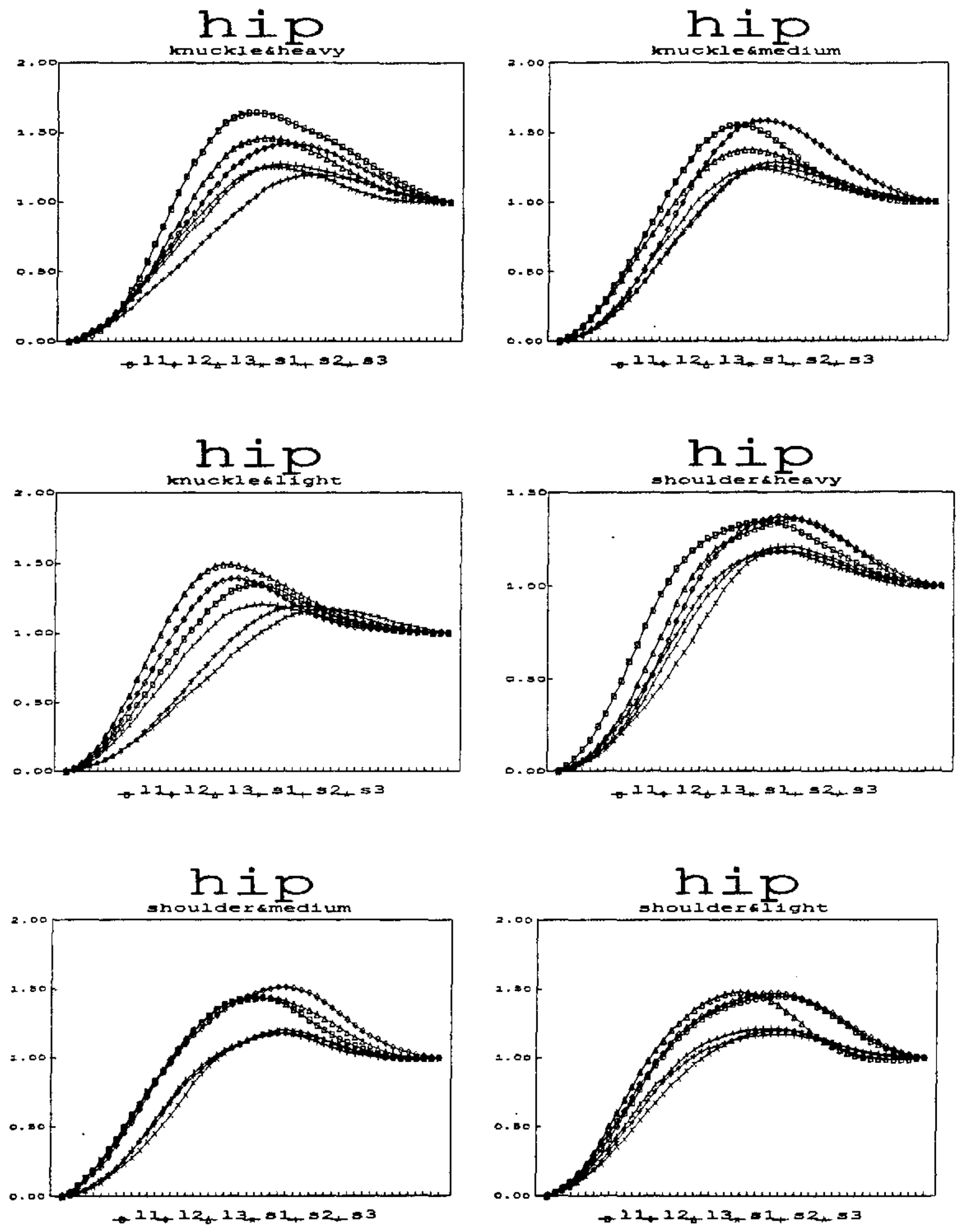

c. hip

Figure A.3 Continued

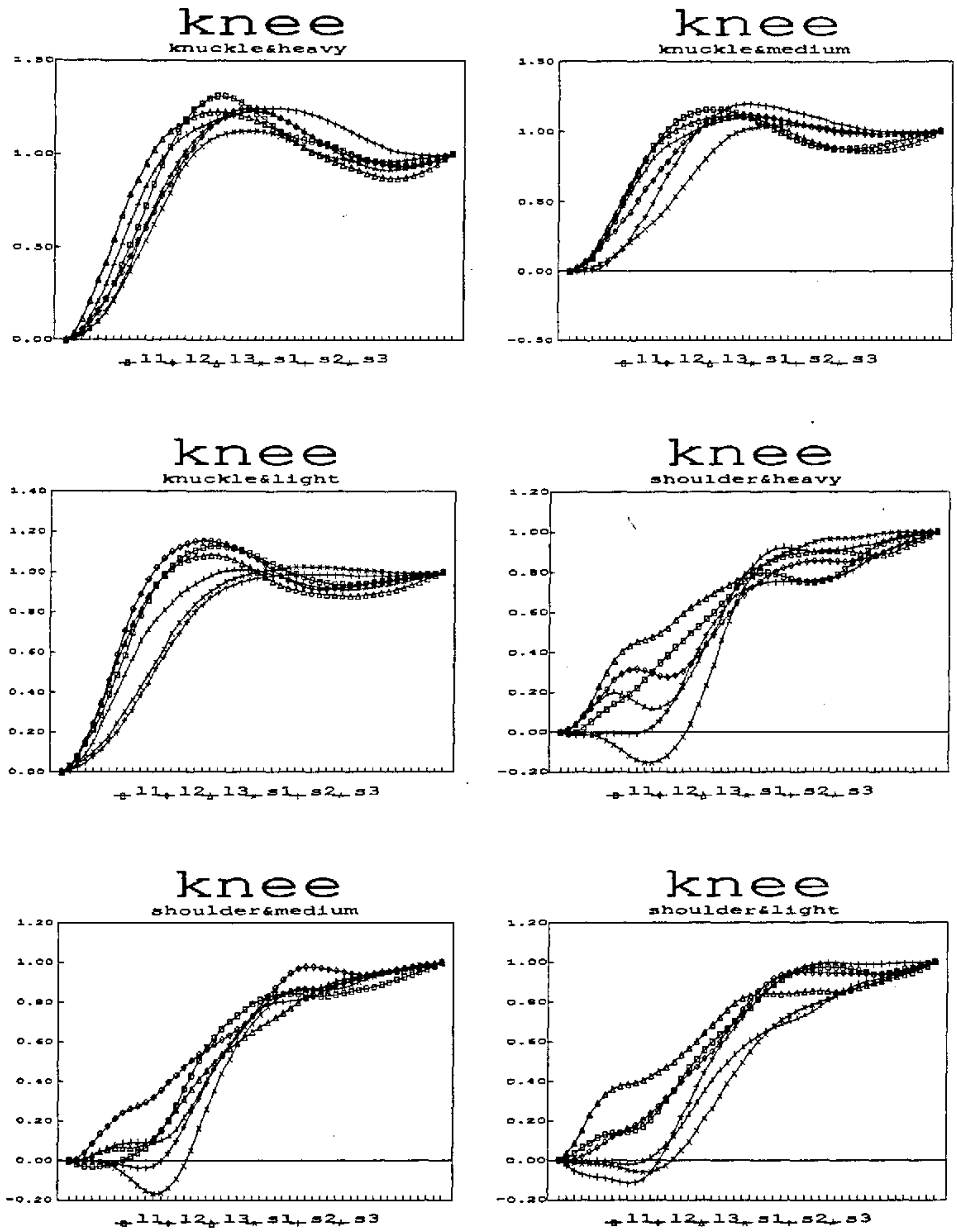

d. knee

Figure A.3 Continued

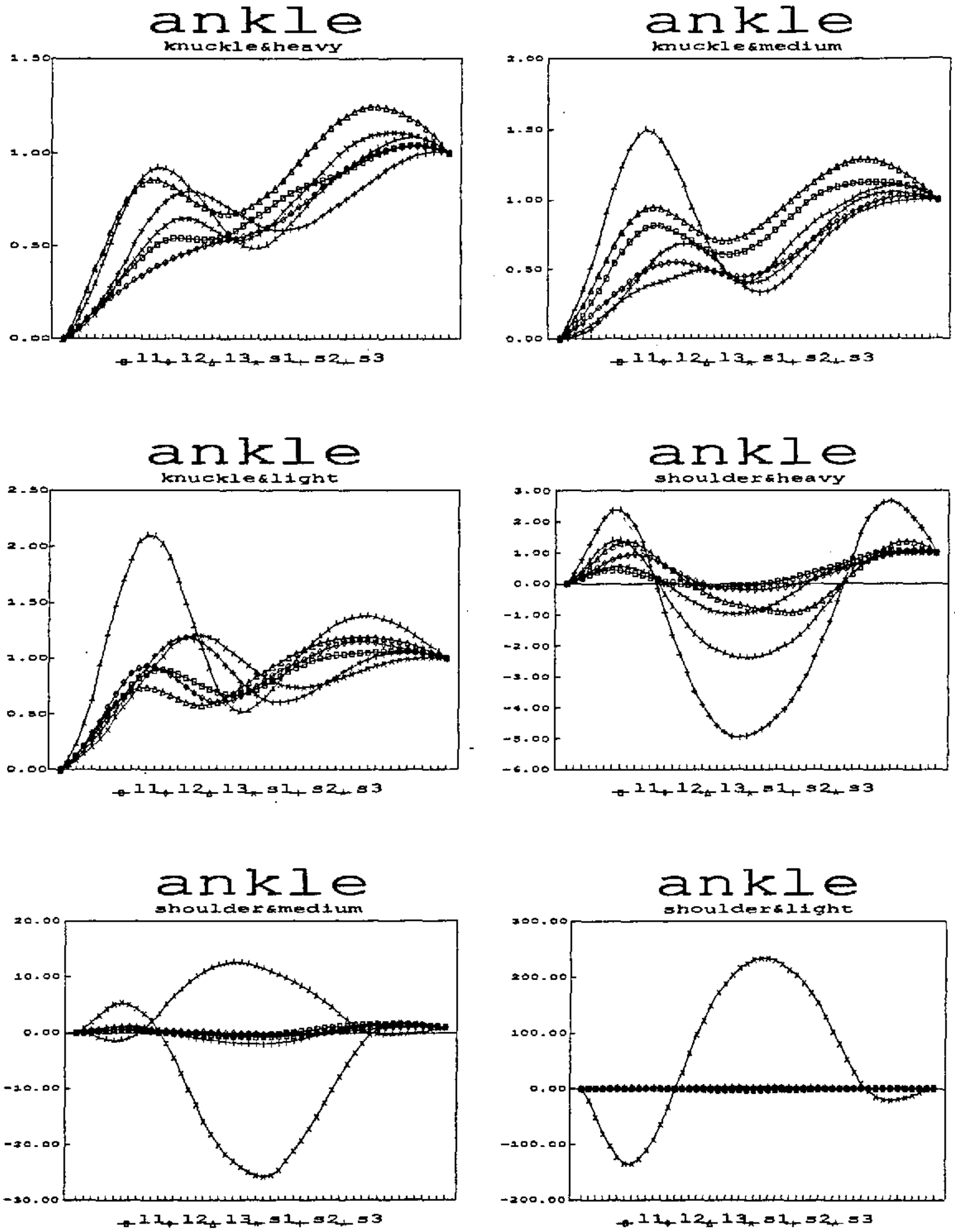

e. ankle

Figure A.3 Continued

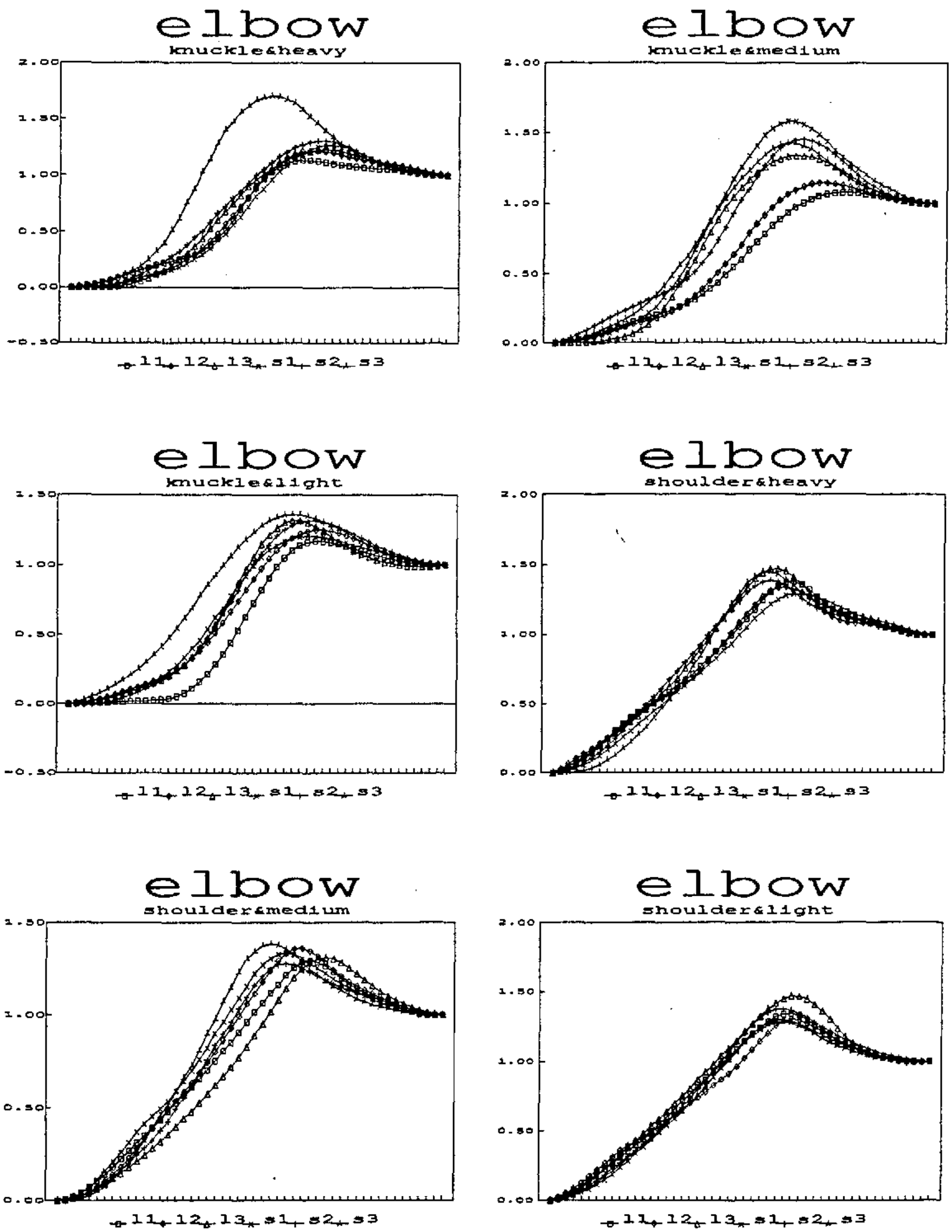

a. elbow

Figure A.4 Normalized trajectories of subject 5

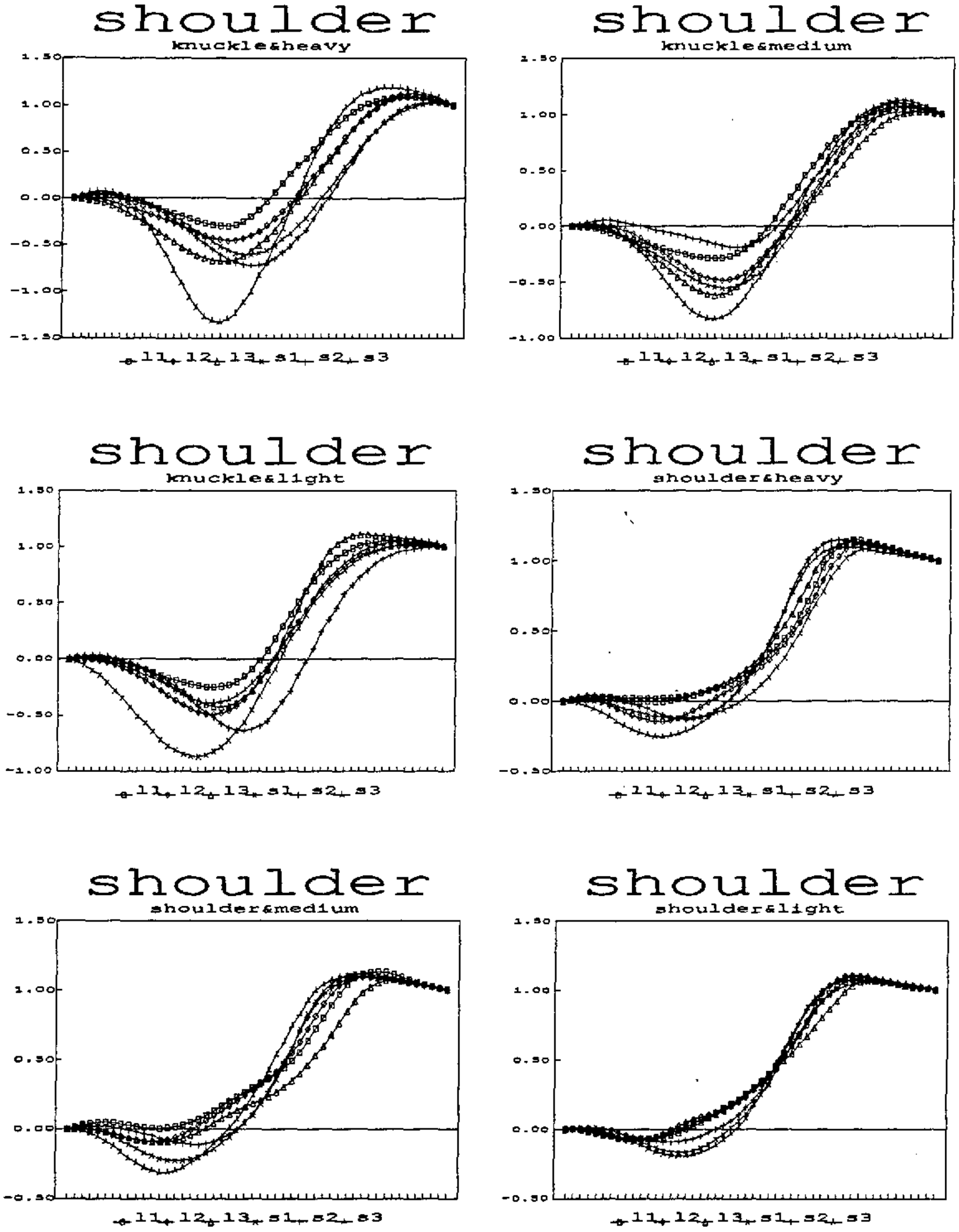

b. shoulder

Figure A.4 Continued

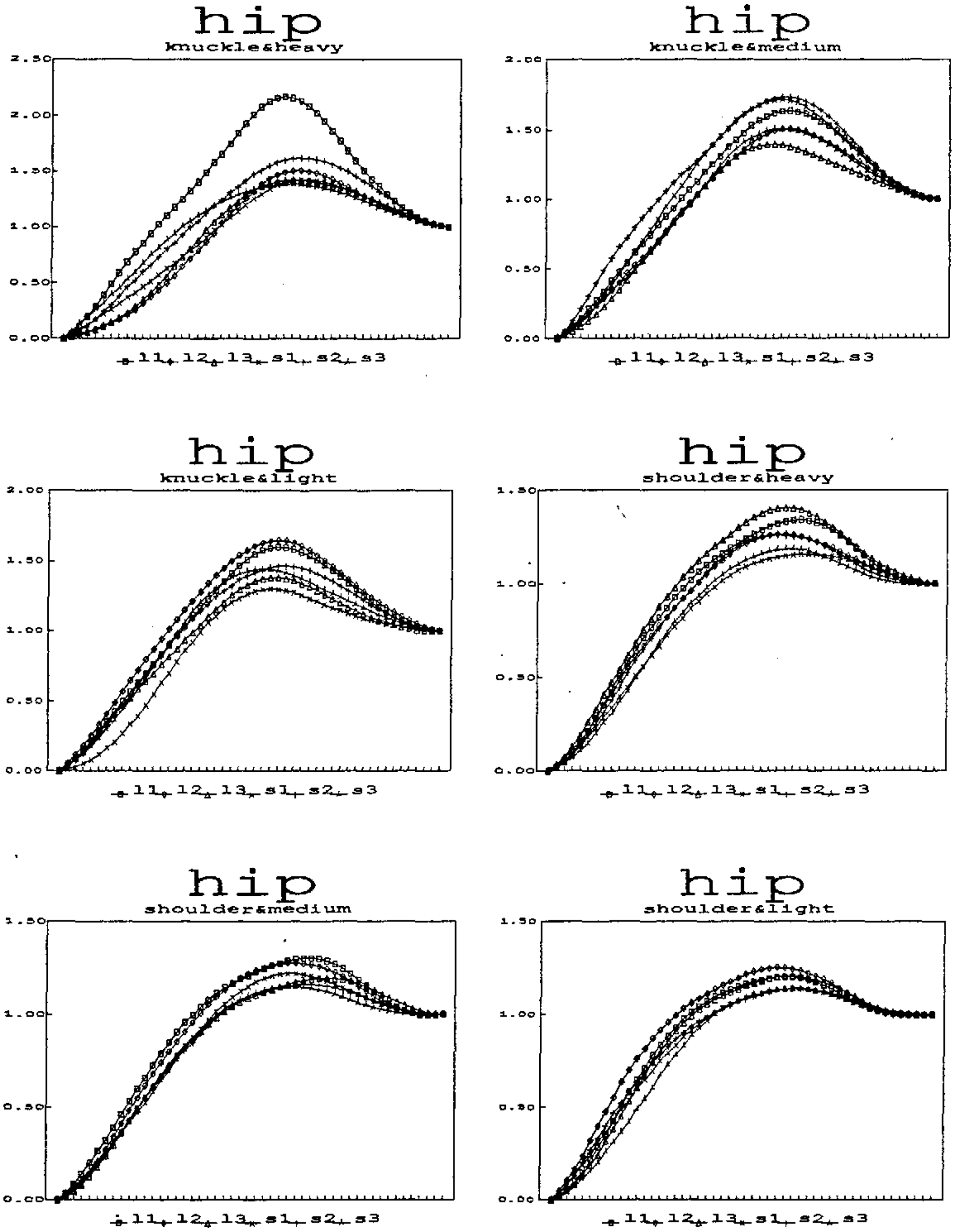

c. hip

Figure A.4 Continued

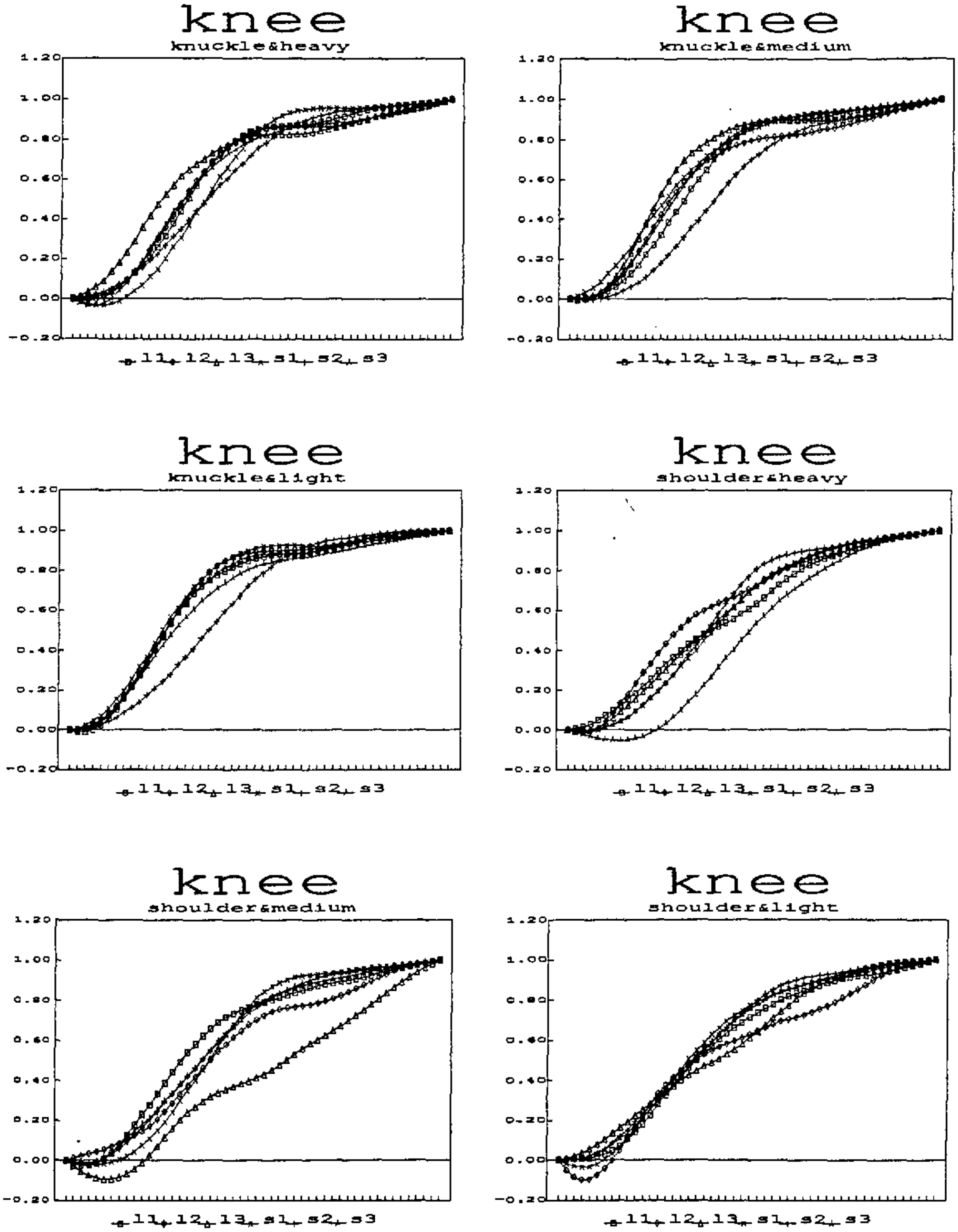

d. knee

Figure A.4 Continued

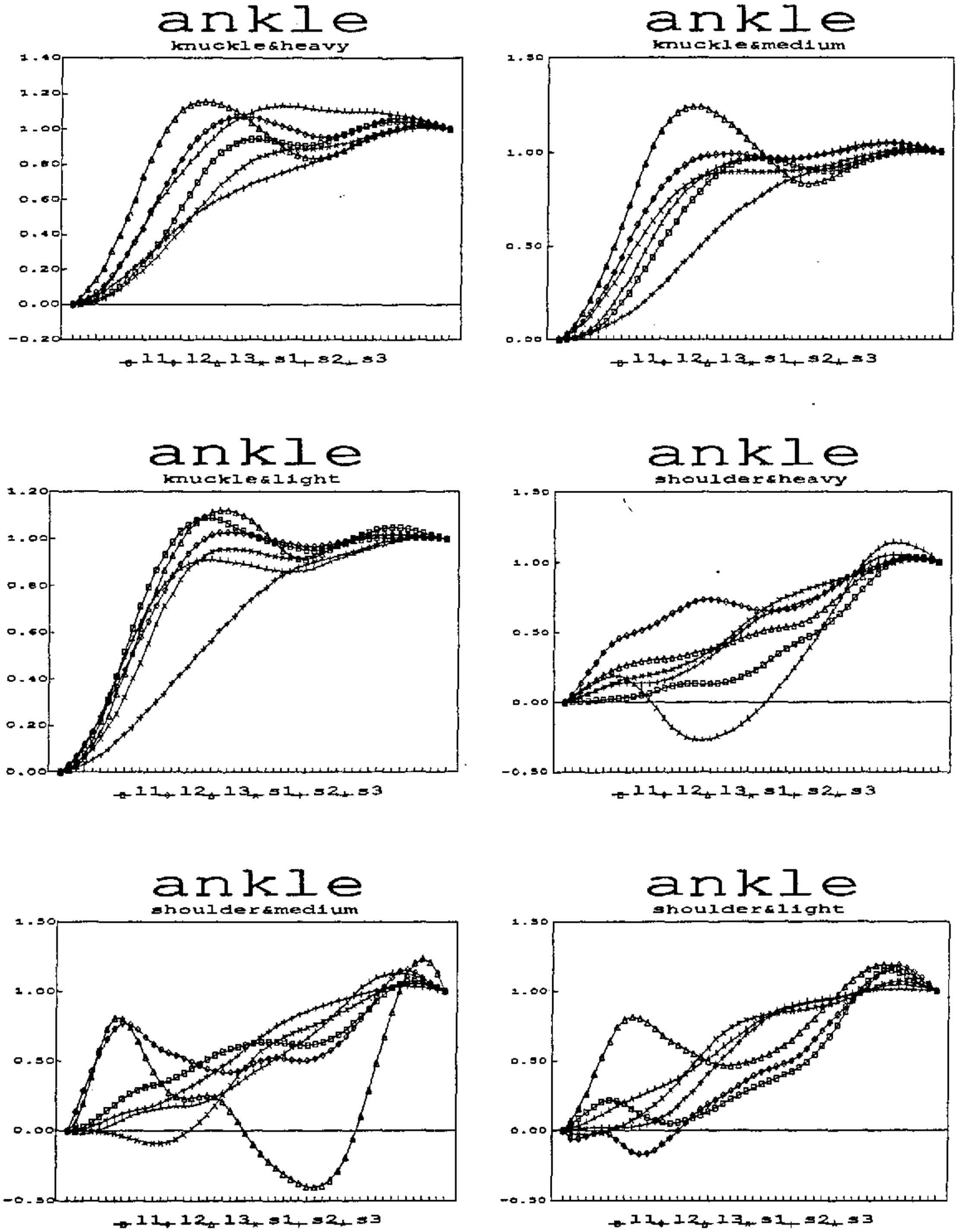

e. ankle

Figure A.4 Continued

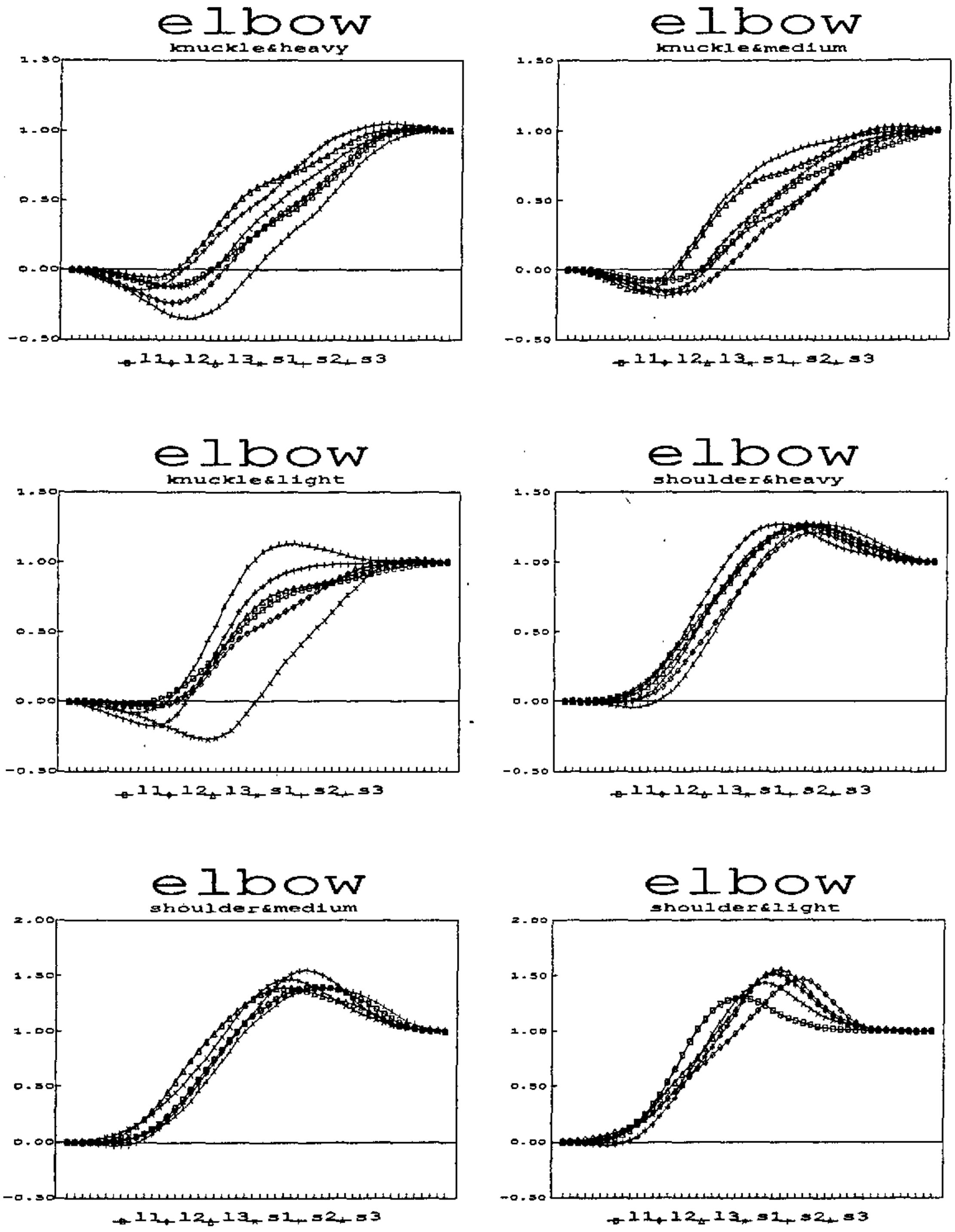

a. elbow

Figure A.5 Normalized trajectories of subject 6

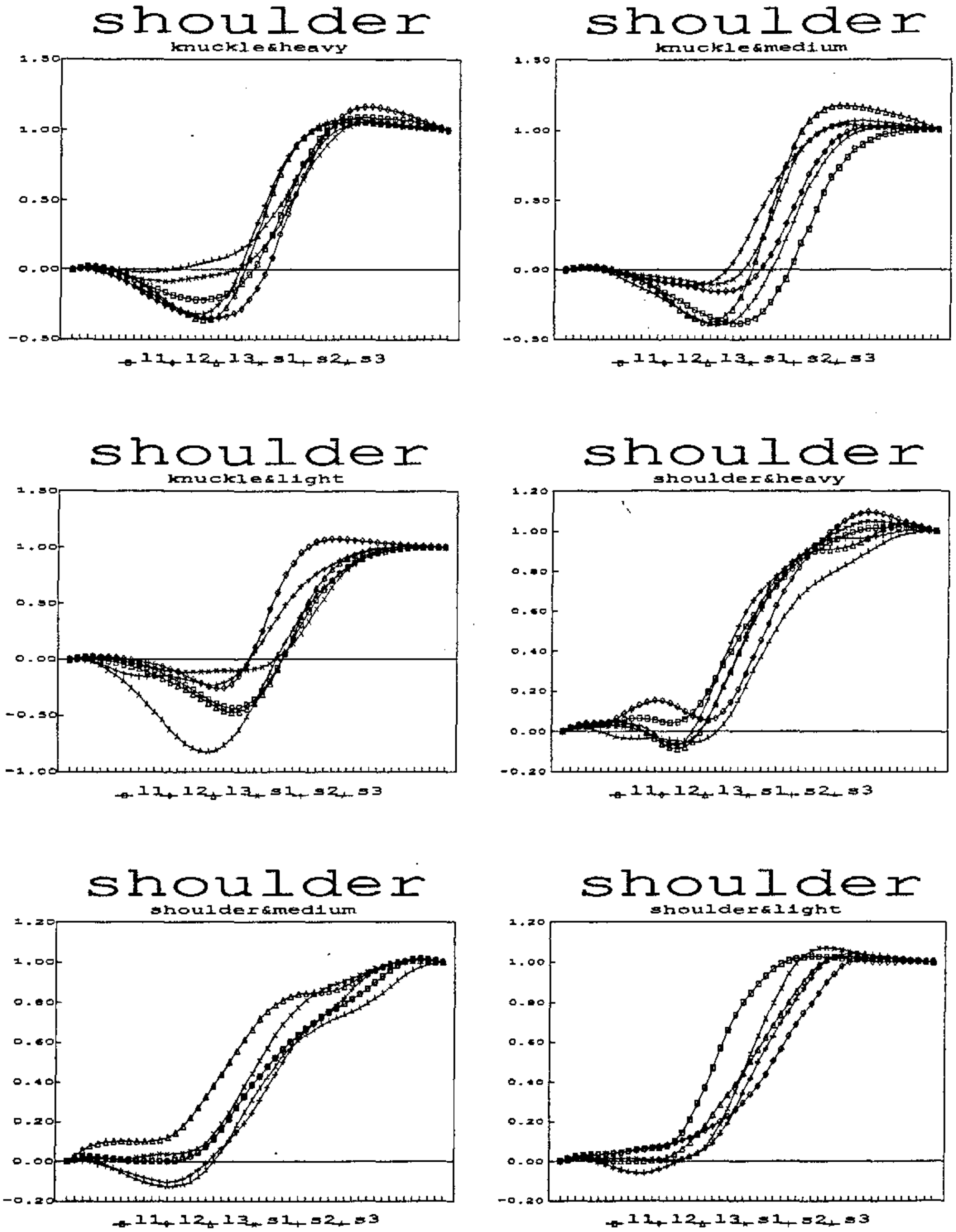

b. shoulder

Figure A.5 Continued

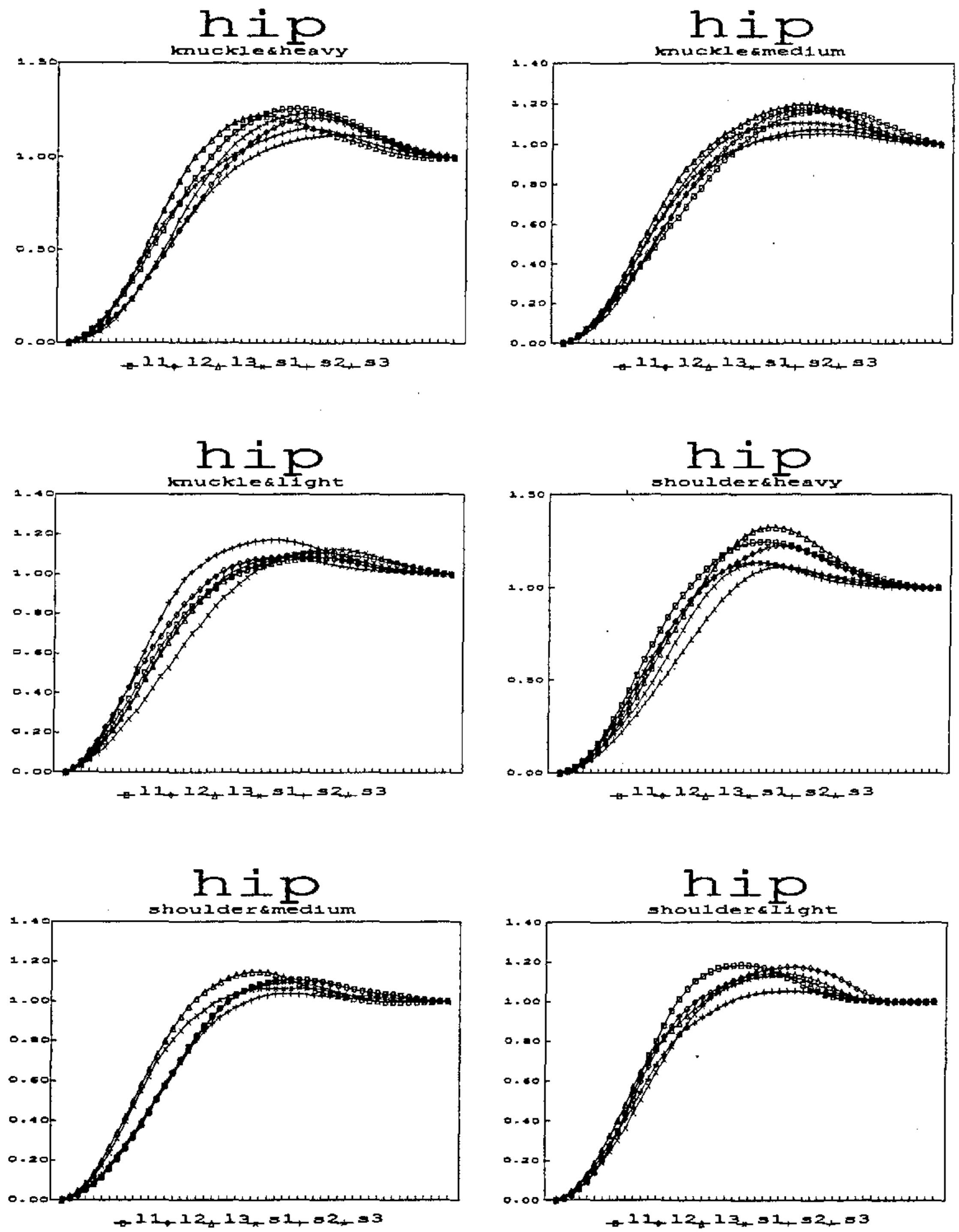

c. hip

Figure A.5 Continued

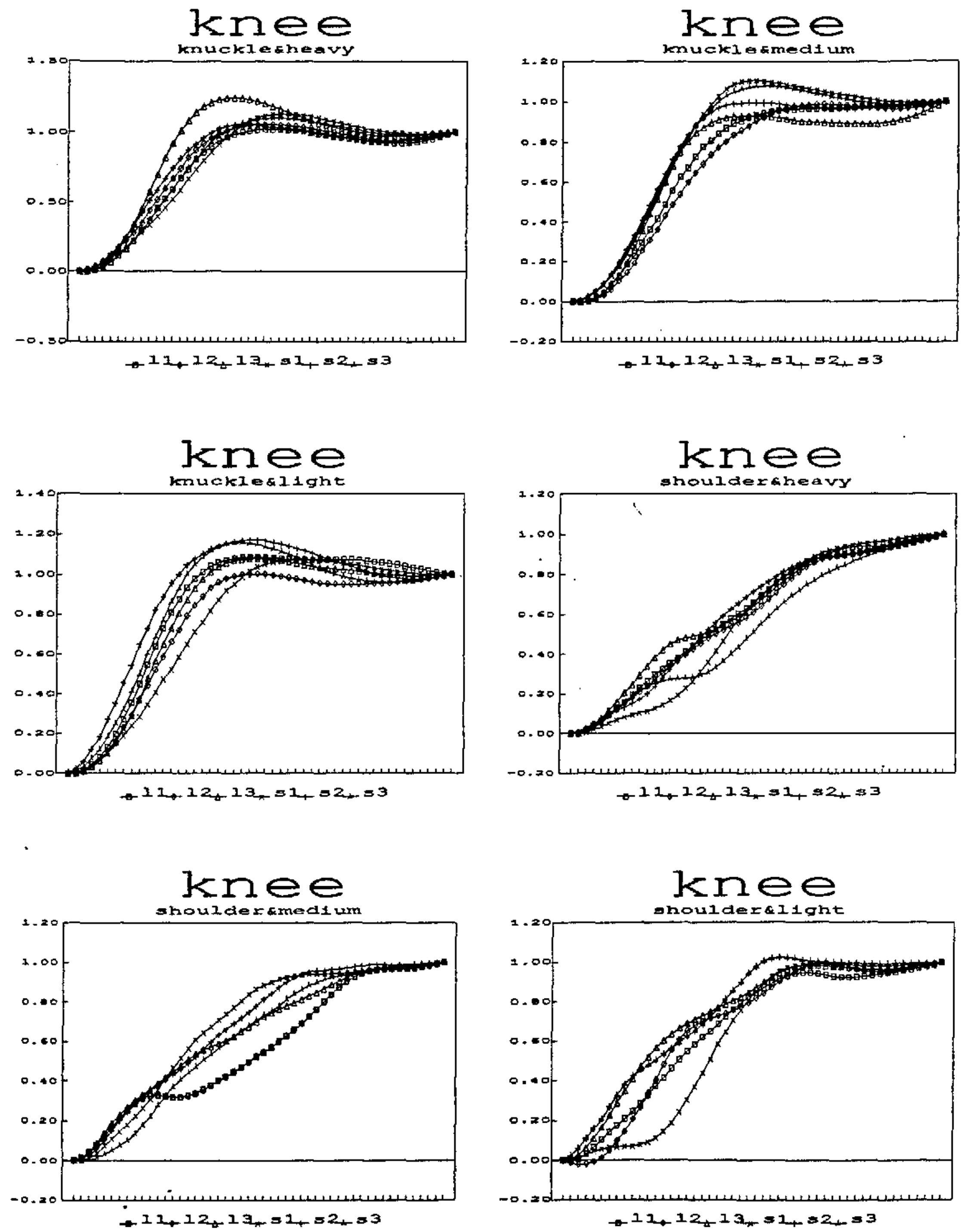

d. knee

Figure A.5 Continued

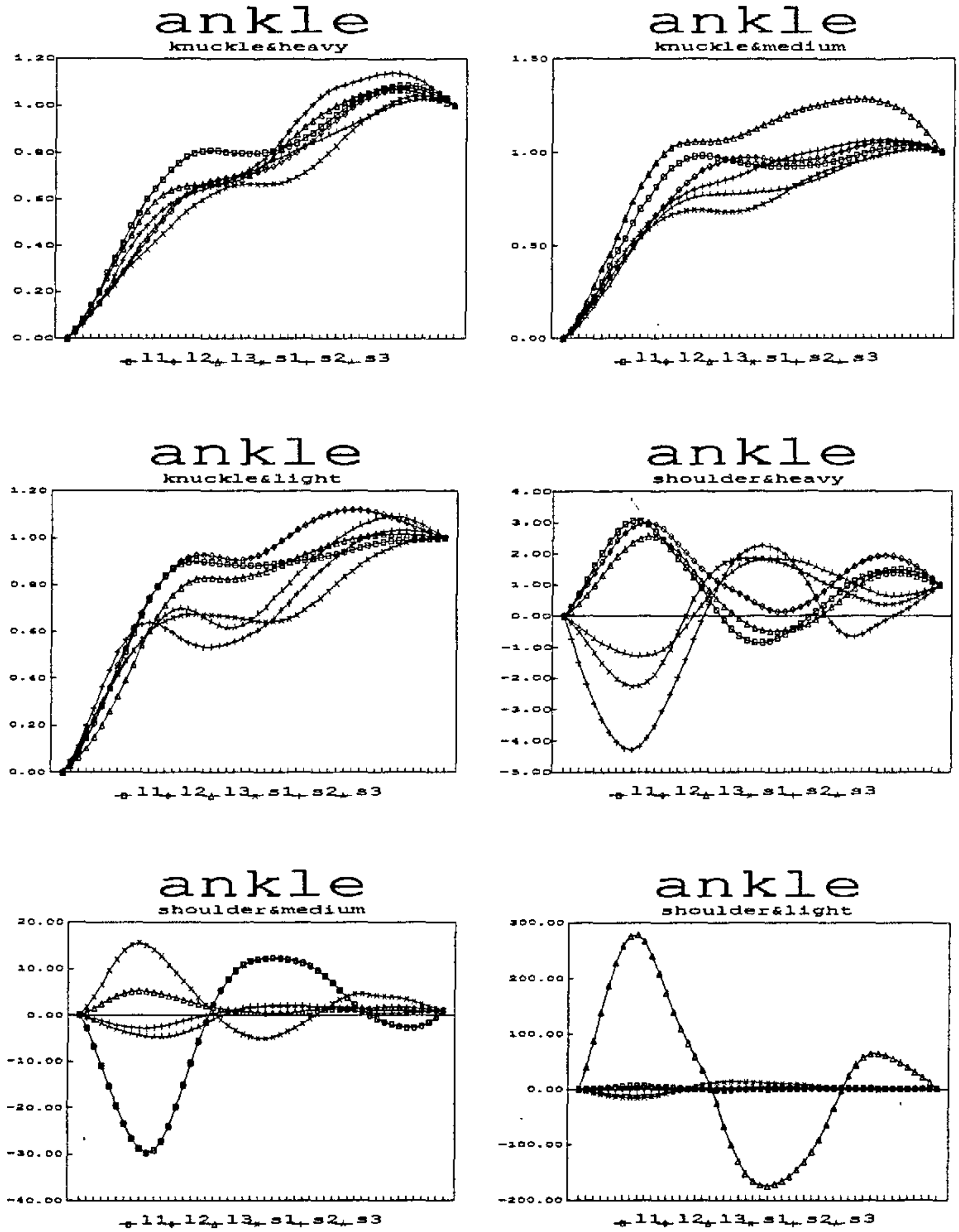

e. ankle

Figure A.5 Continued

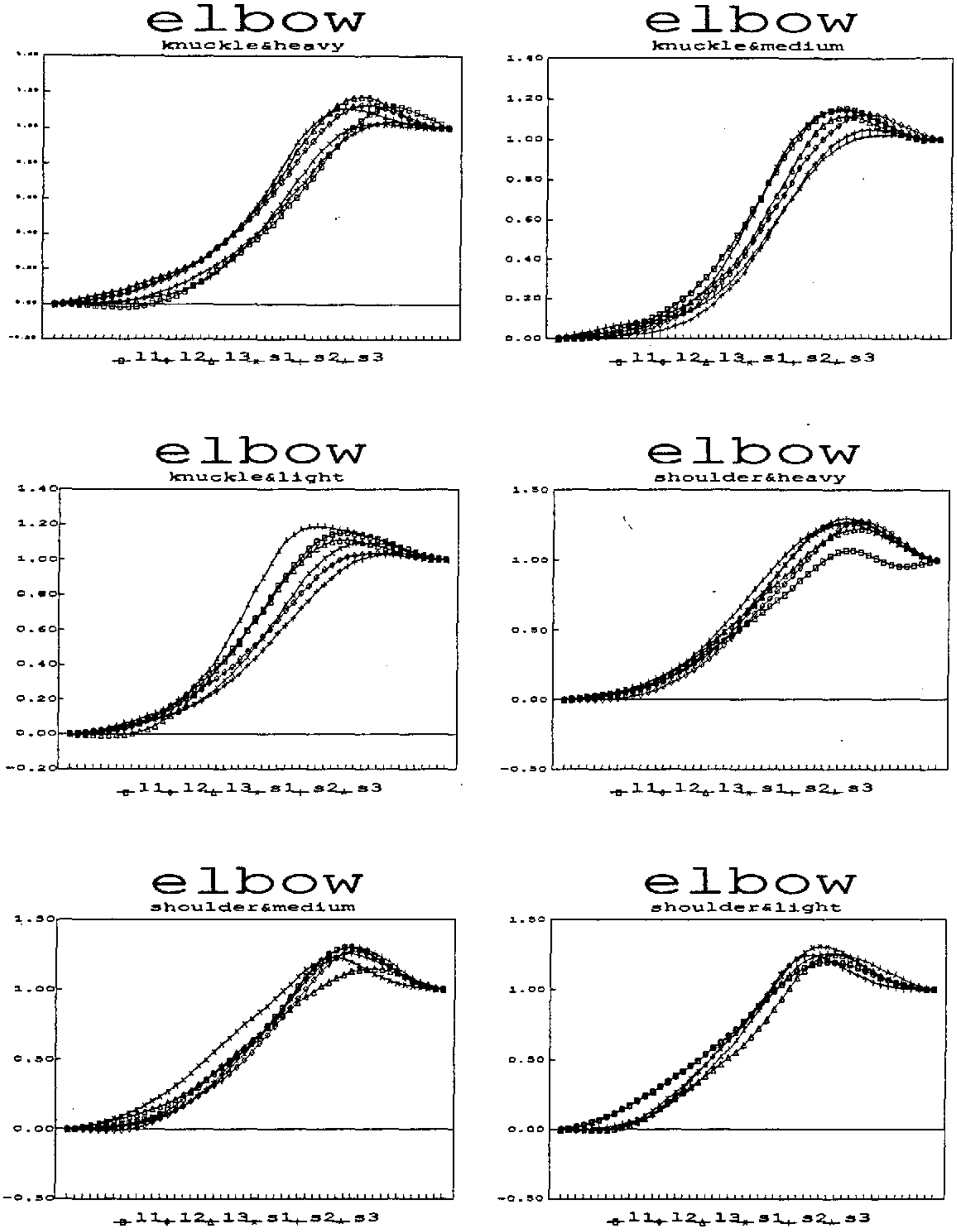

a. elbow

Figure A.6 Normalized trajectories of subject 7

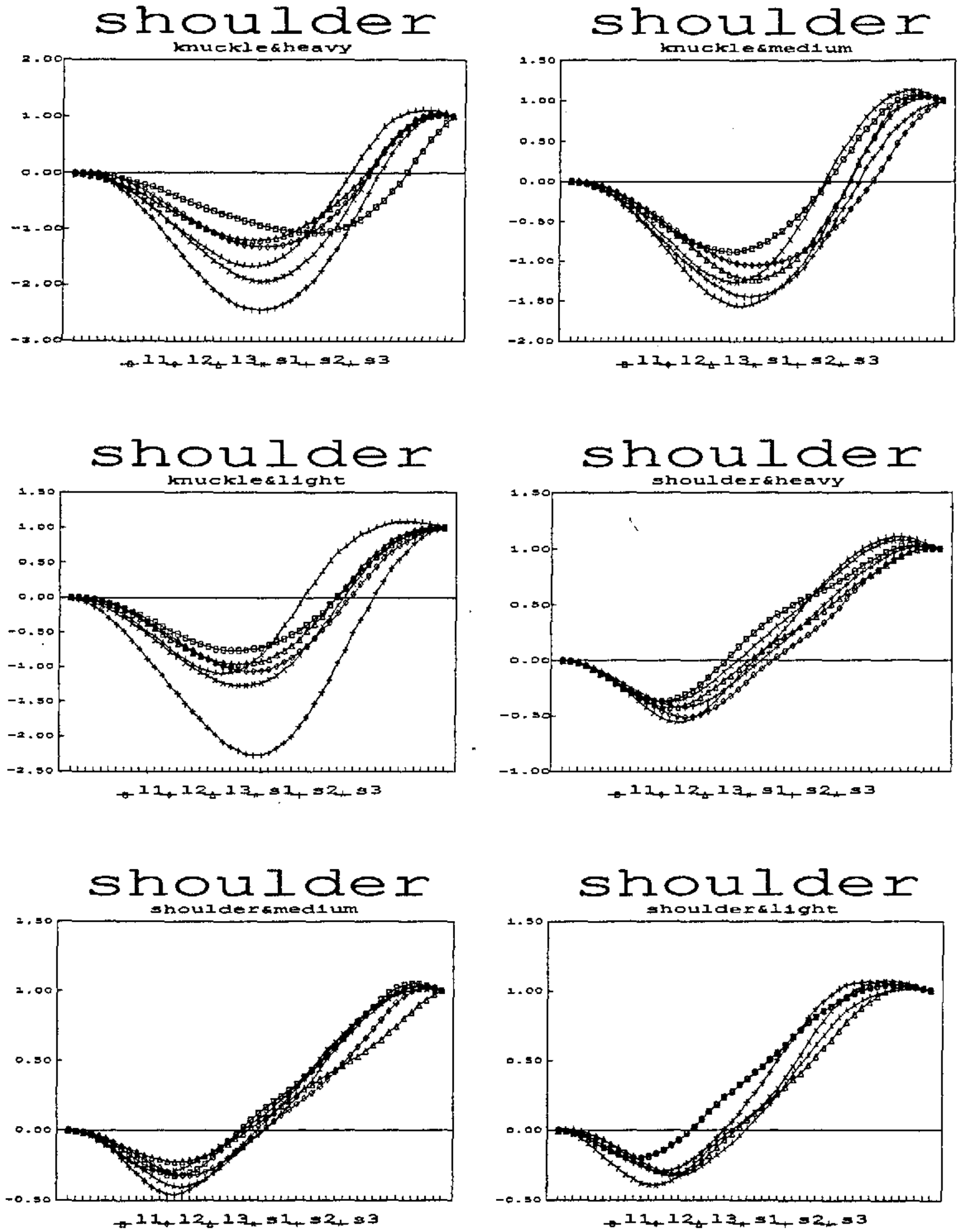

b. shoulder

Figure A.6 Continued

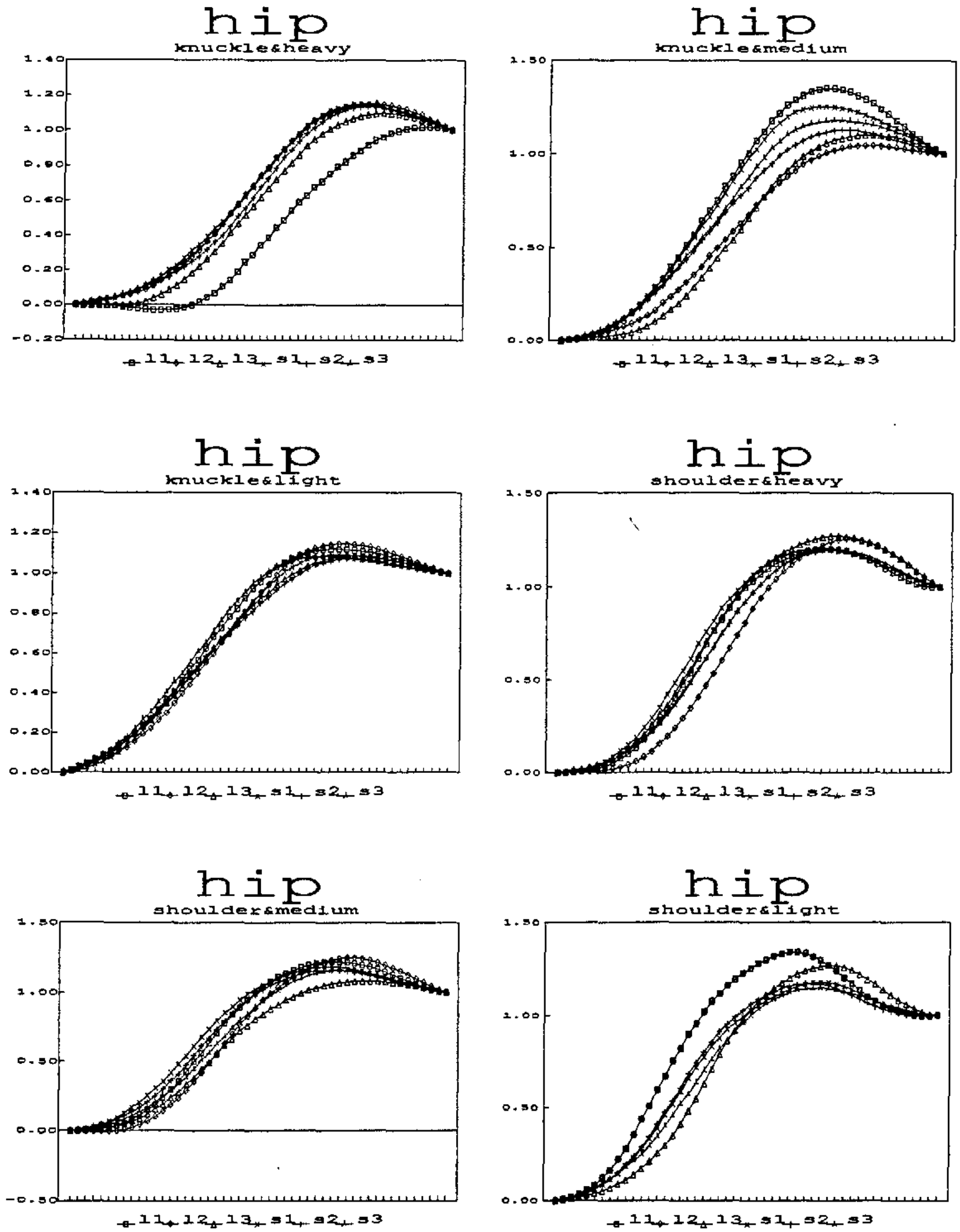

c. hip

Figure A.6 Continued

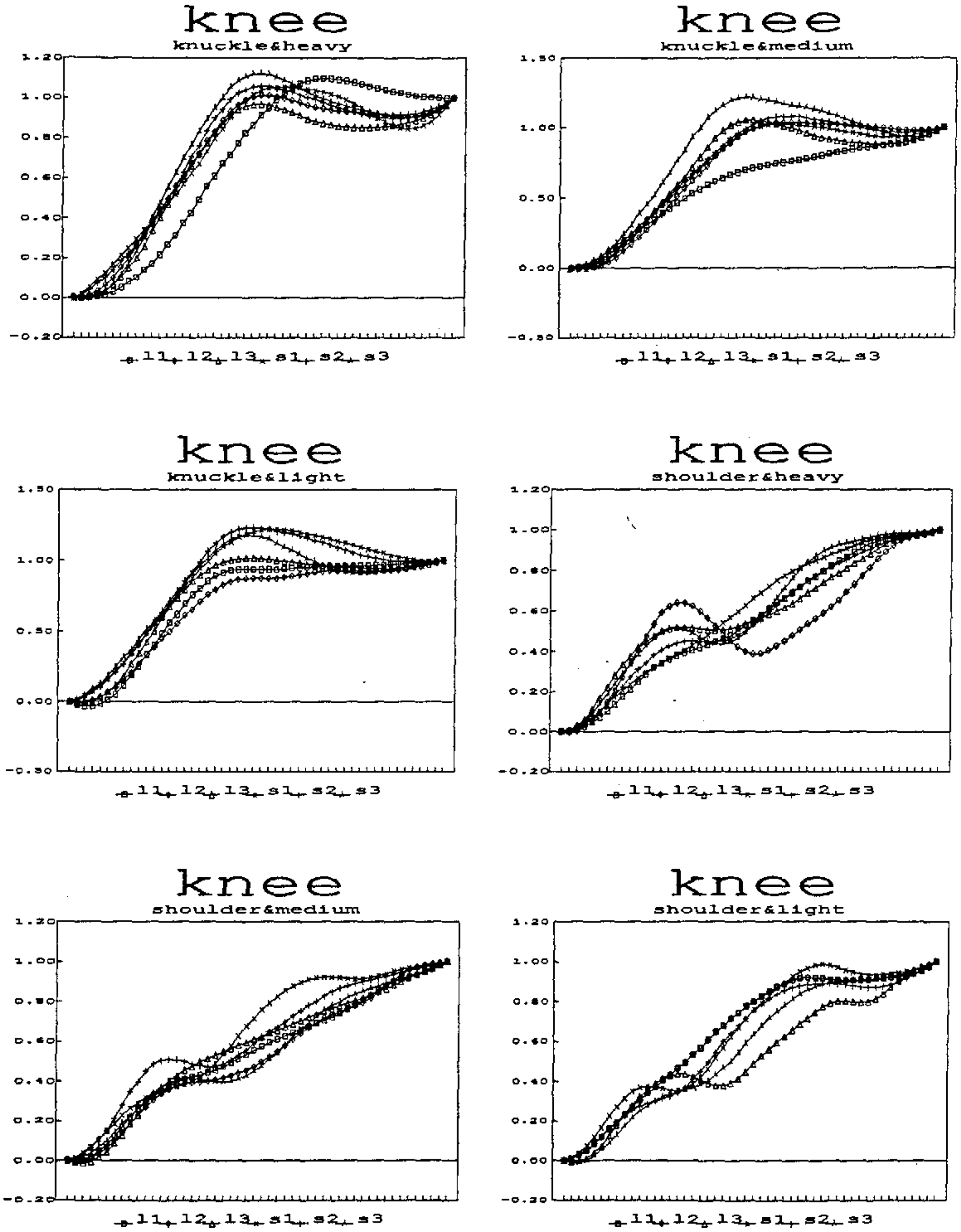

d. knee

Figure A.6 Continued

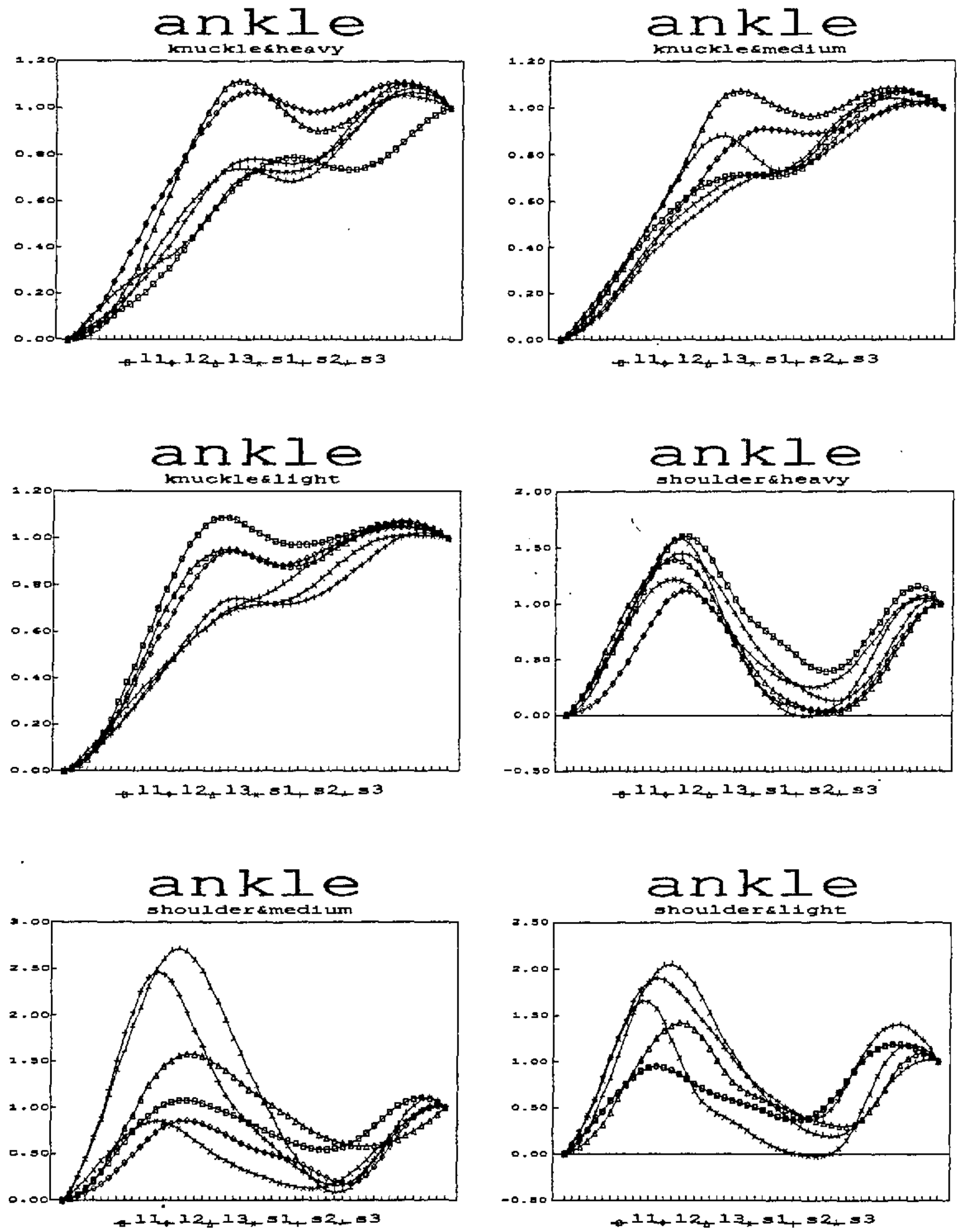

e. ankle

Figure A.6 Continued

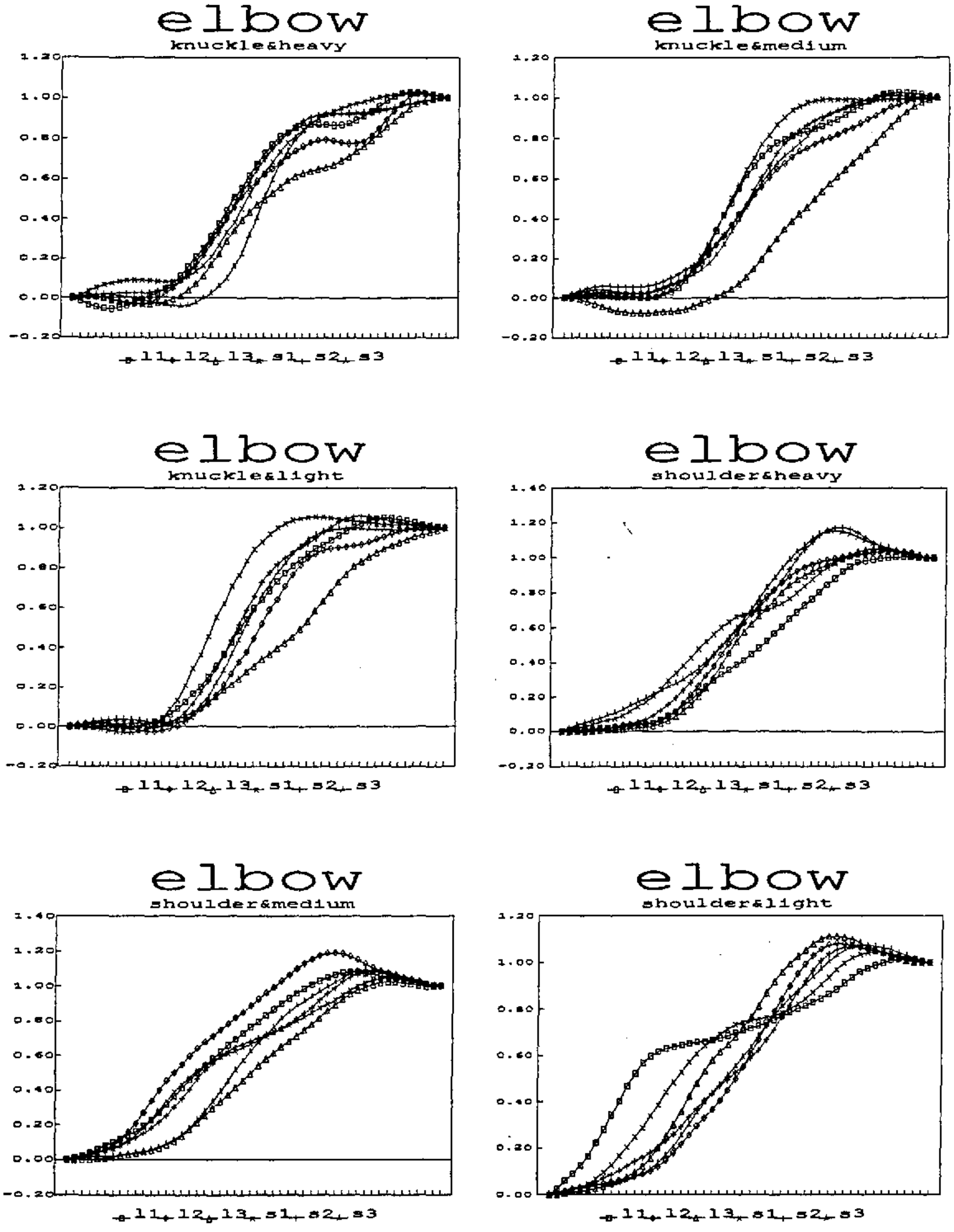

a. elbow

Figure A.7 Normalized trajectories of subject 8

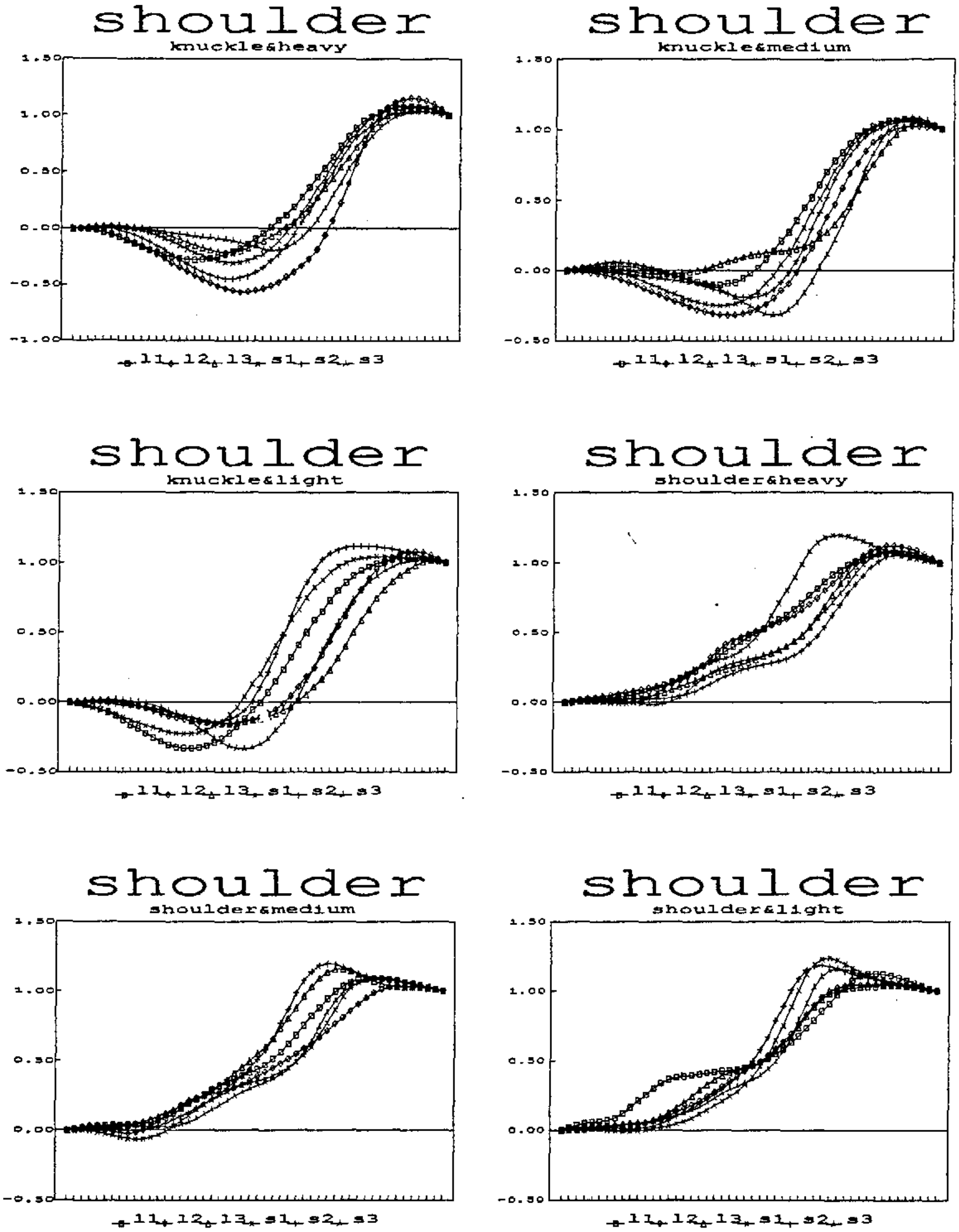

b. shoulder

Figure A.7 Continued

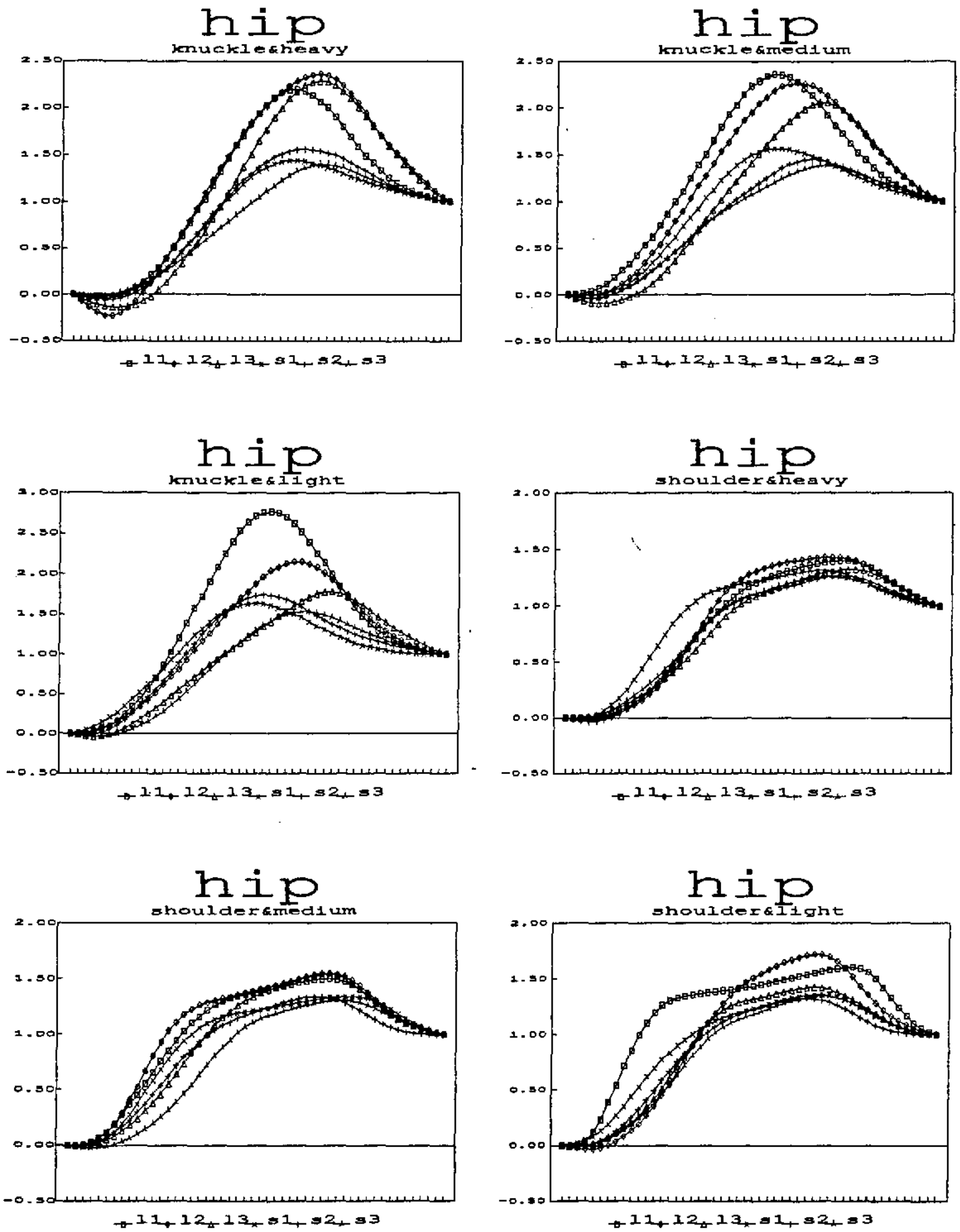

c. hip

Figure A.7 Continued

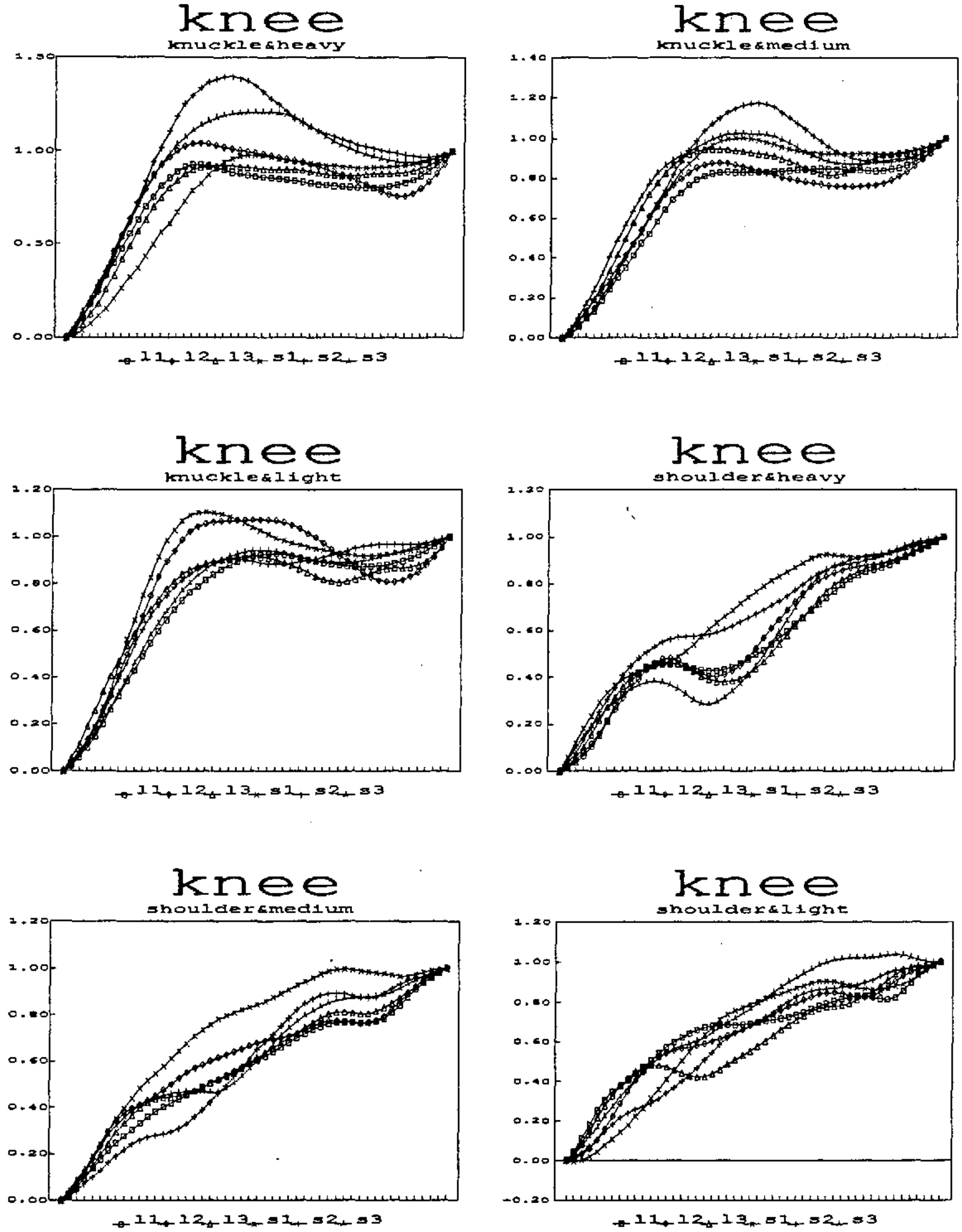

d. knee

Figure A.7 Continued

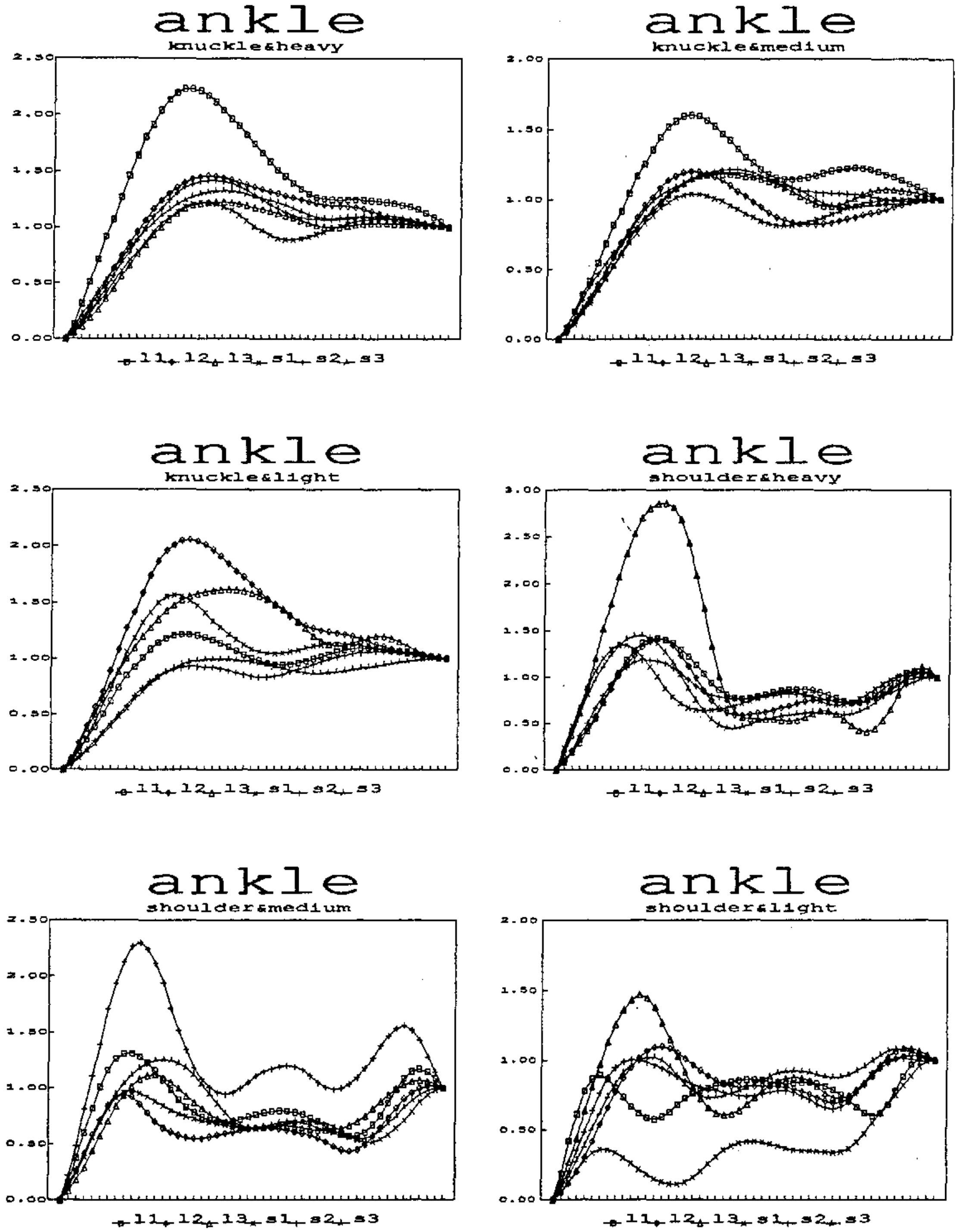

e. ankle

Figure A.7 Continued

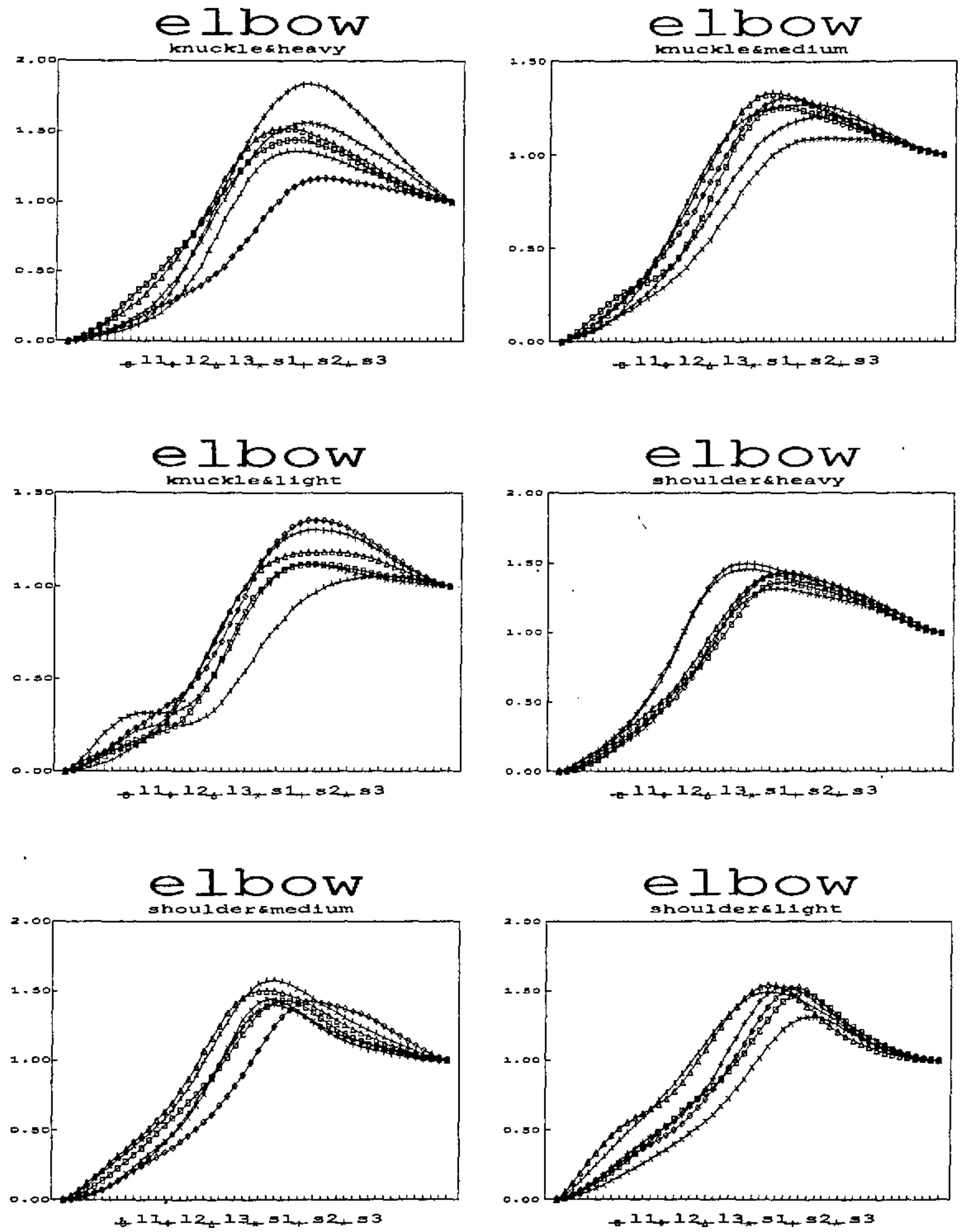

a. elbow

Figure A.8 Normalized trajectories of subject 9, who performed squat lifts

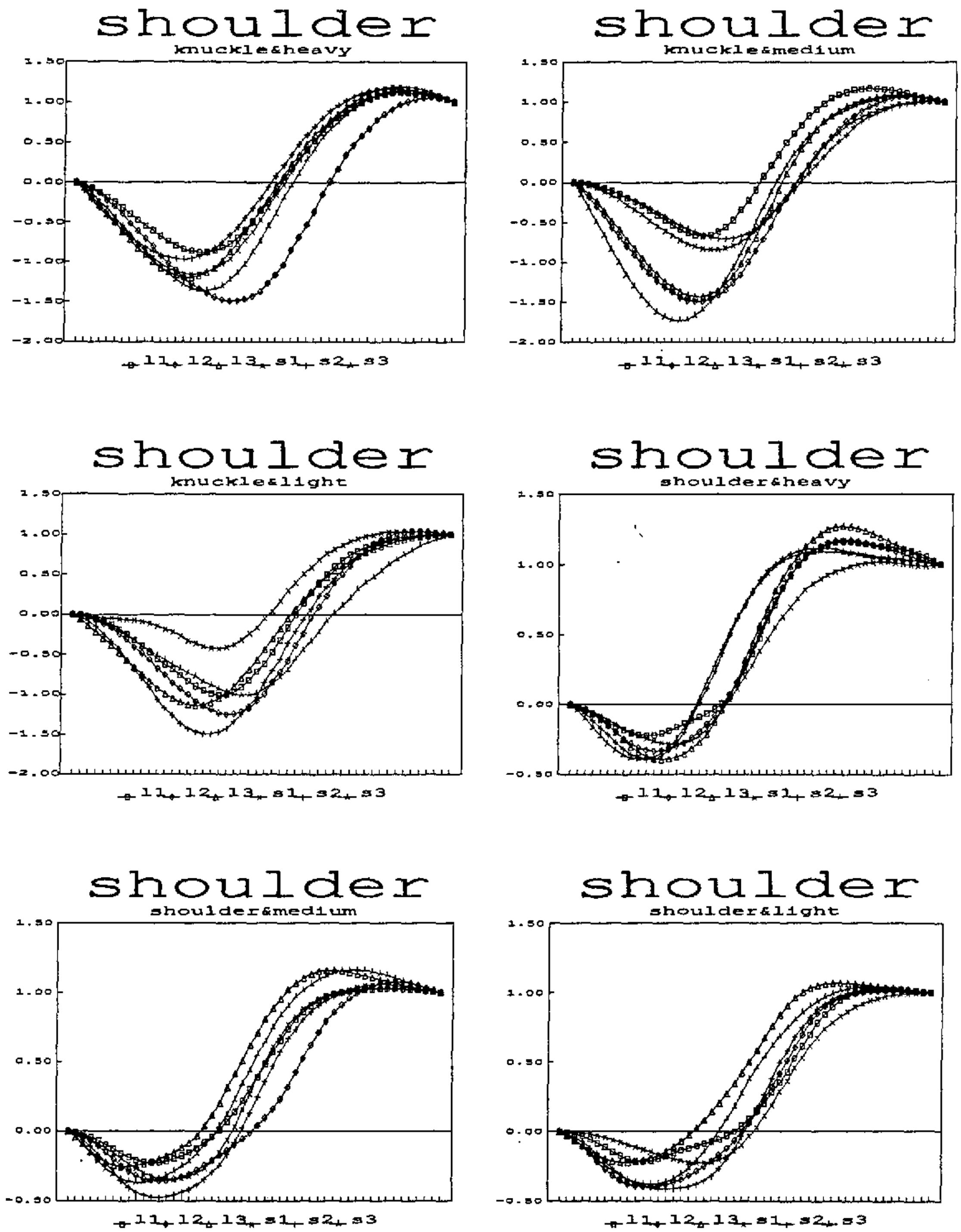

b. shoulder

Figure A.8 Continued

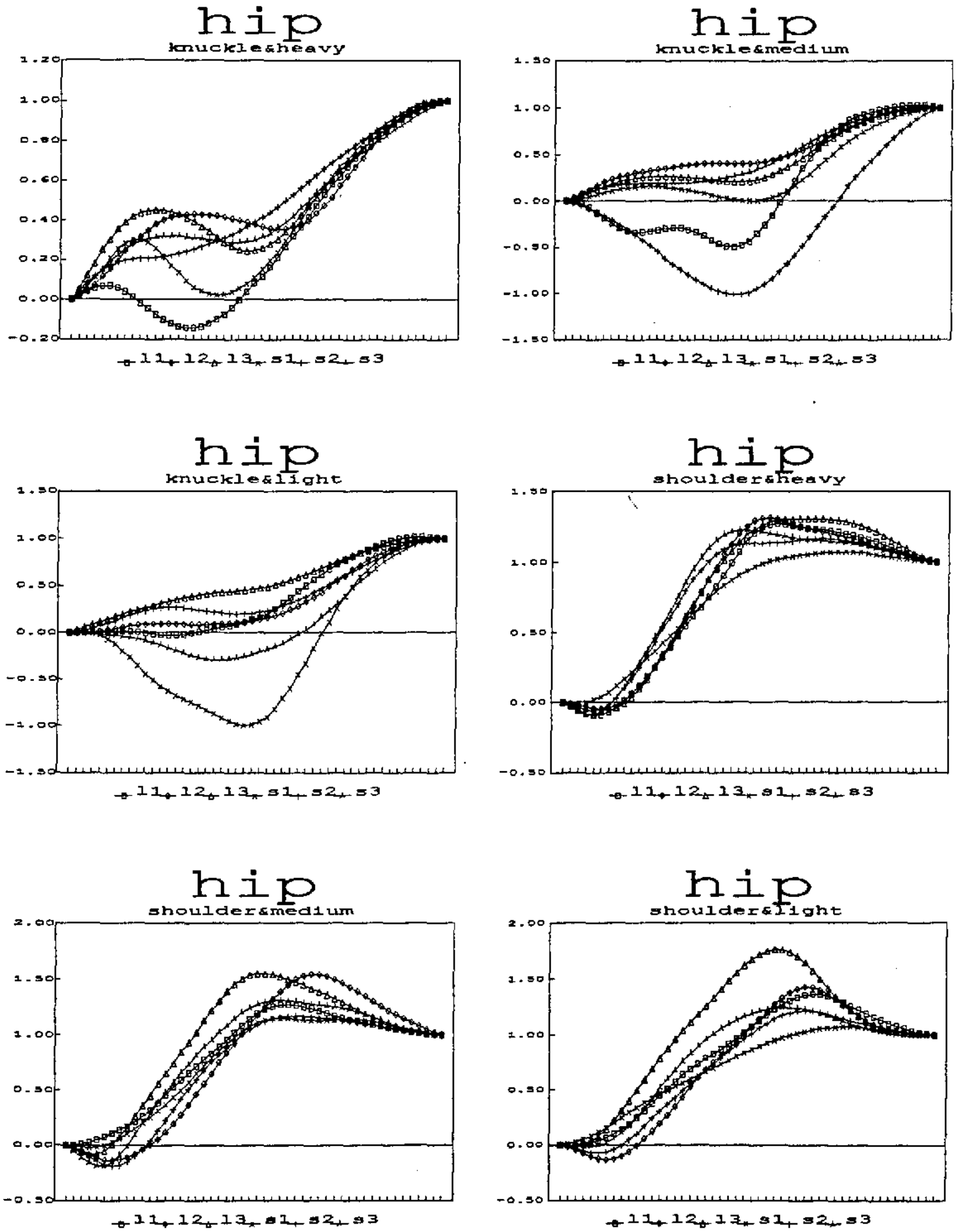

c. hip

Figure A.8 Continued

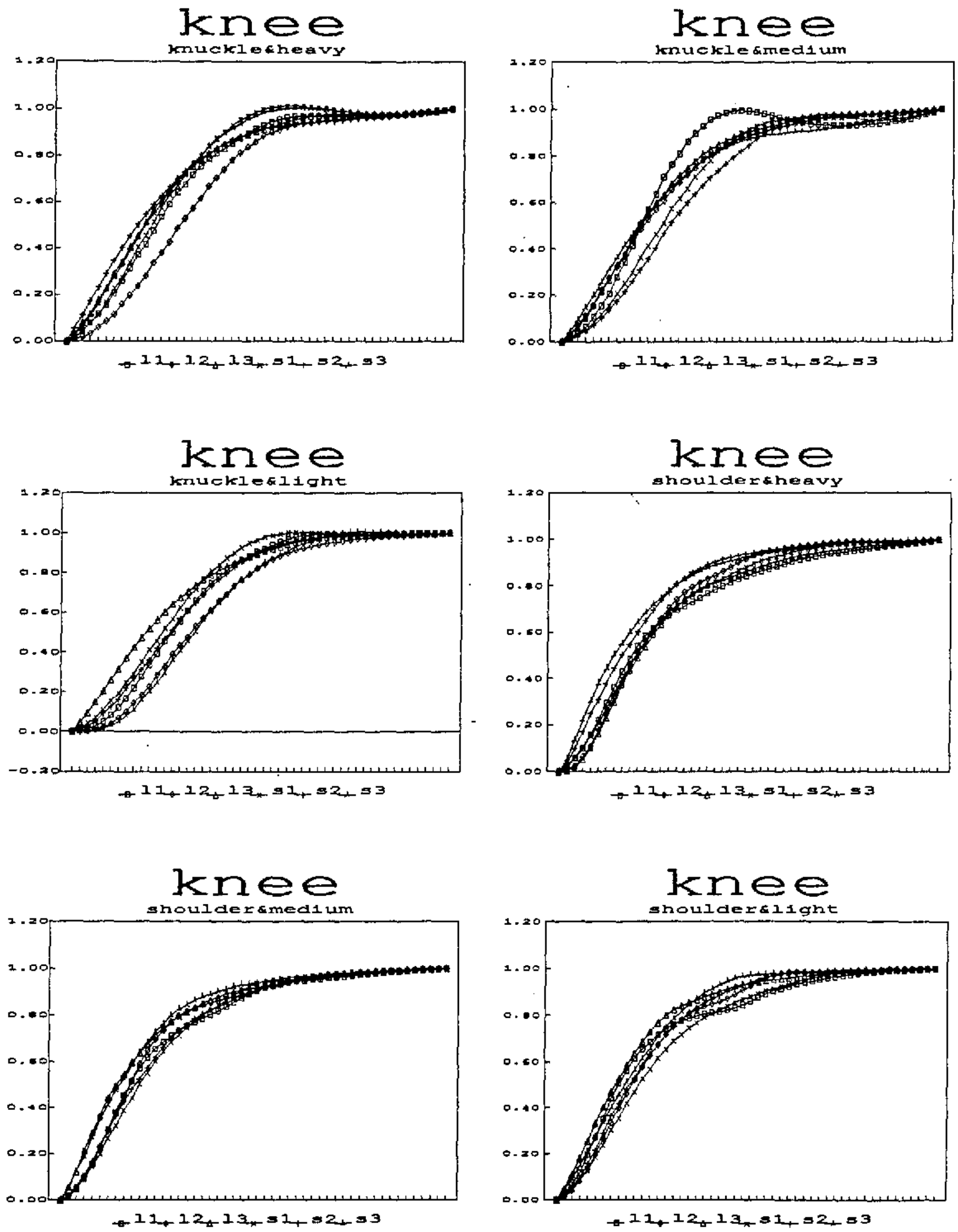

d. knee

Figure A.8 Continued

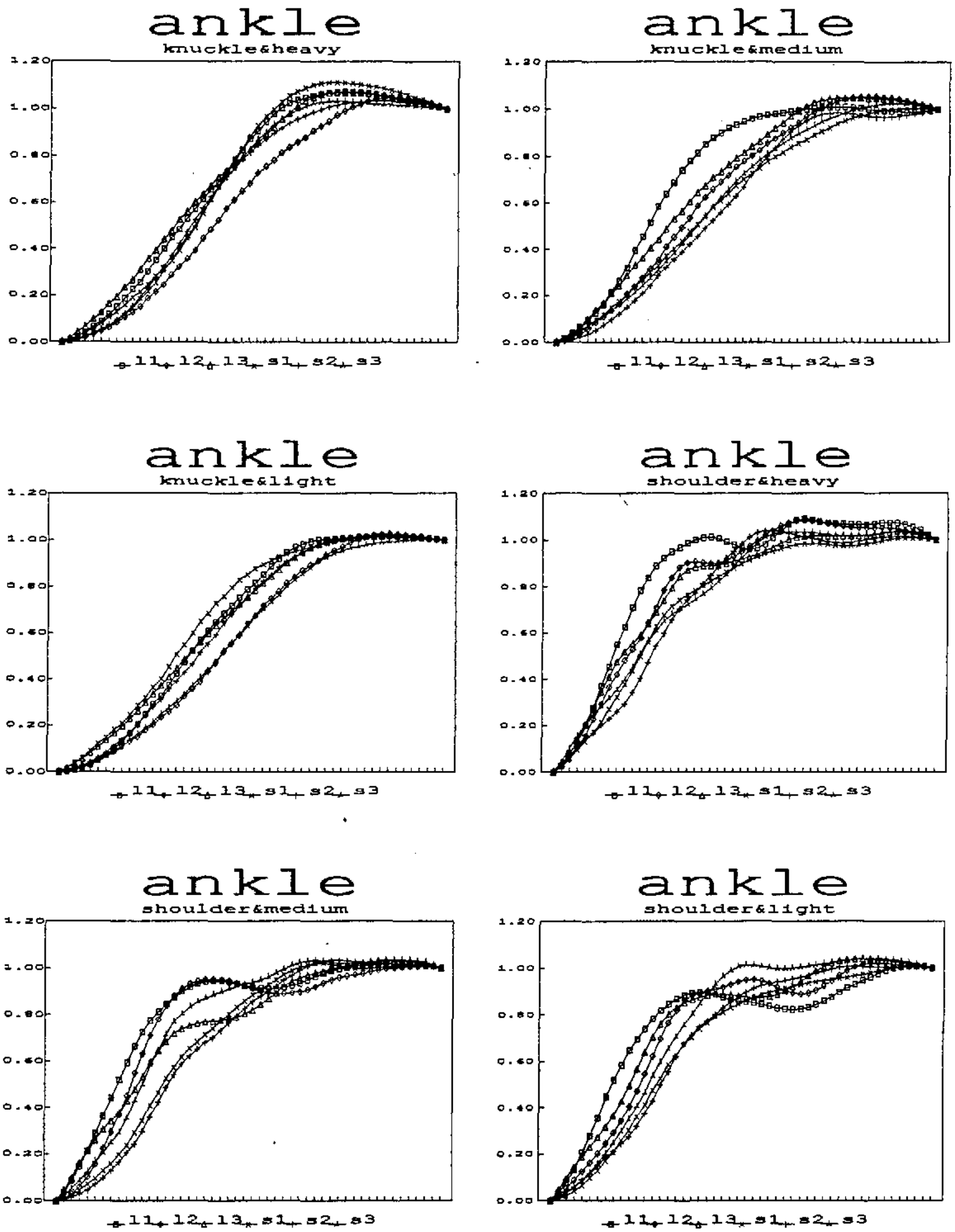

e. ankle

Figure A.8 Continued

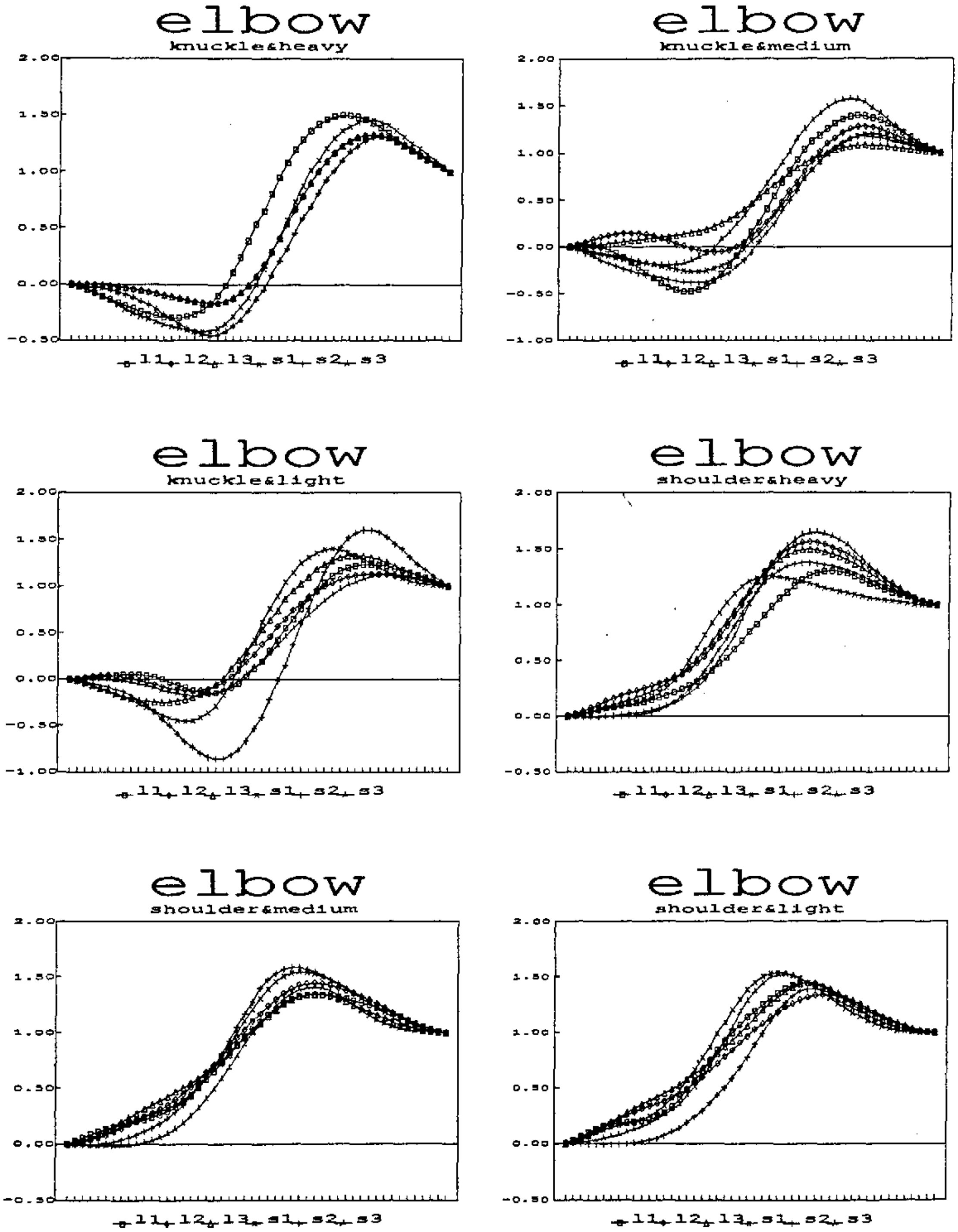

a. elbow

Figure A.9 Normalized trajectories of subject 10, who performed squat lifts

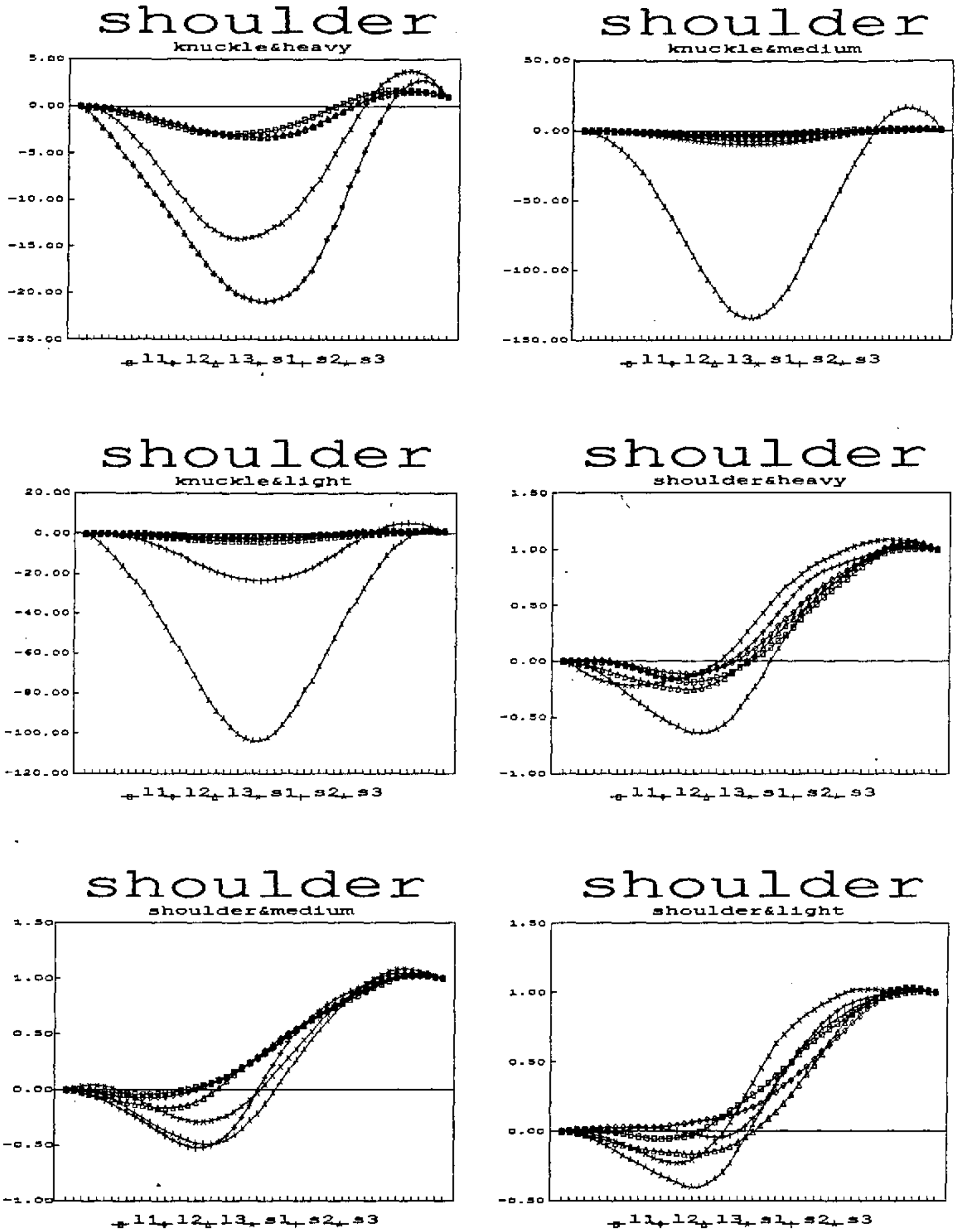

b. shoulder

Figure A.9 Continued

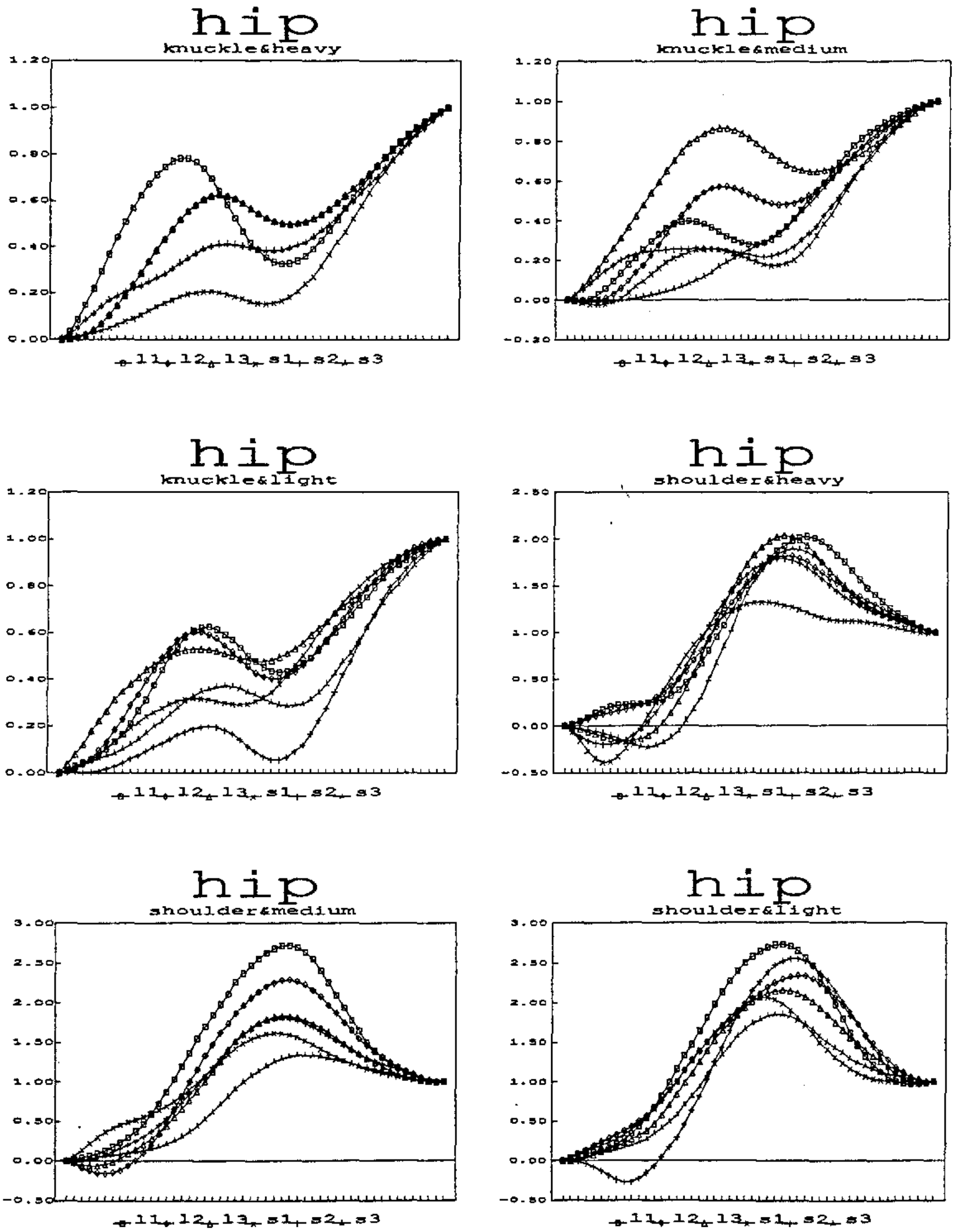

c. hip

Figure A.9 Continued

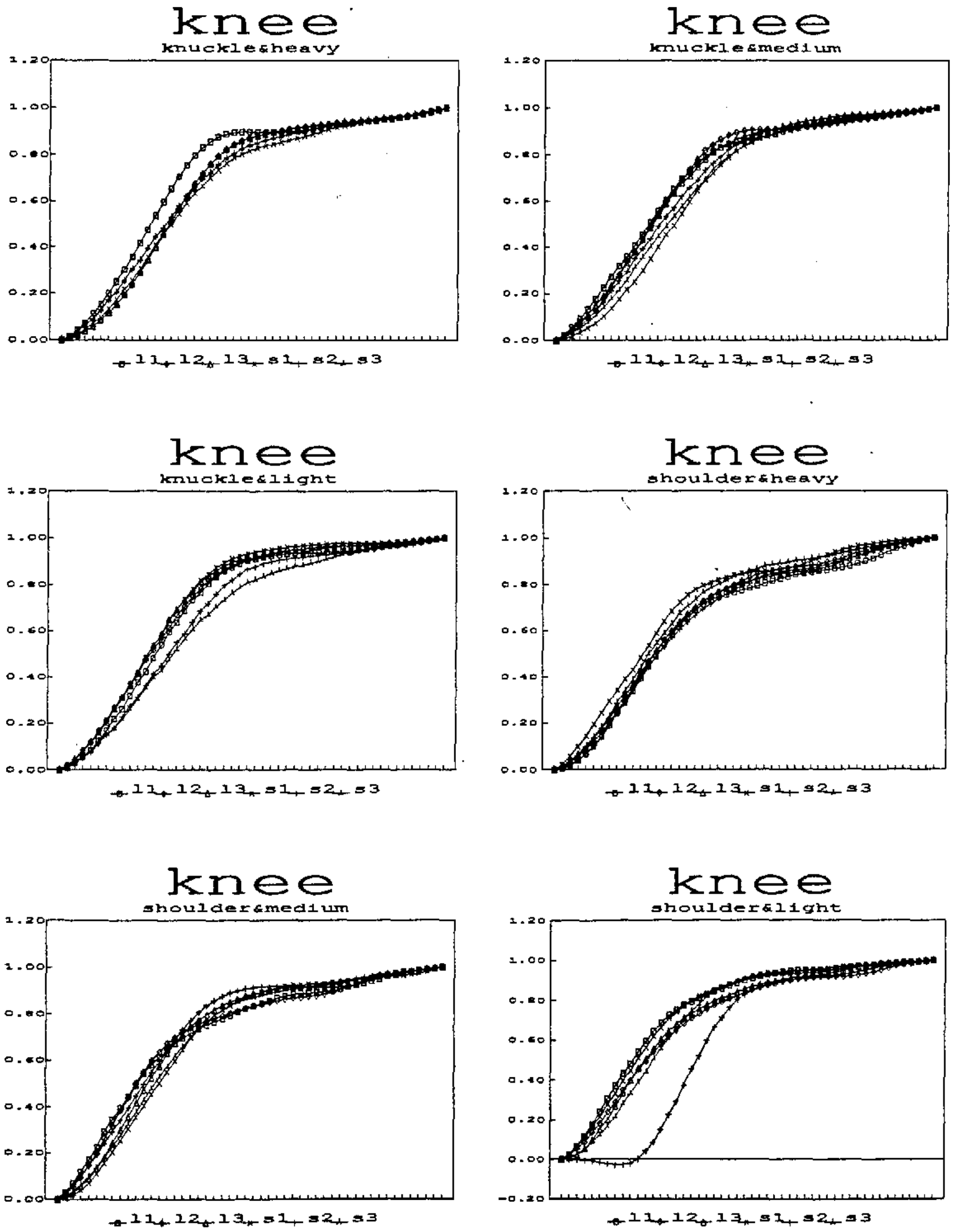

d. knee

Figure A.9 Continued

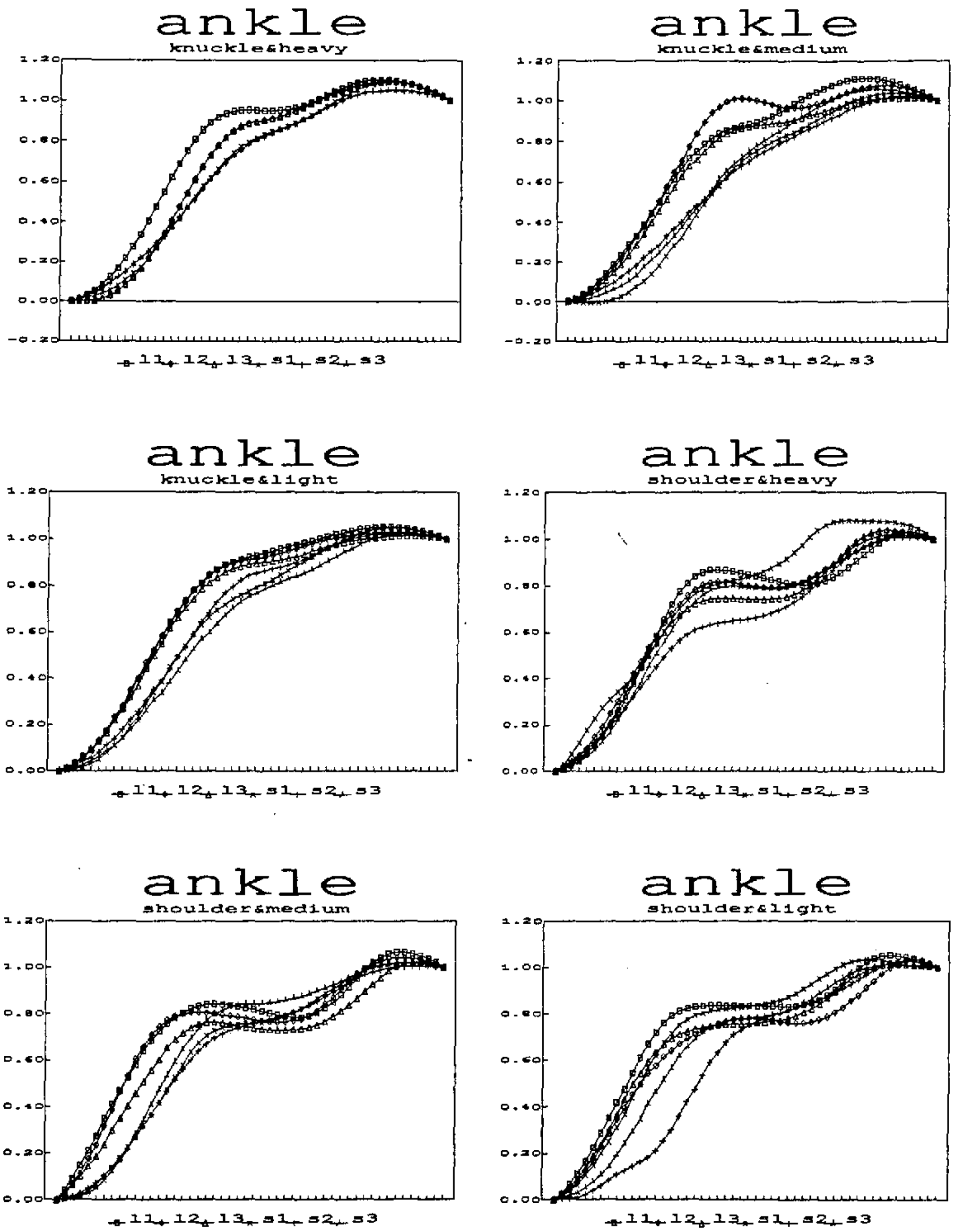

e. ankle

Figure A.9 Continued

APPENDIX B
ACTUAL VERSUS SIMULATED TRAJECTORIES FOR ADDITIONAL SUBJECTS

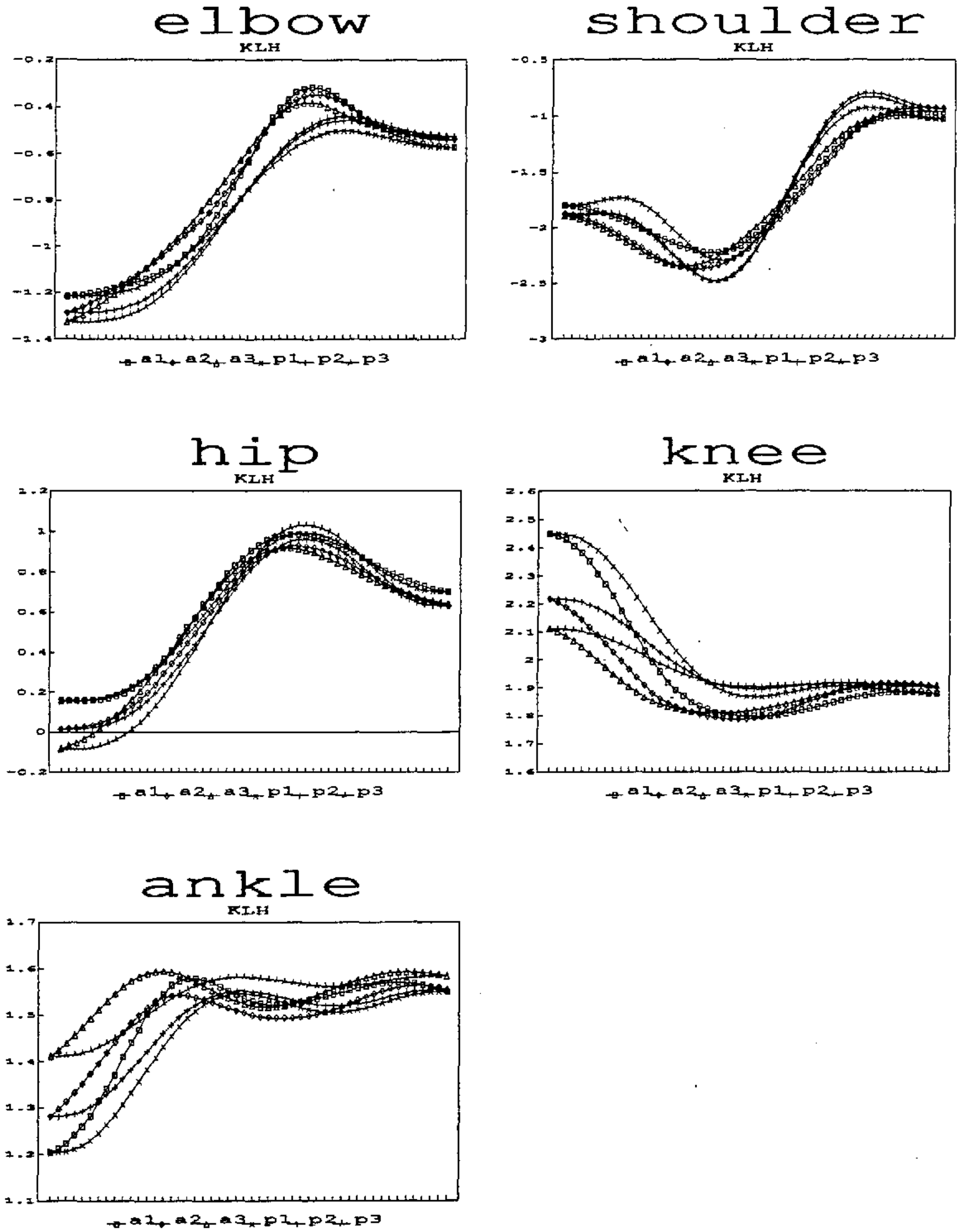

a. KLH

Figure B.1 Actual versus simulated trajectories for subject 2

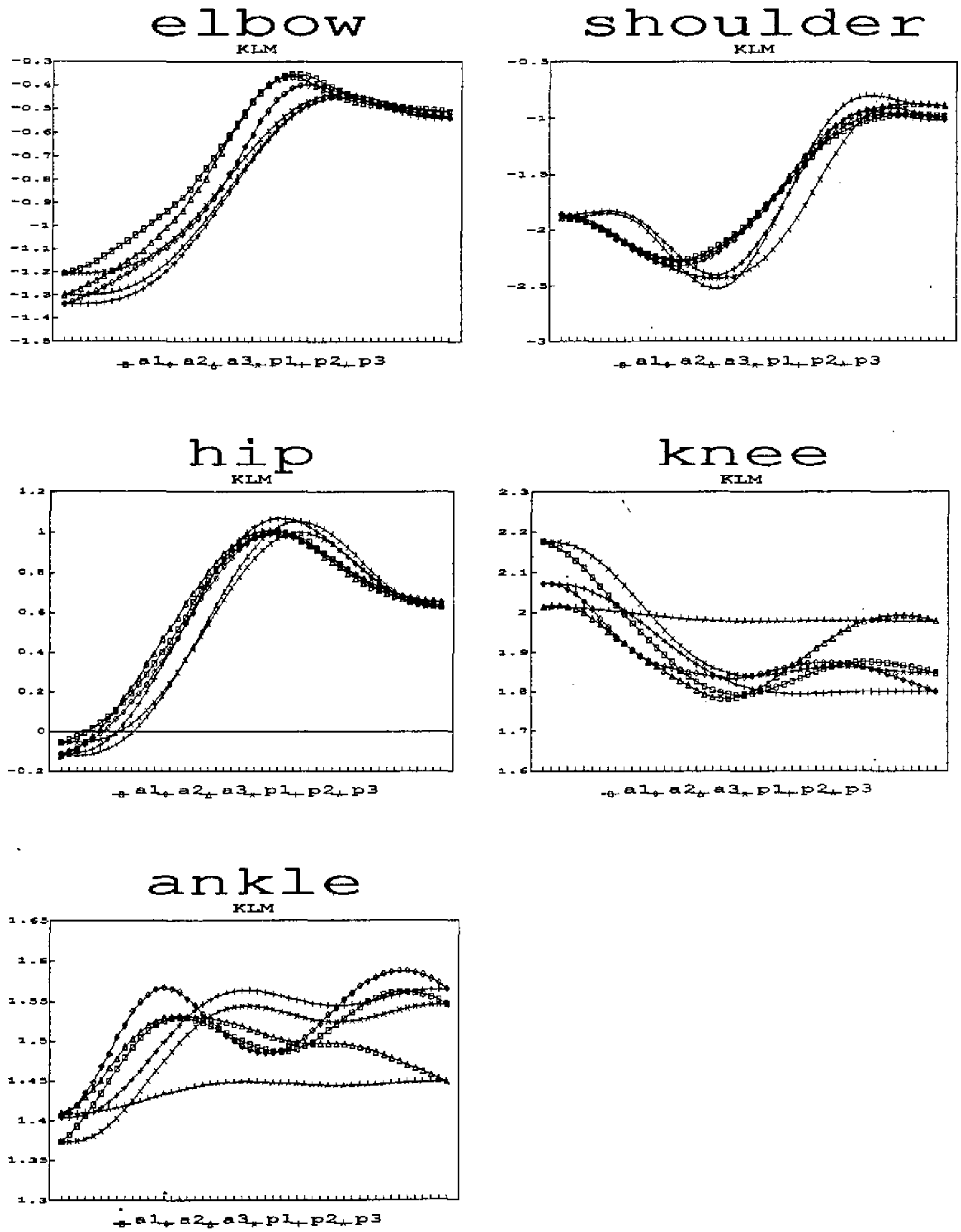

b. KLM

Figure B.1 Continued

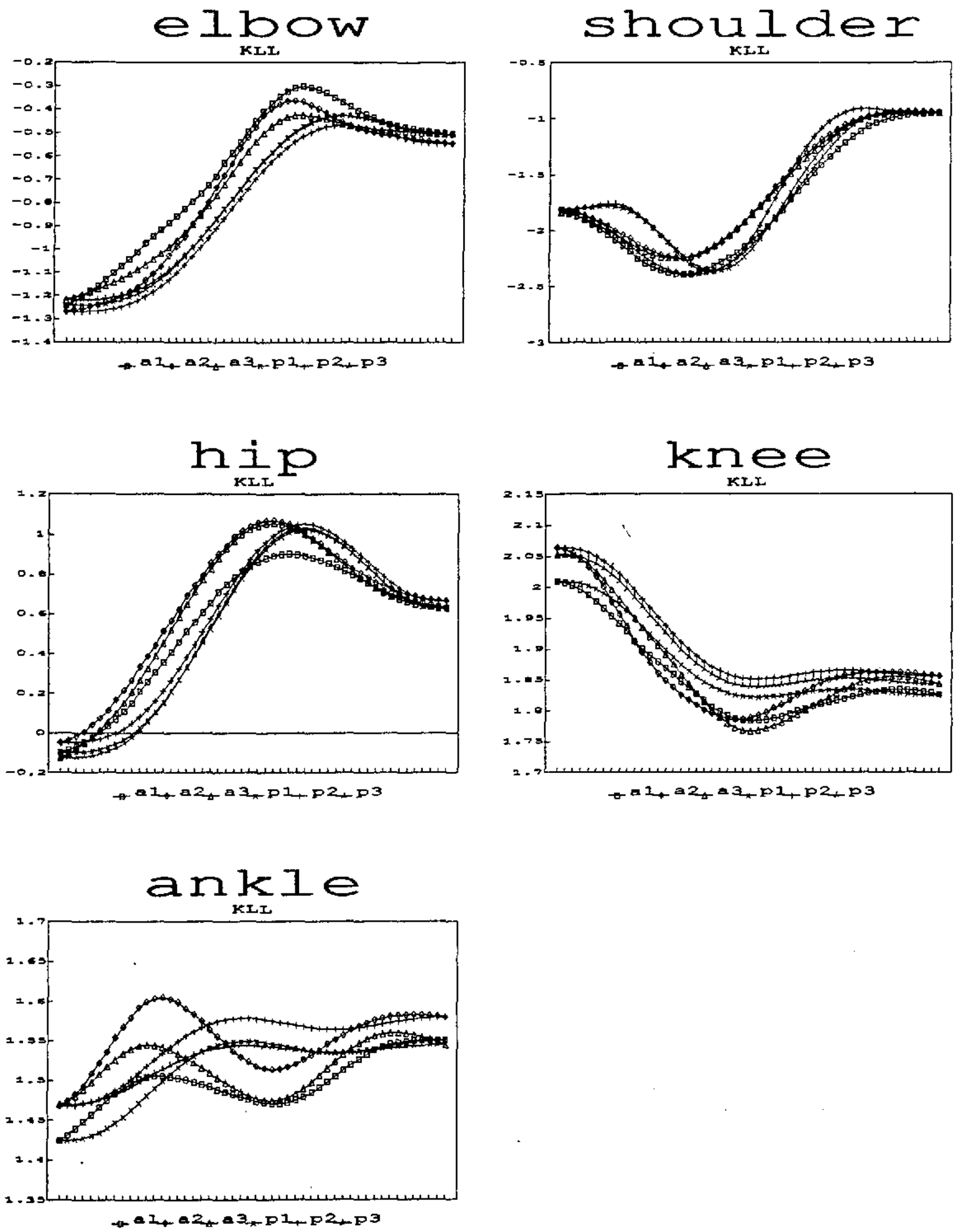

c. KLL

Figure B.1 Continued

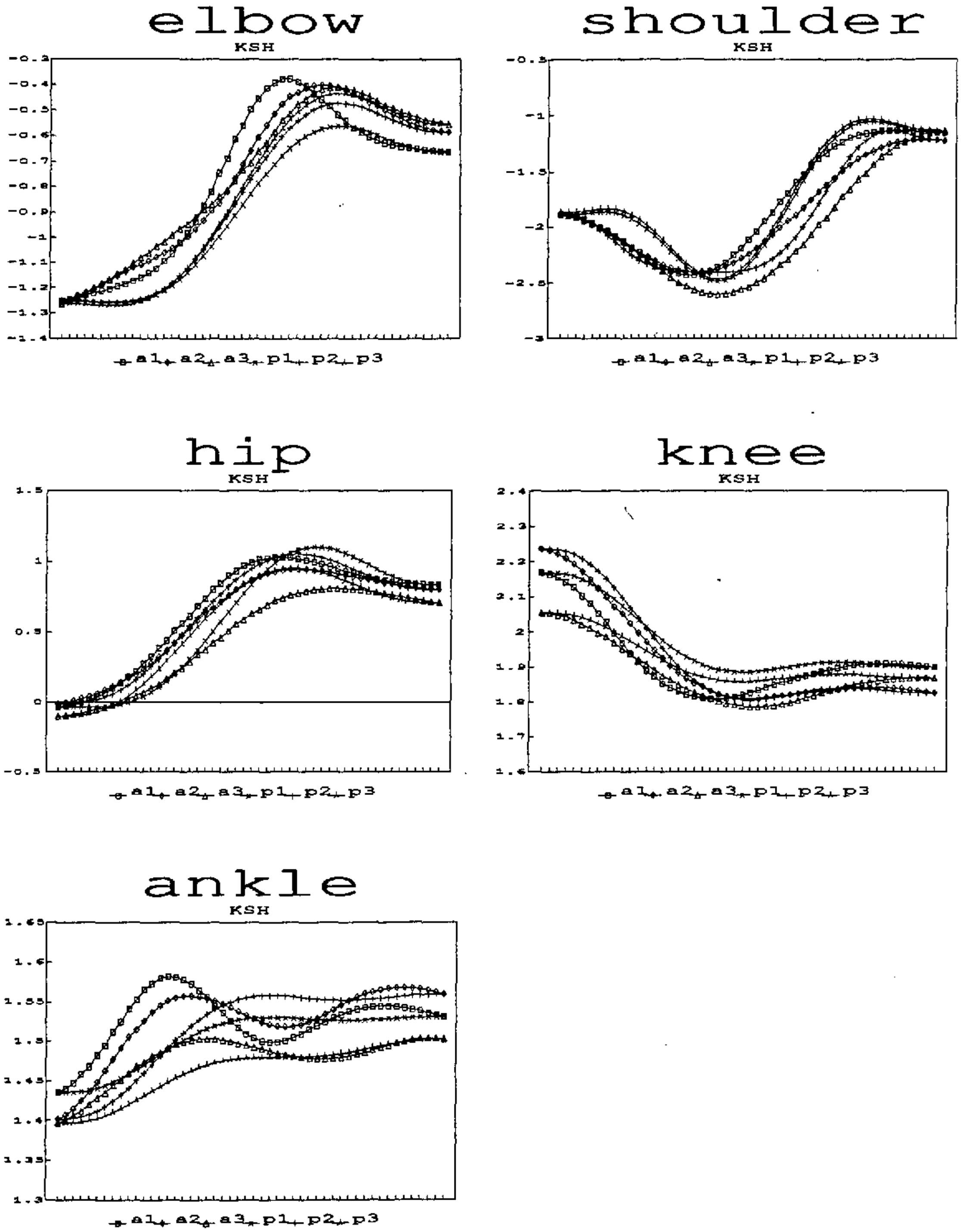

d. KSH

Figure B.1 Continued

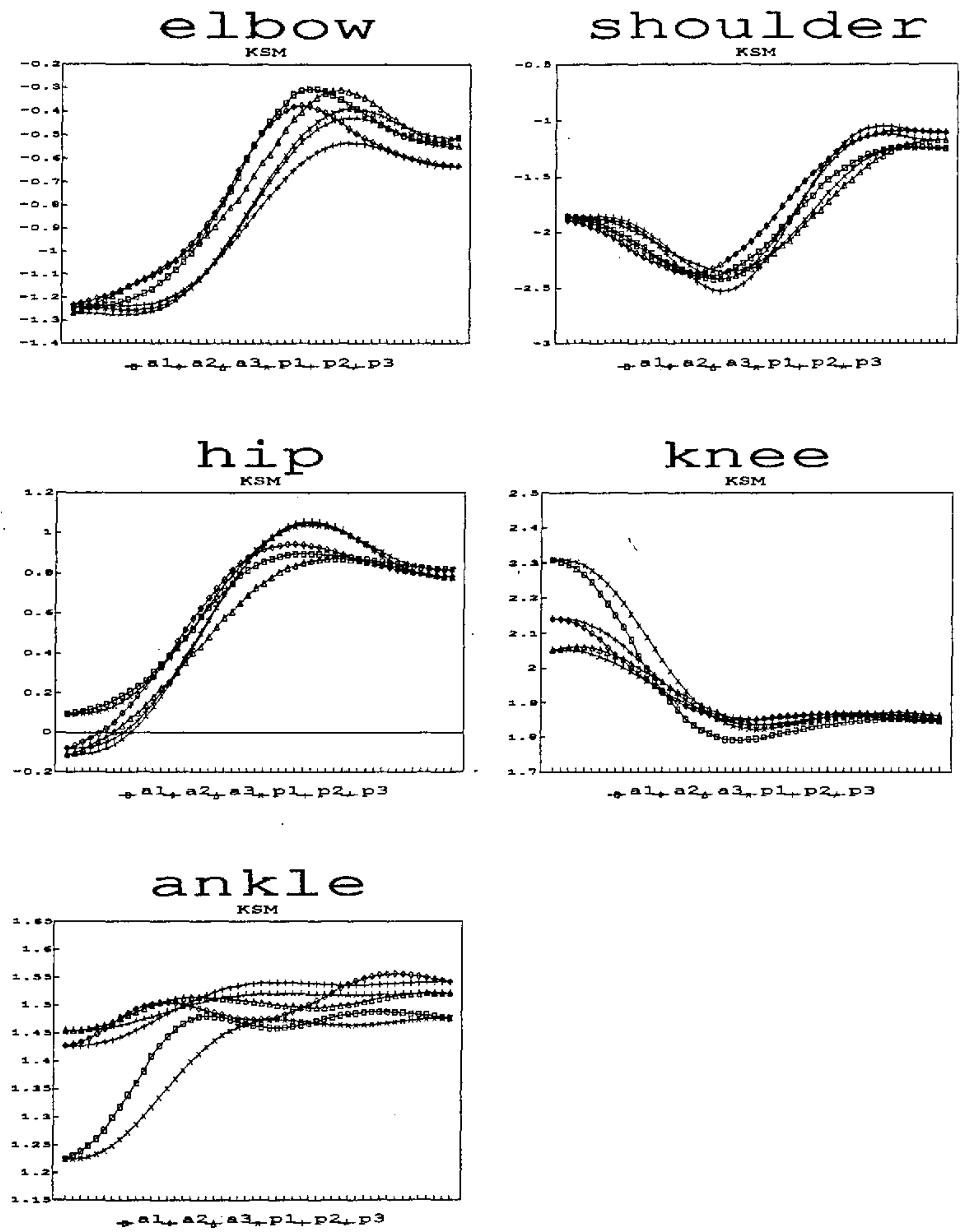

e. KSM

Figure B.1 Continued

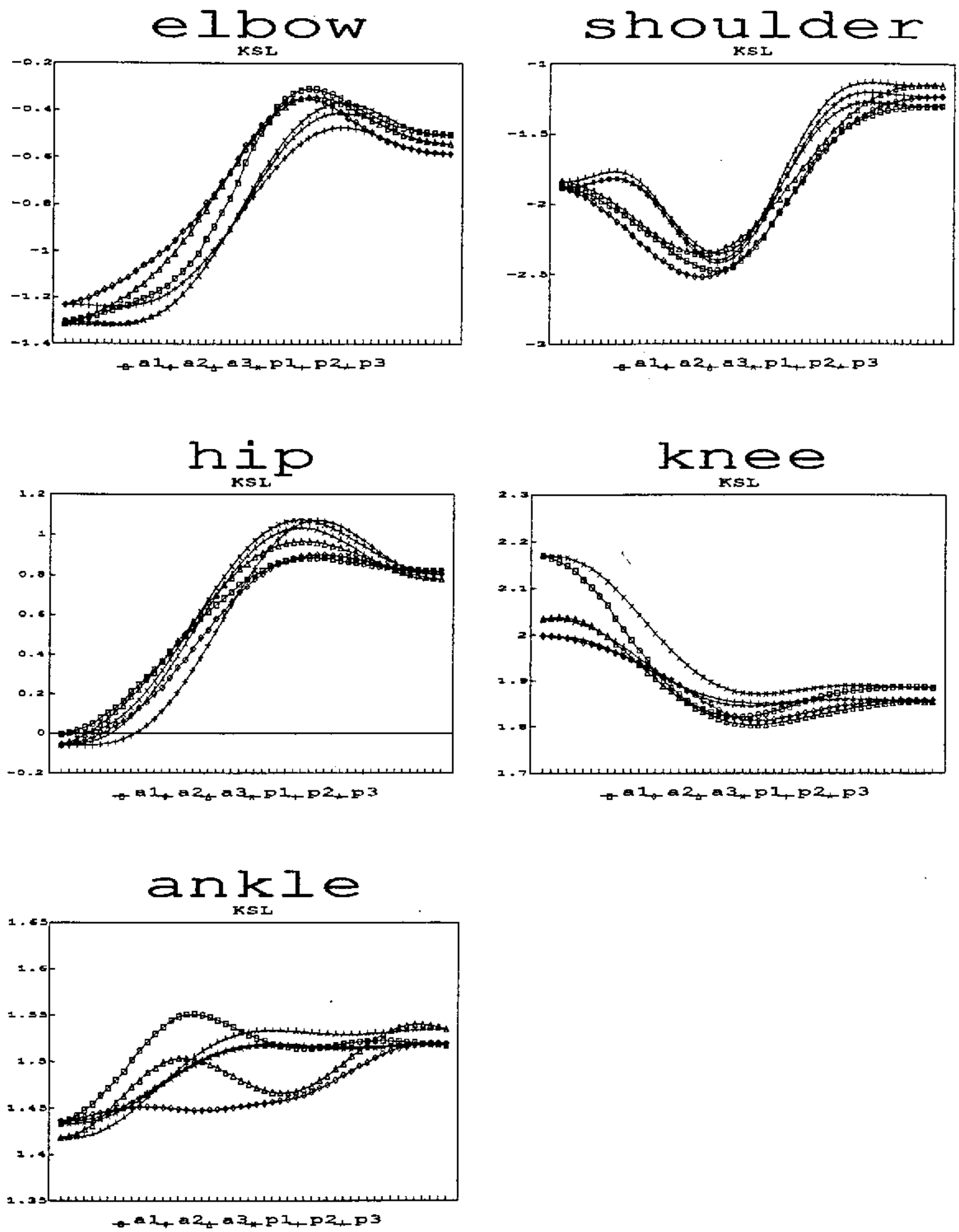

f. KSL

Figure B.1 Continued

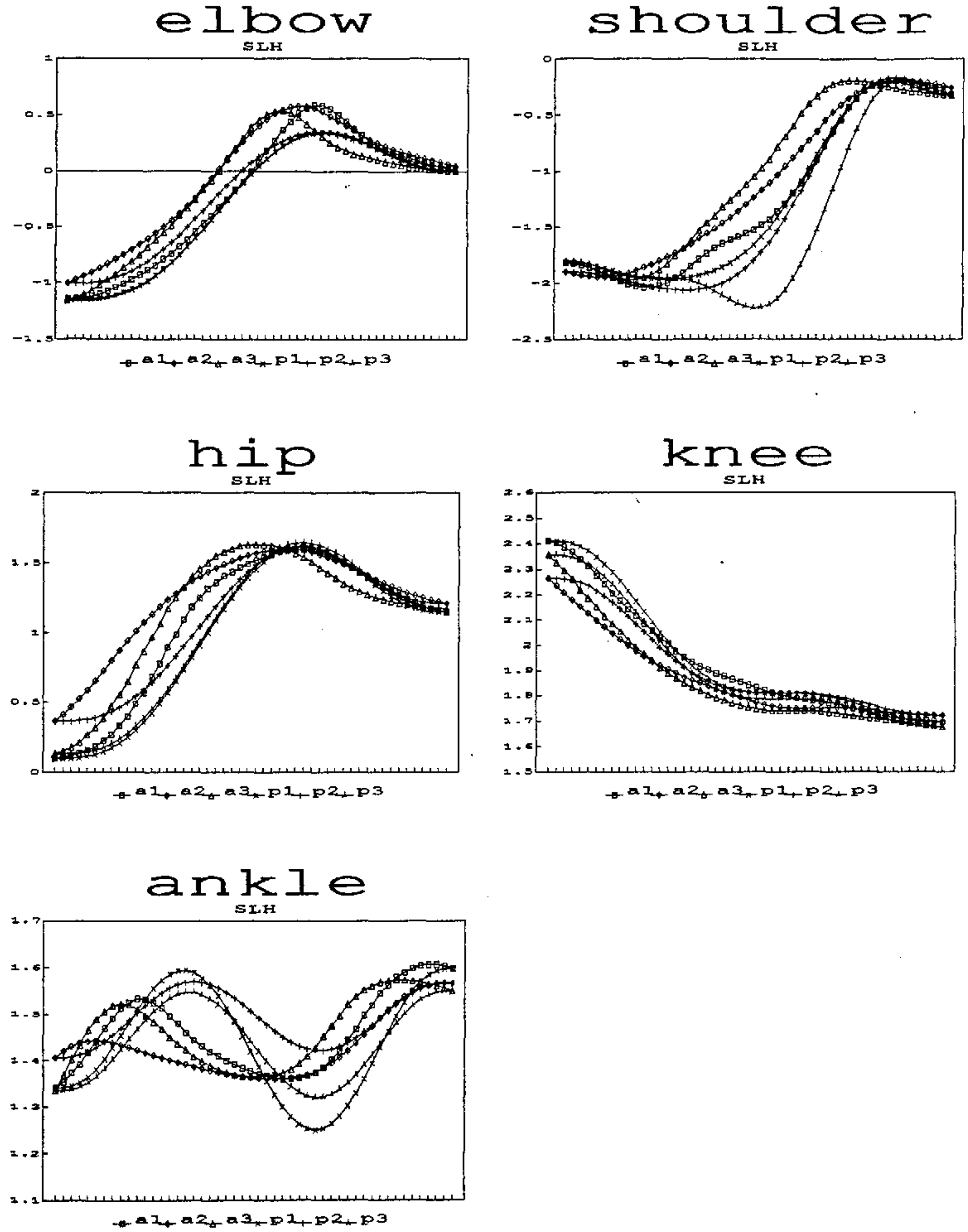

g. SLH

Figure B.1 Continued

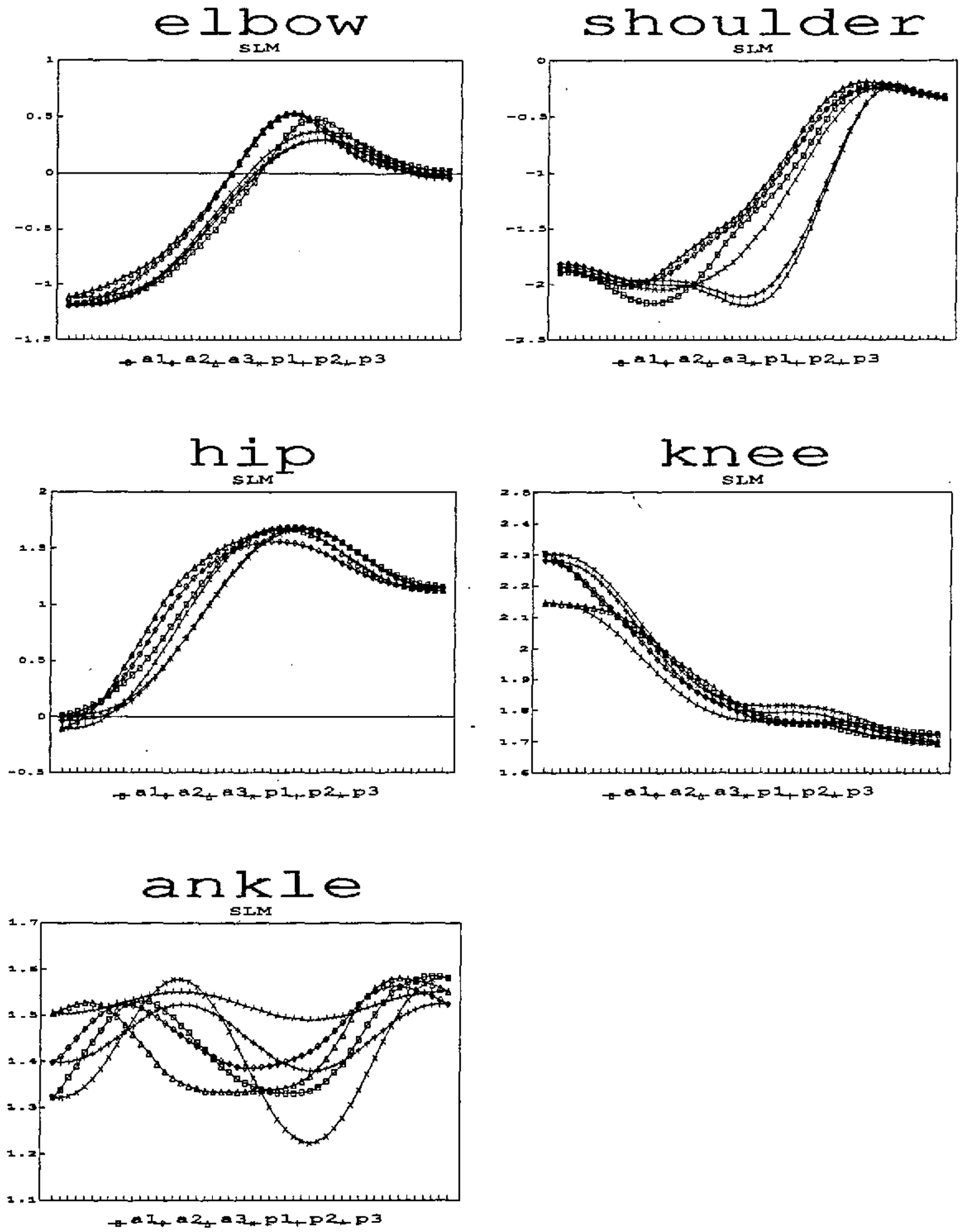

h. SLM

Figure B.1 Continued

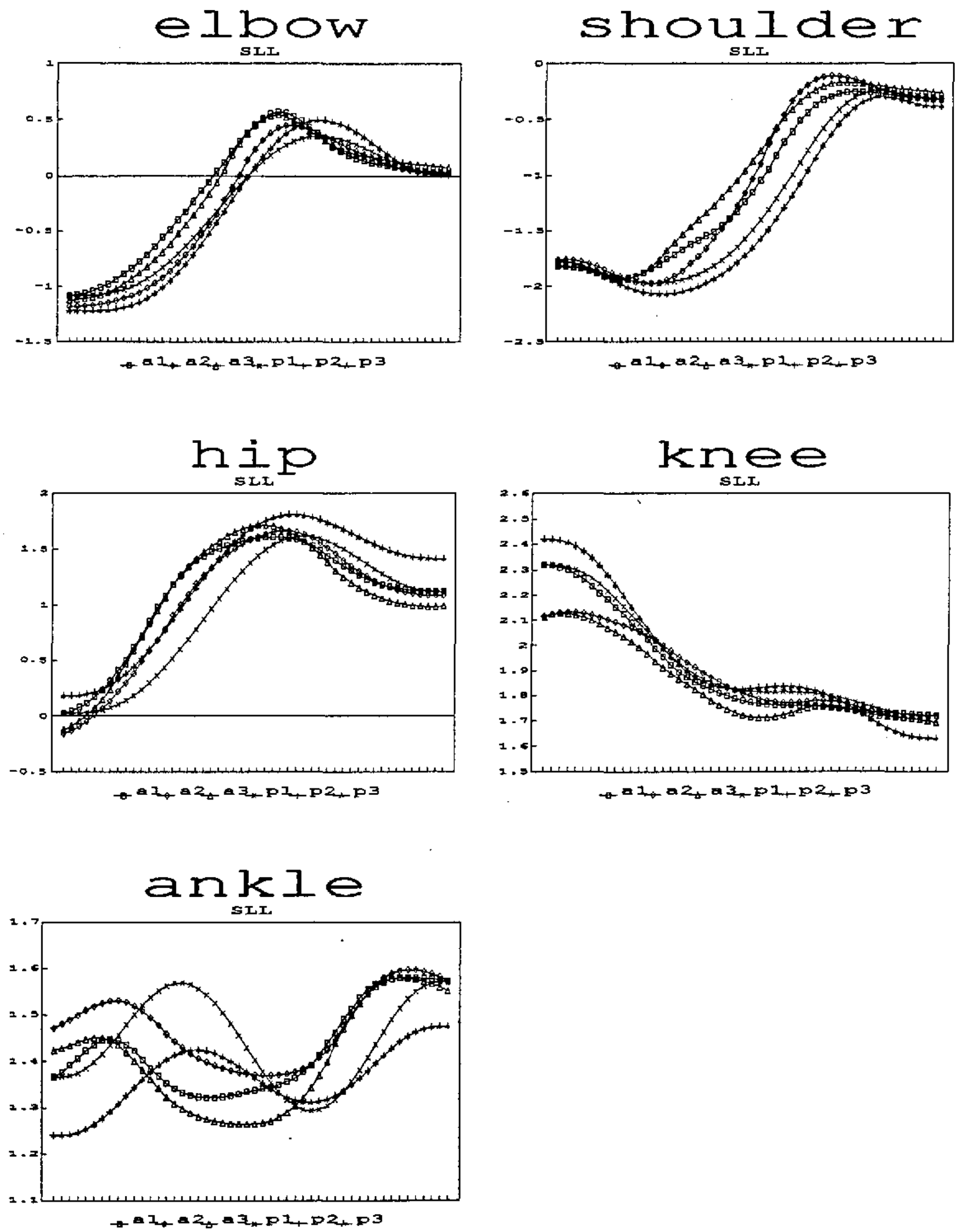

i. SLL

Figure B.1 Continued

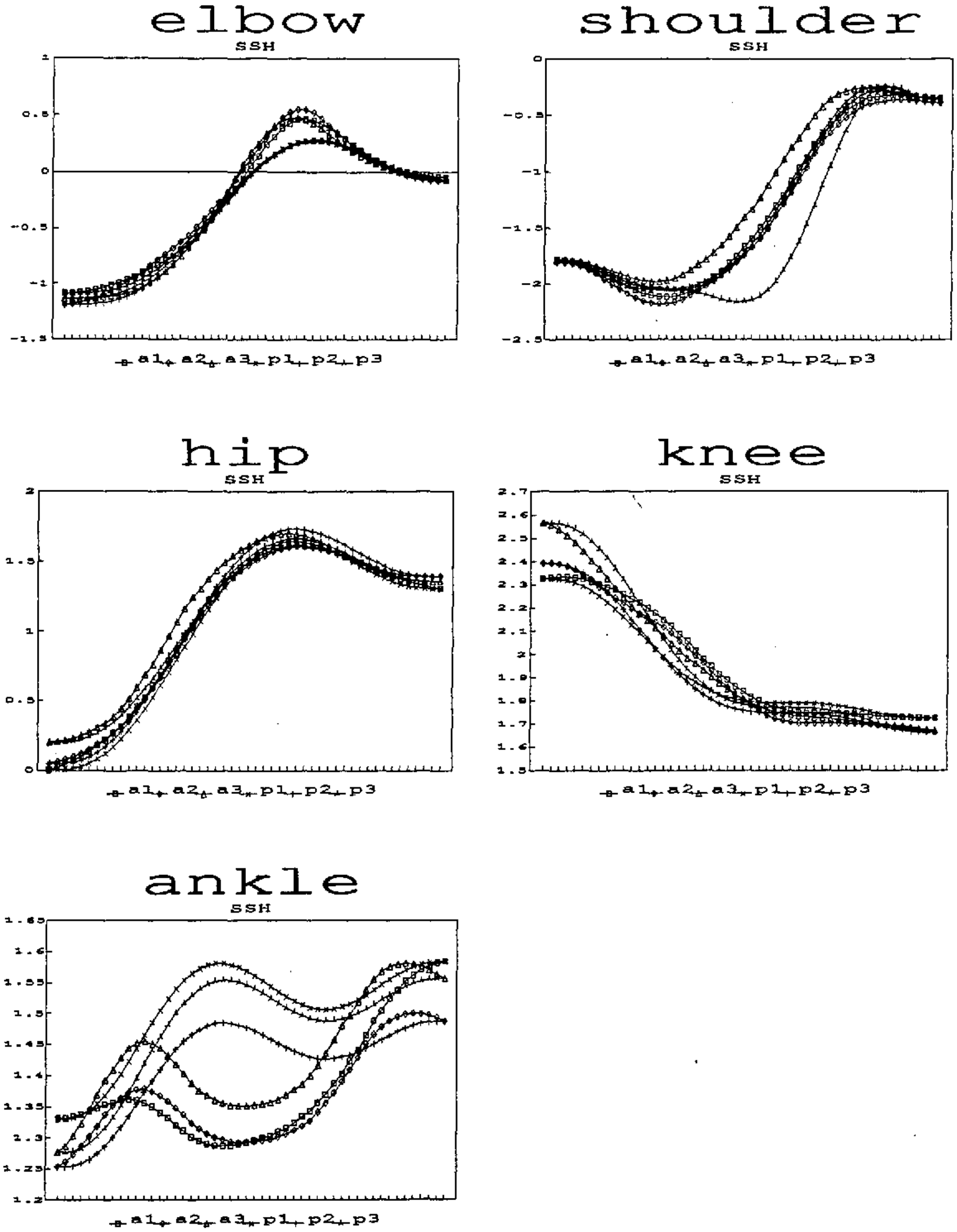

j. SSH

Figure B.1 Continued

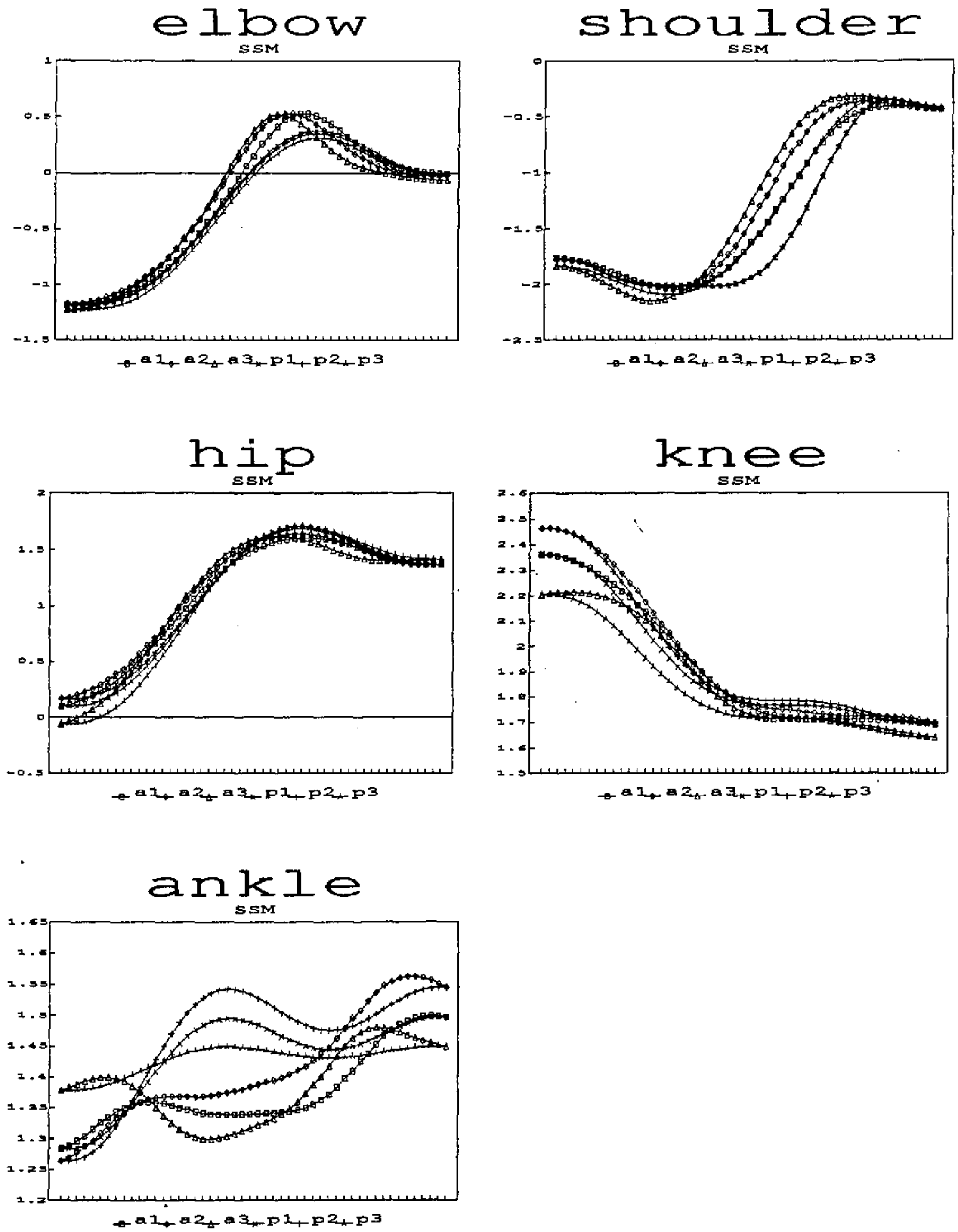

k. SSM

Figure B.1 Continued

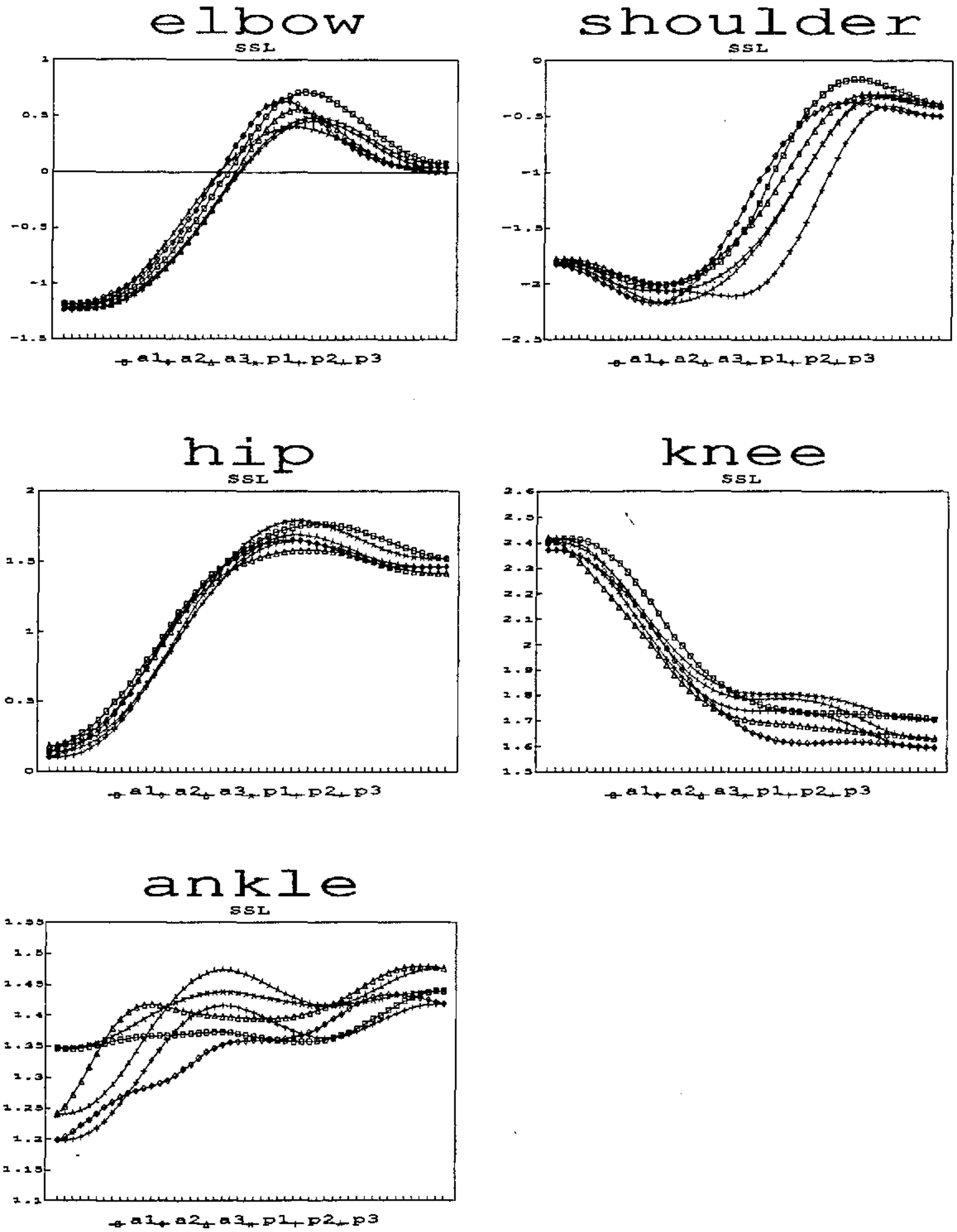

l. SSL

Figure B.1 Continued

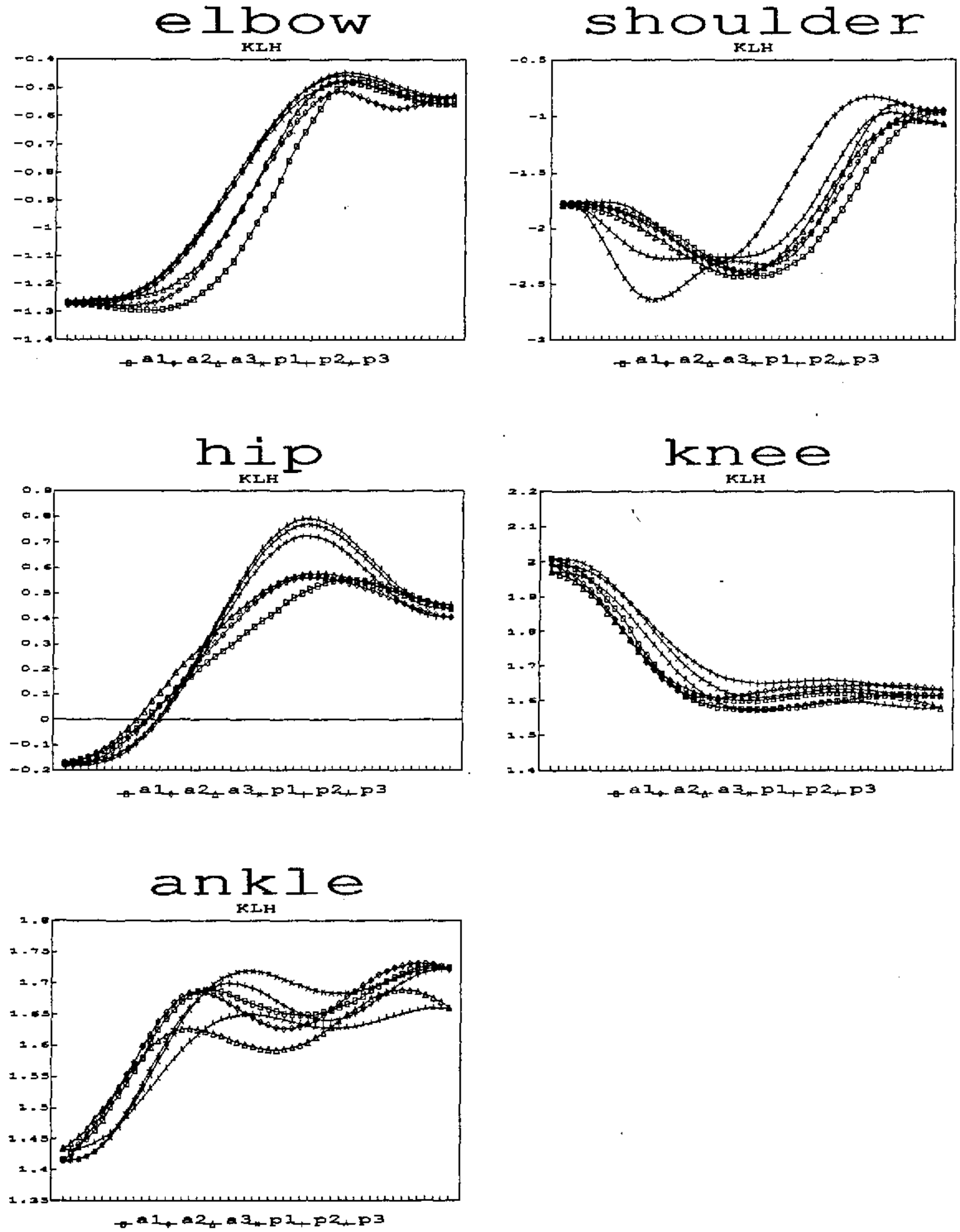

a. KLH

Figure B.2 Actual versus simulated trajectories for subject 3

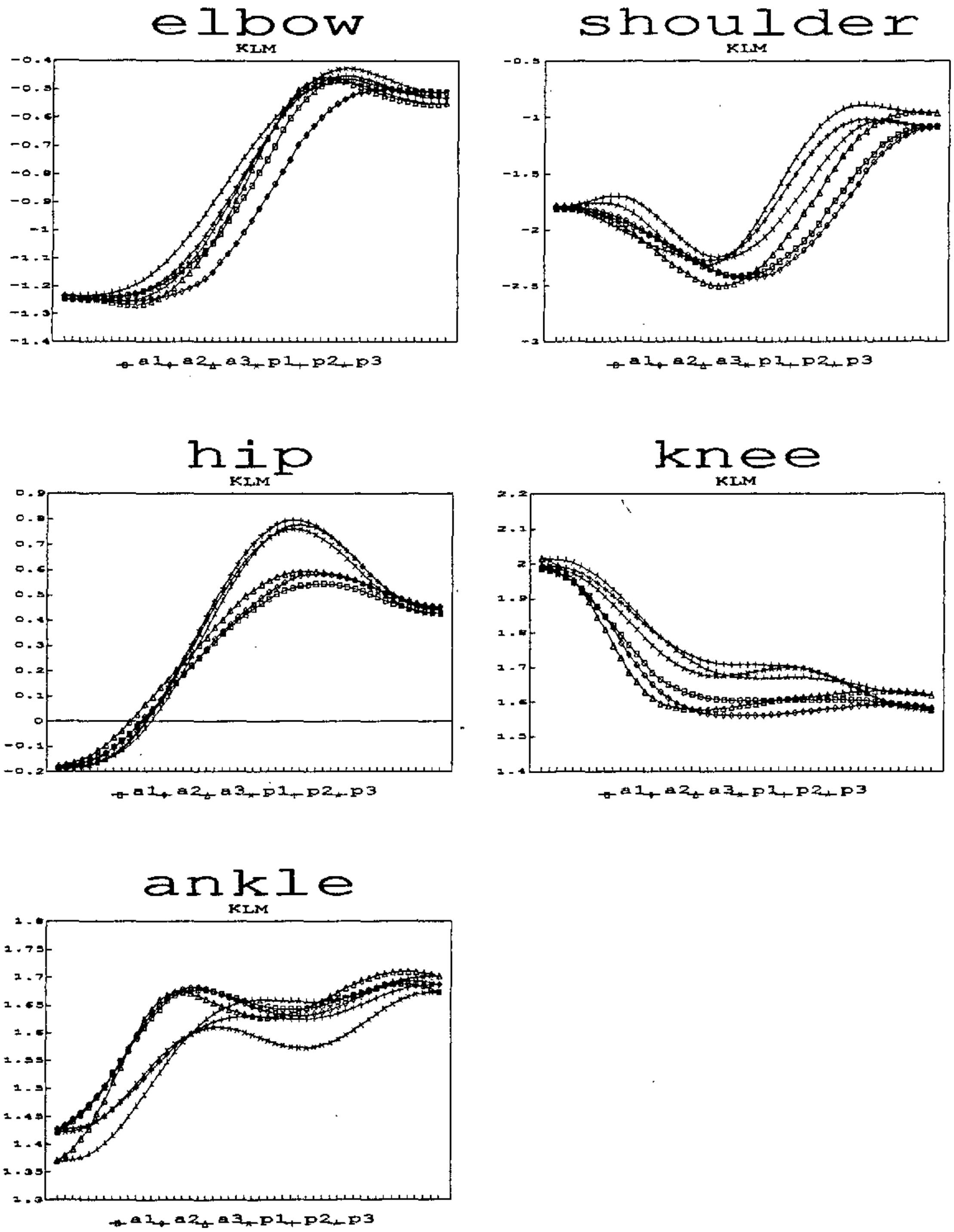

b. KLM

Figure B.2 Continued

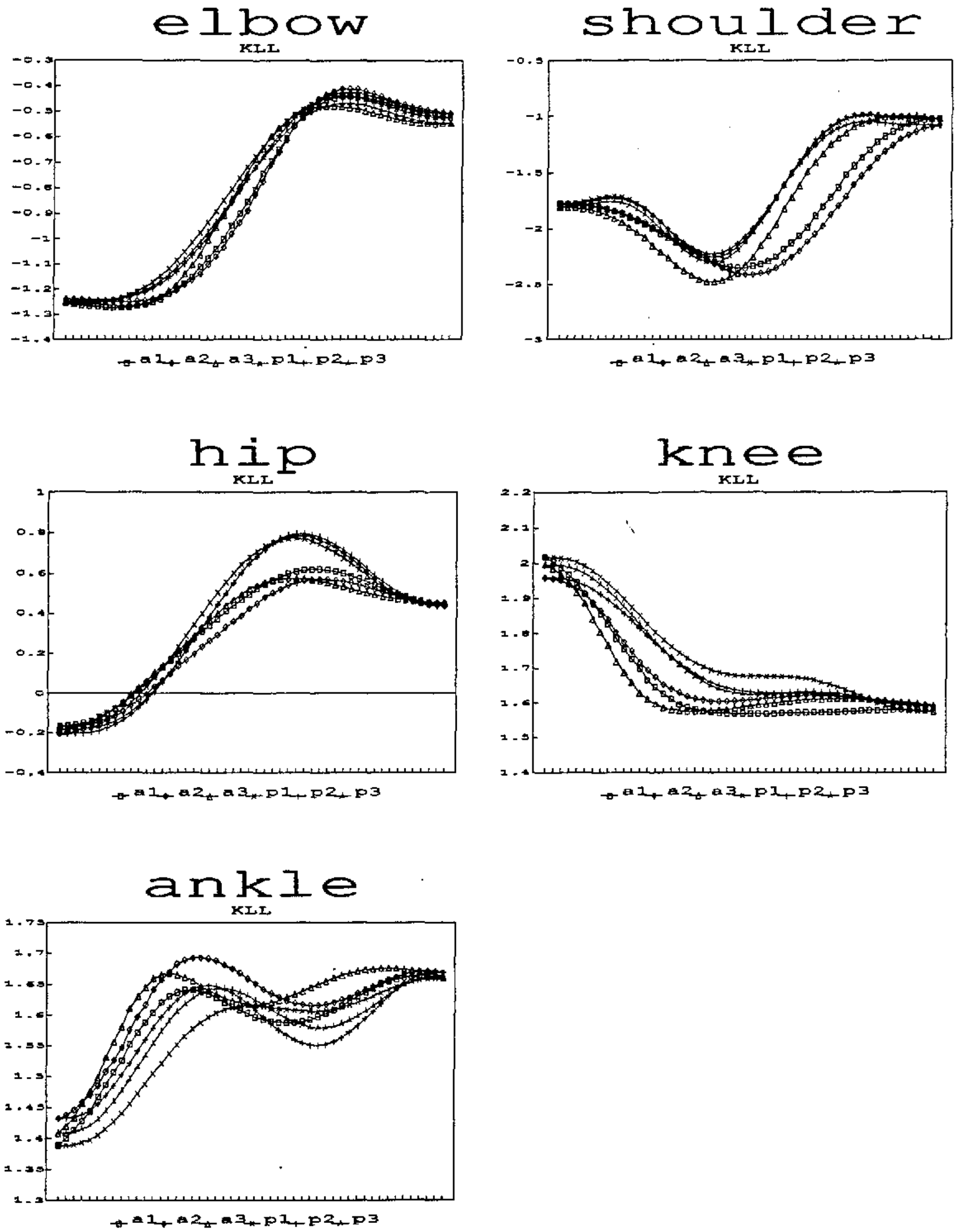

c. KLL

Figure B.2 Continued

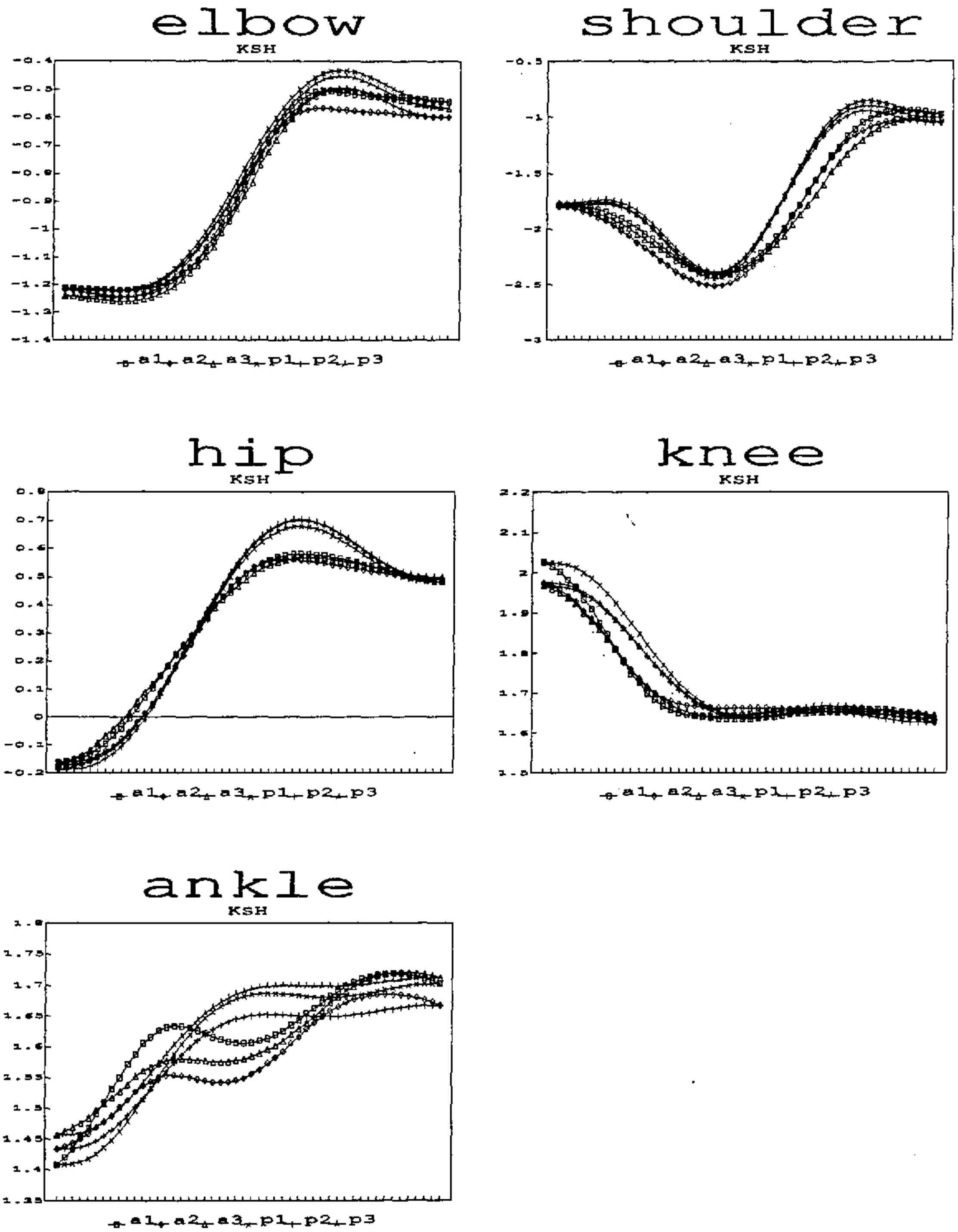

d. KSH

Figure B.2 Continued

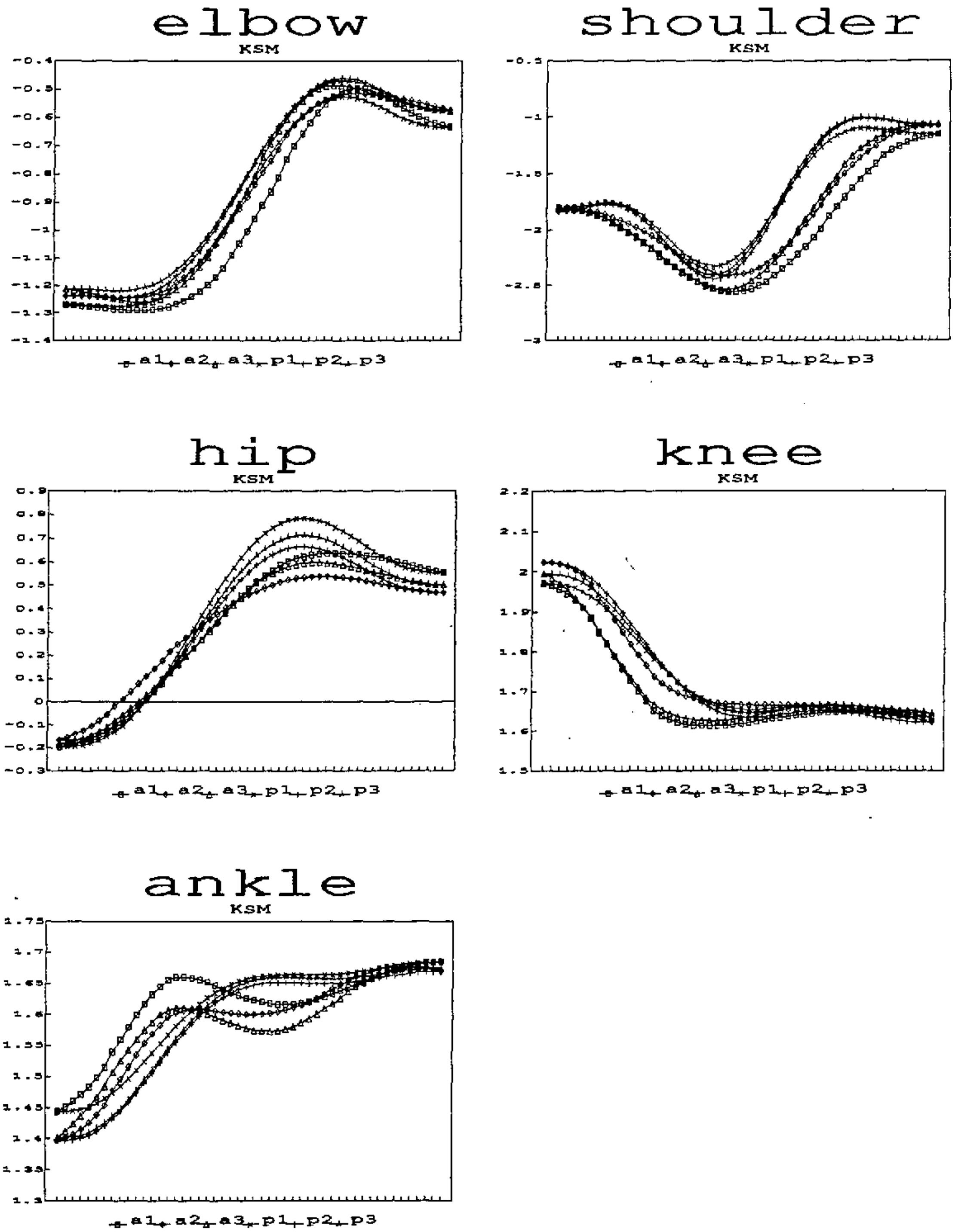

e. KSM

Figure B.2 Continued

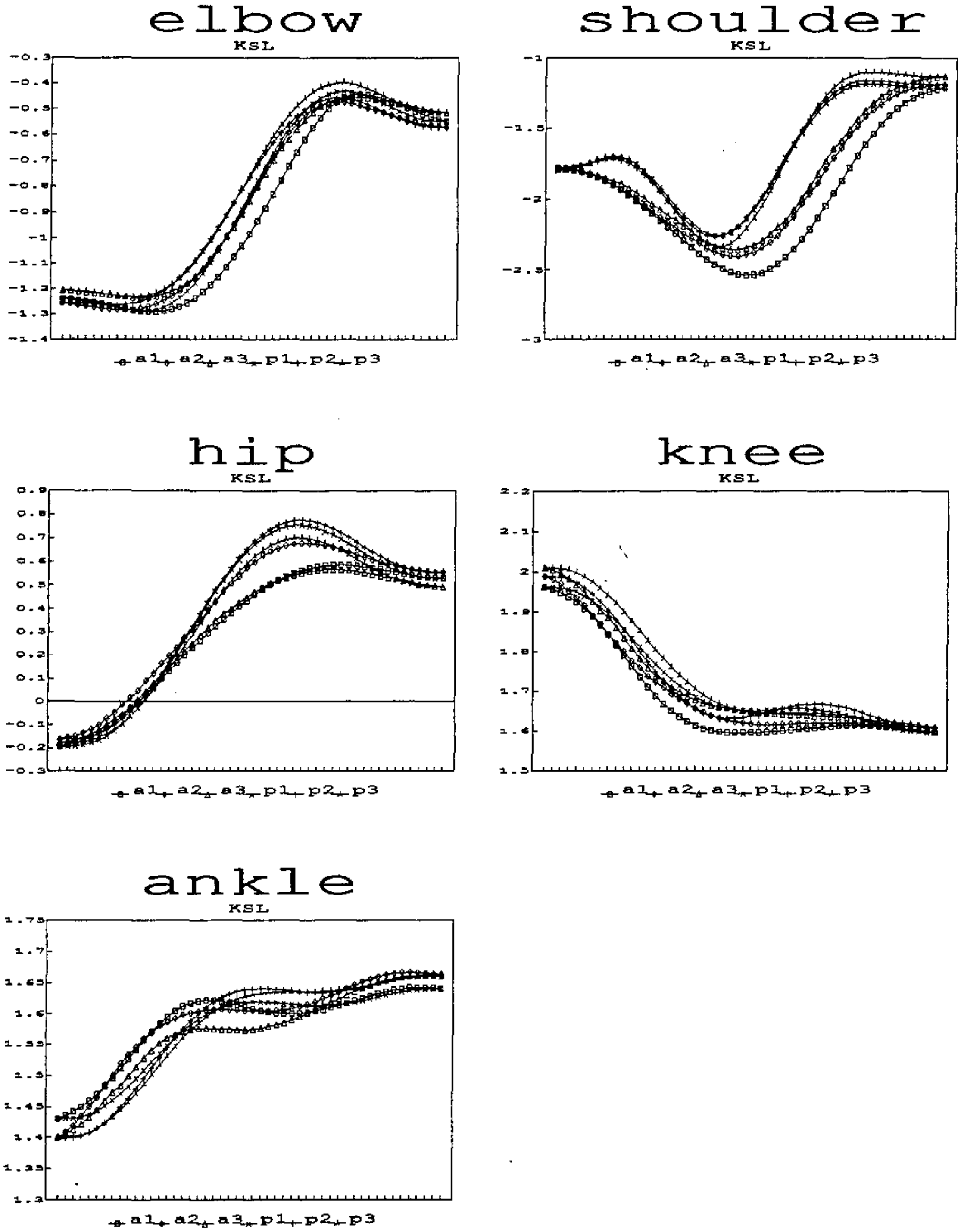

f. KSL

Figure B.2 Continued

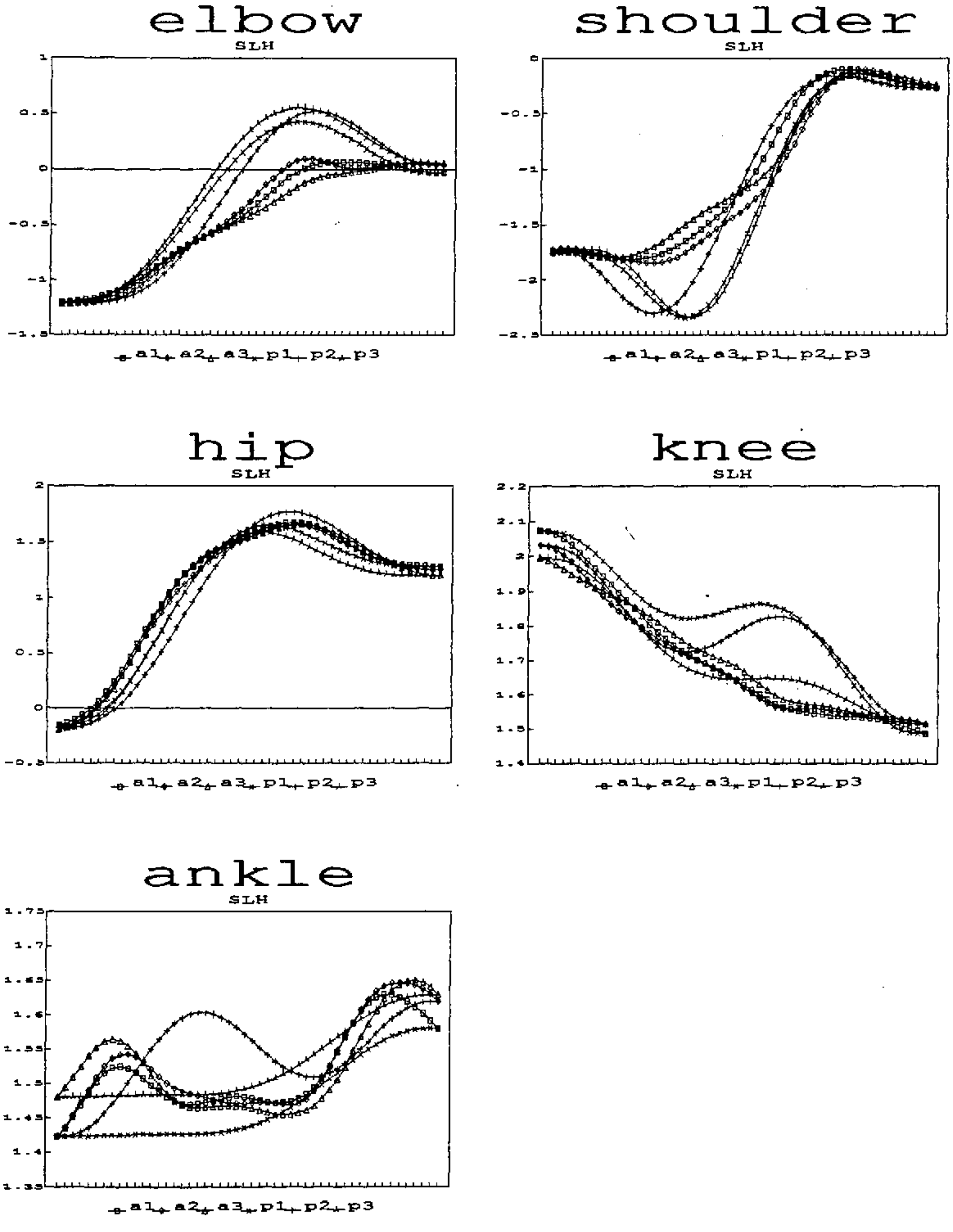

g. SLH

Figure B.2 Continued

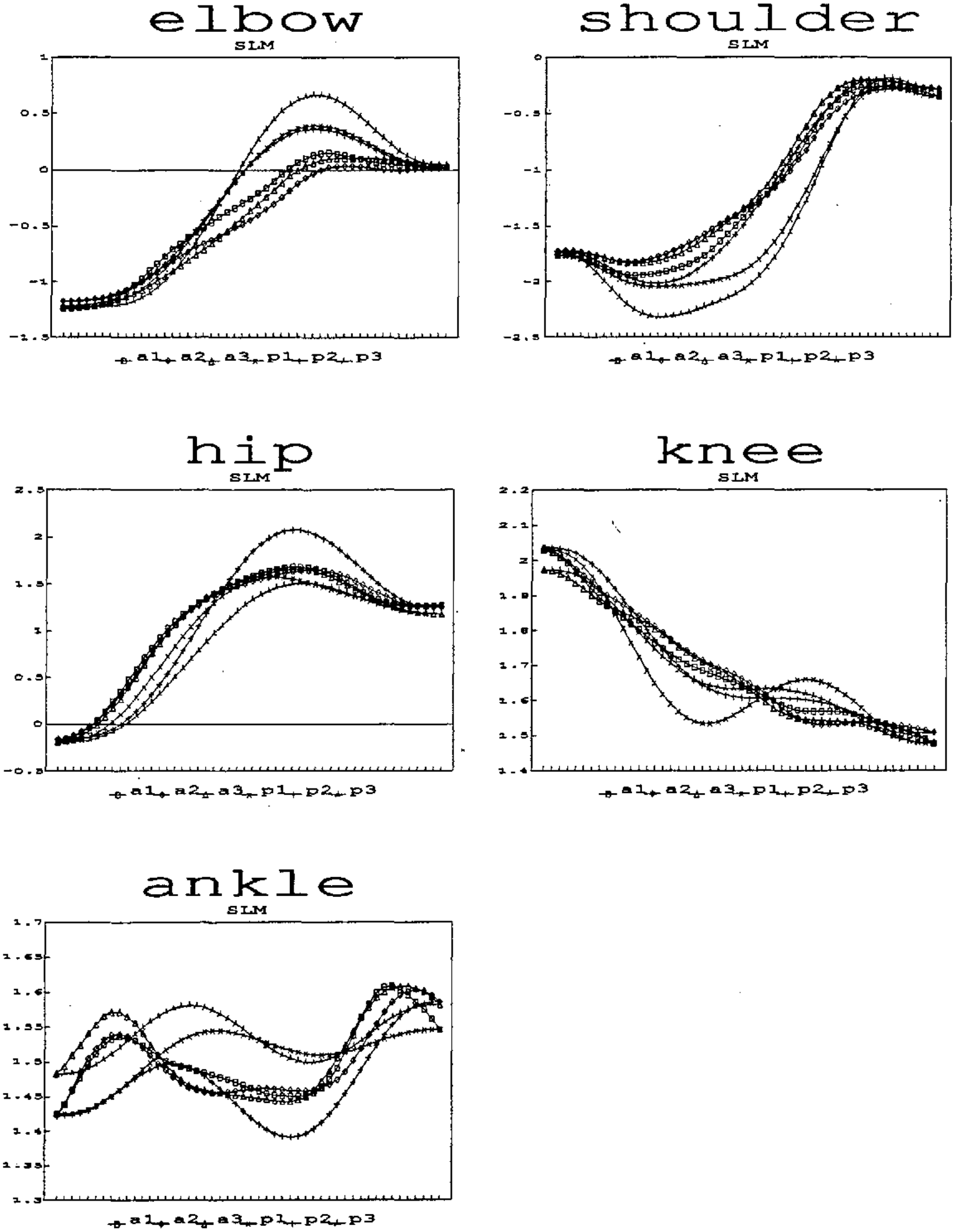

h. SLM

Figure B.2 Continued

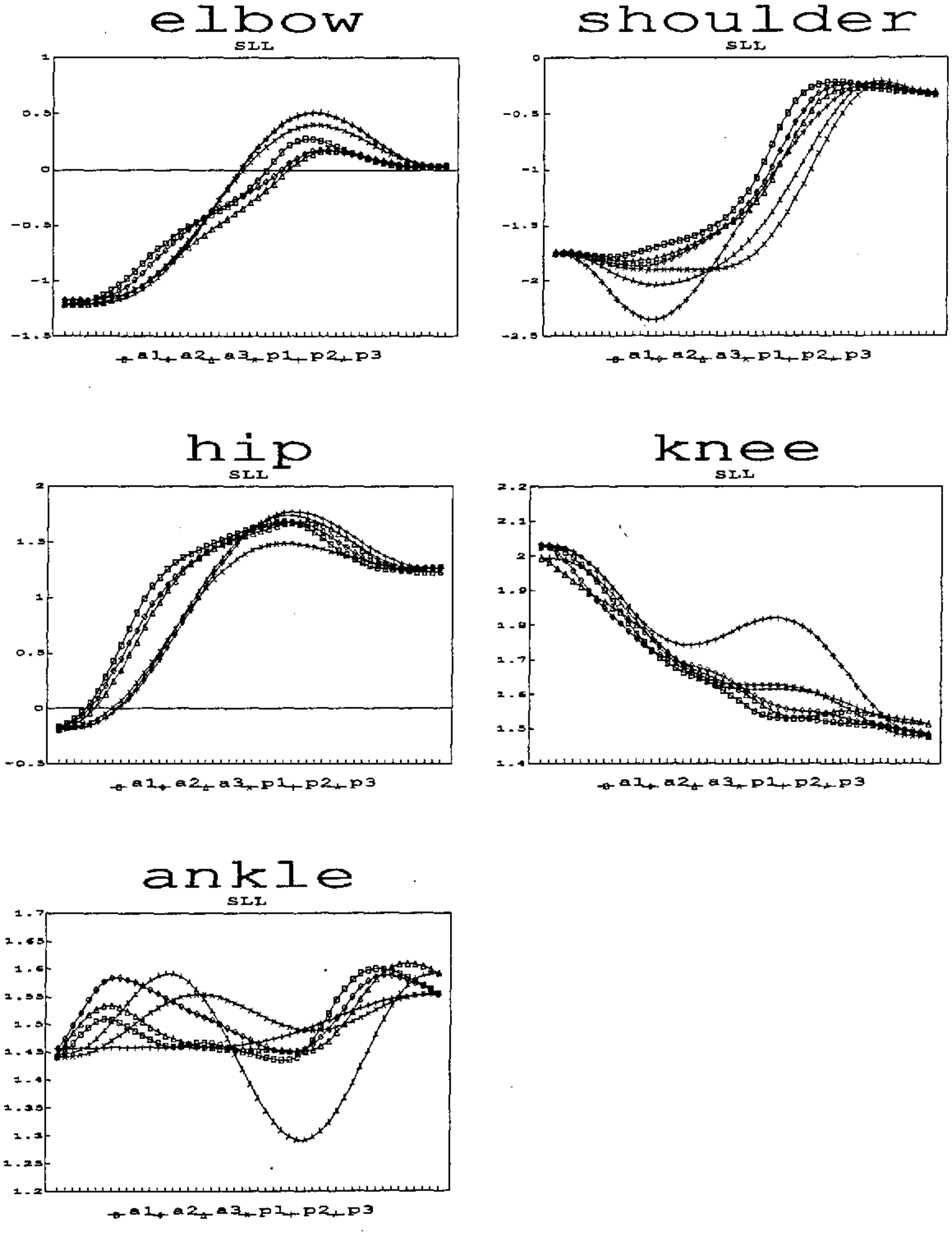

i. SLL

Figure B.2 Continued

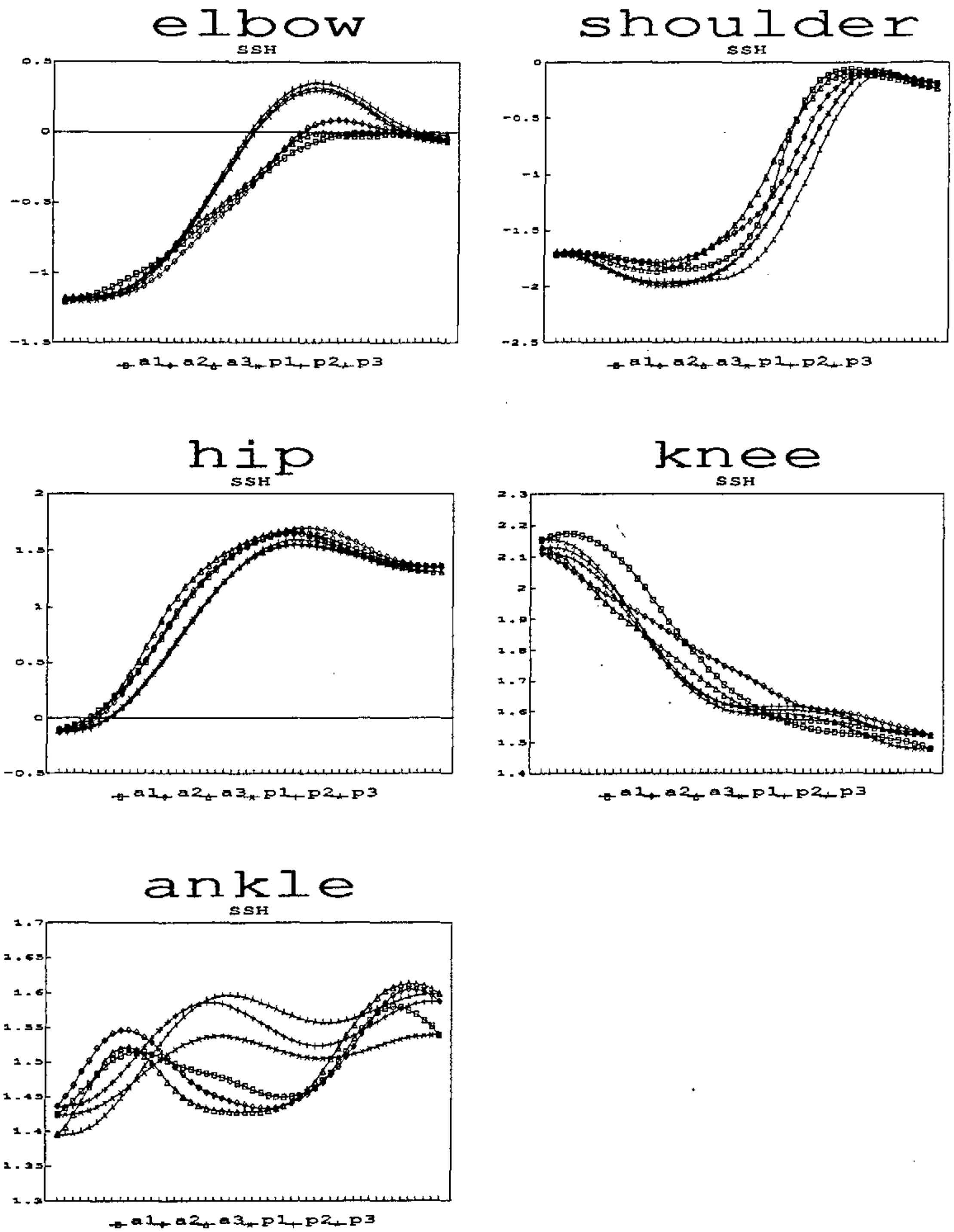

j. SSH

Figure B.2 Continued

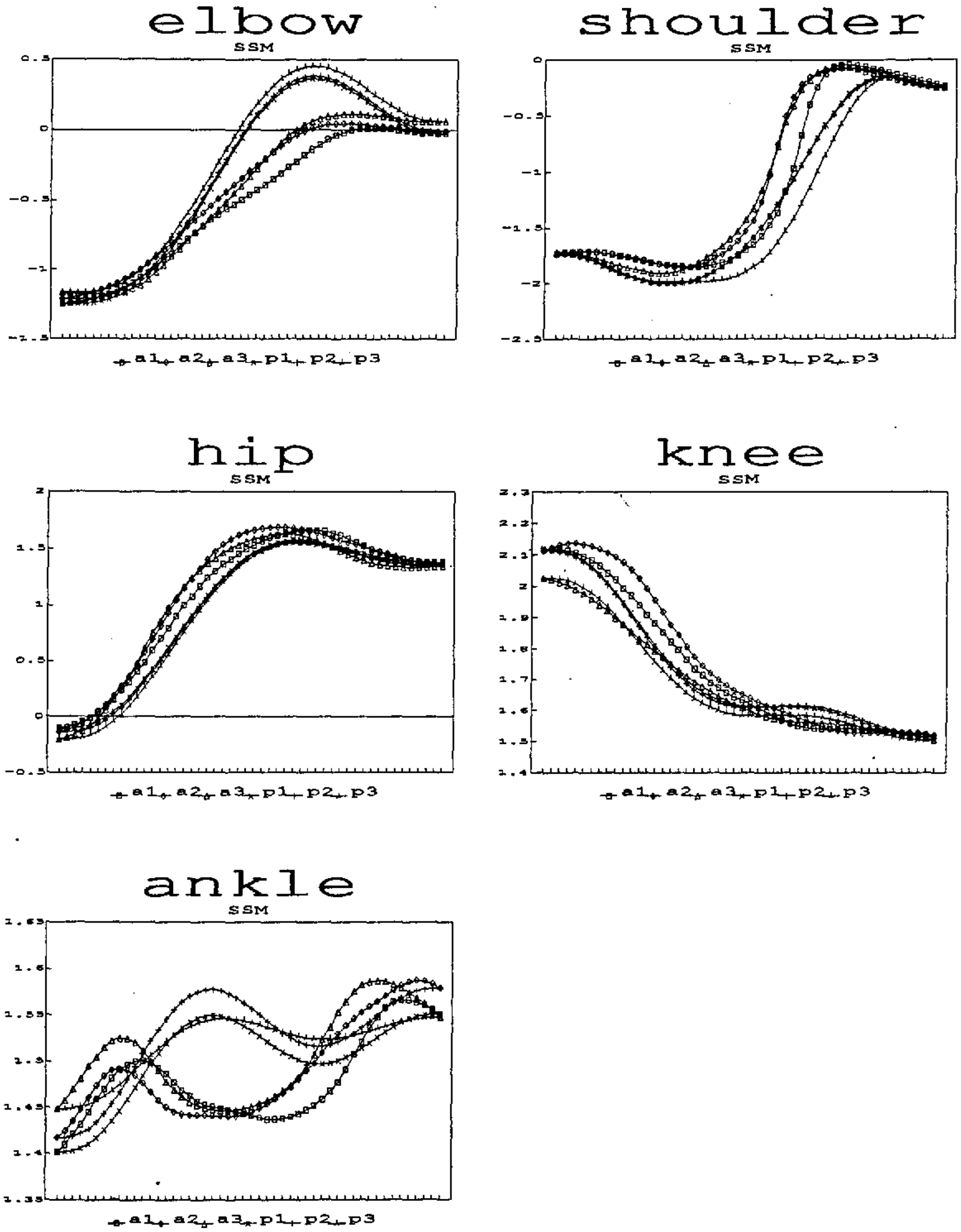

k. SSM

Figure B.2 Continued

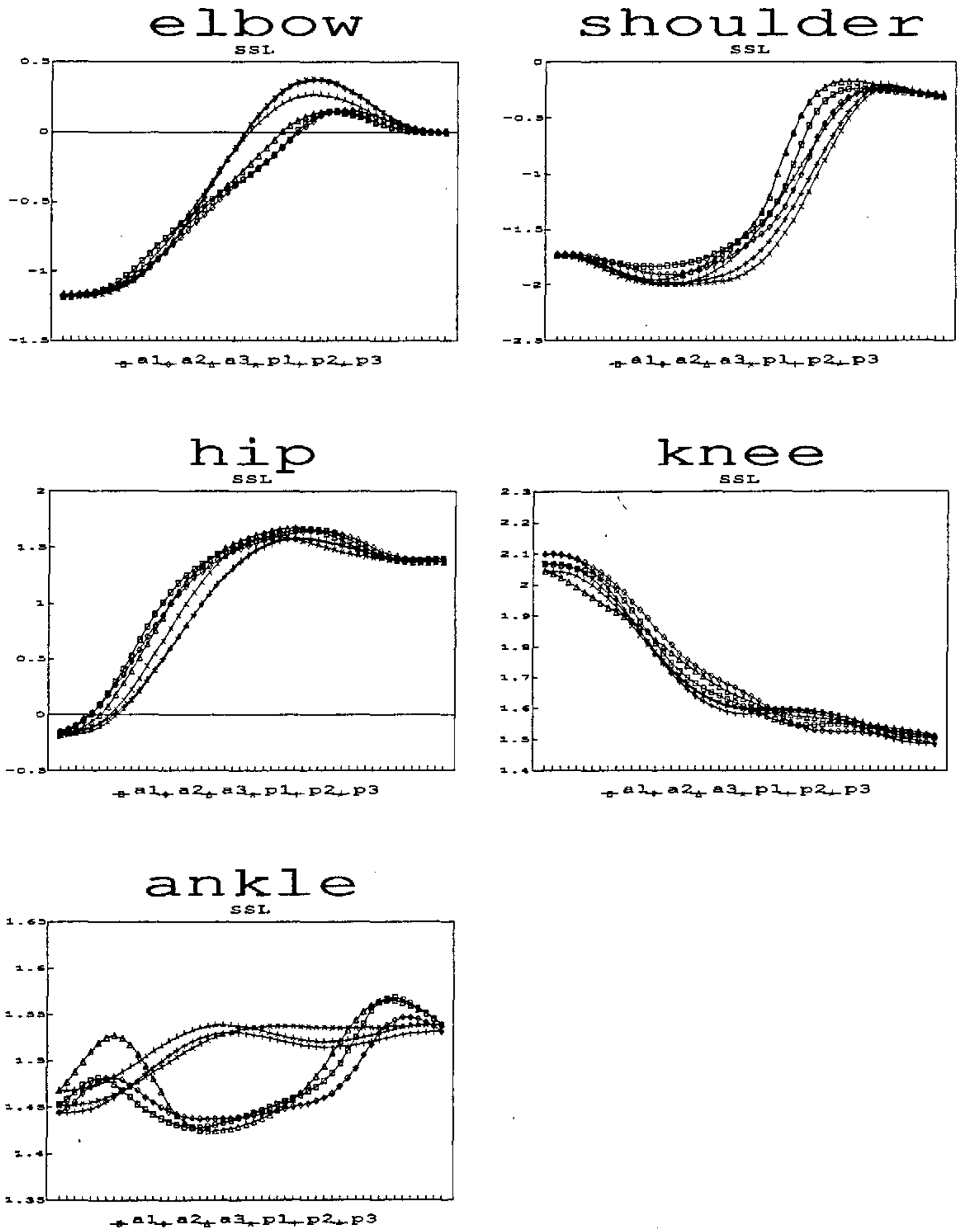

1. SSL

Figure B.2 Continued

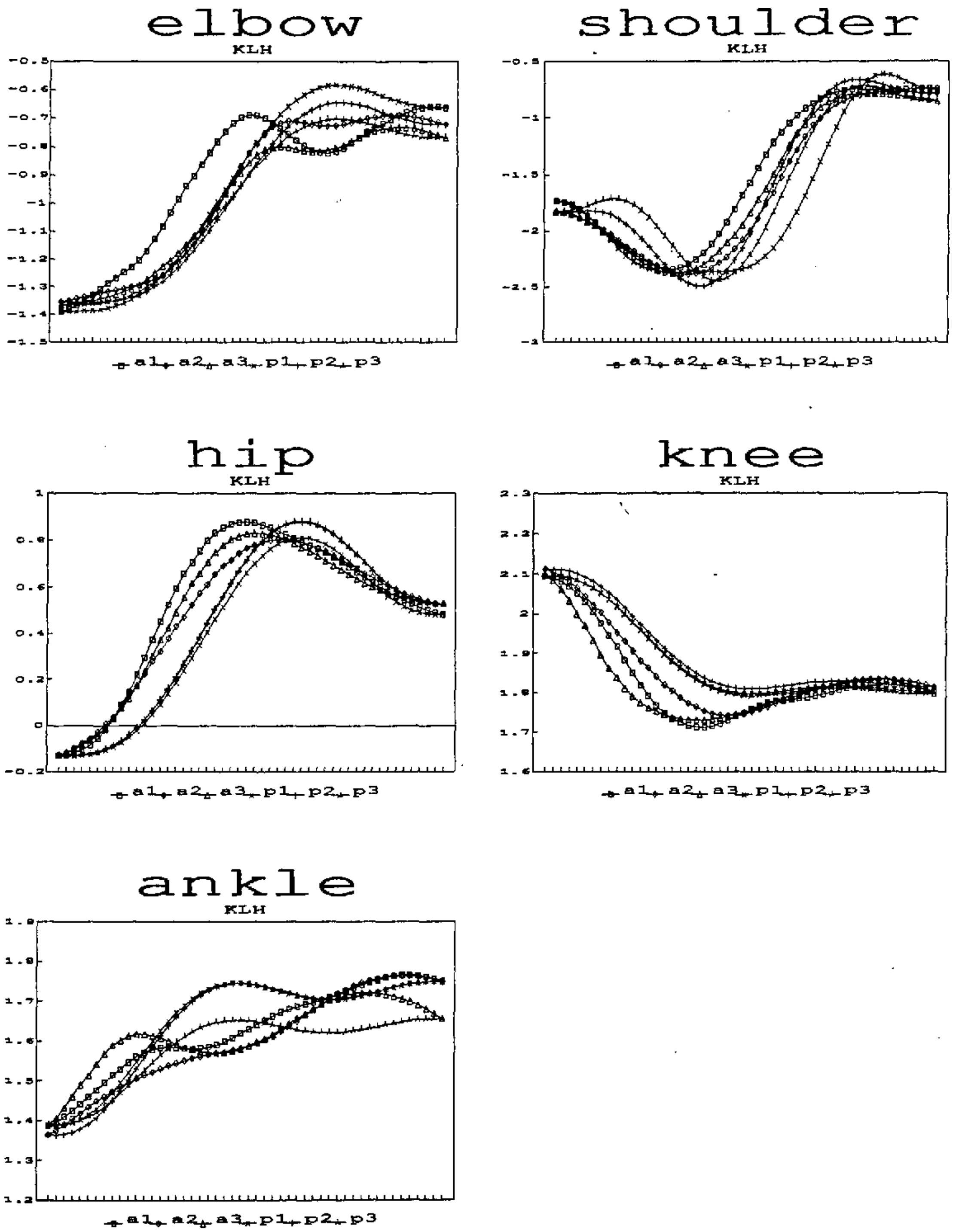

a. KLH

Figure B.3 Actual versus simulated trajectories for subject 4

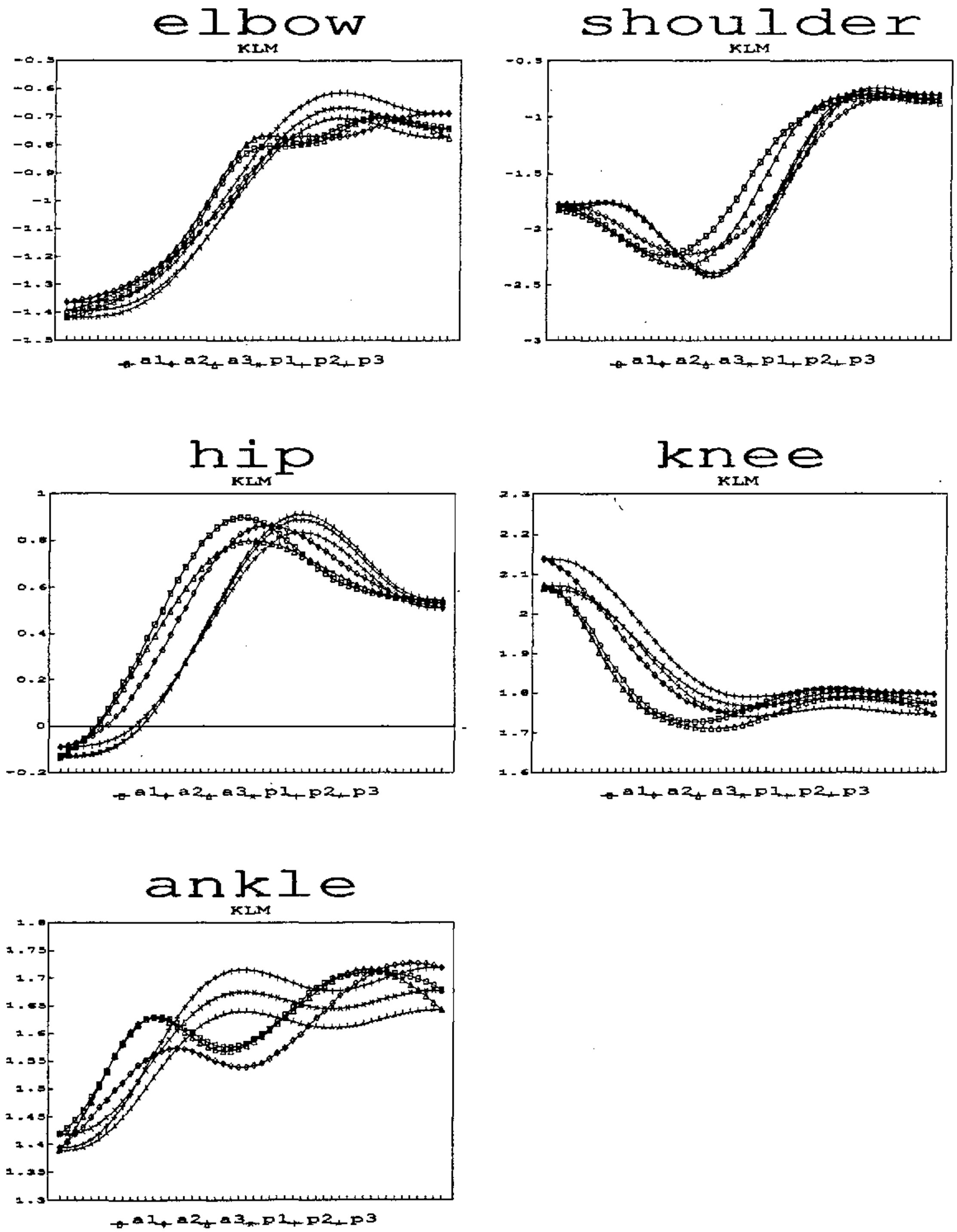

b. KLM

Figure B.3 Continued

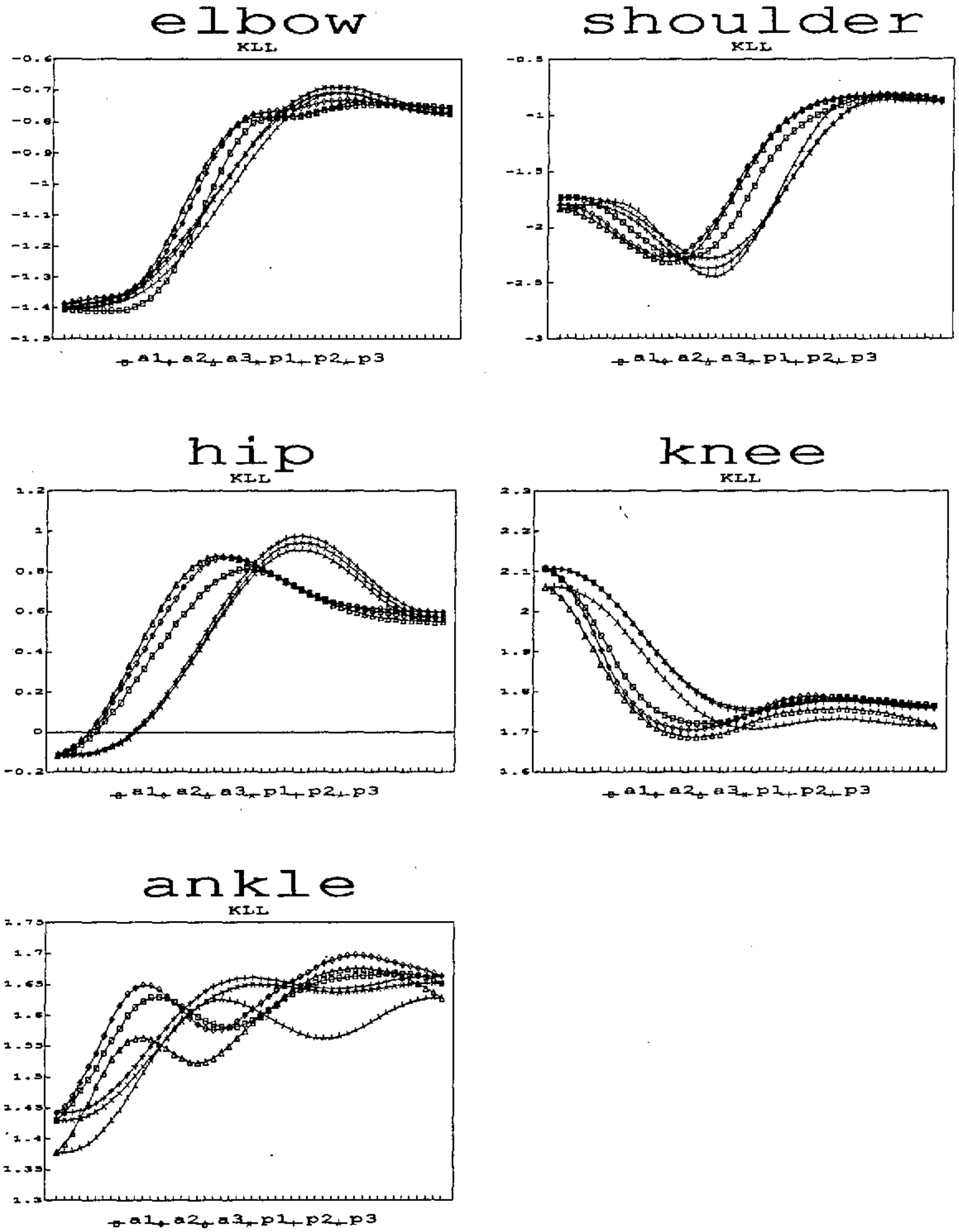

c. KLL

Figure B.3 Continued

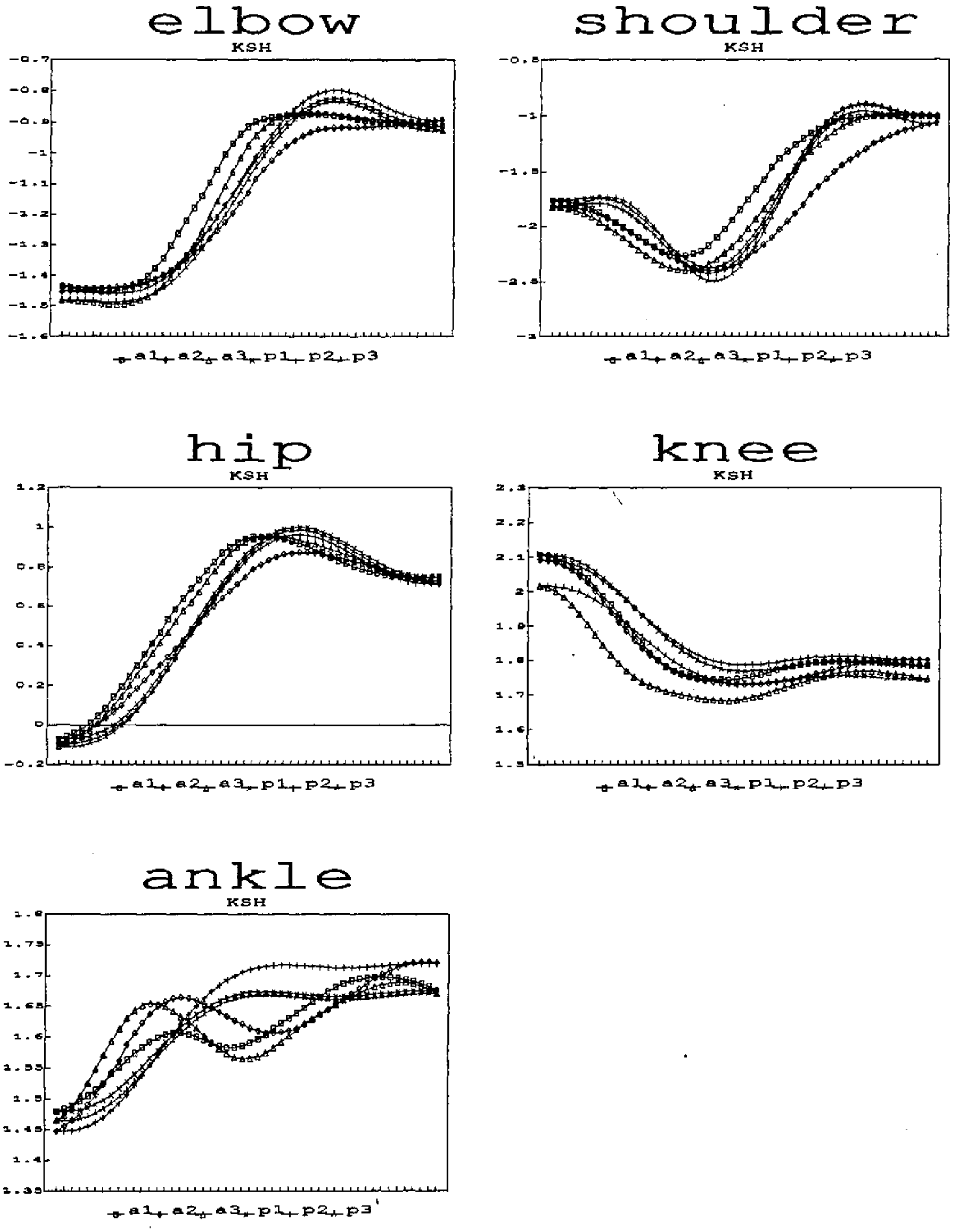

d. KSH

Figure B.3 Continued

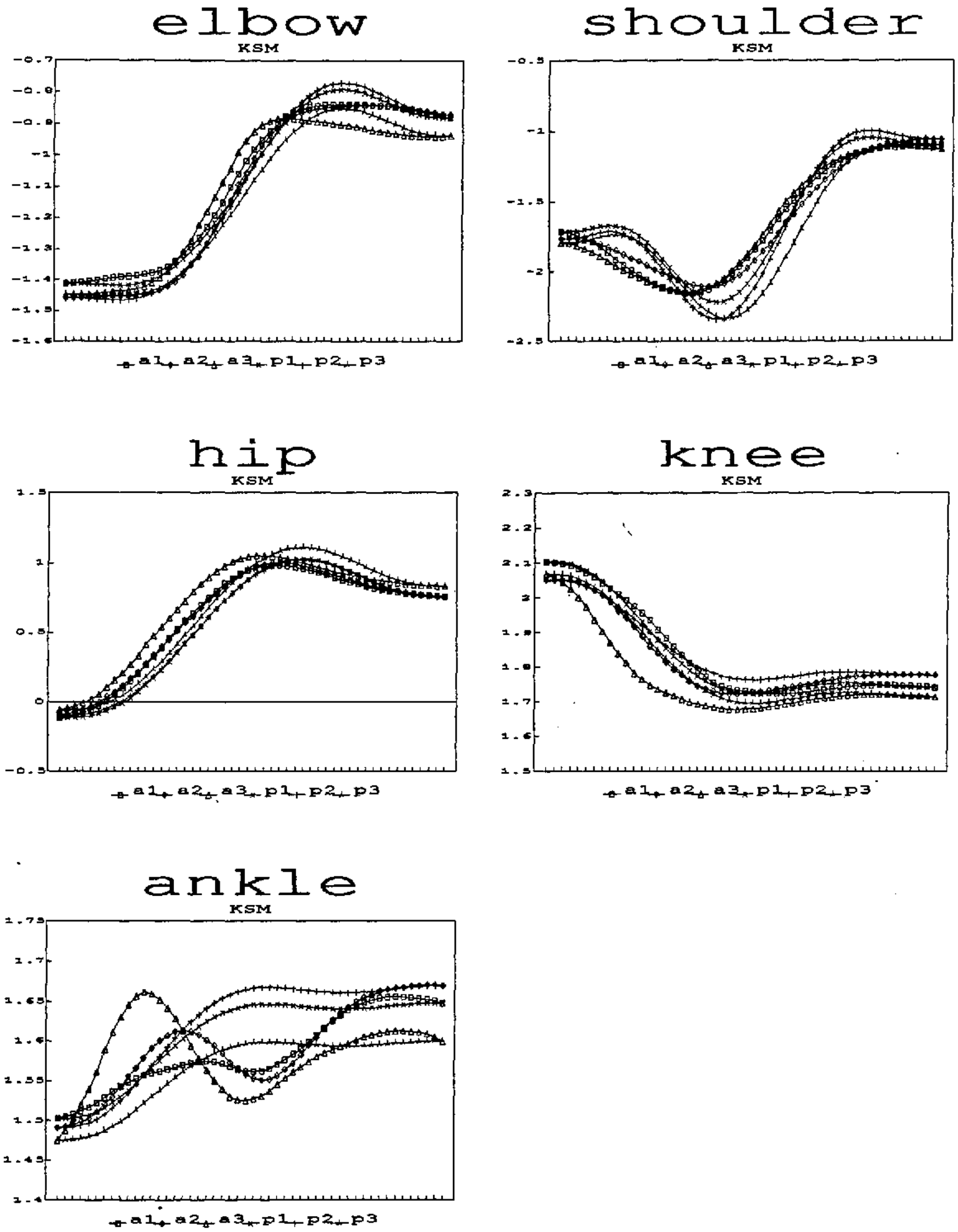

e. KSM

Figure B.3 Continued

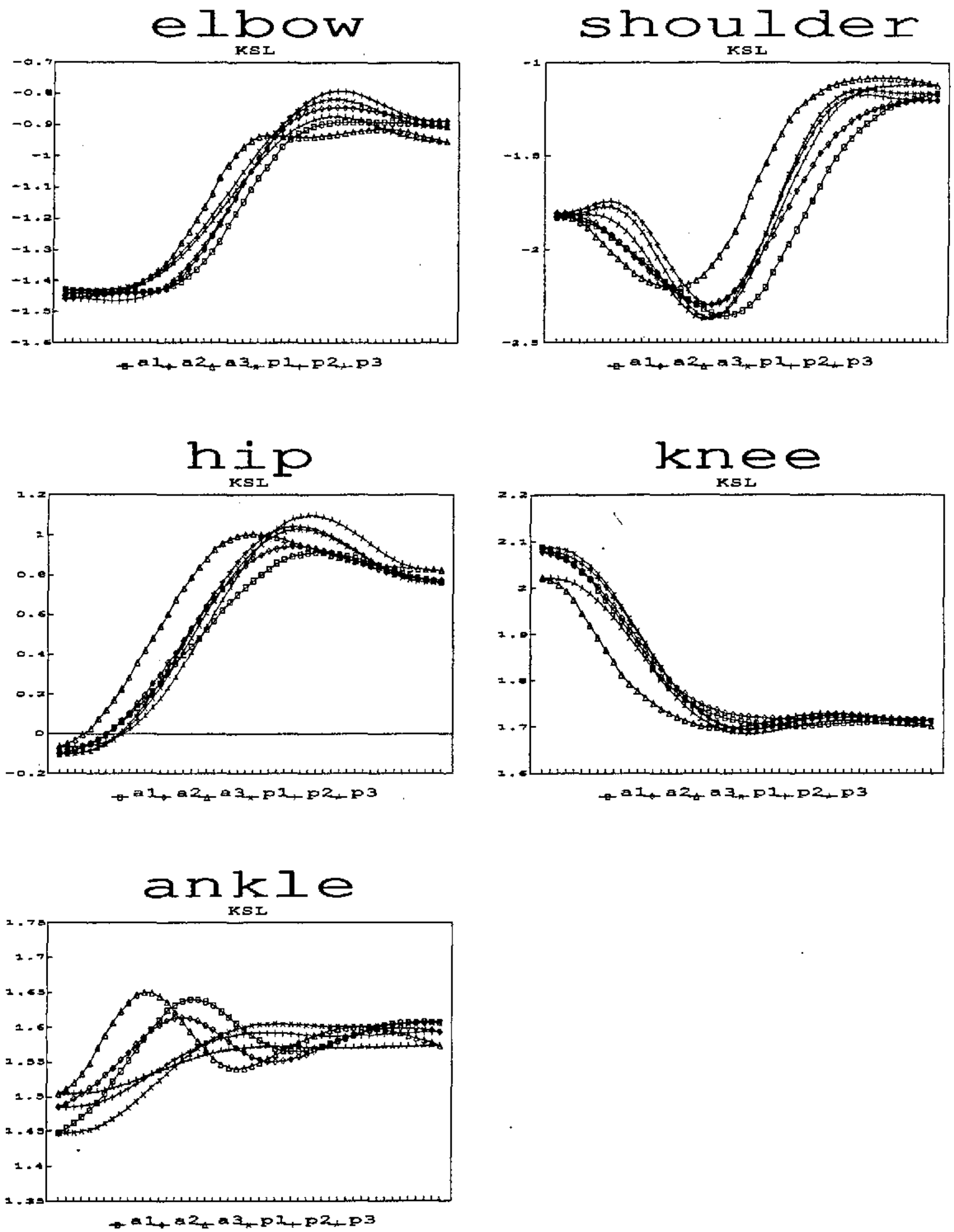

f. KSL

Figure B.3 Continued

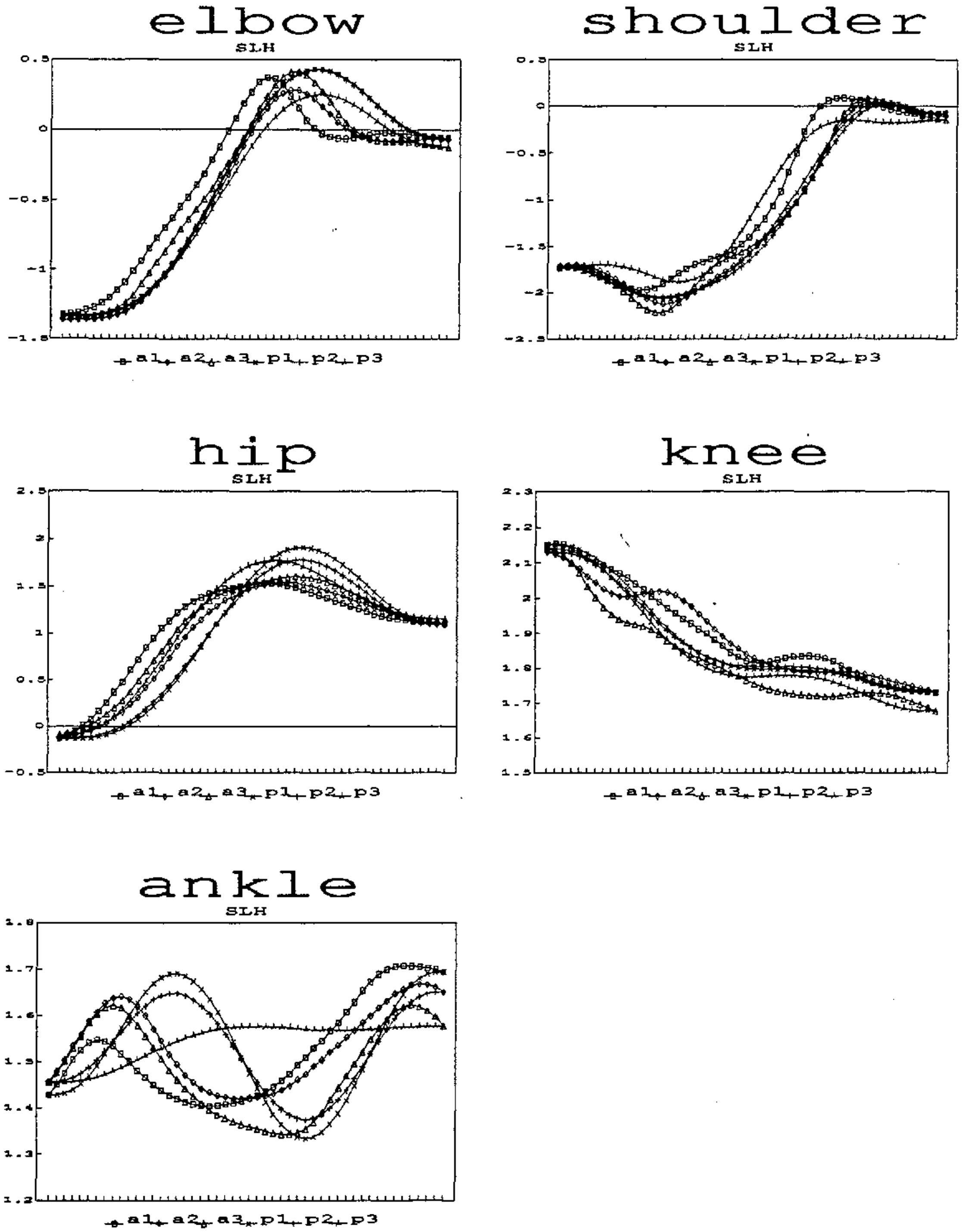

g. SLH

Figure B.3 Continued

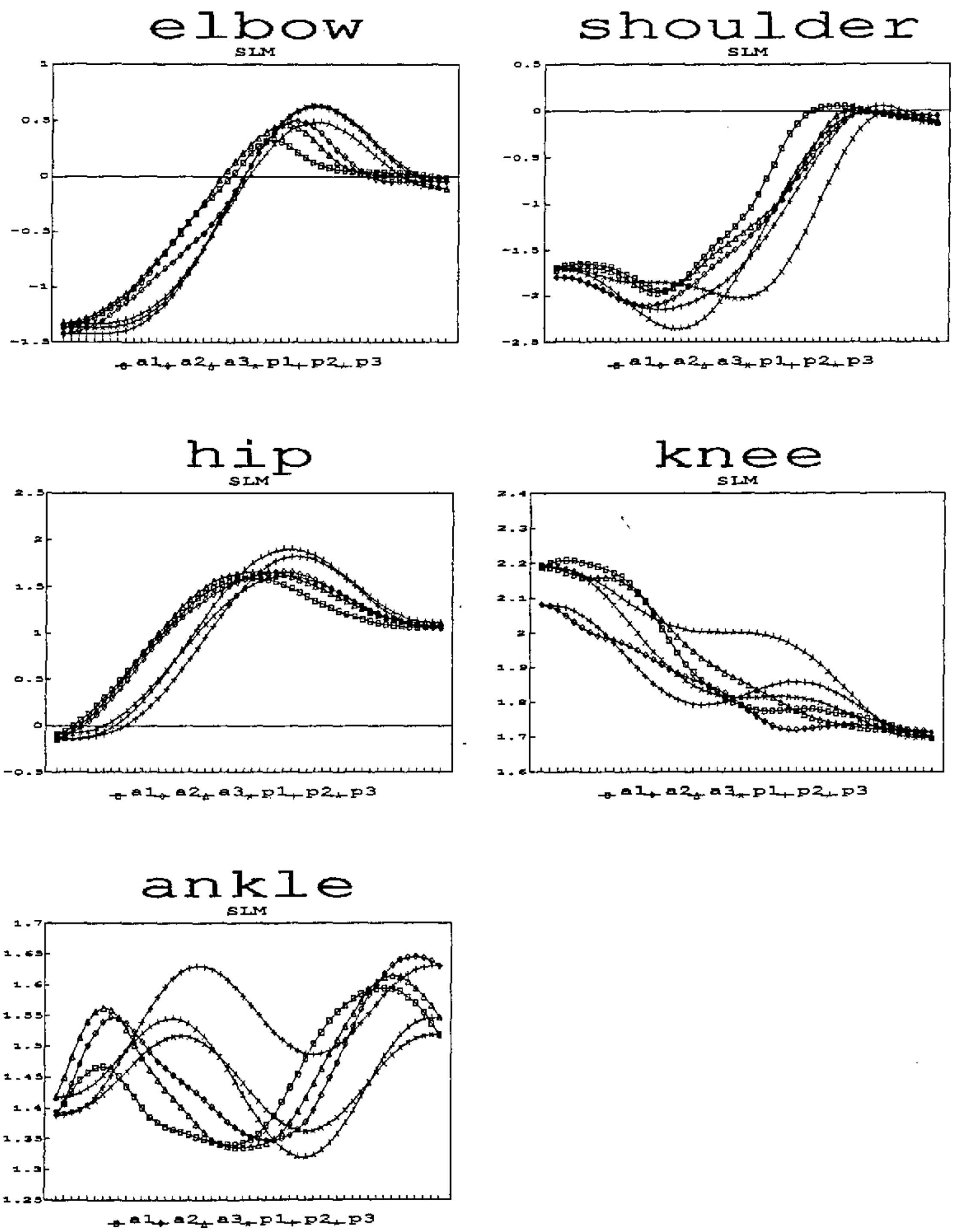

h. SLM

Figure B.3 Continued

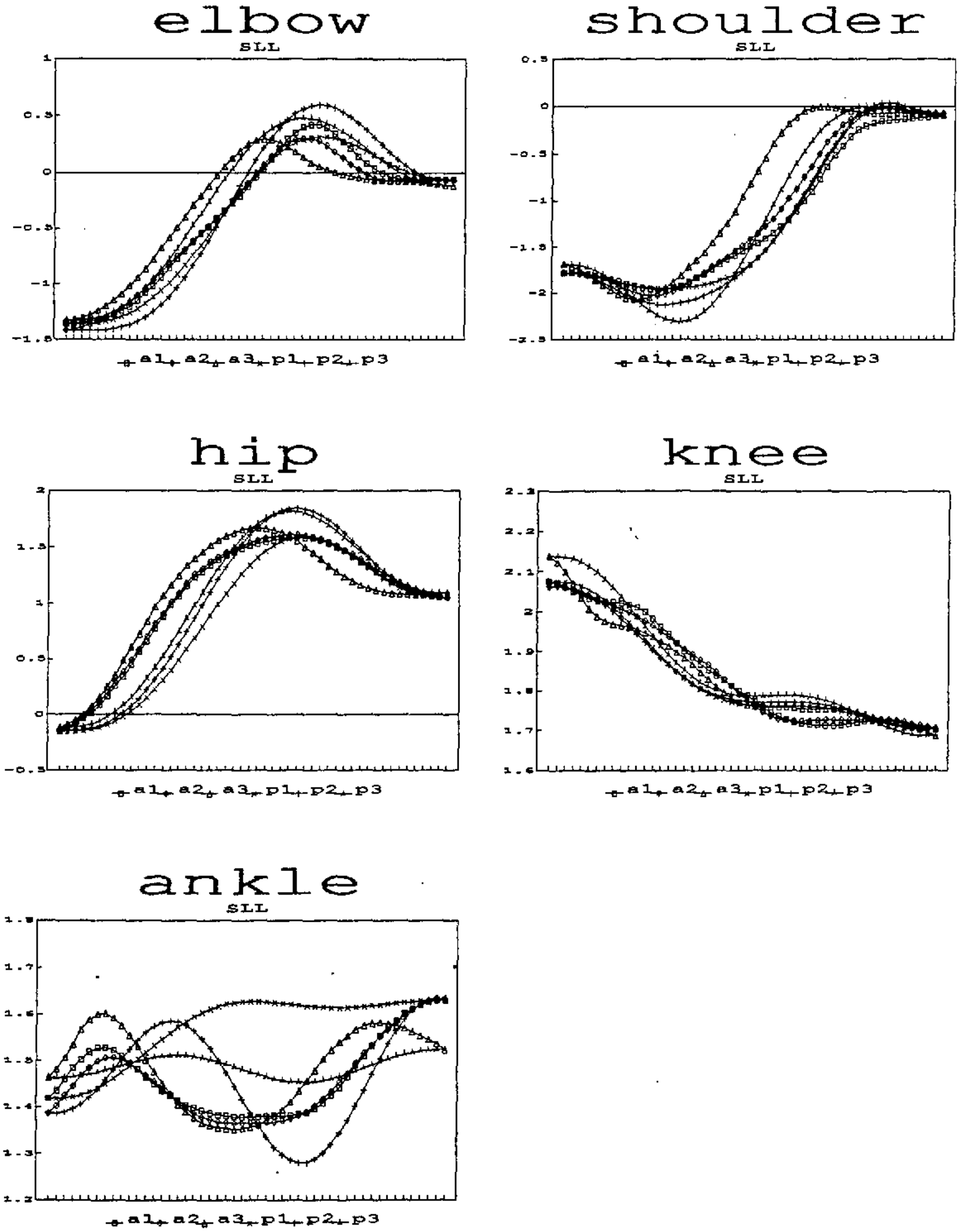

i. SLL

Figure B.3 Continued

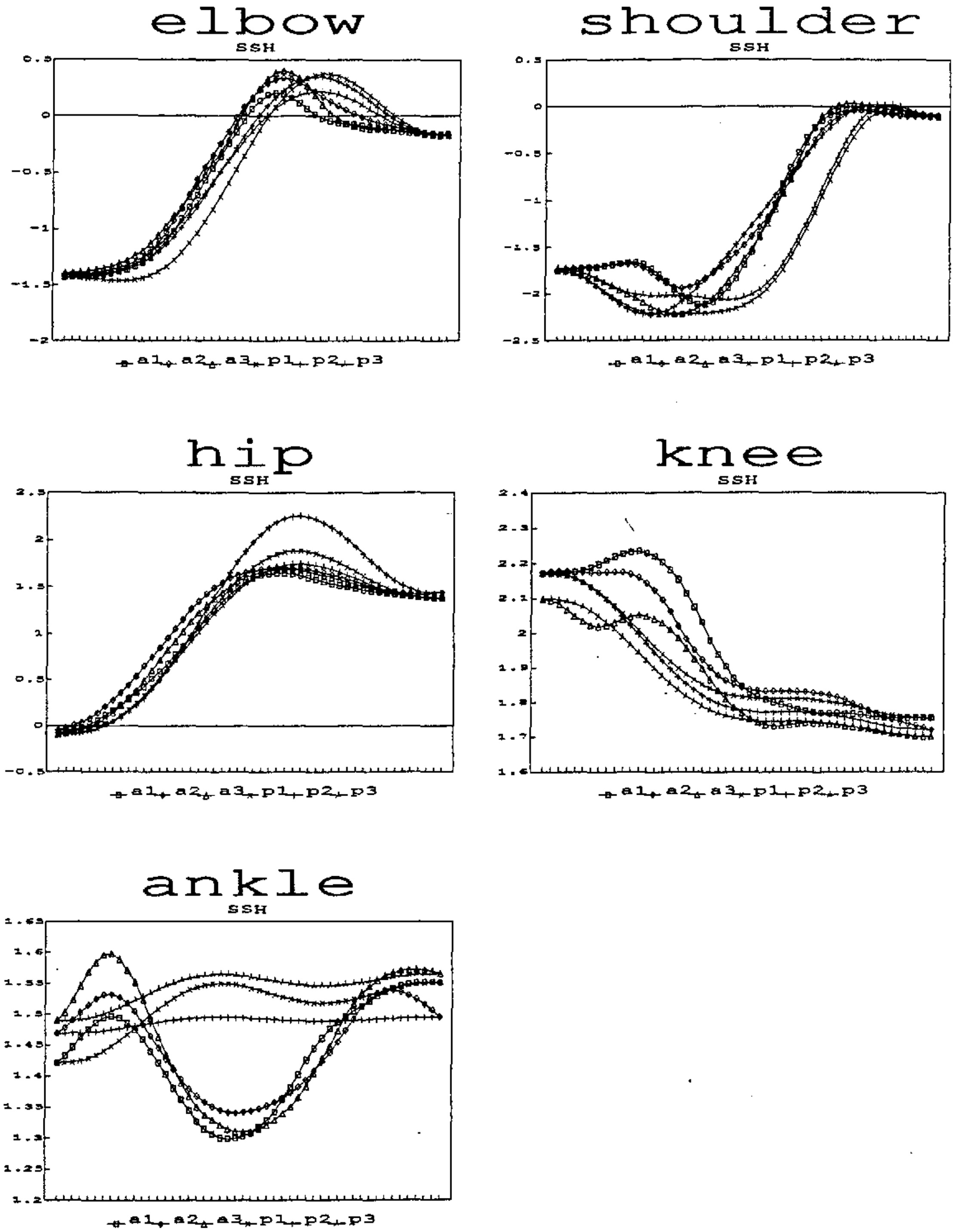

j. SSH

Figure B.3 Continued

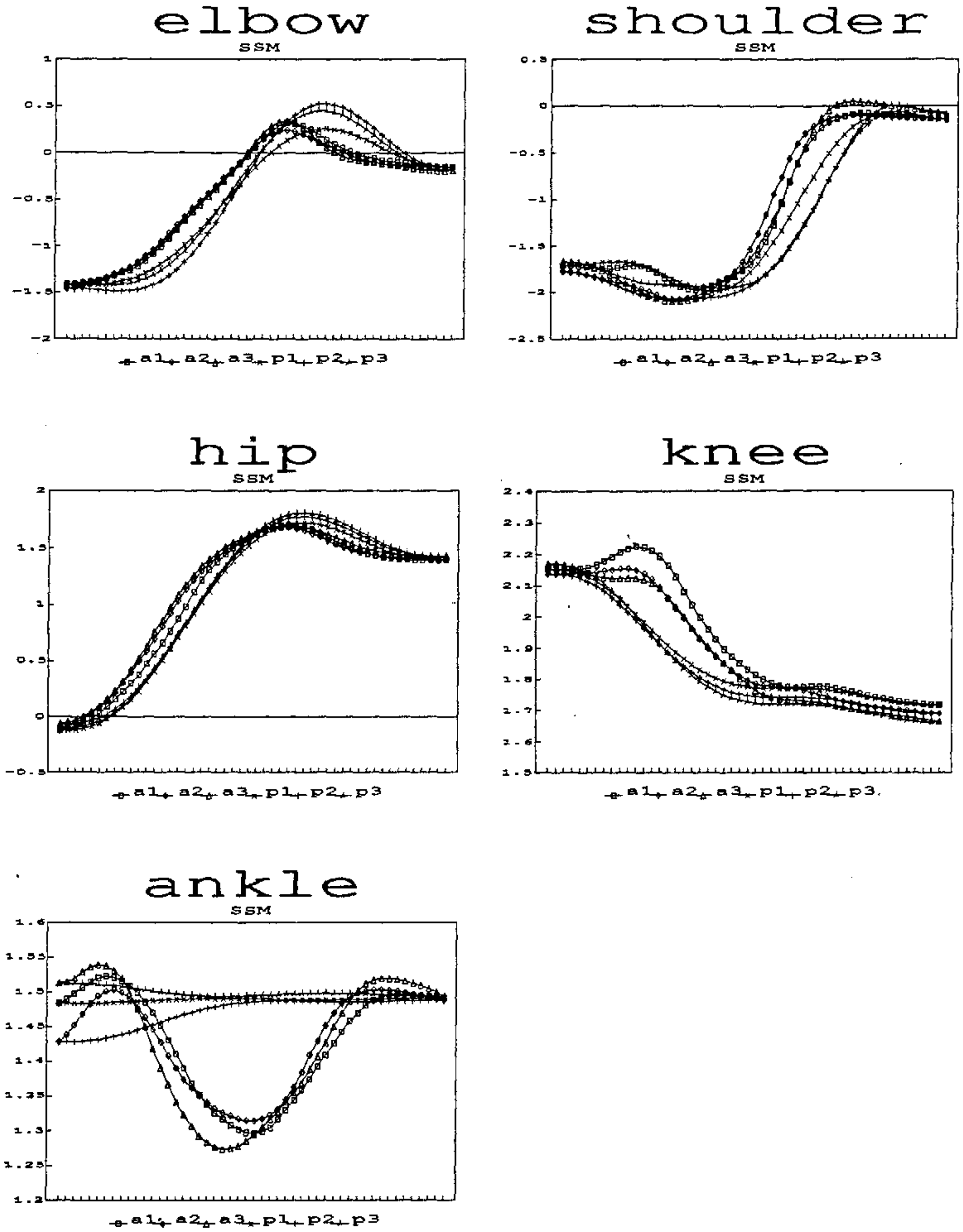

k. SSM

Figure B.3 Continued

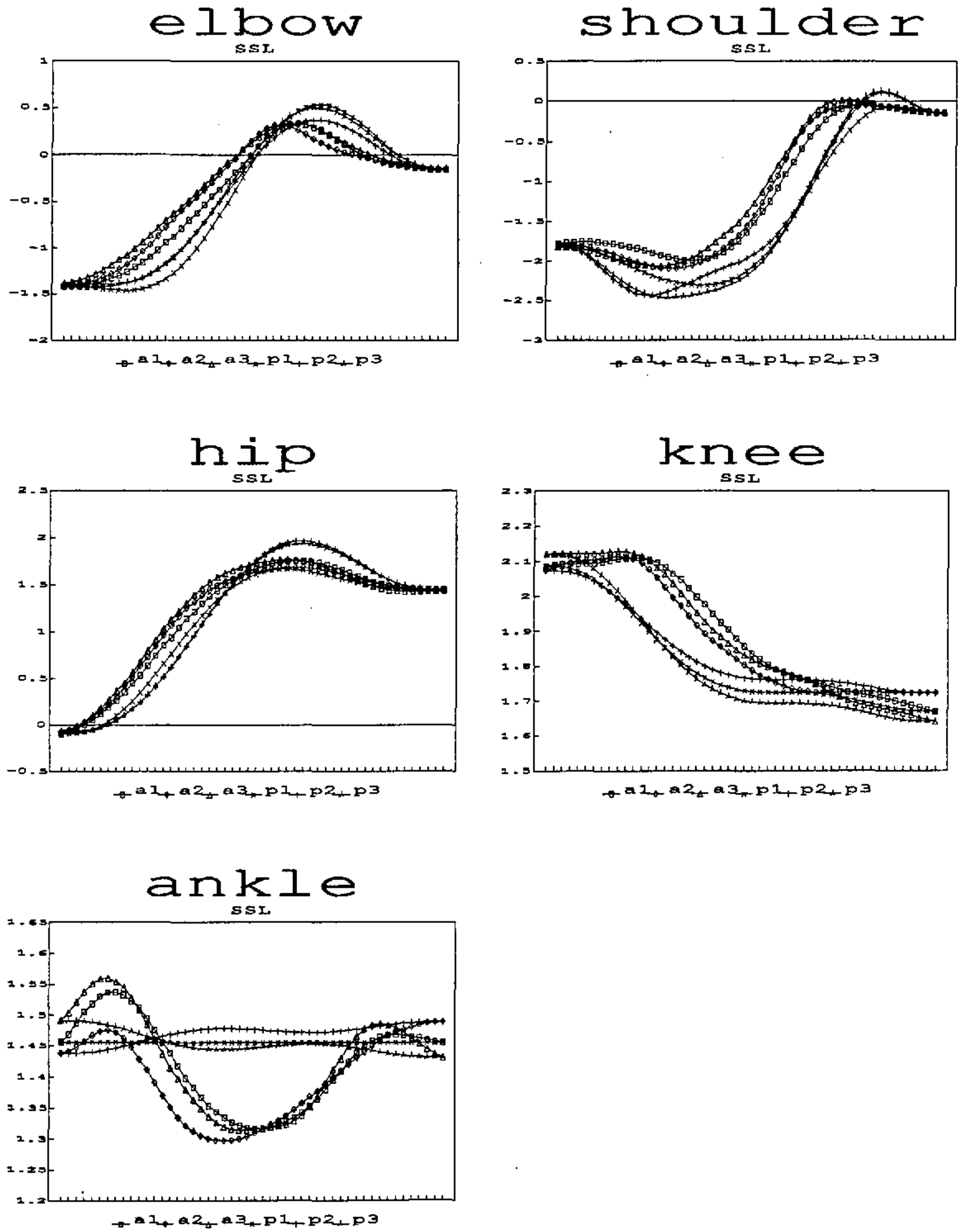

1. SSL

Figure B.3 Continued

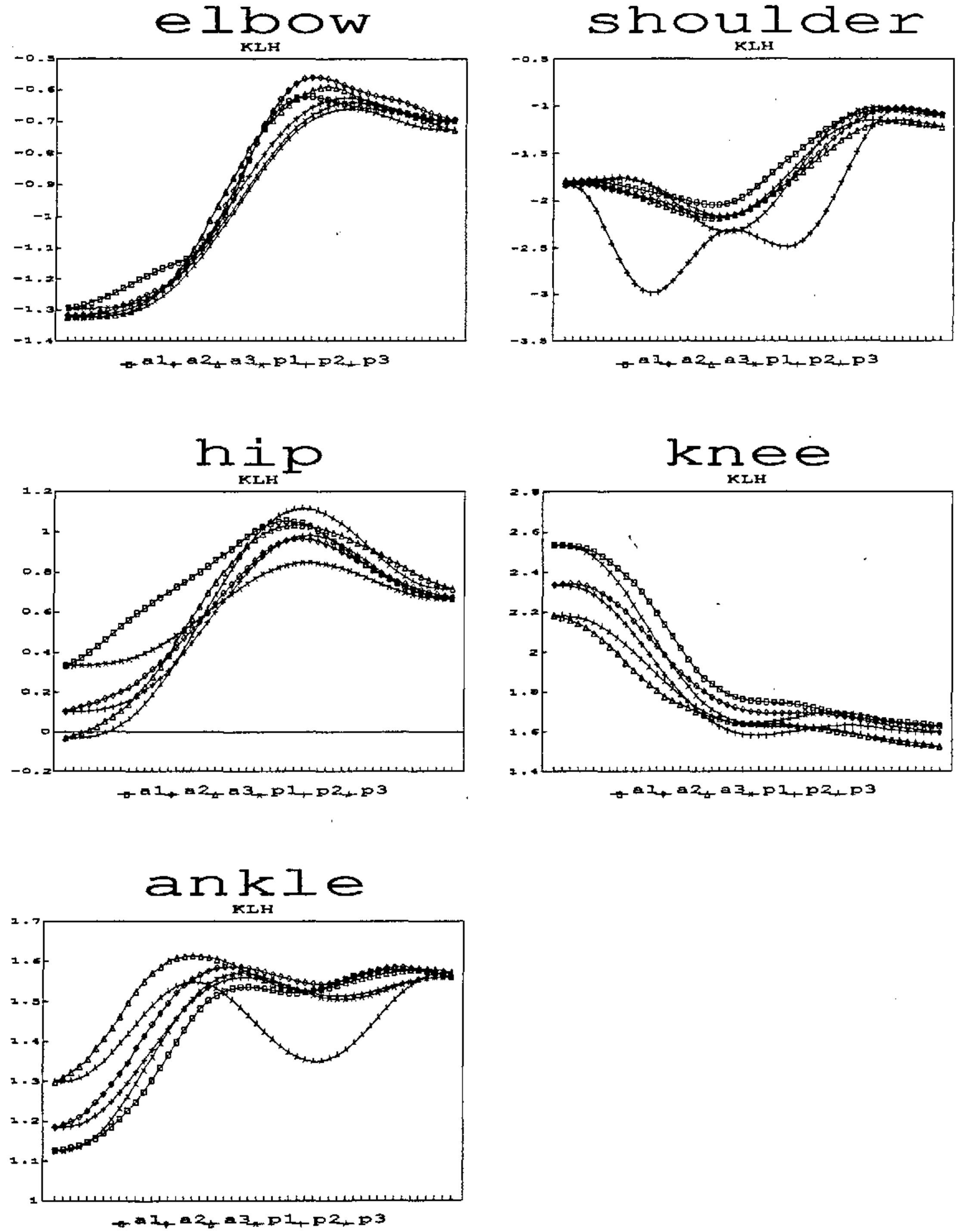

a. KLH

Figure B.4 Actual versus simulated trajectories for subject 5

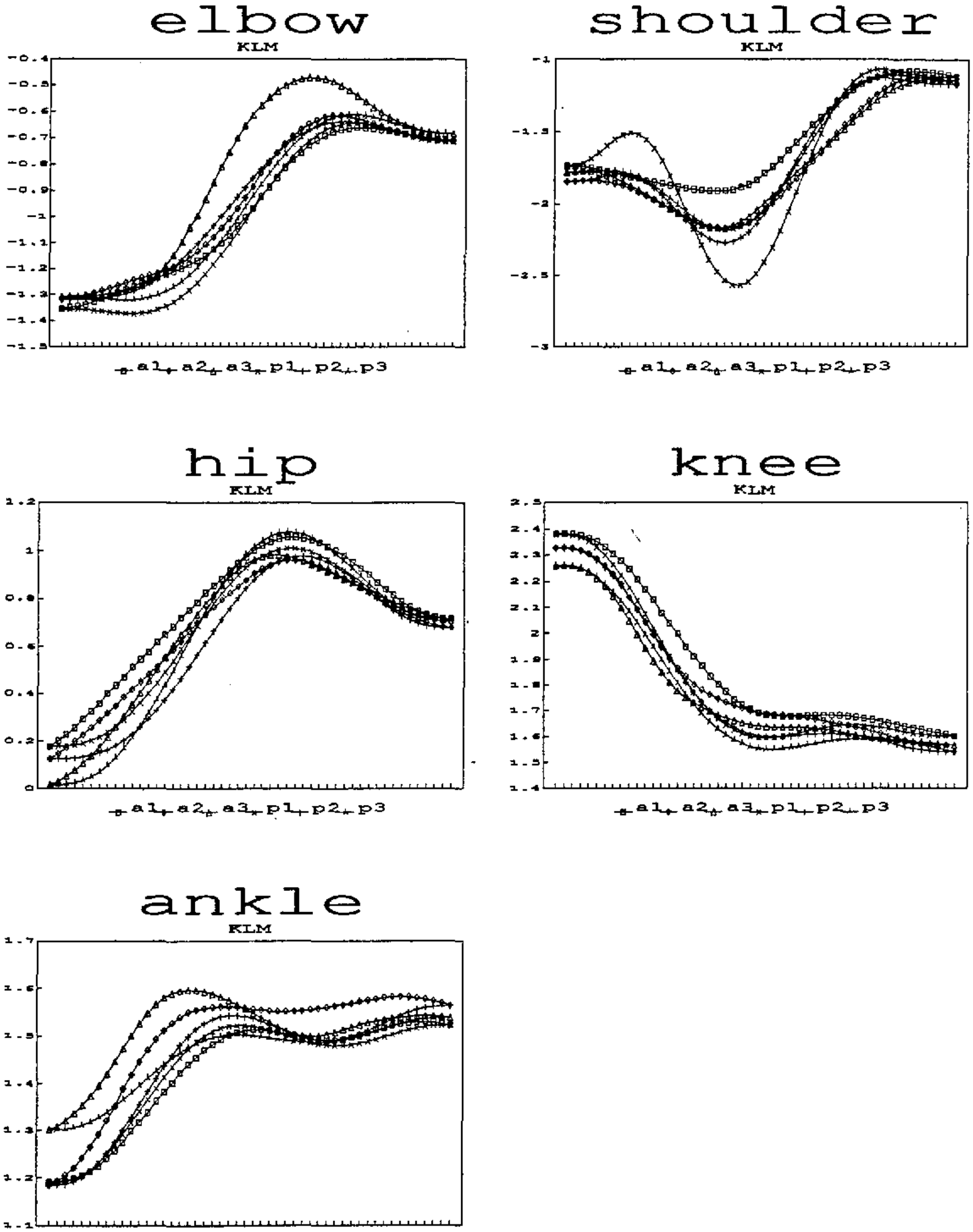

b. KLM

Figure B.4 Continued

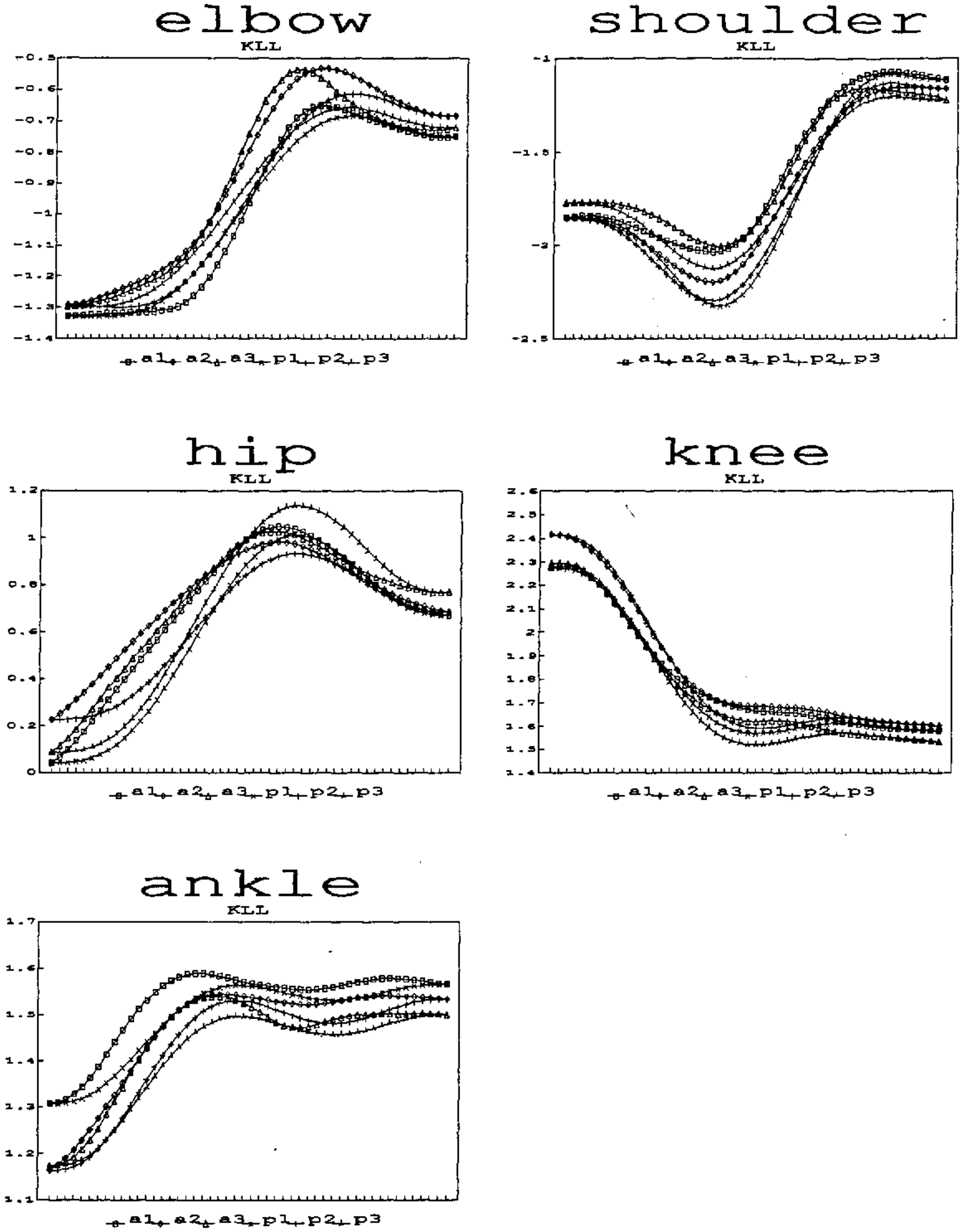

c. KLL

Figure B.4 Continued

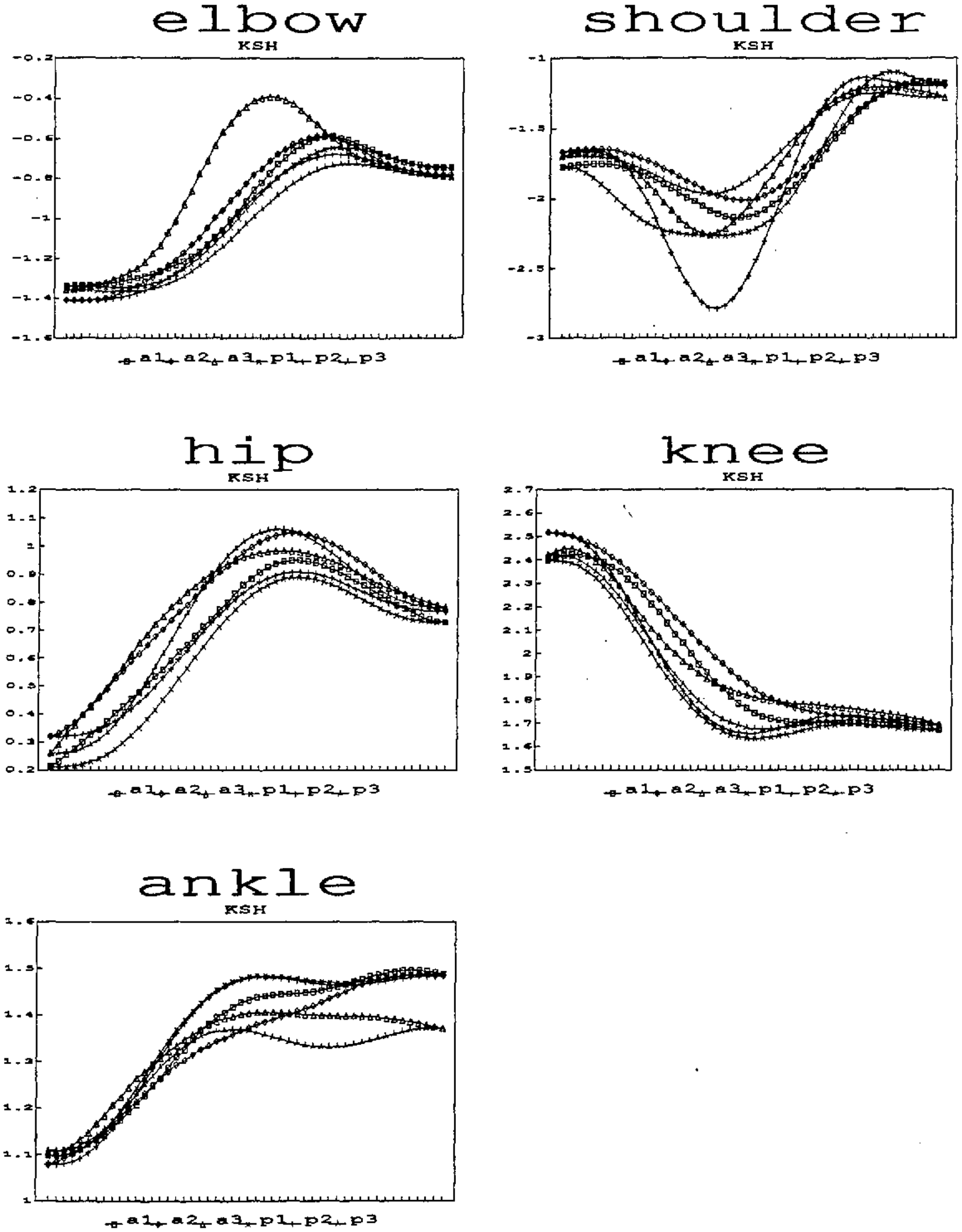

d. KSH

Figure B.4 Continued

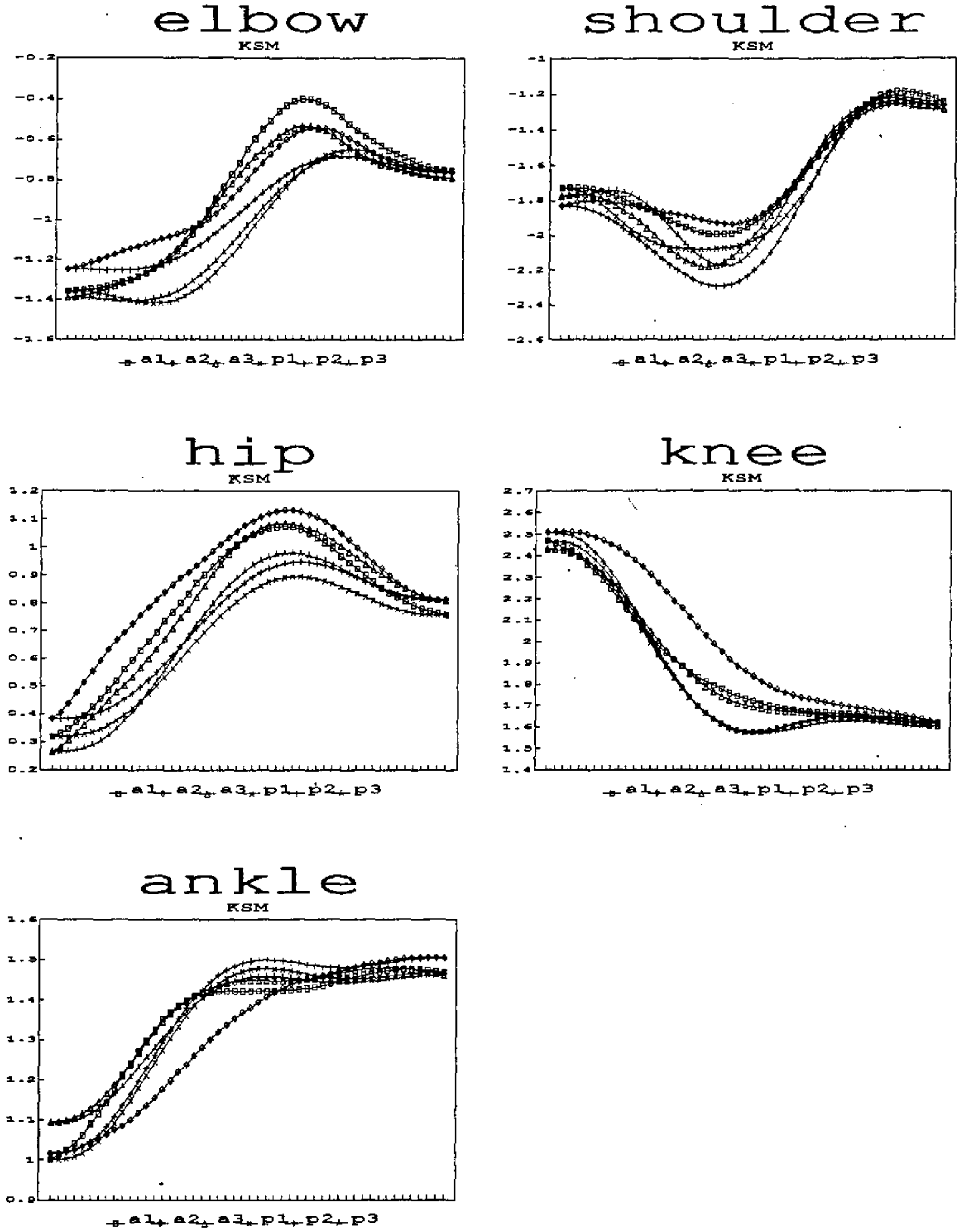

e. KSM

Figure B.4 Continued

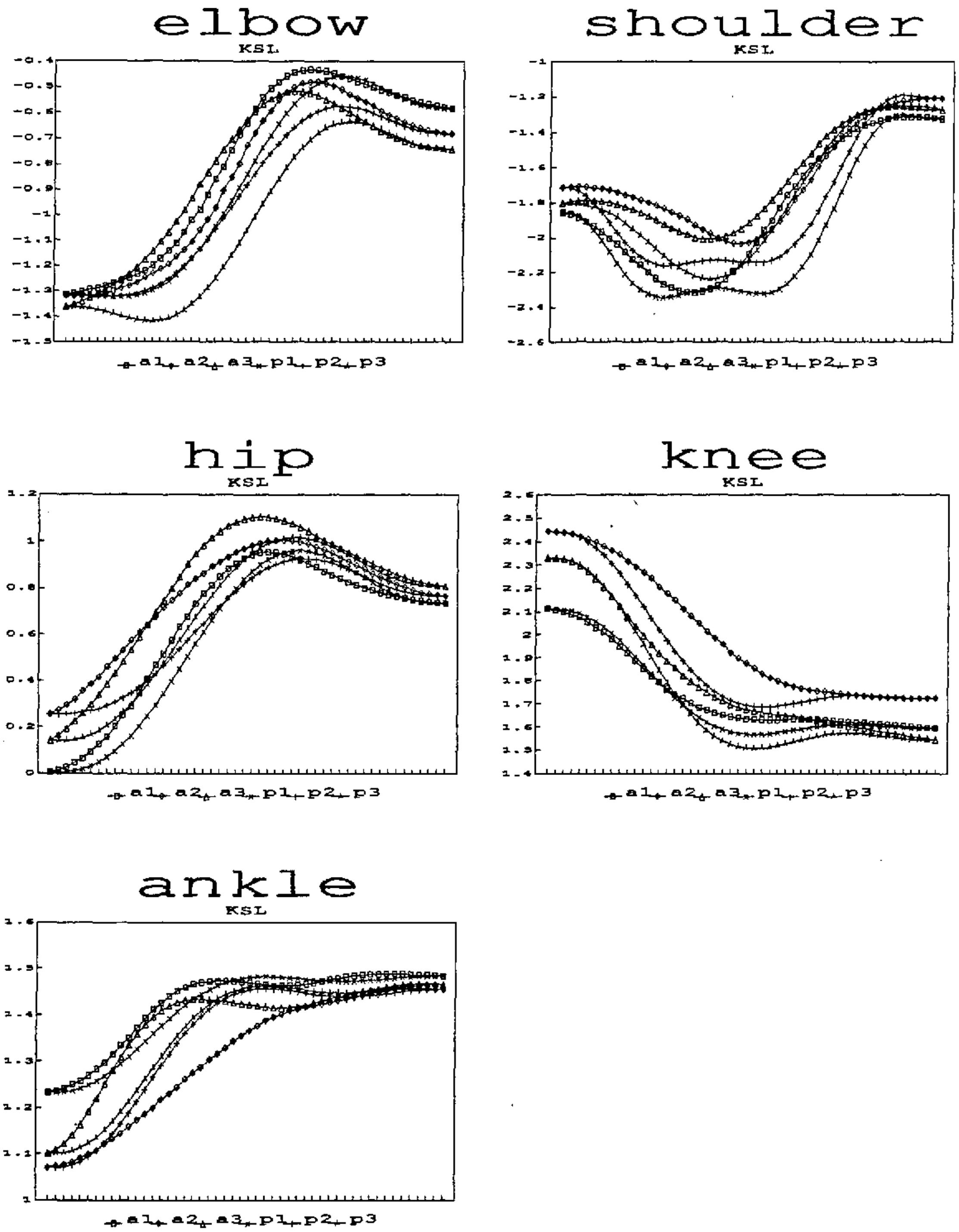

f. KSL

Figure B.4 Continued

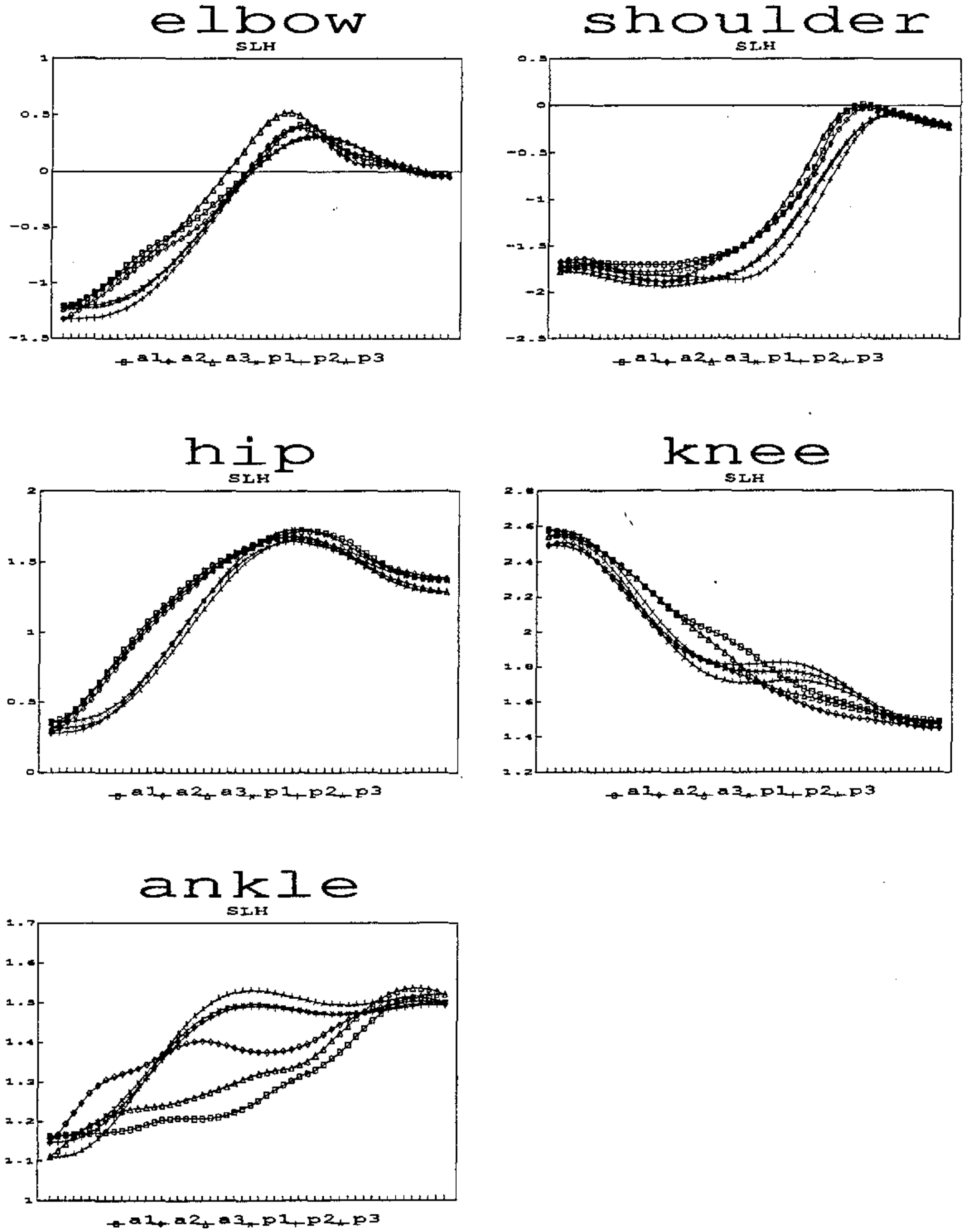

g. SLH

Figure B.4 Continued

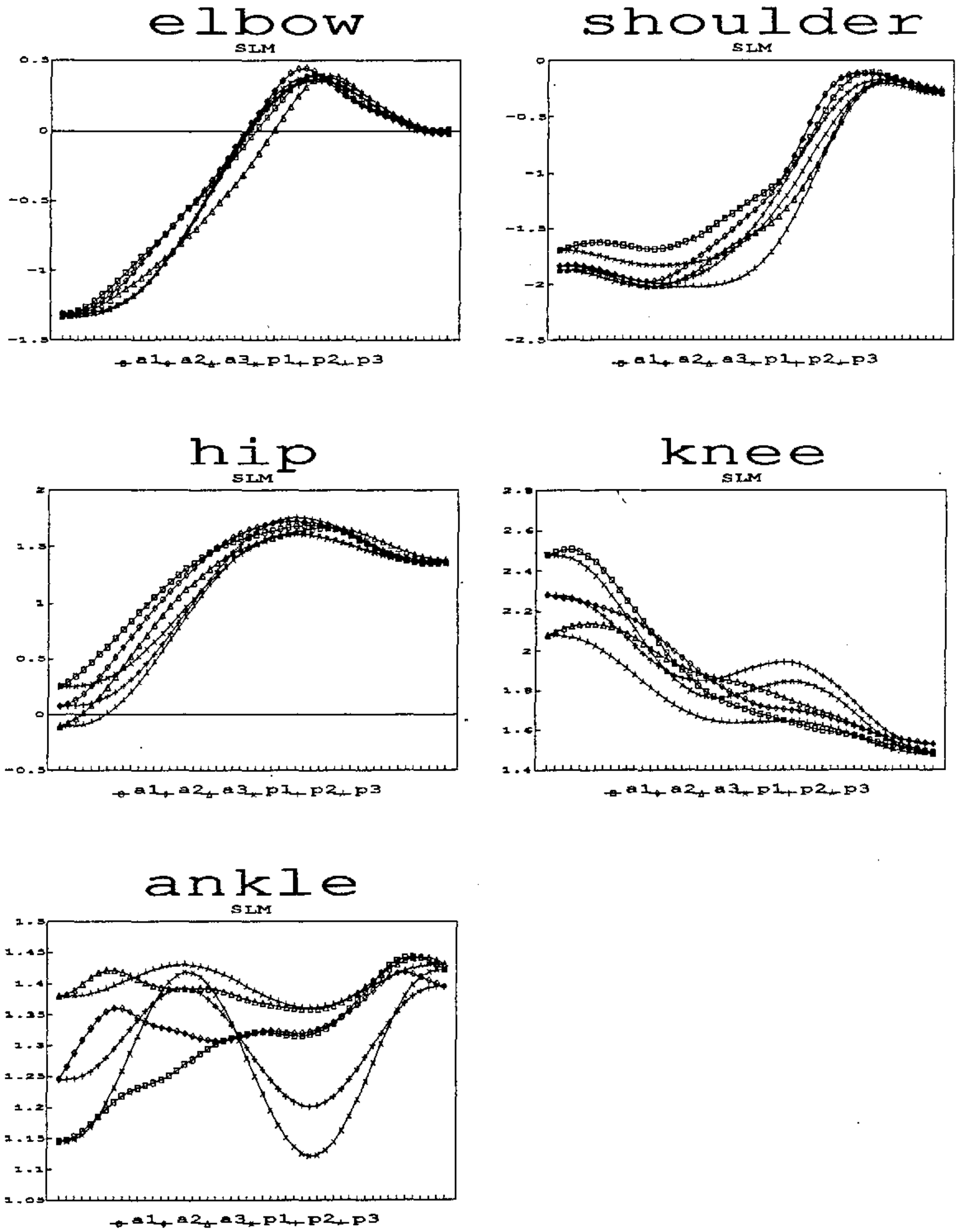

h. SLM

Figure B.4 Continued

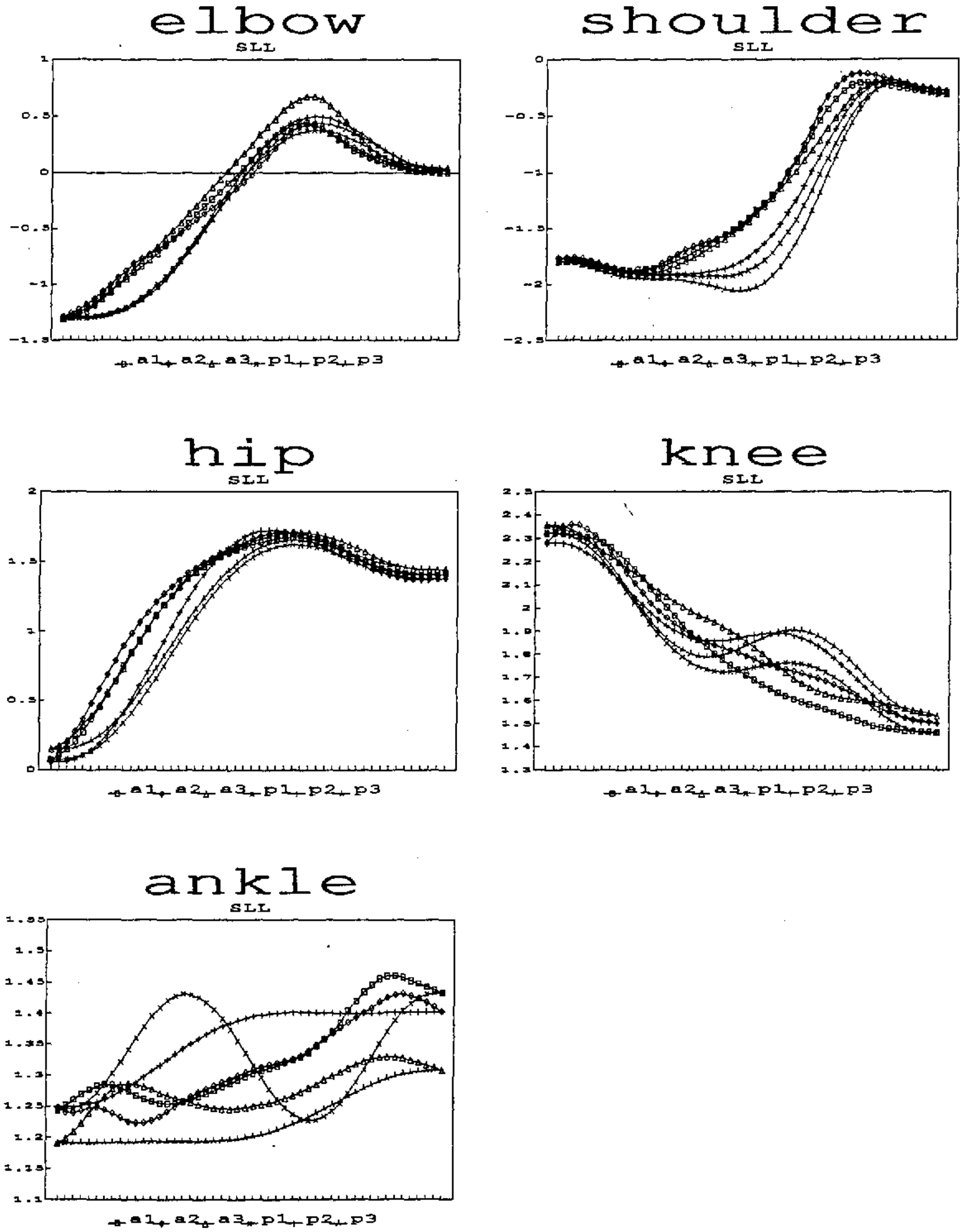

i. SLL

Figure B.4 Continued

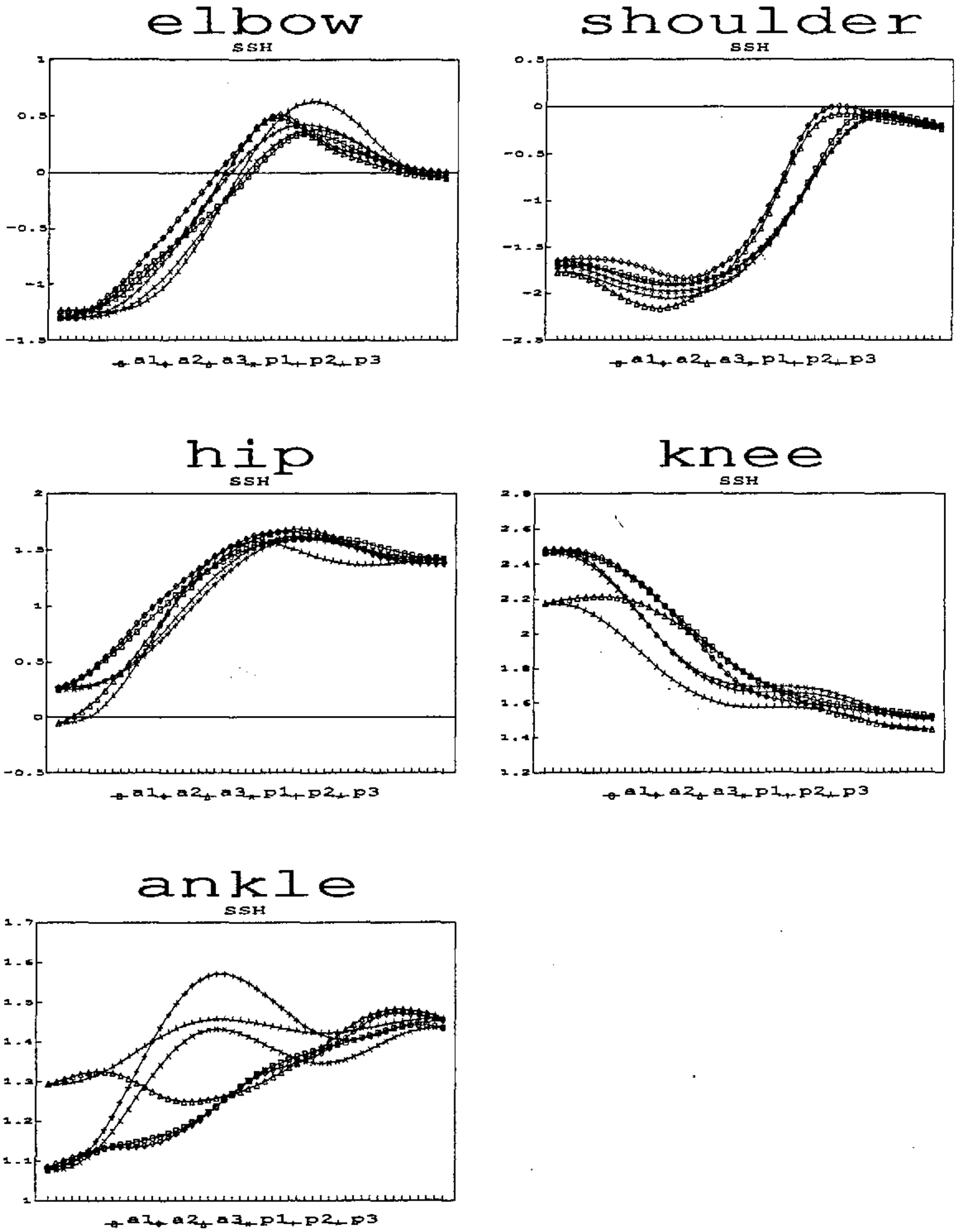

j. SSH

Figure B.4 Continued

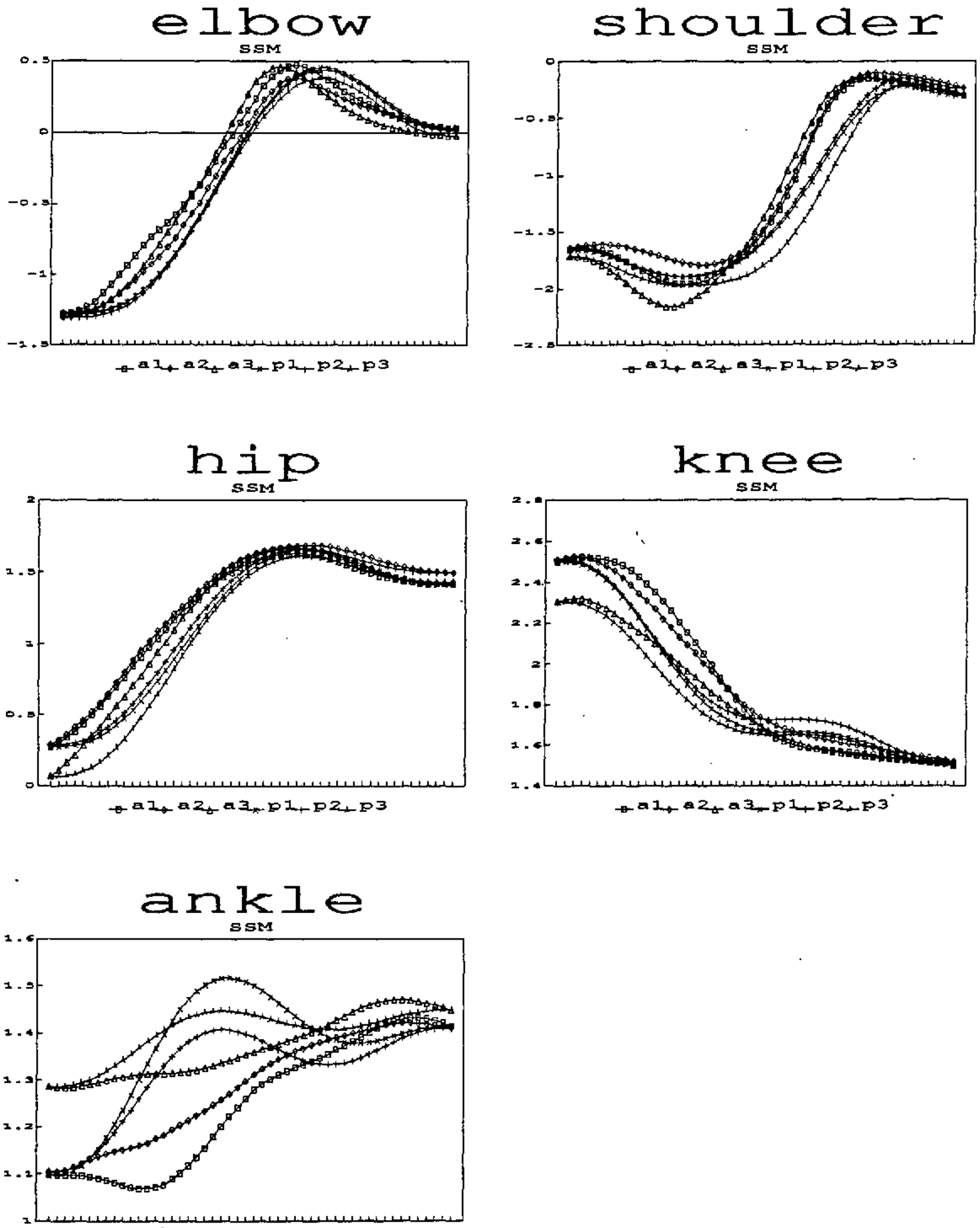

k. SSM

Figure B.4 Continued

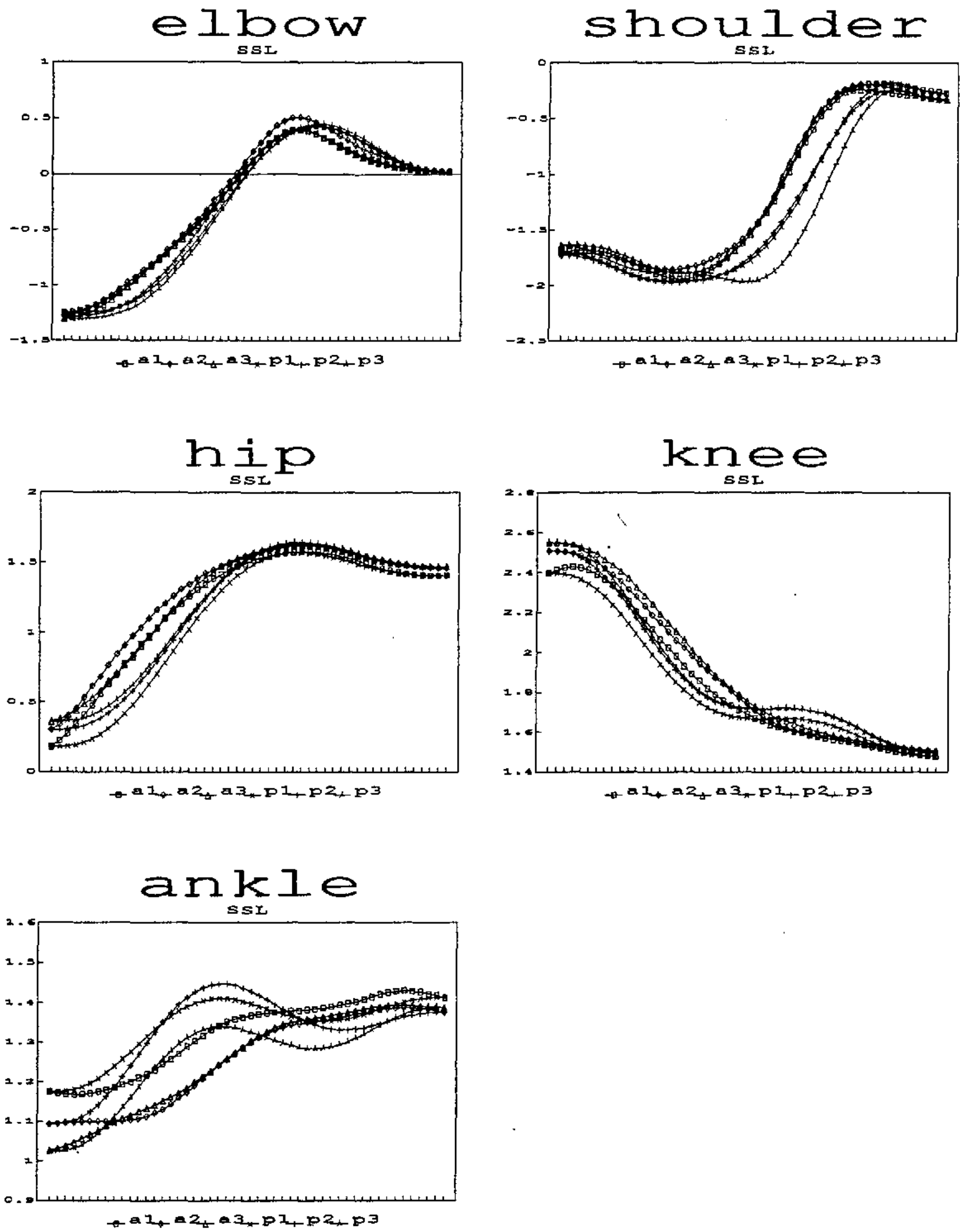

1. SSL

Figure B.4 Continued

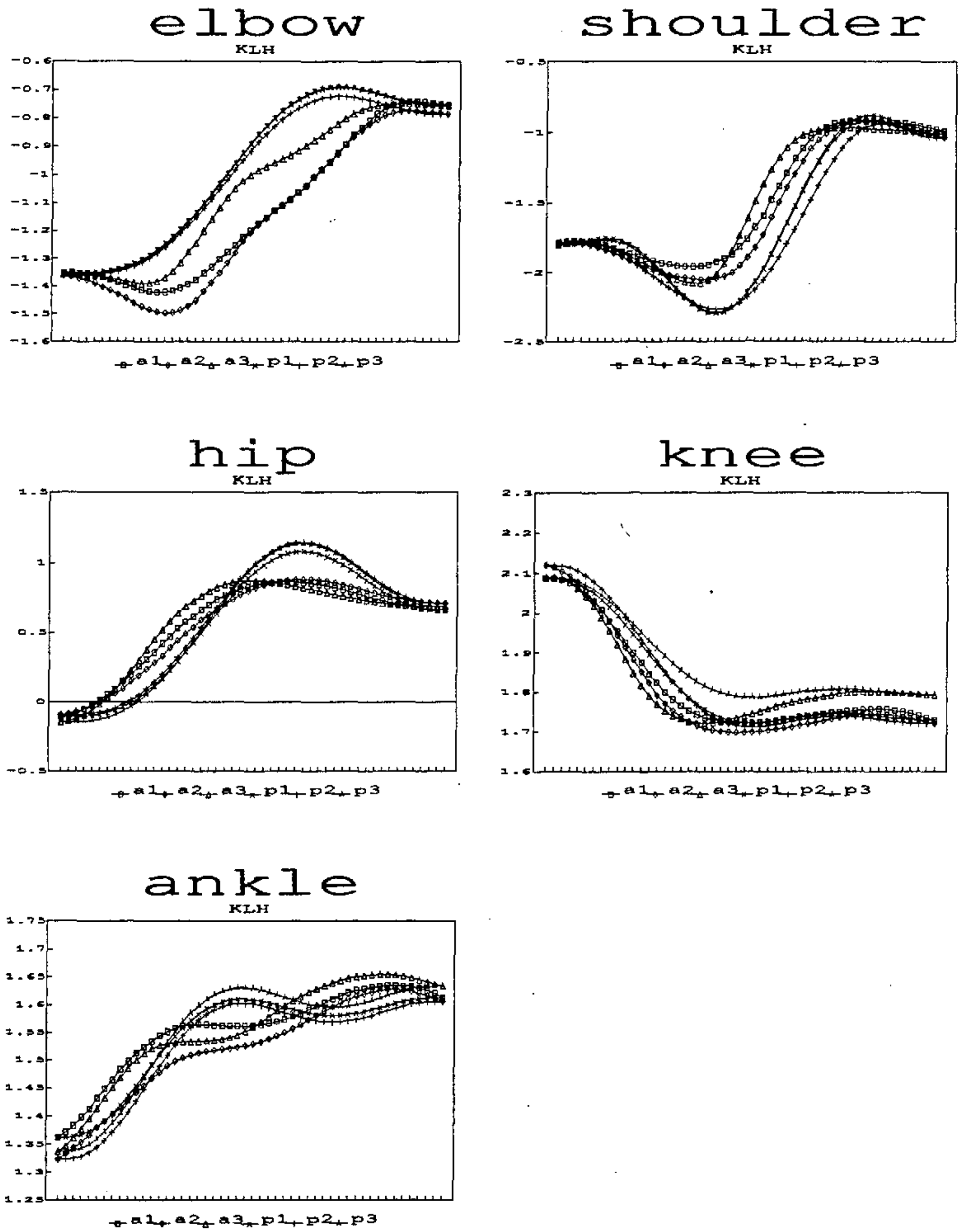

a. KLH

Figure B.5 Actual versus simulated trajectories for subject 6

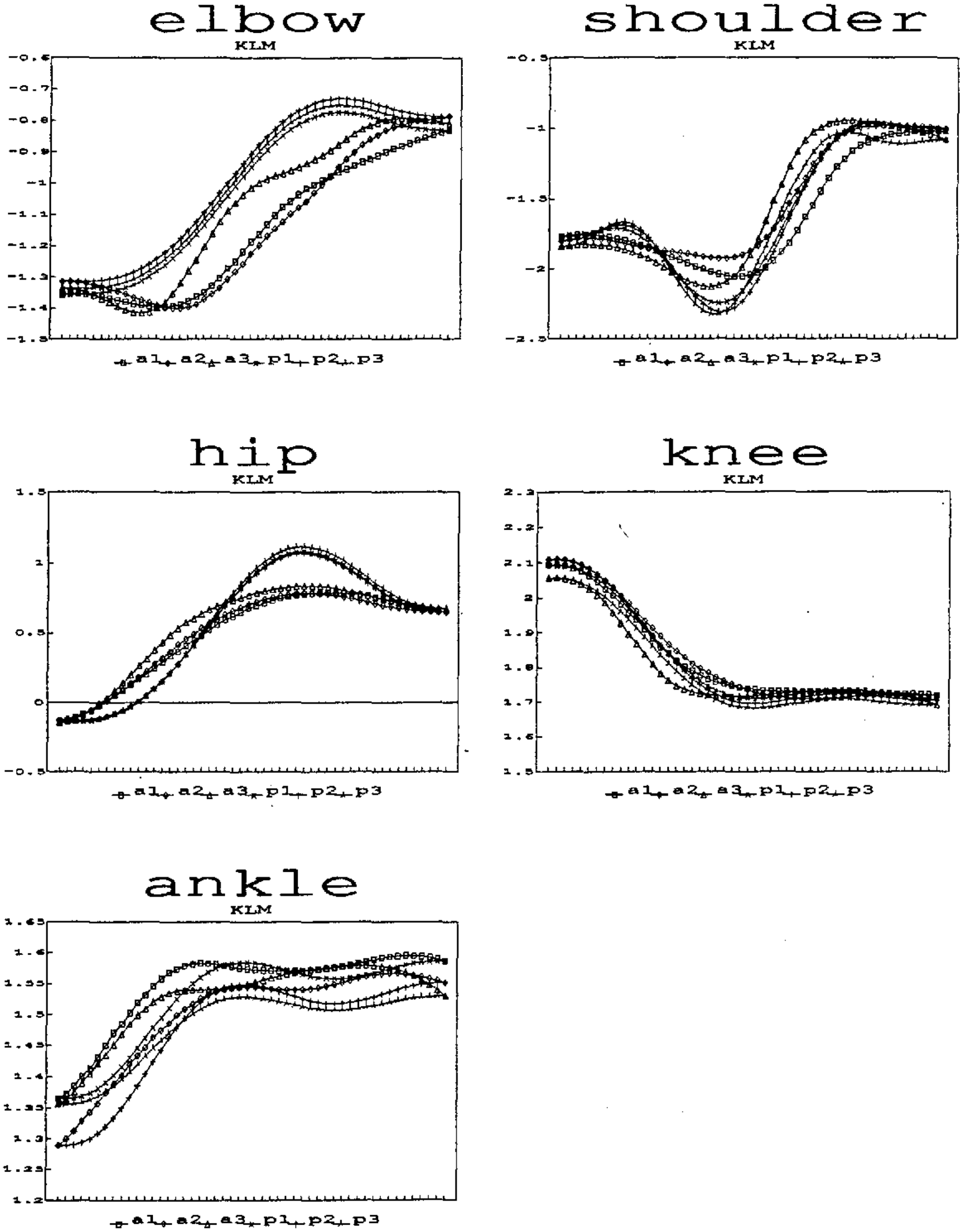

b. KLM

Figure B.5 Continued

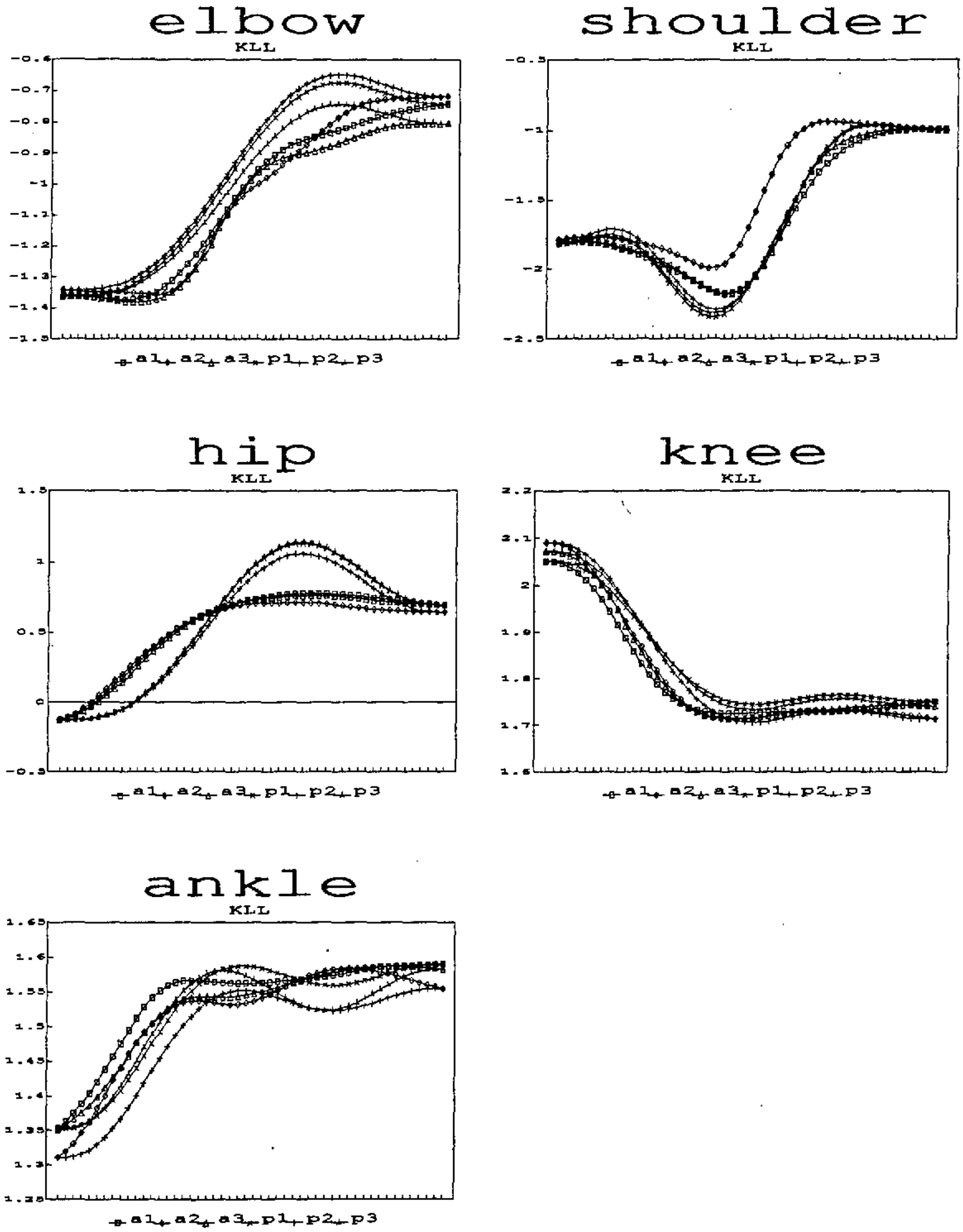

c. KLL

Figure B.5 Continued

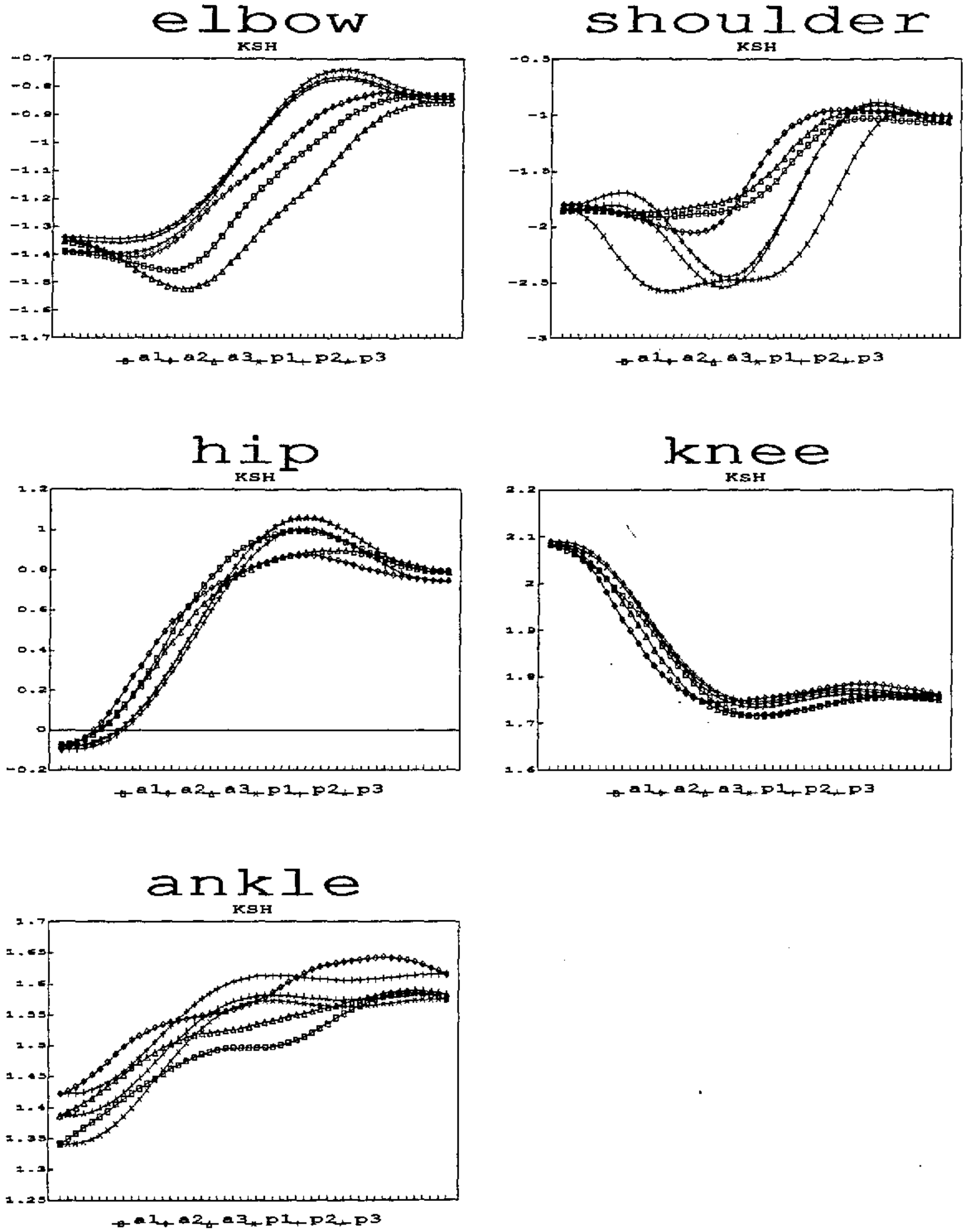

d. KSH

Figure B.5 Continued

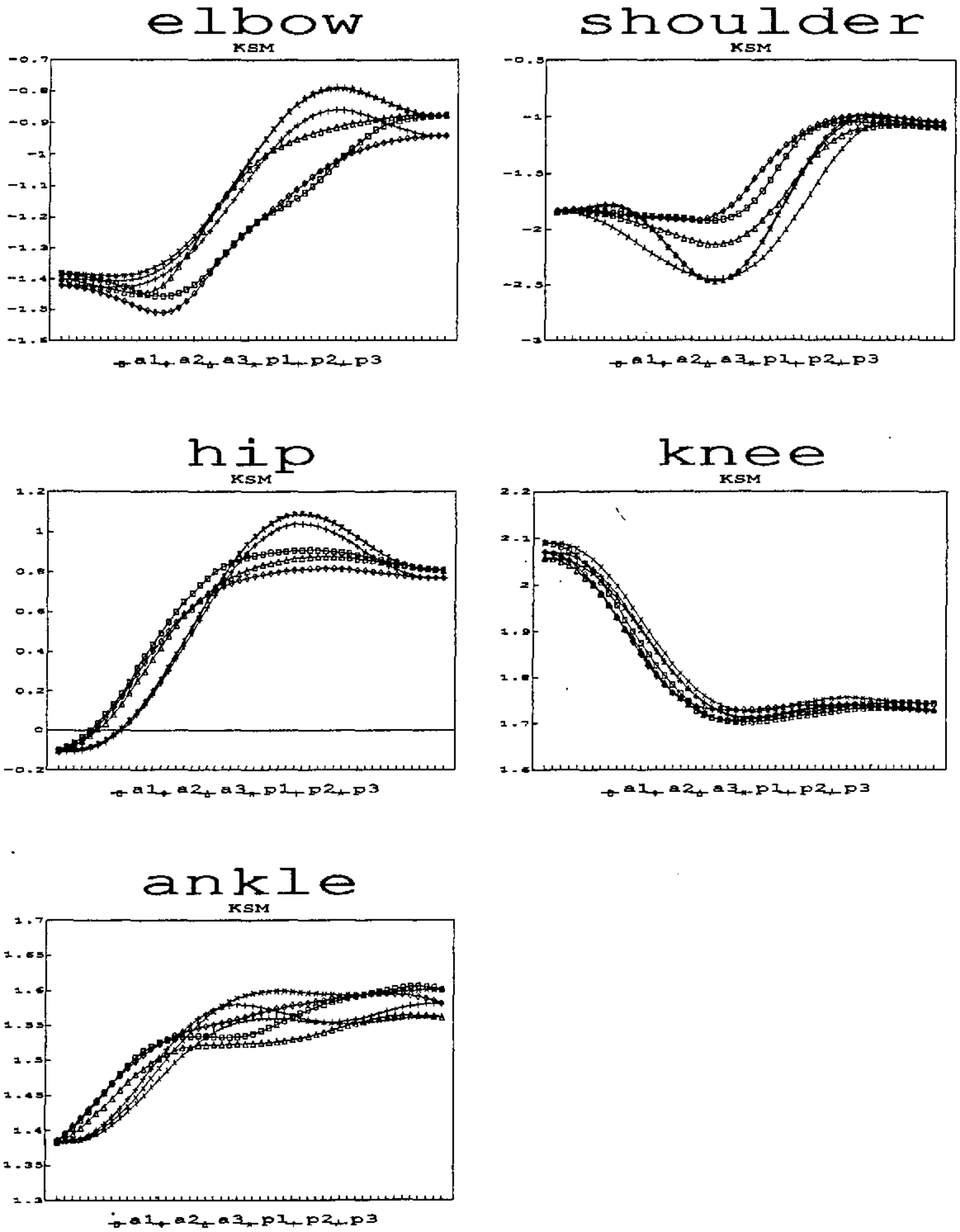

e. KSM

Figure B.5 Continued

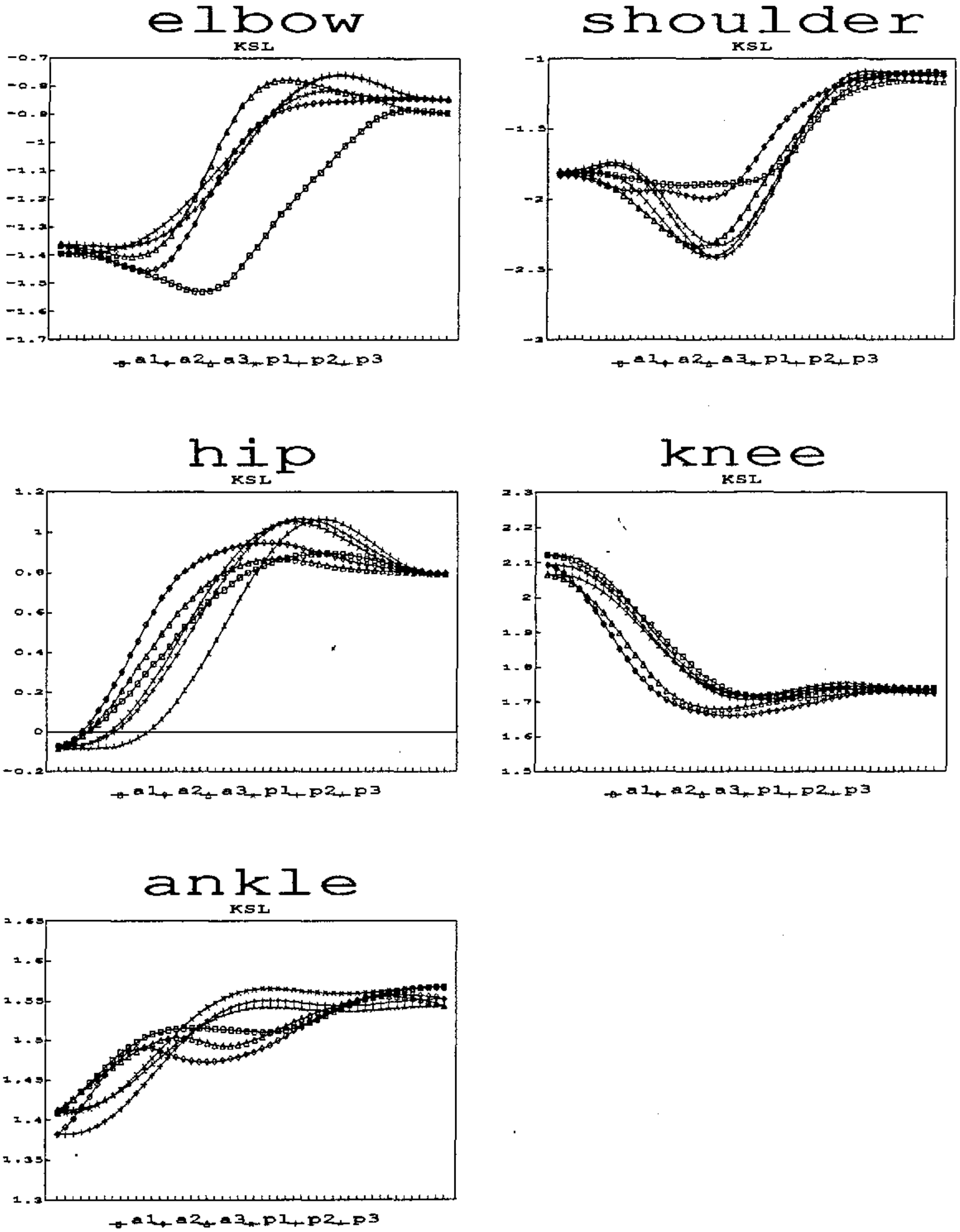

f. KSL

Figure B.5 Continued

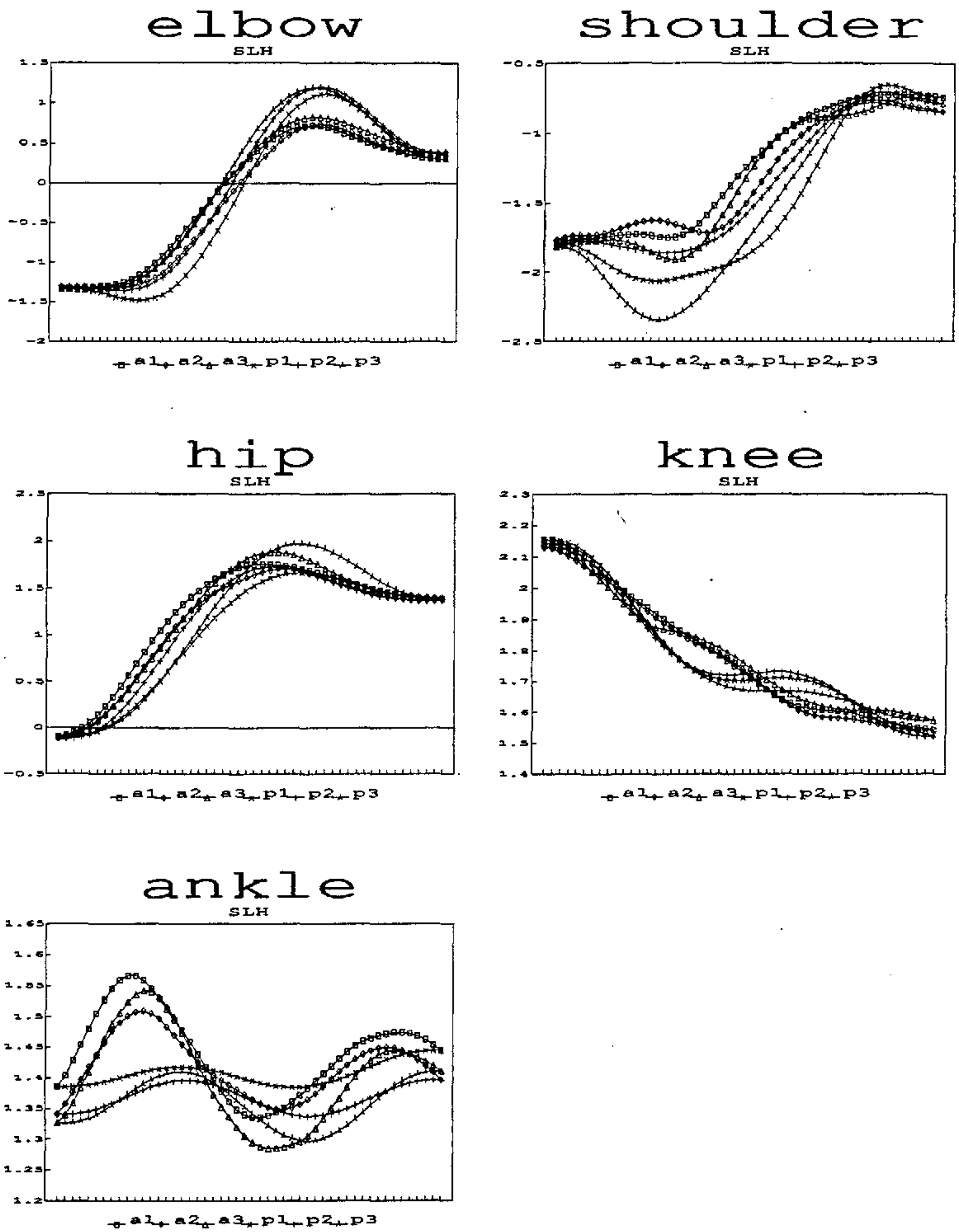

g. SLH

Figure B.5 Continued

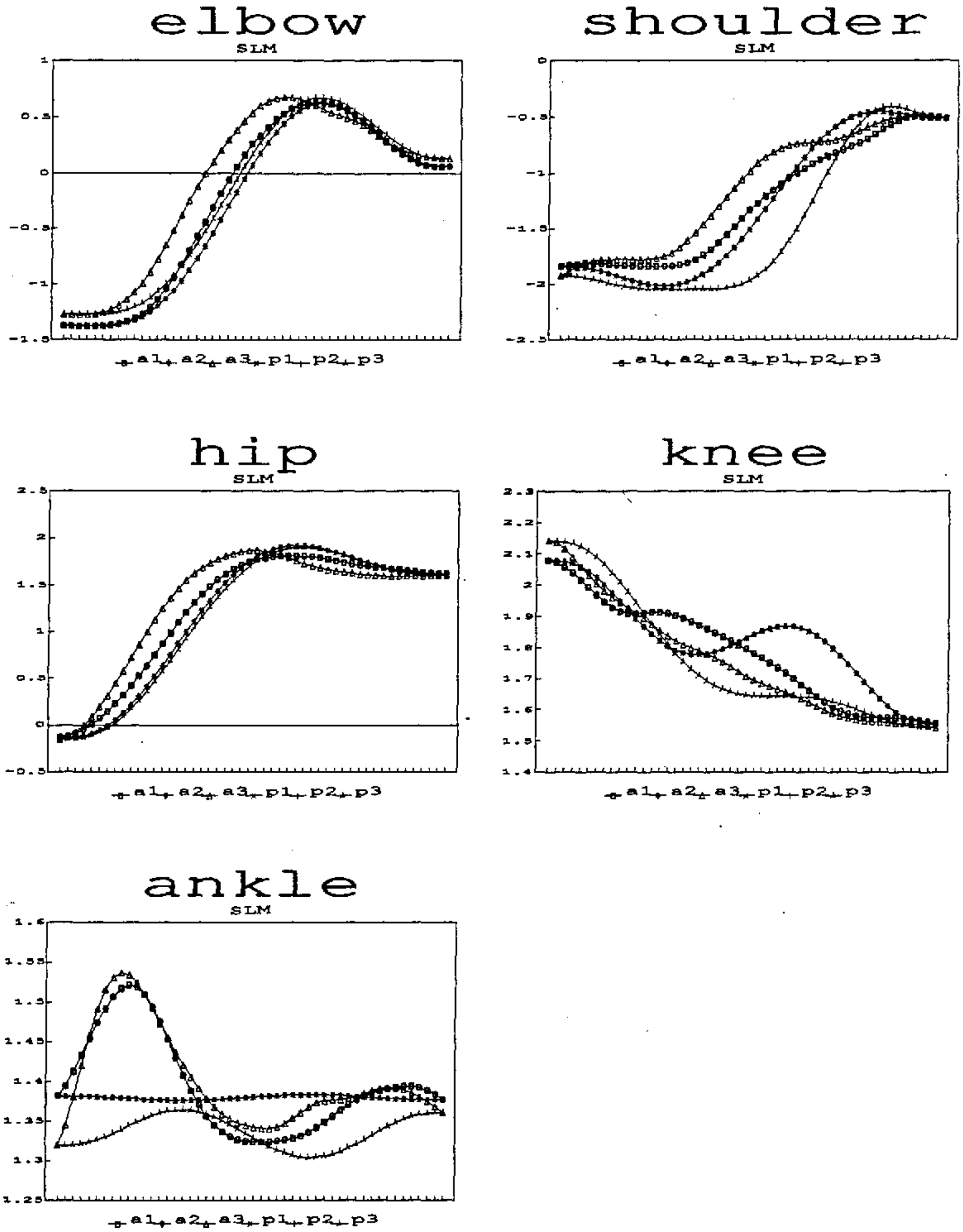

h. SLM

Figure B.5 Continued

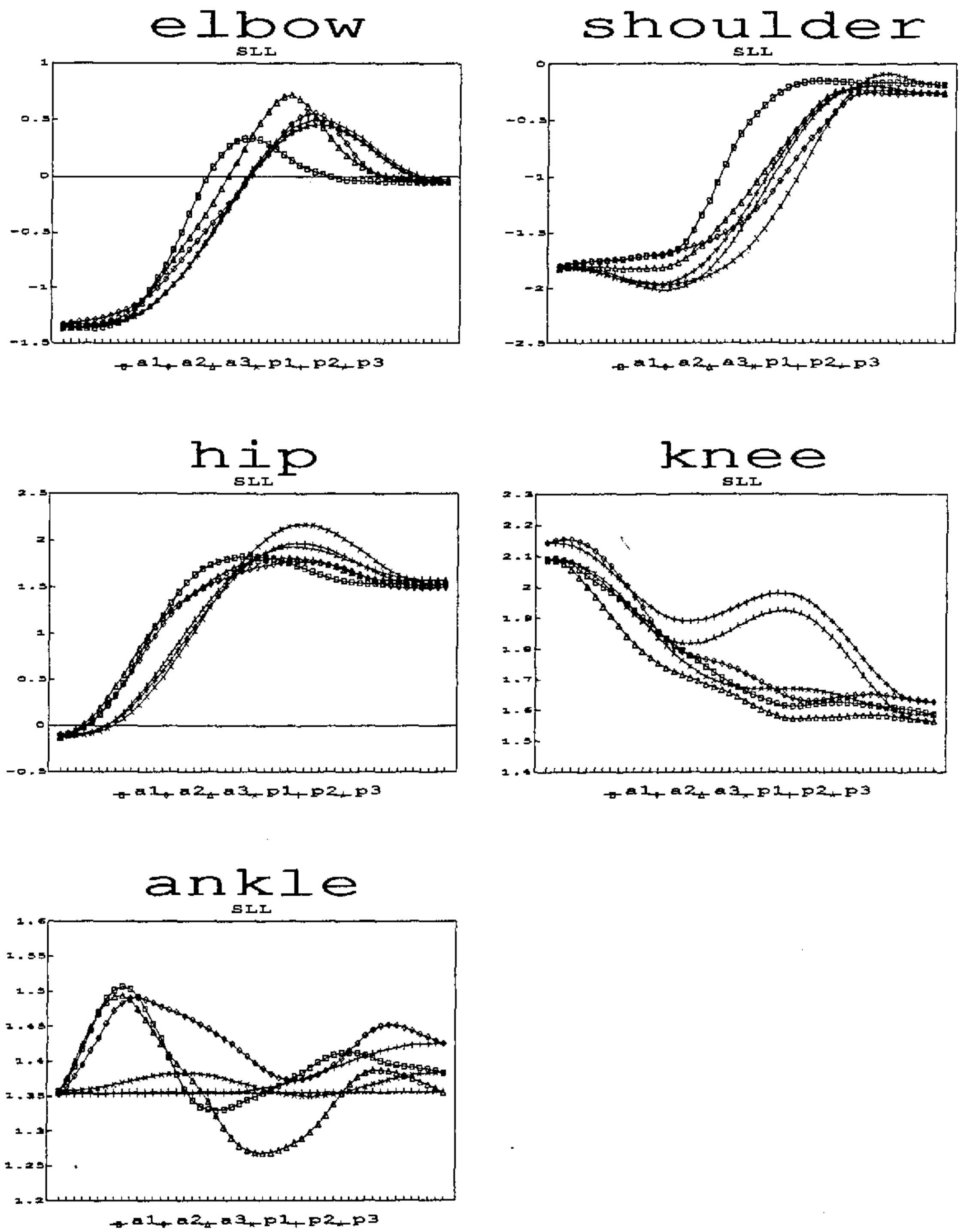

i. SLL

Figure B.5 Continued

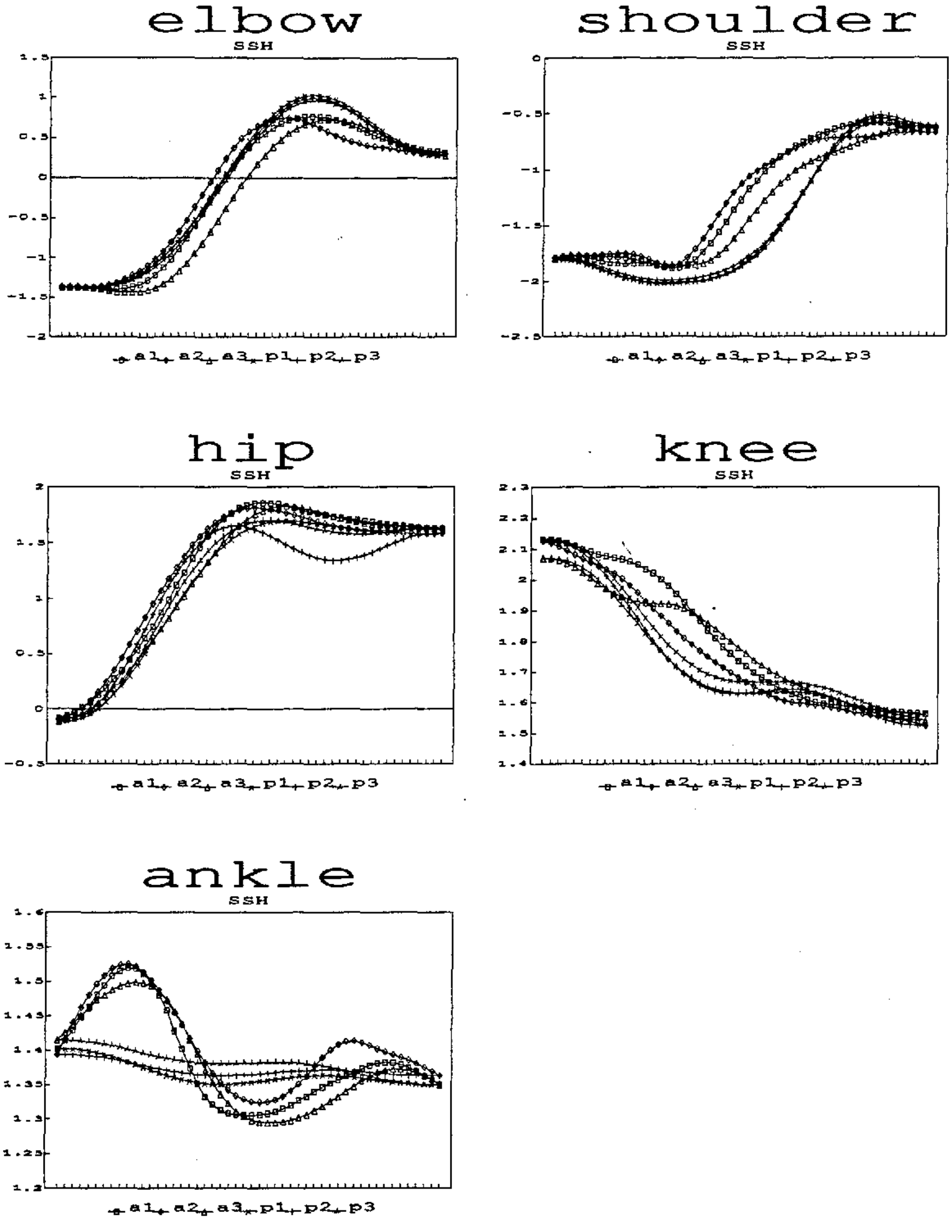

j. SSH

Figure B.5 Continued

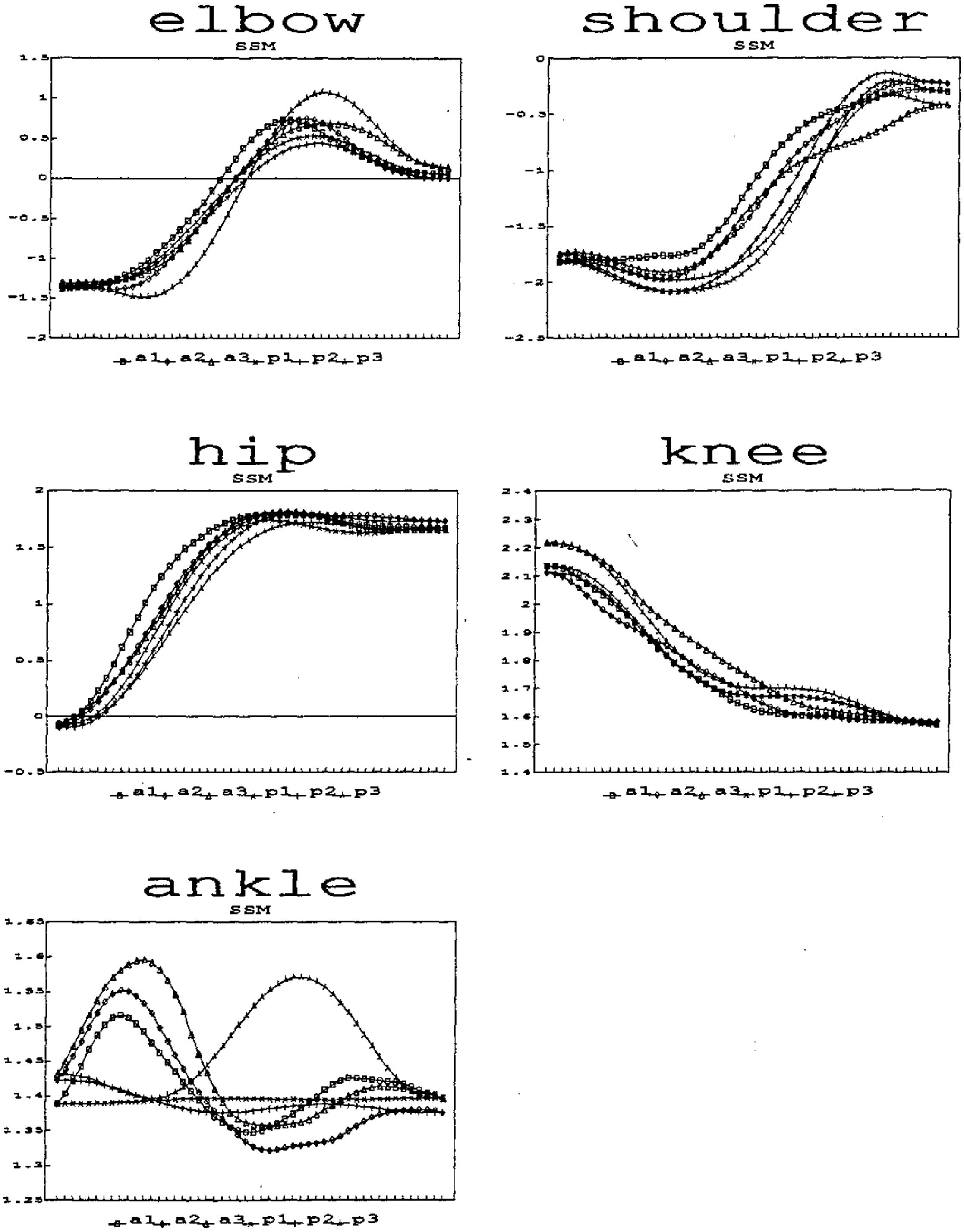

k. SSM

Figure B.5 Continued

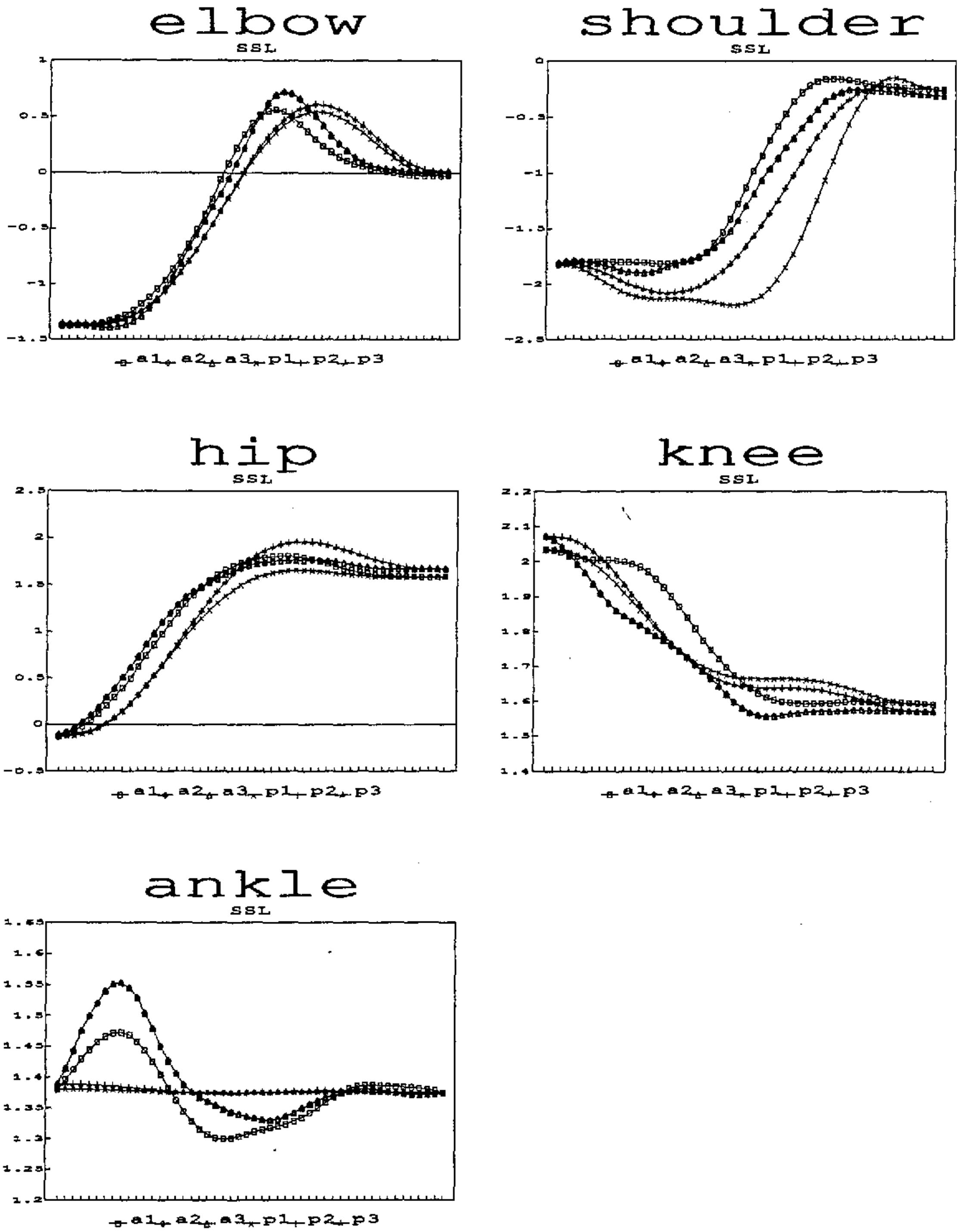

1. SSL

Figure B.5 Continued

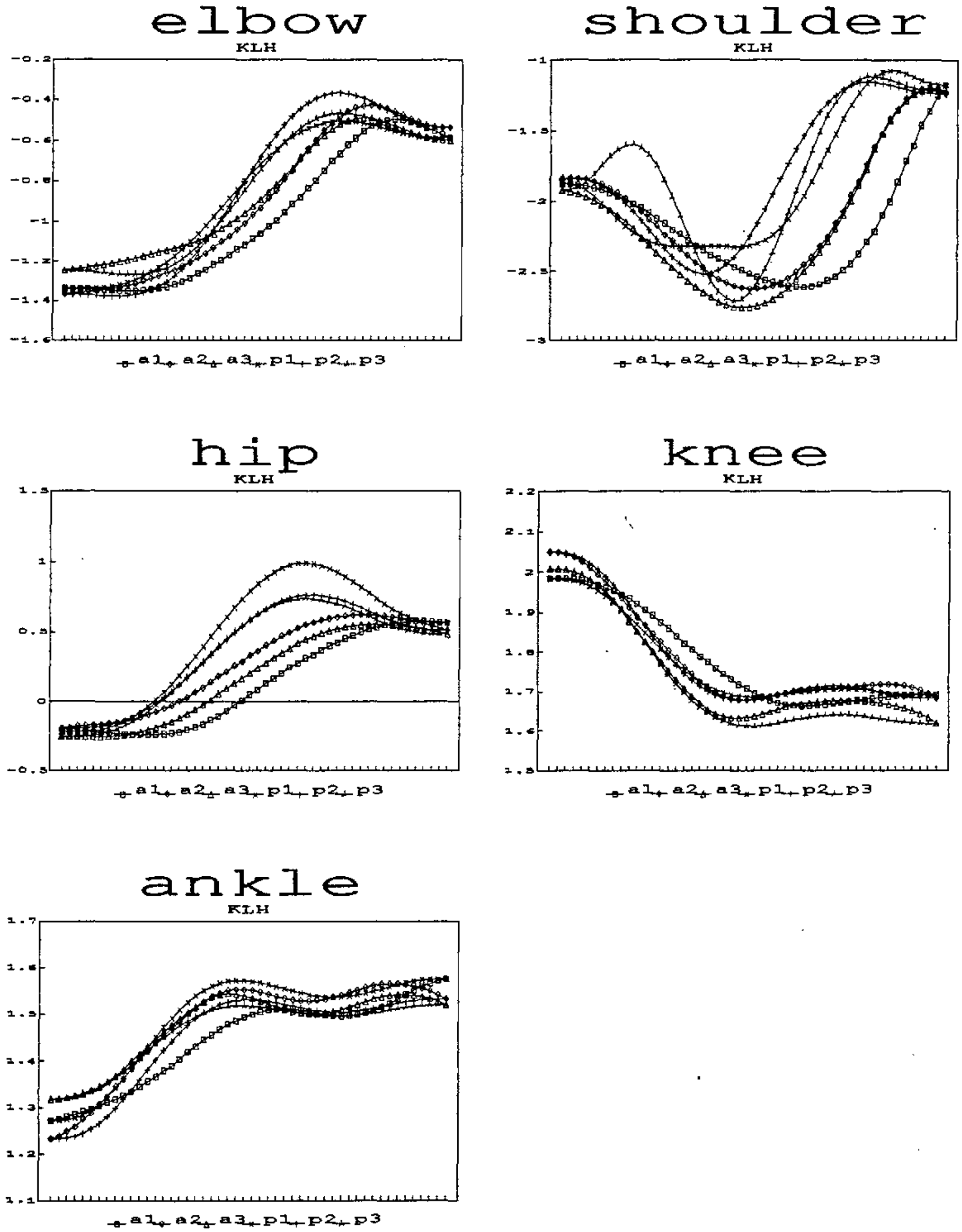

a. KLH

Figure B.6 Actual versus simulated trajectories for subject 7

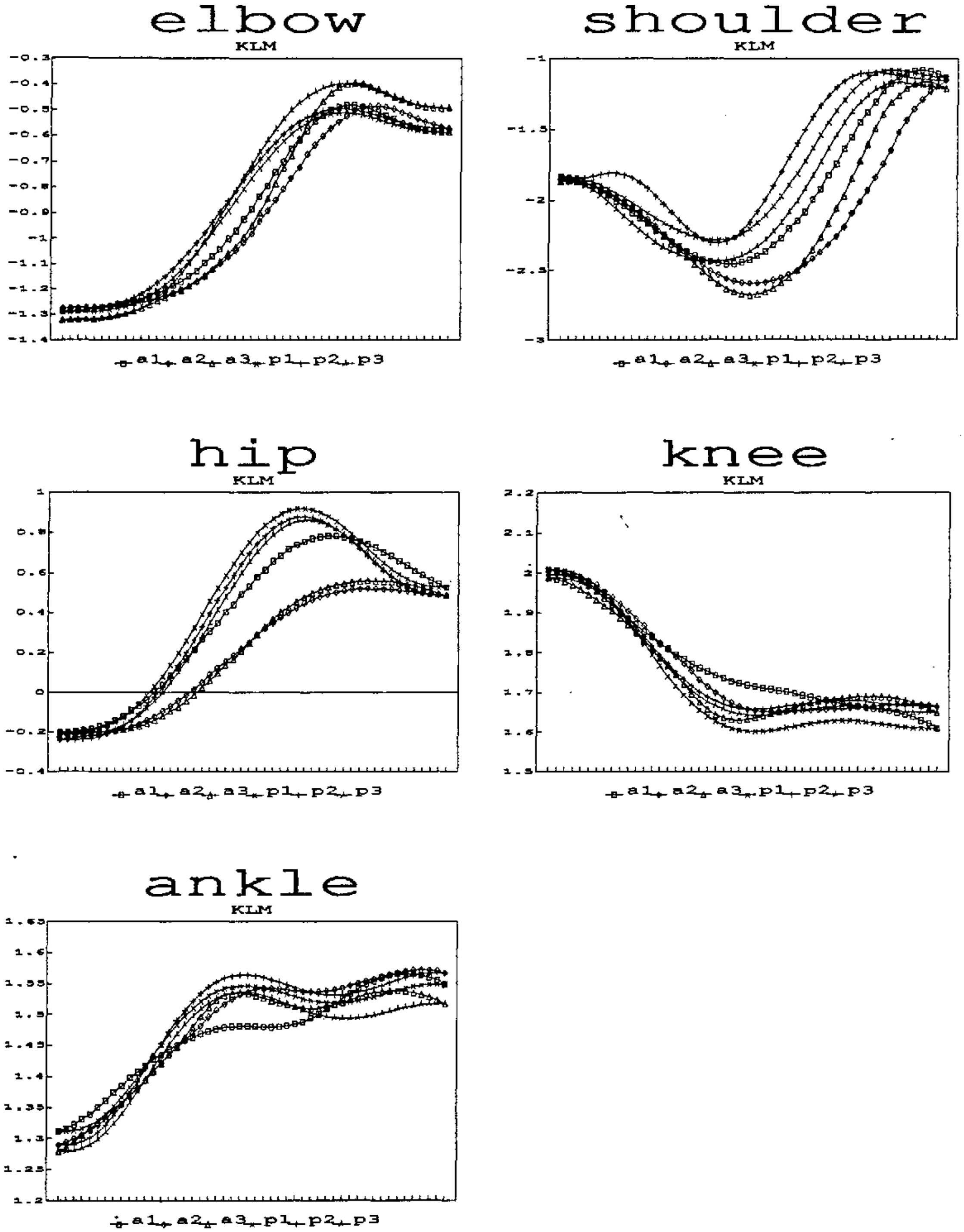

b. KLM

Figure B.6 Continued

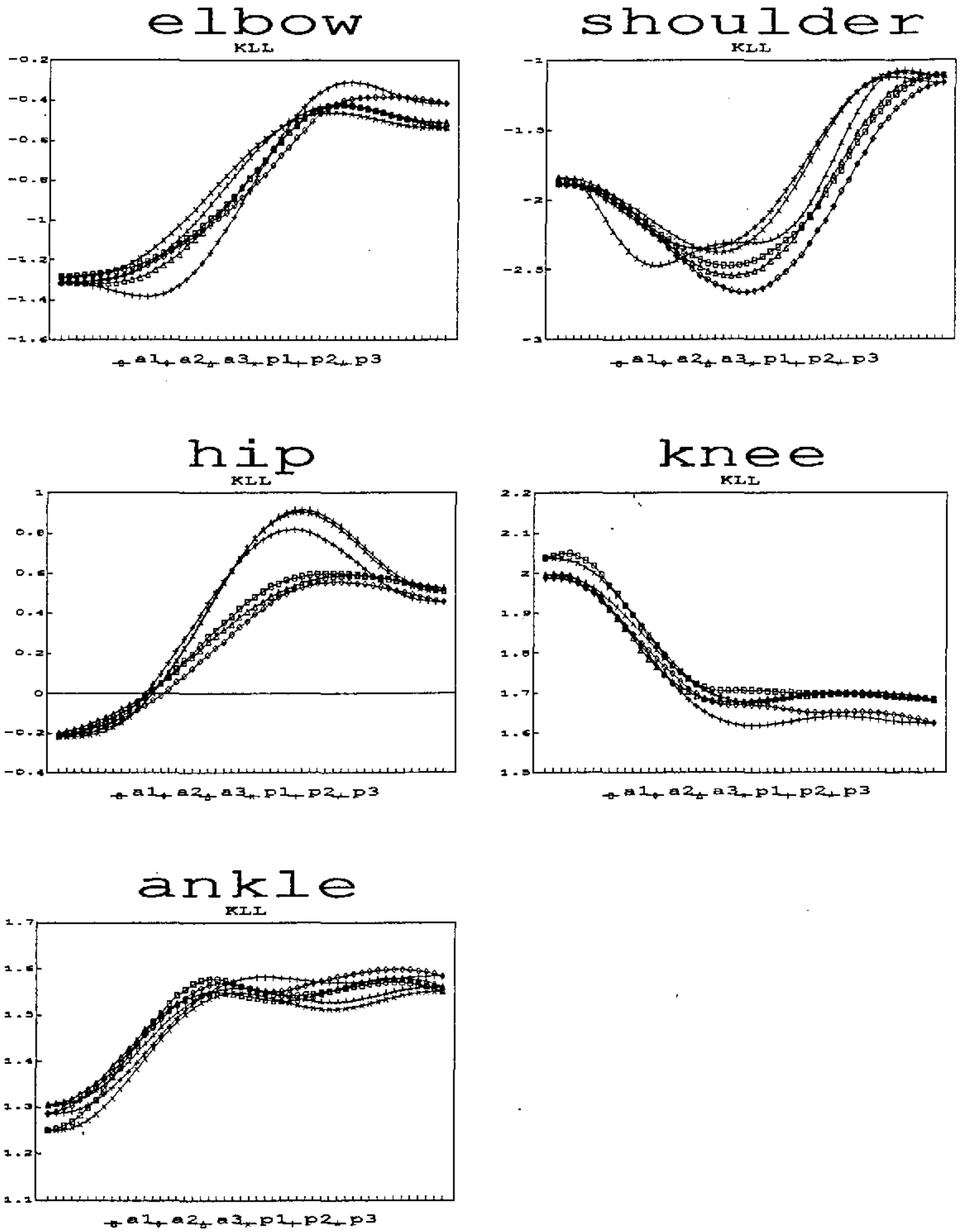

c. KLL

Figure B.6 Continued

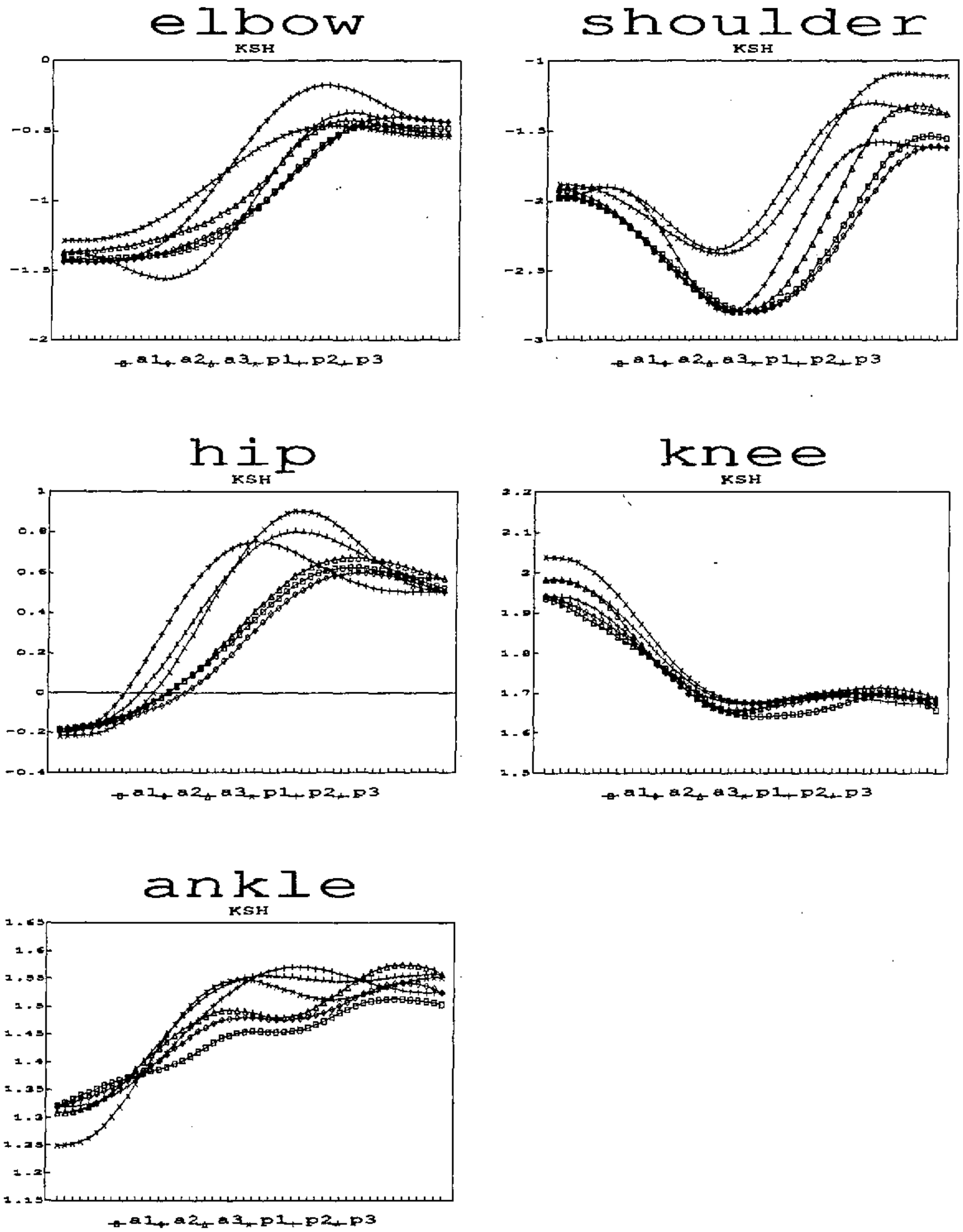

d. KSH

Figure B.6 Continued

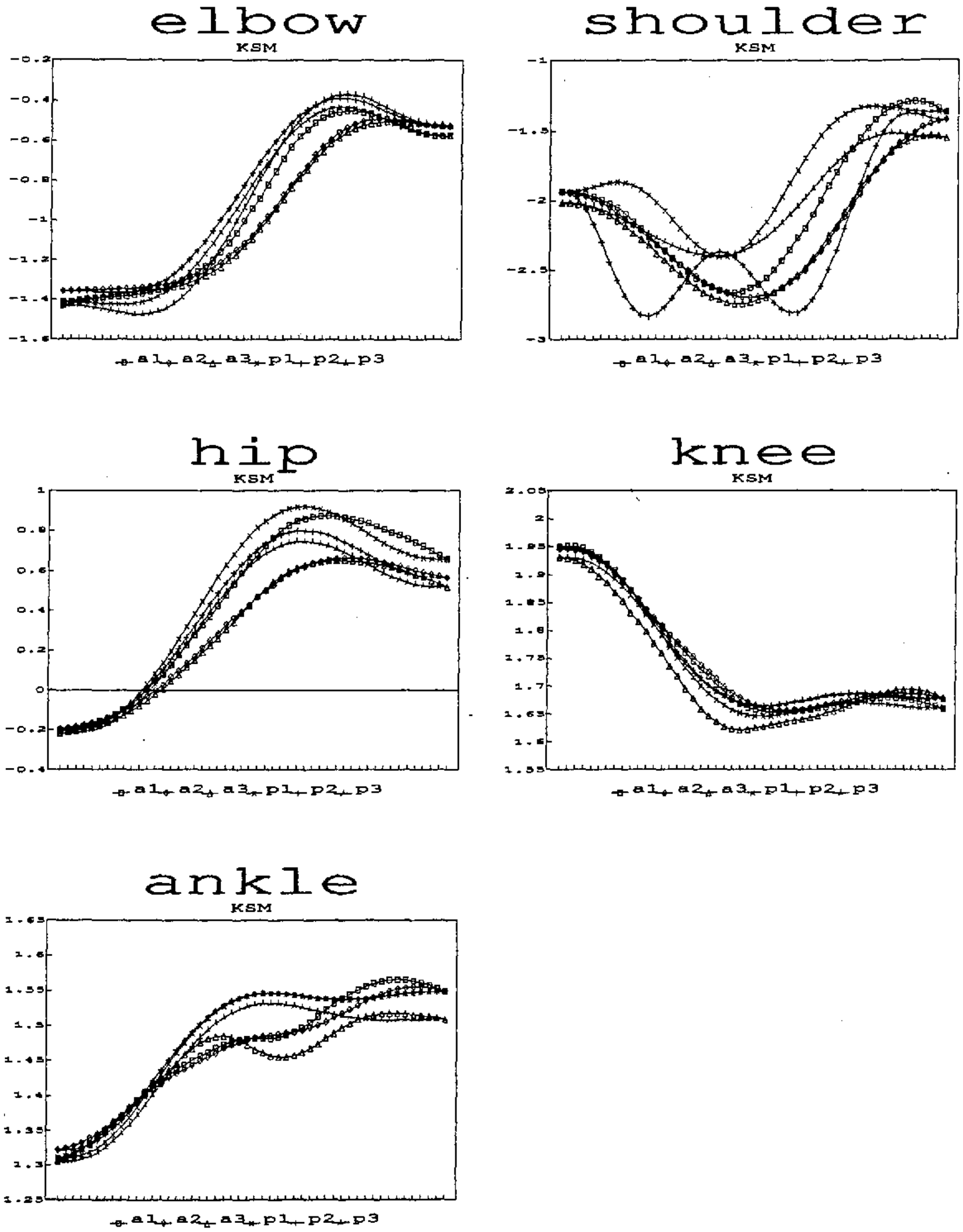

e. KSM

Figure B.6 Continued

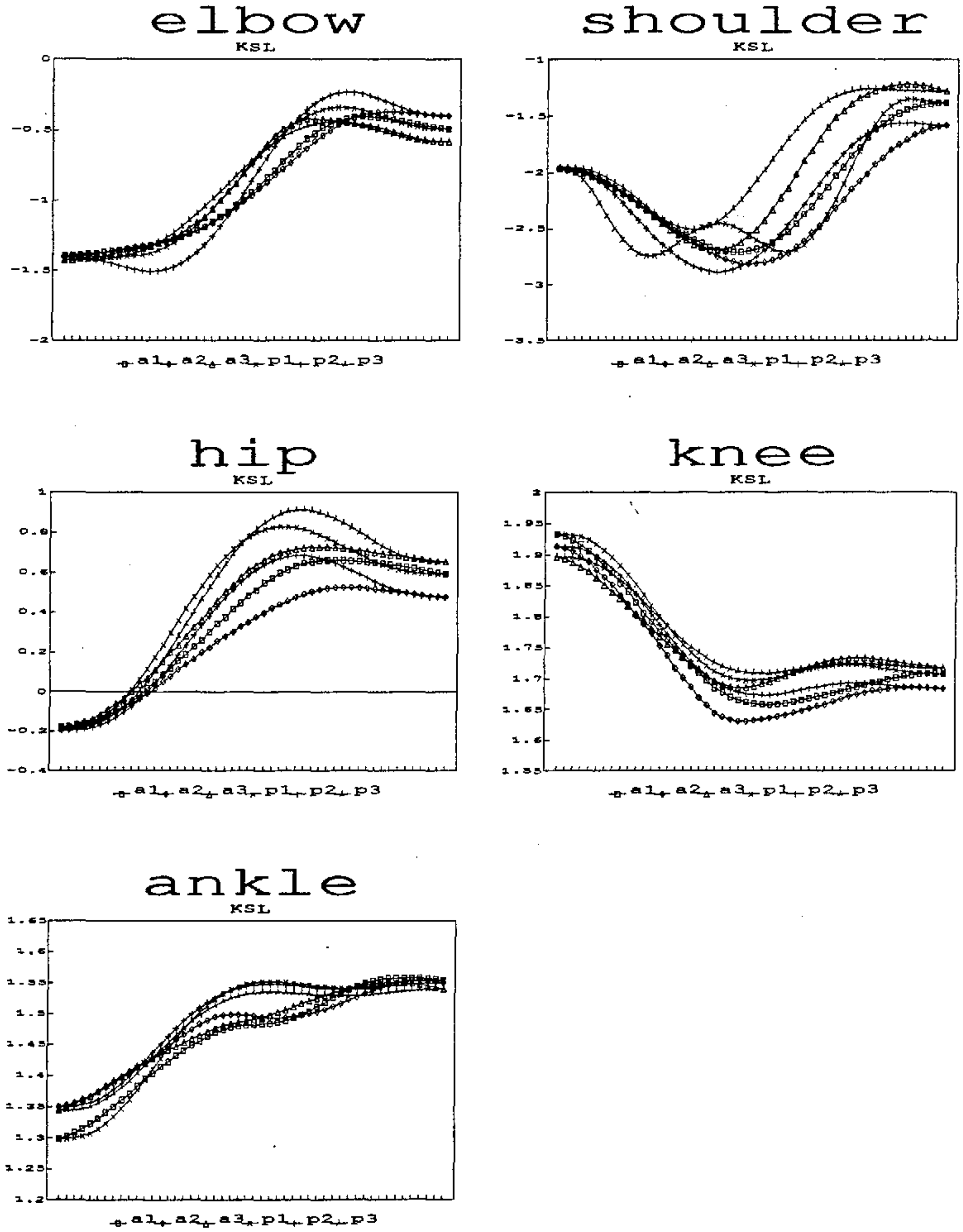

f. KSL

Figure B.6 Continued

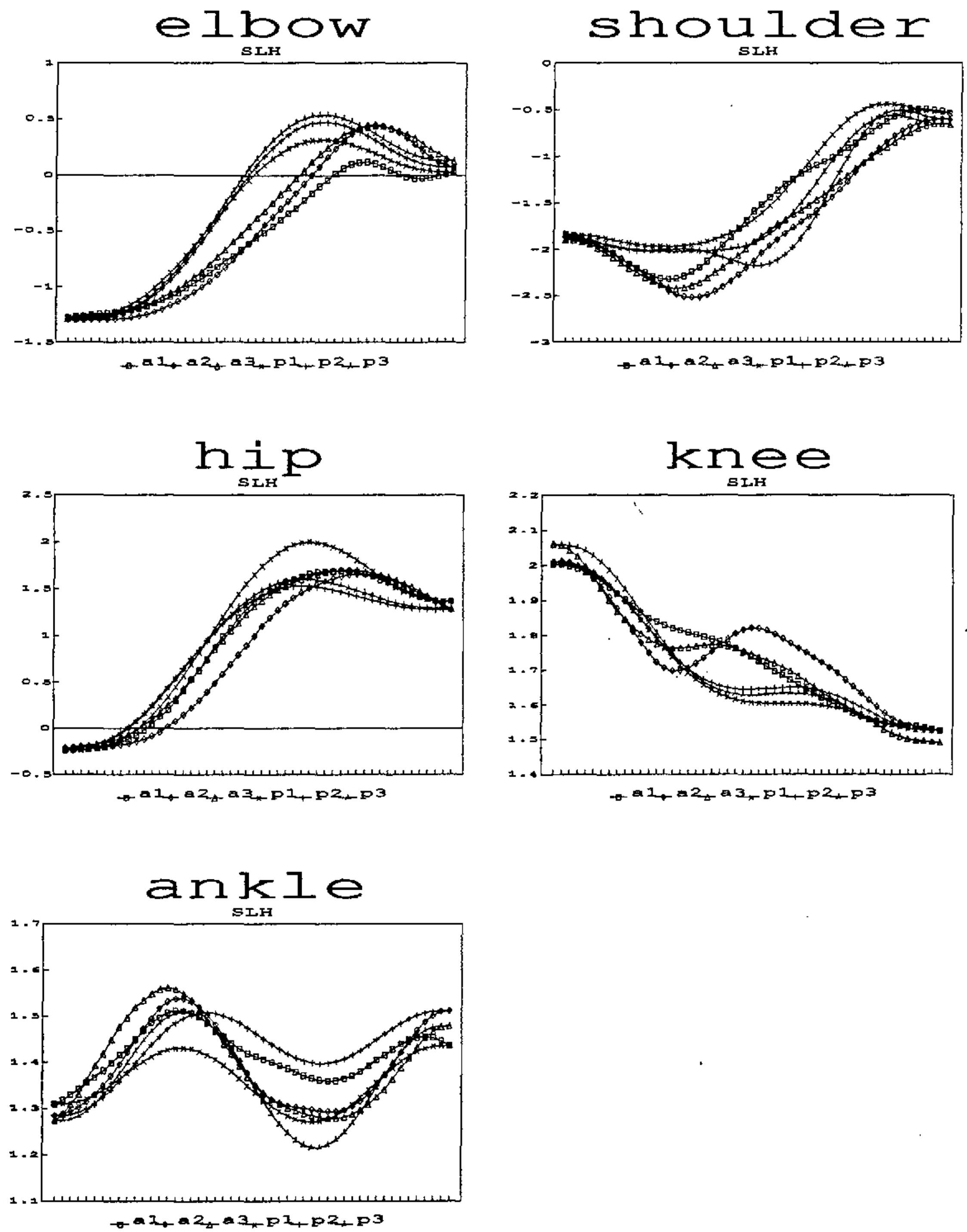

g. SLH

Figure B.6 Continued

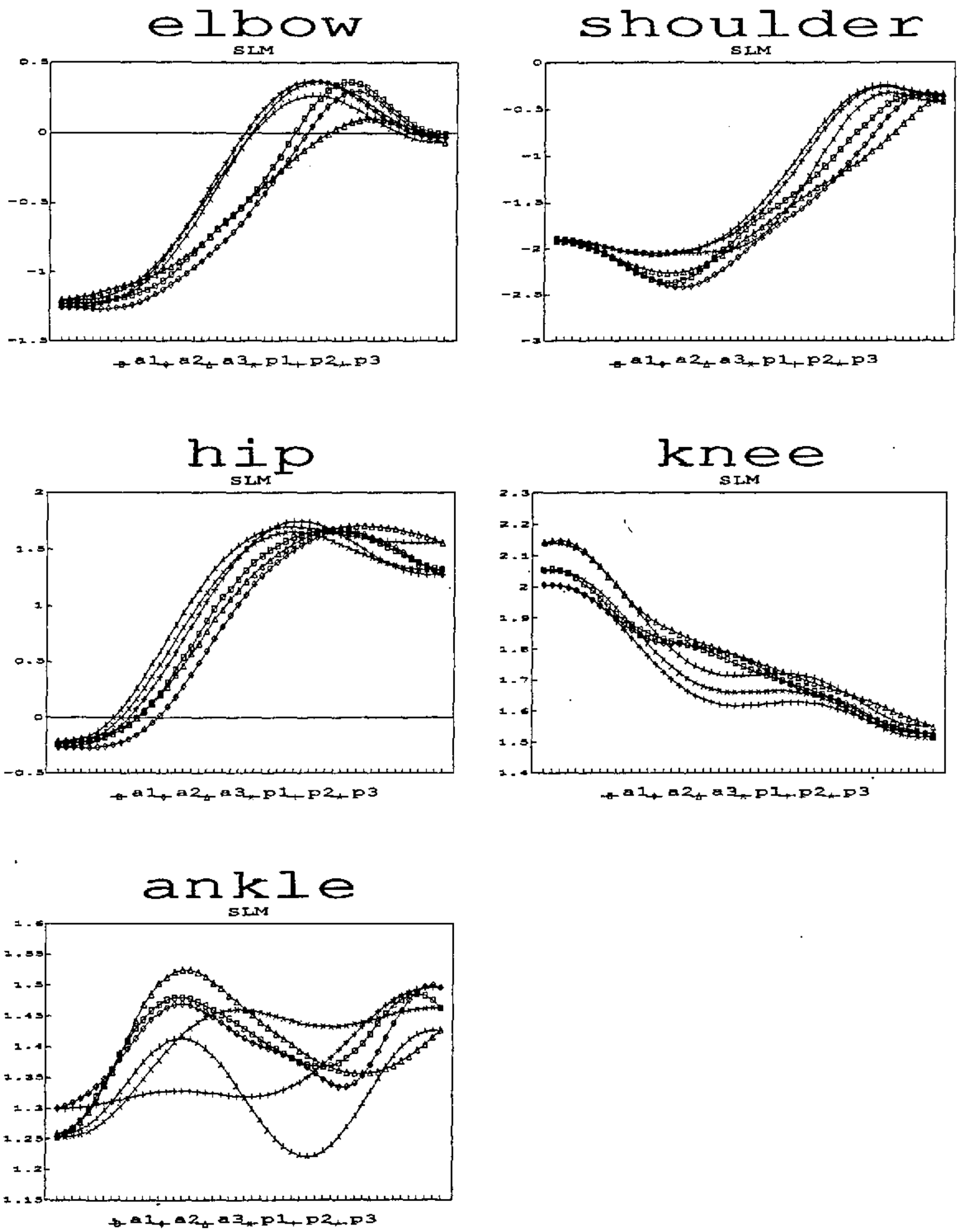

h. SLM

Figure B.6 Continued

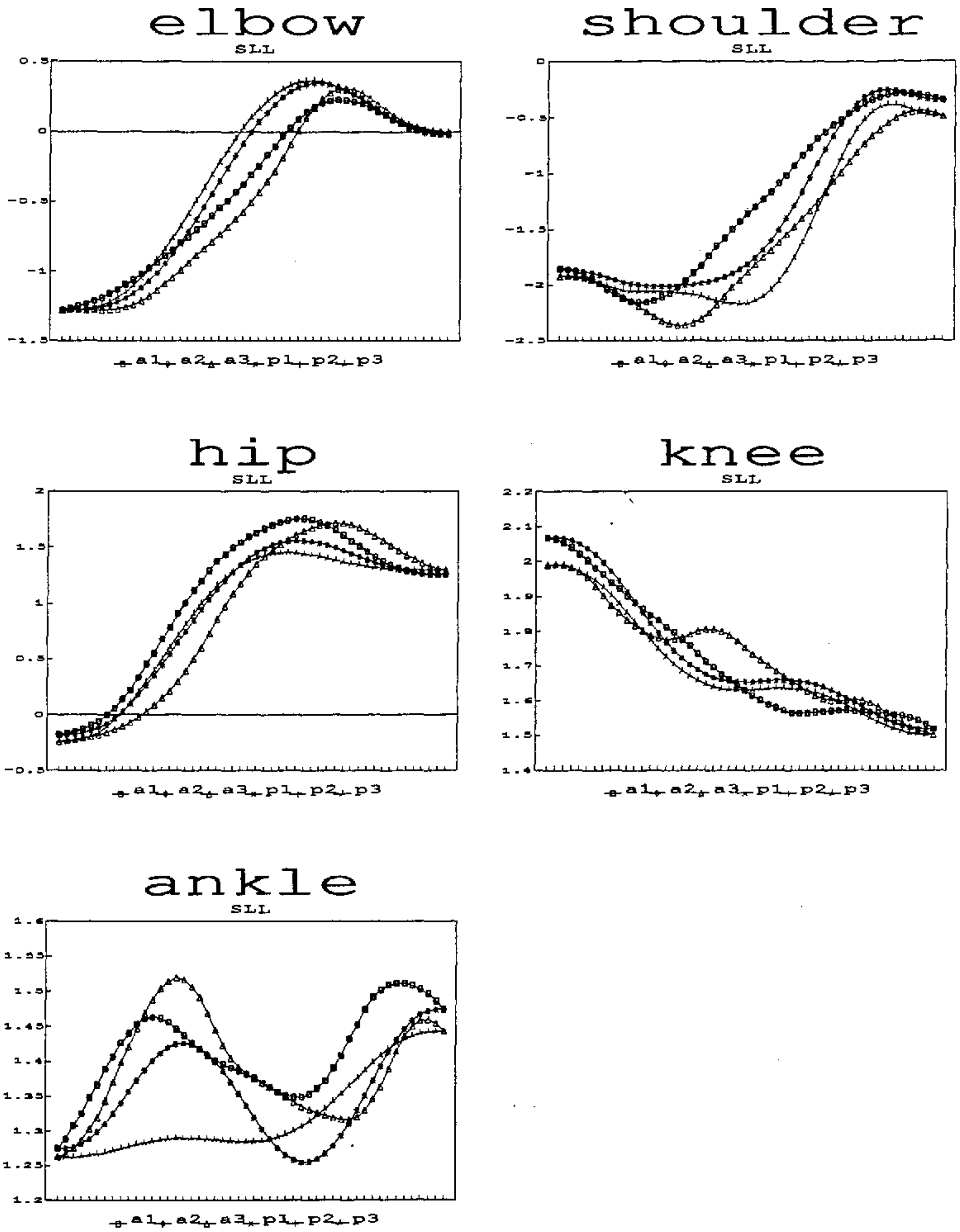

i. SLL

Figure B.6 Continued

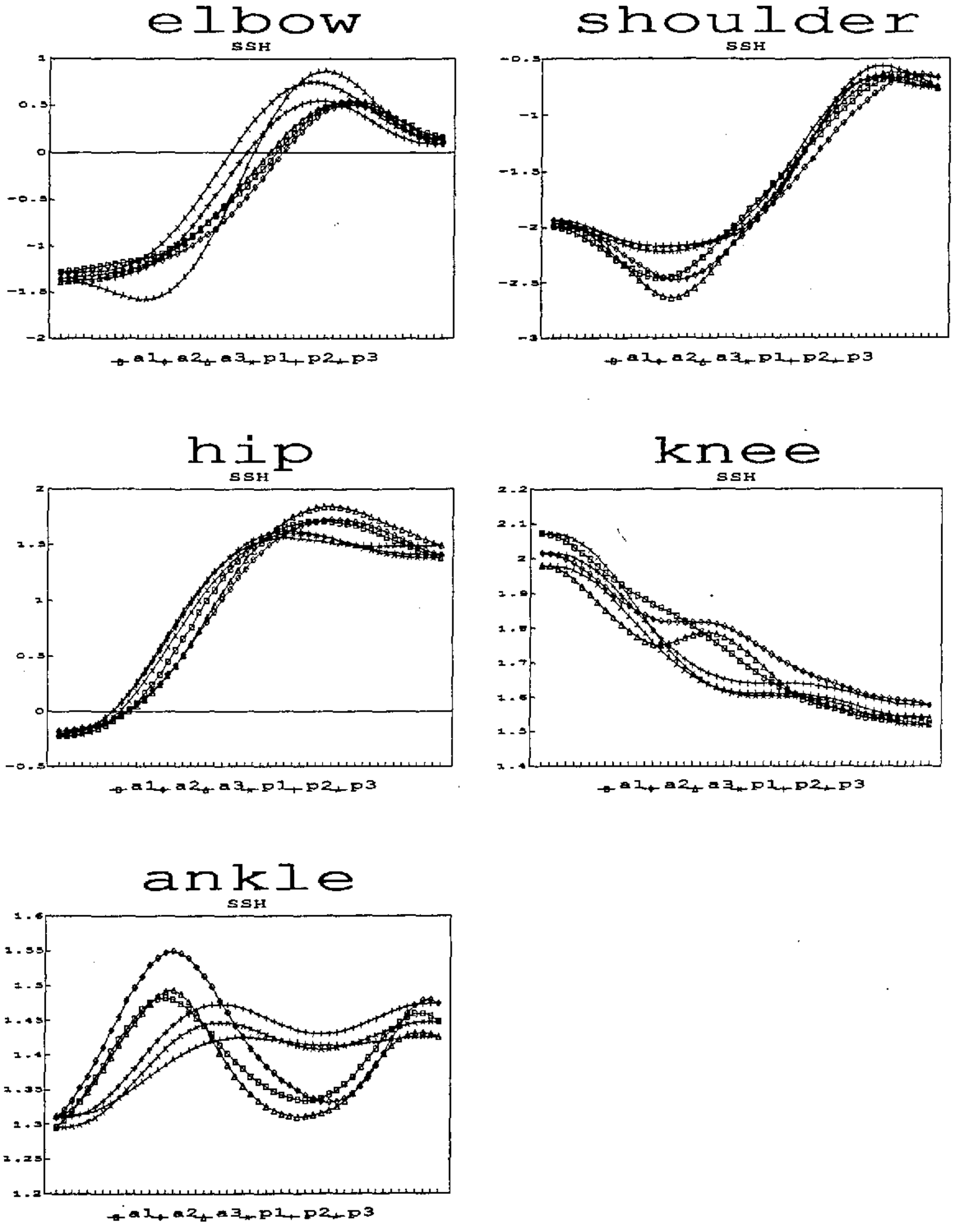

j. SSH

Figure B.6 Continued

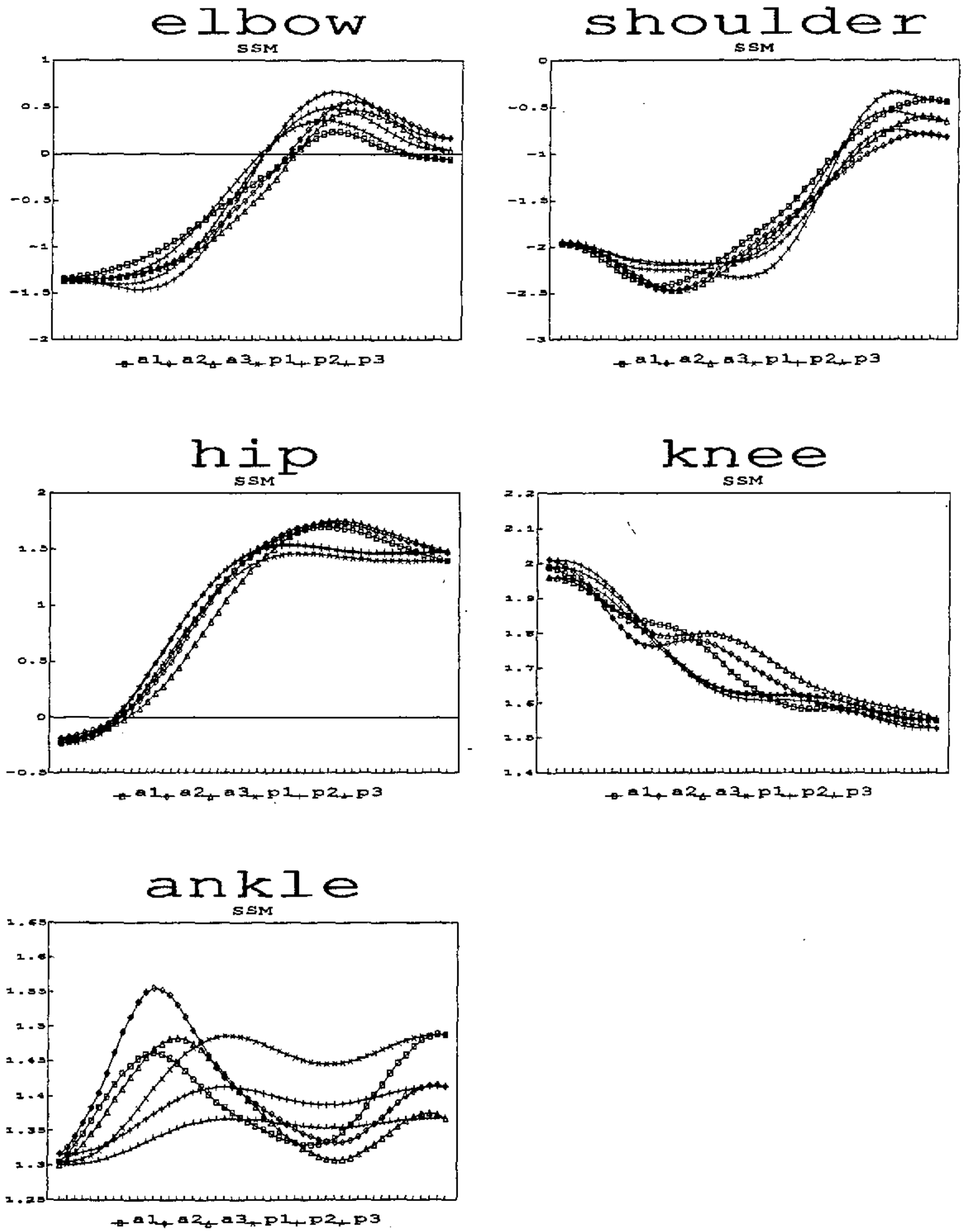

k. SSM

Figure B.6 Continued

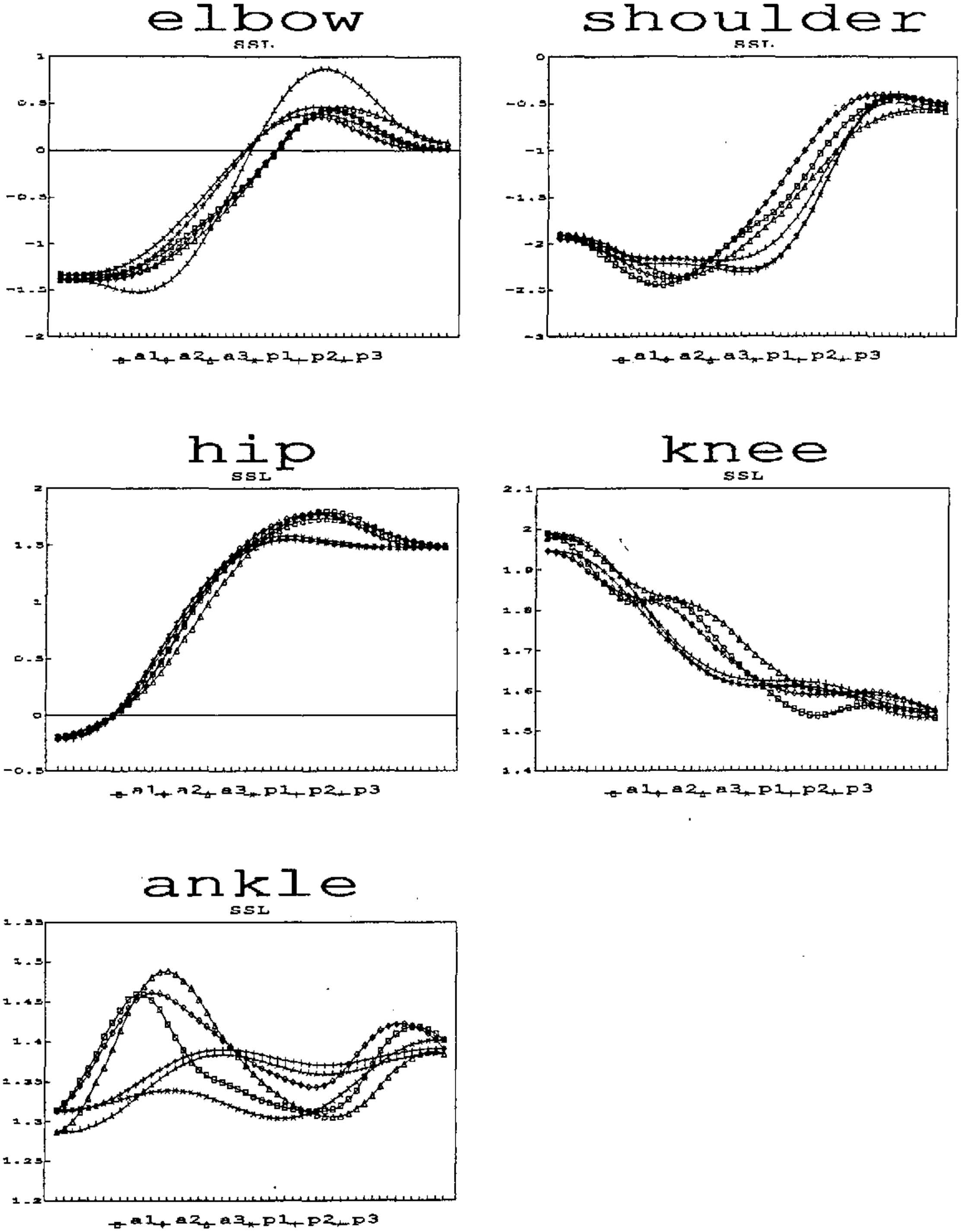

1. SSL

Figure B.6 Continued

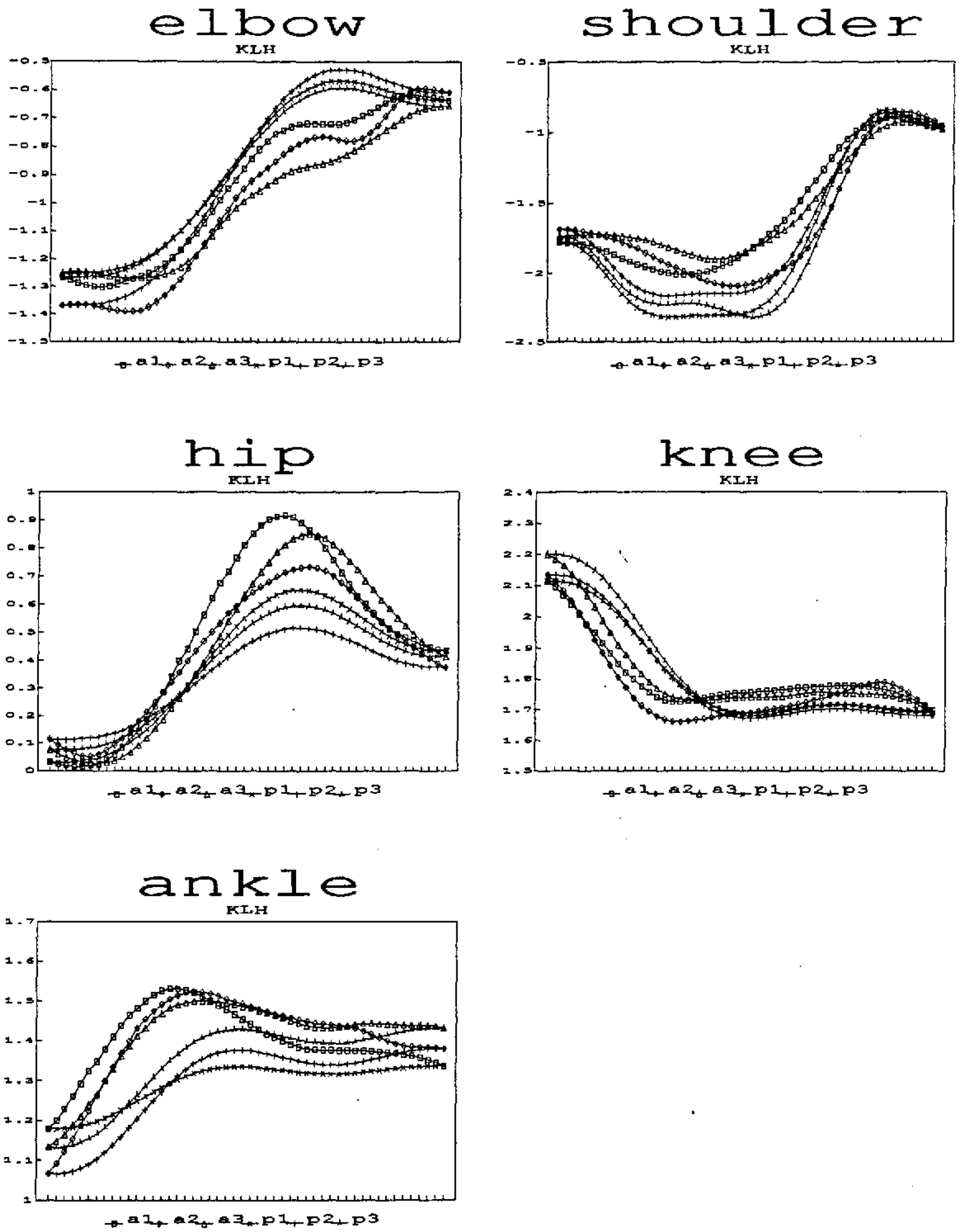

a. KLH

Figure B.7 Actual versus simulated trajectories for subject 8

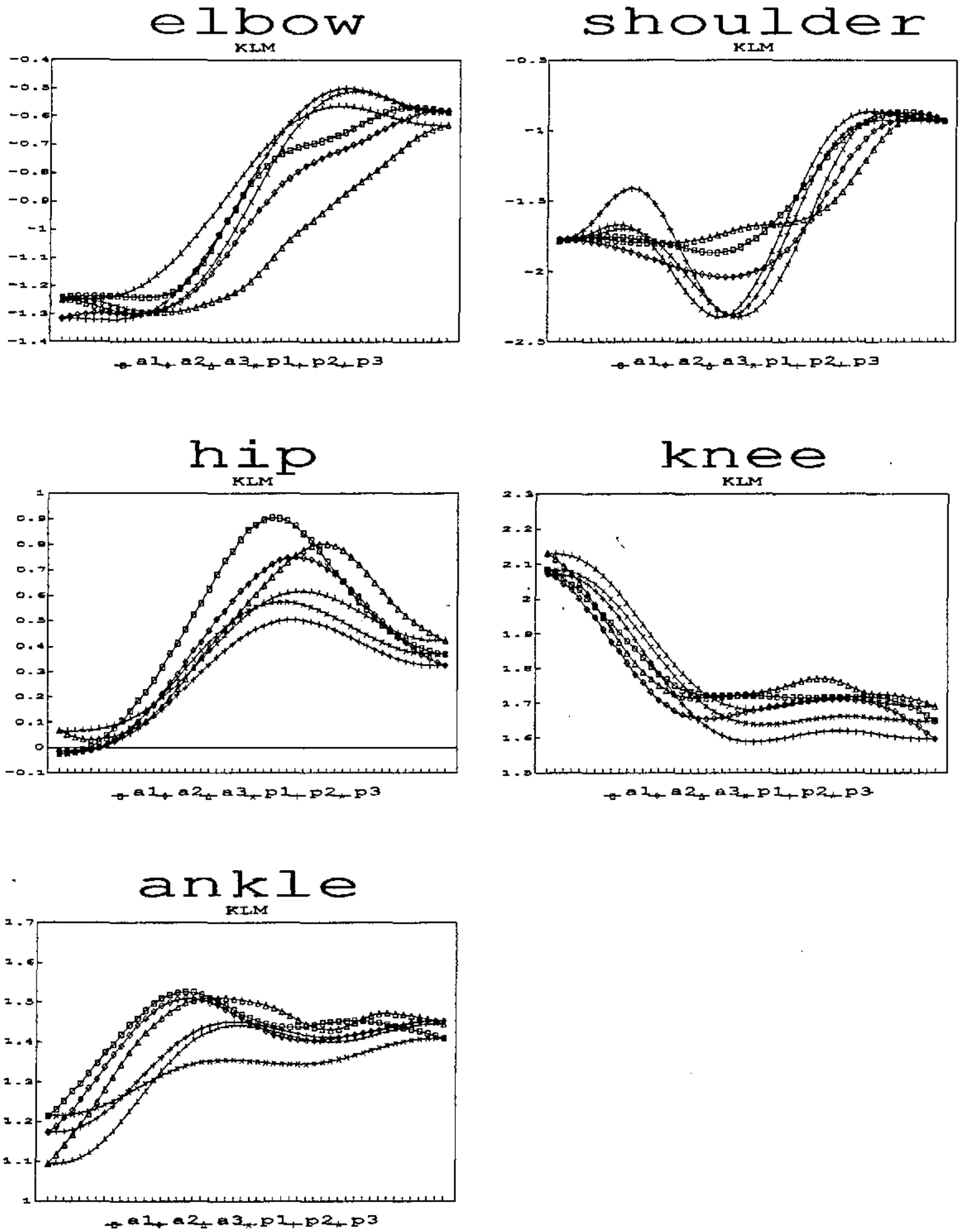

b. KLM

Figure B.7 Continued

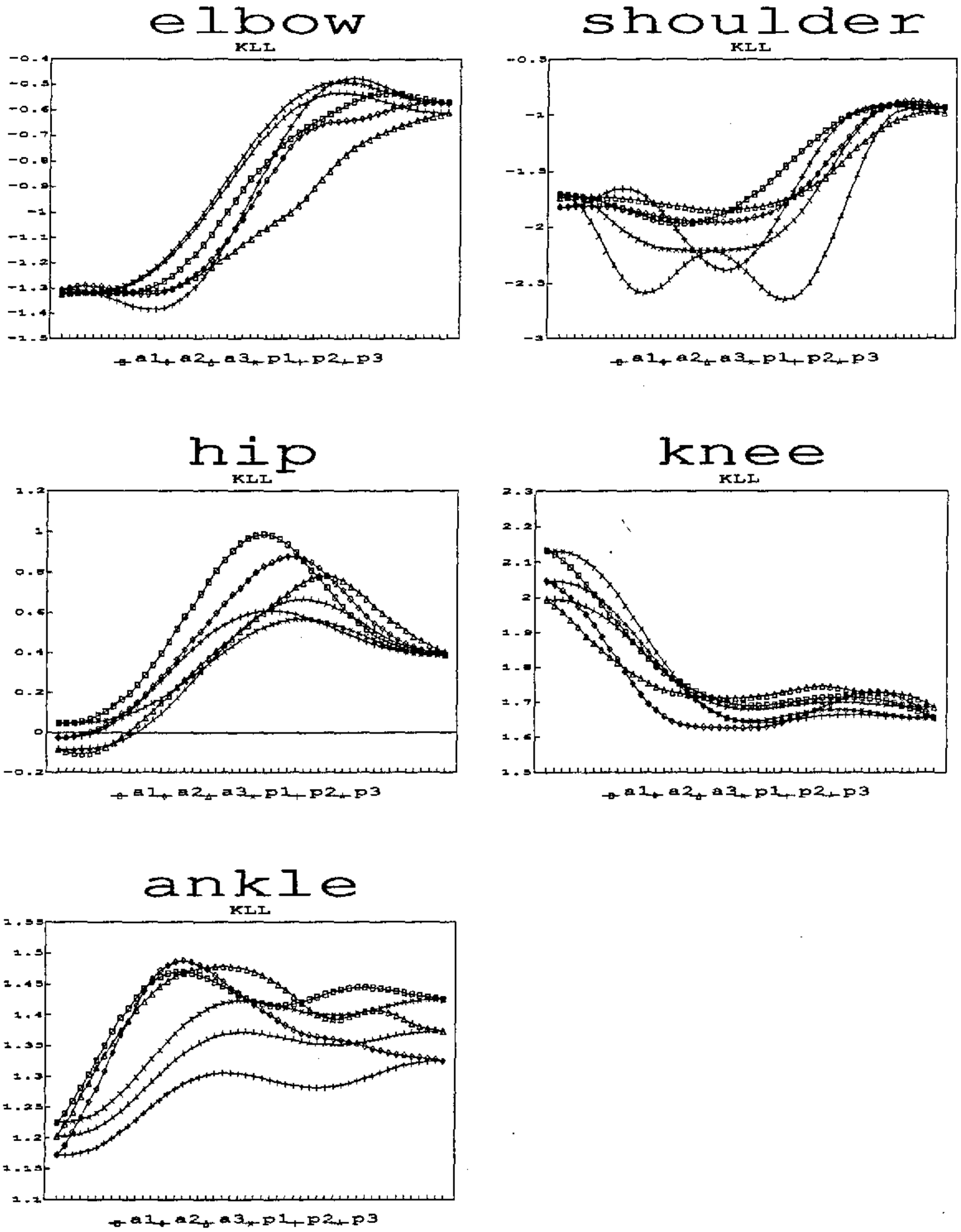

c. KLL

Figure B.7 Continued

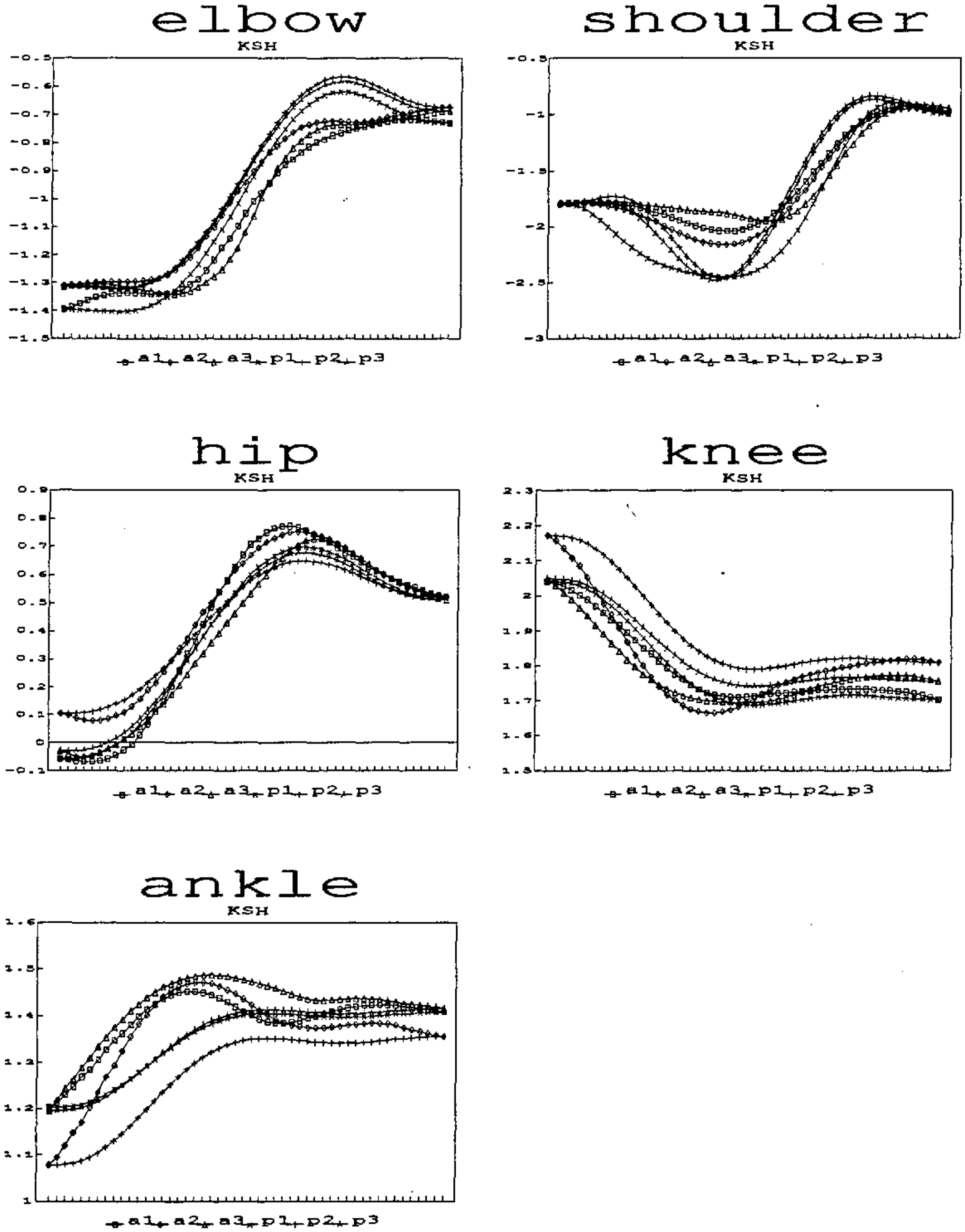

d. KSH

Figure B.7 Continued

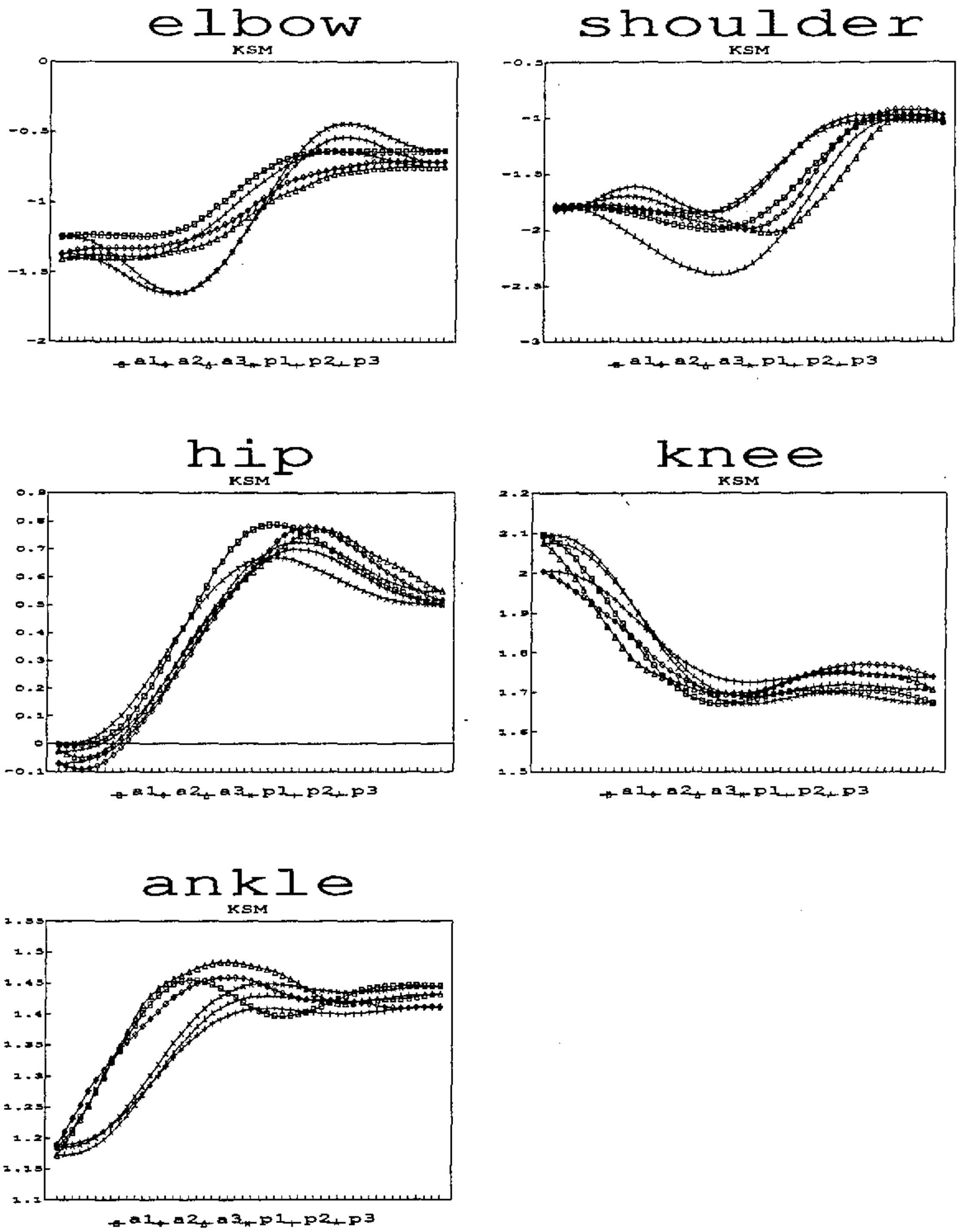

e. KSM

Figure B.7 Continued

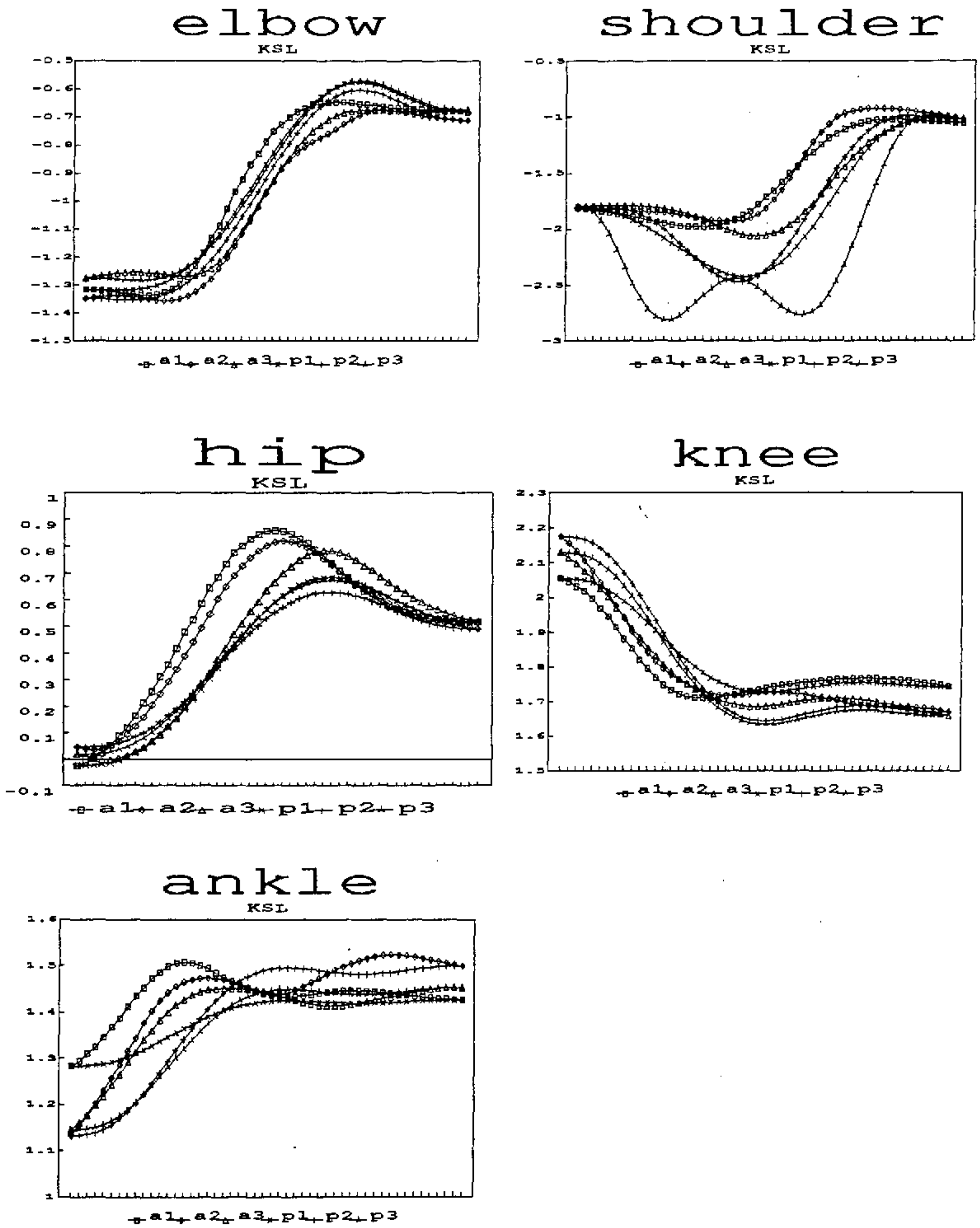

f. KSL

Figure B.7 Continued

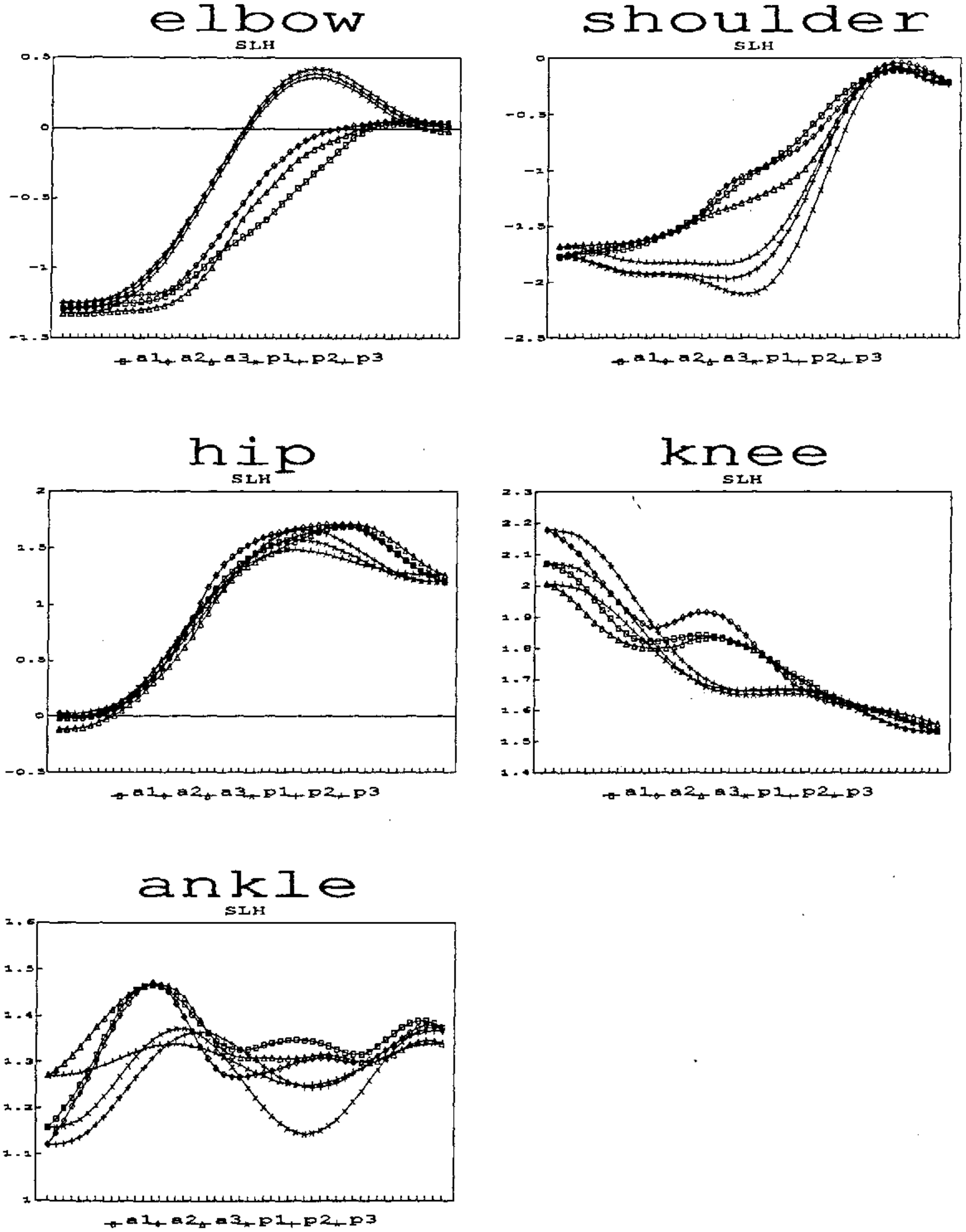

g. SLH

Figure B.7 Continued

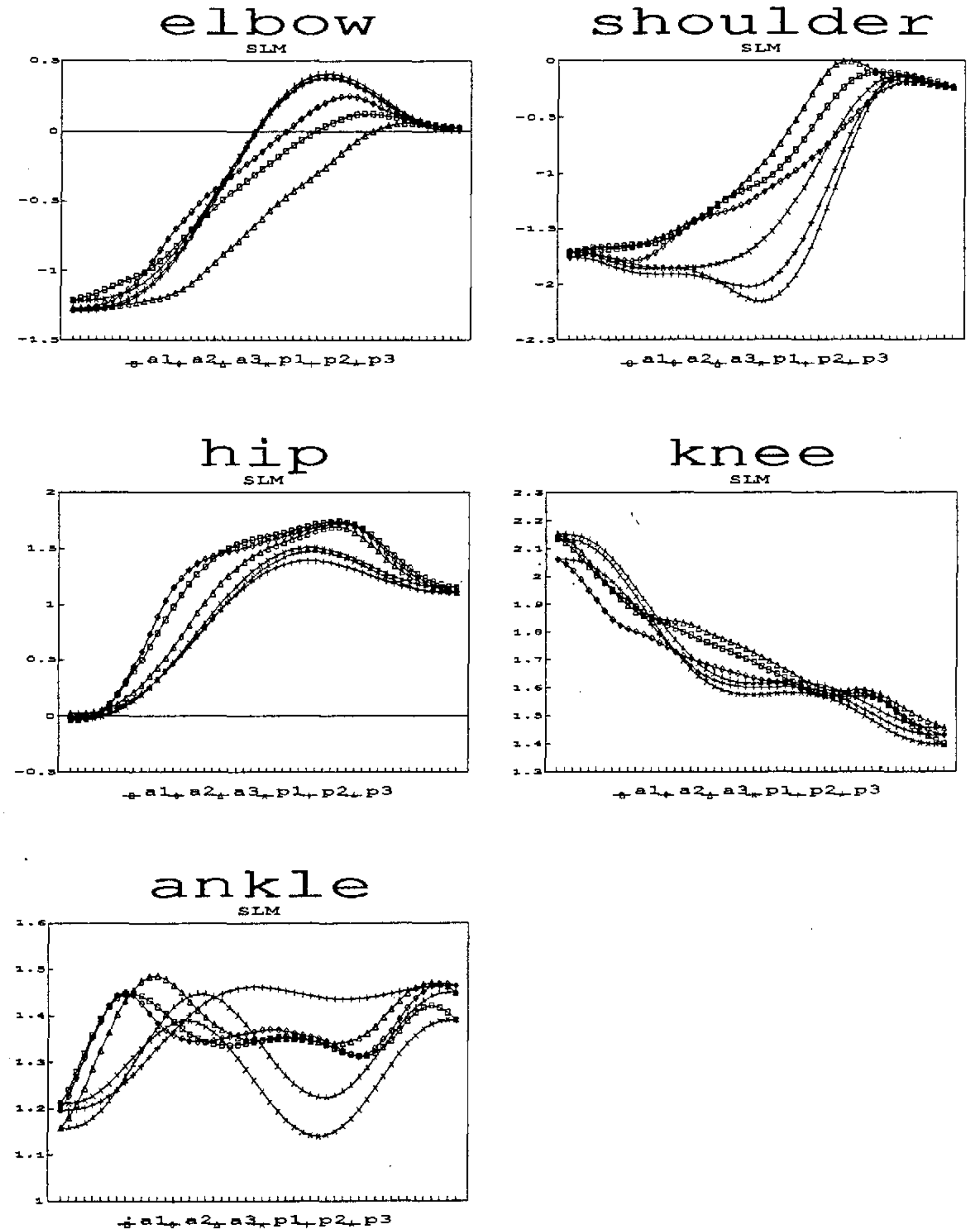

h. SLM

Figure B.7 Continued

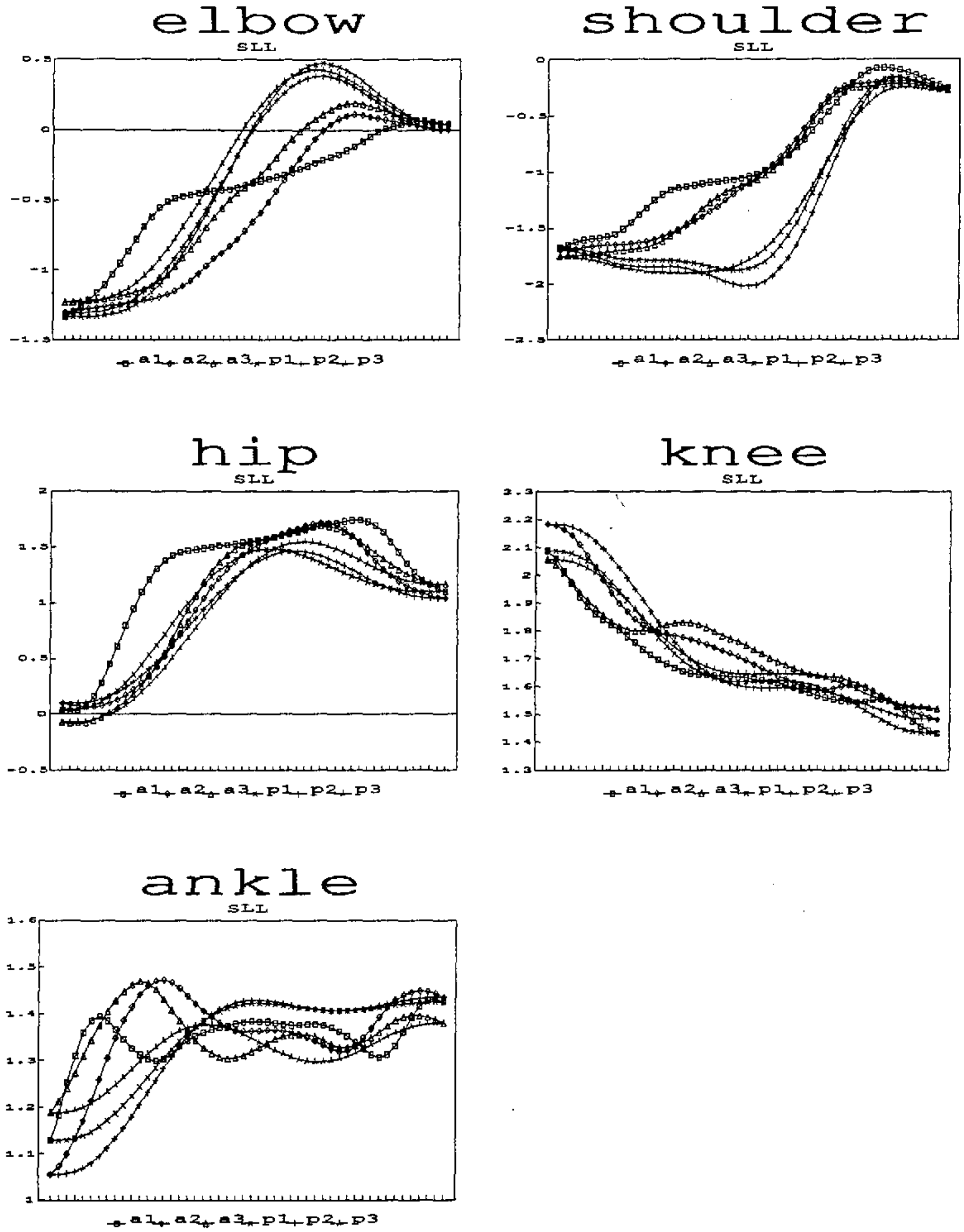

i. SLL

Figure B.7 Continued

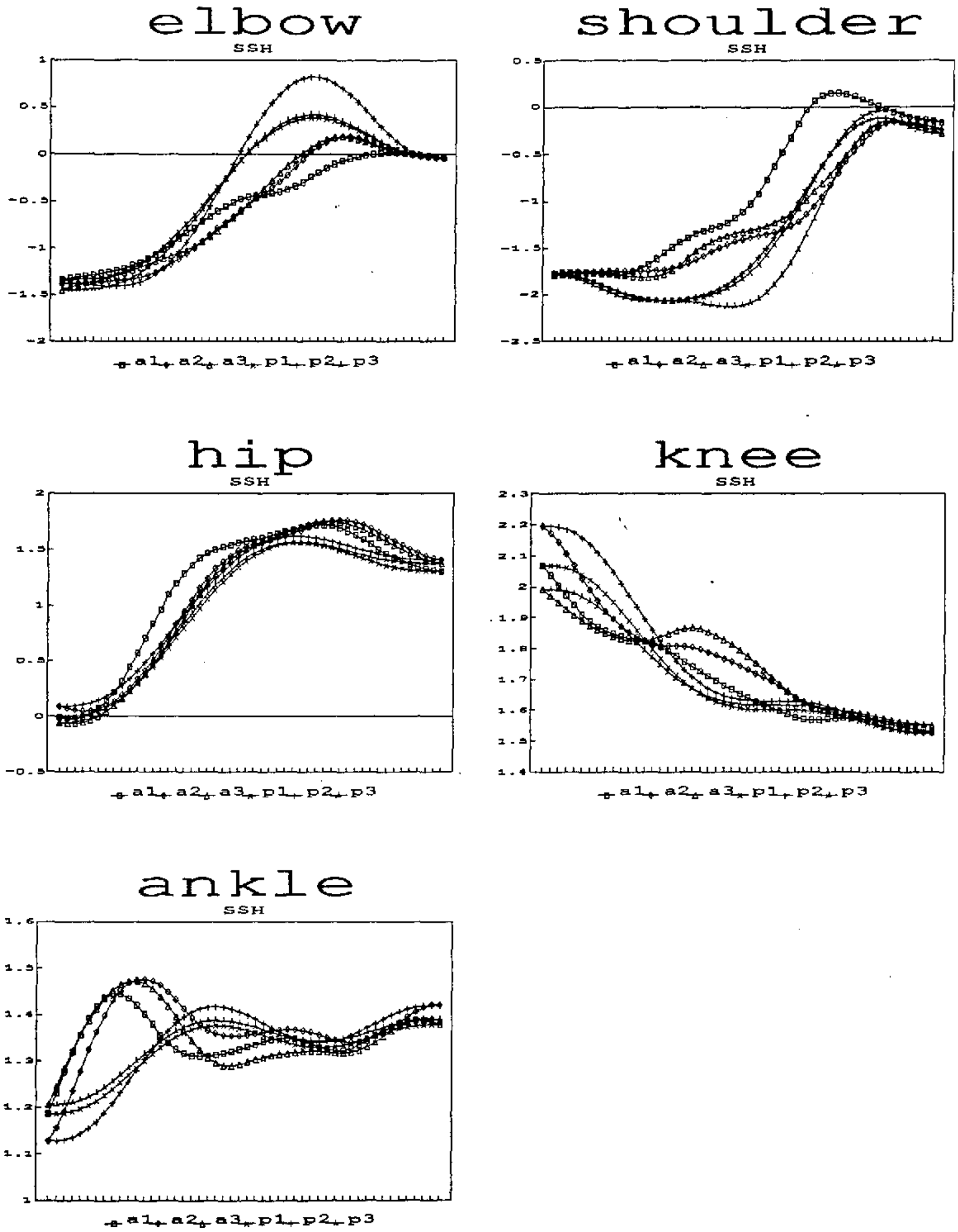

j. SSH

Figure B.7 Continued

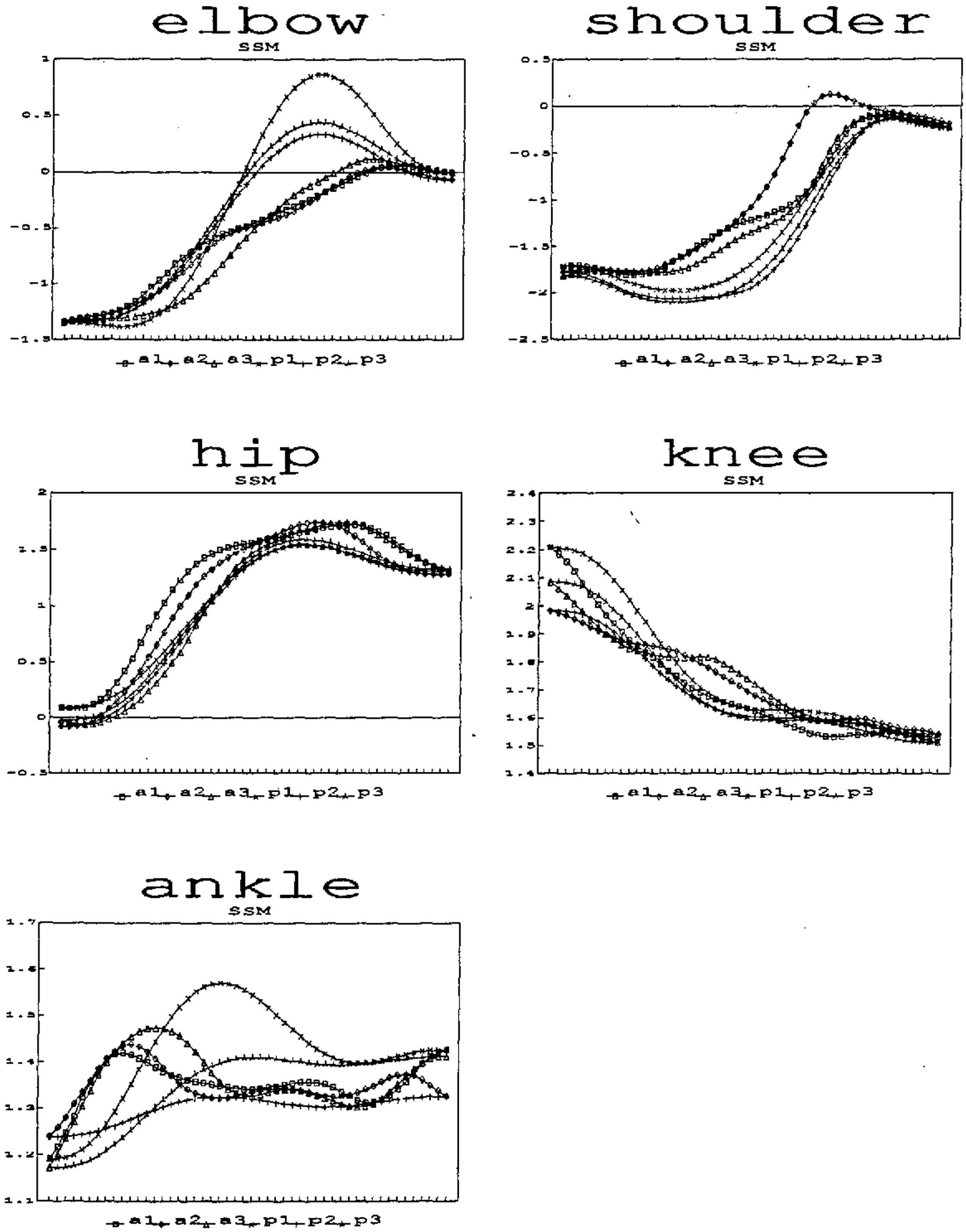

k. SSM

Figure B.7 Continued

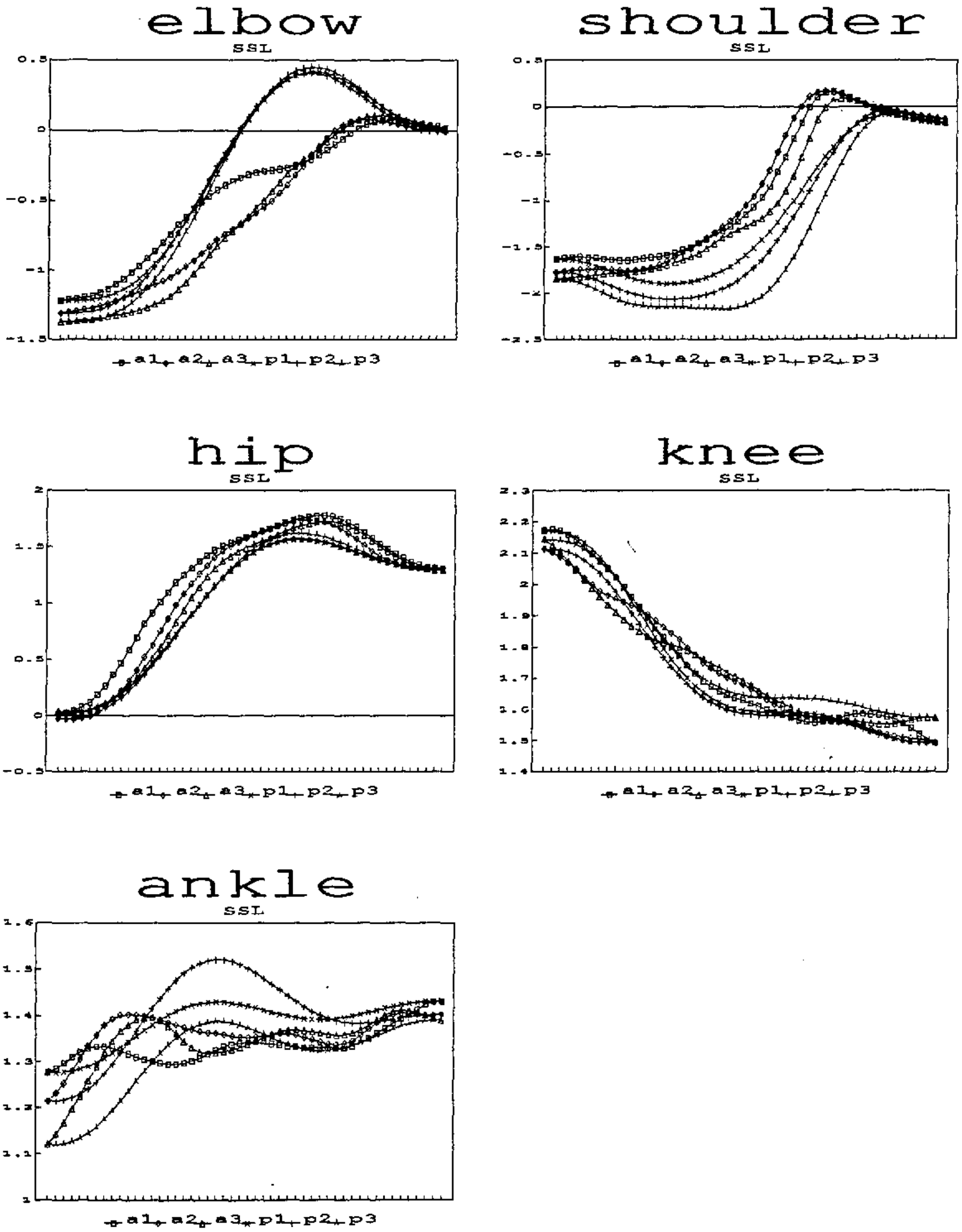

1. SSL

Figure B.7 Continued

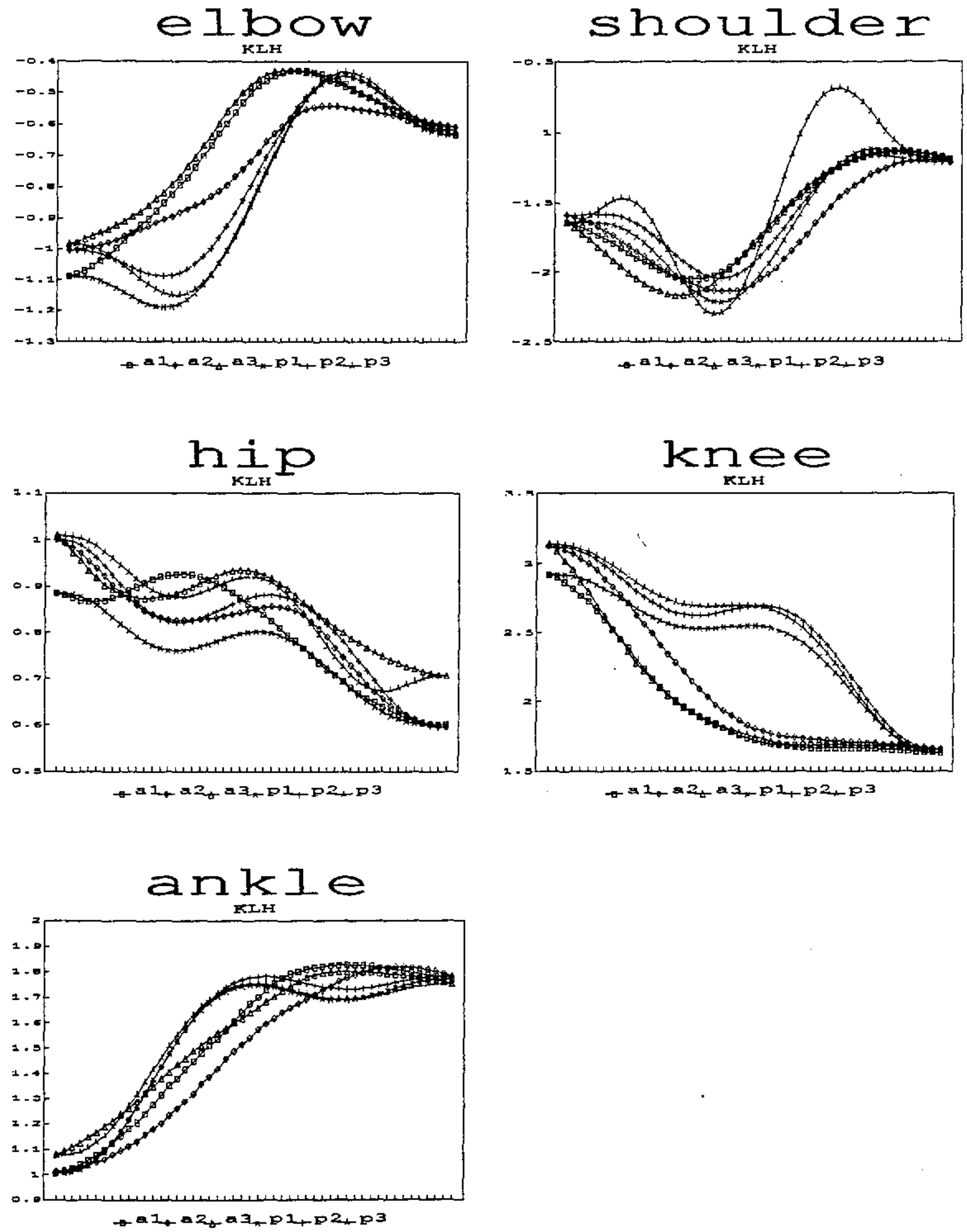

a. KLH

Figure B.8 Actual versus simulated trajectories for subject 9, who performed squat lifts

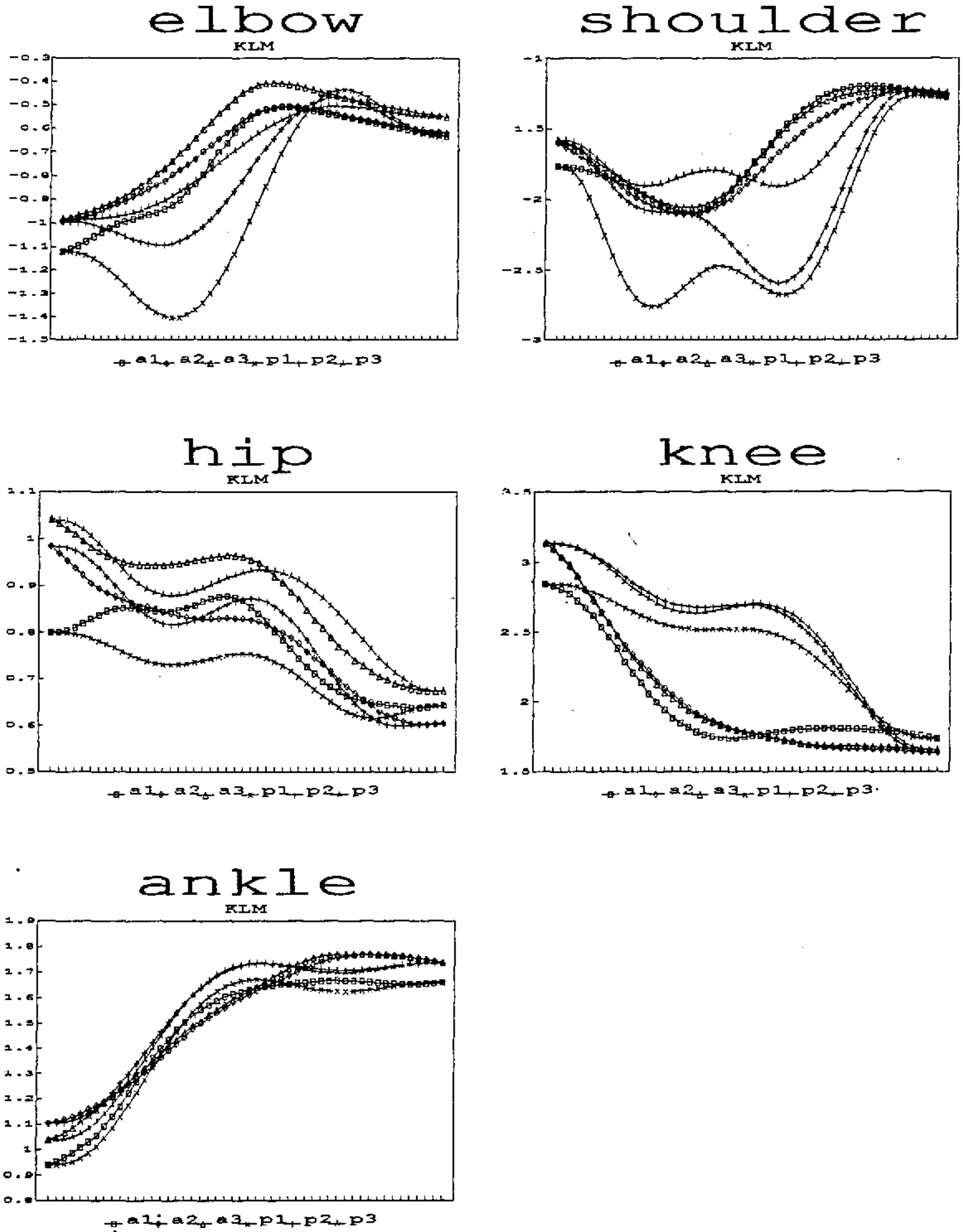

b. KLM

Figure B.8 Continued

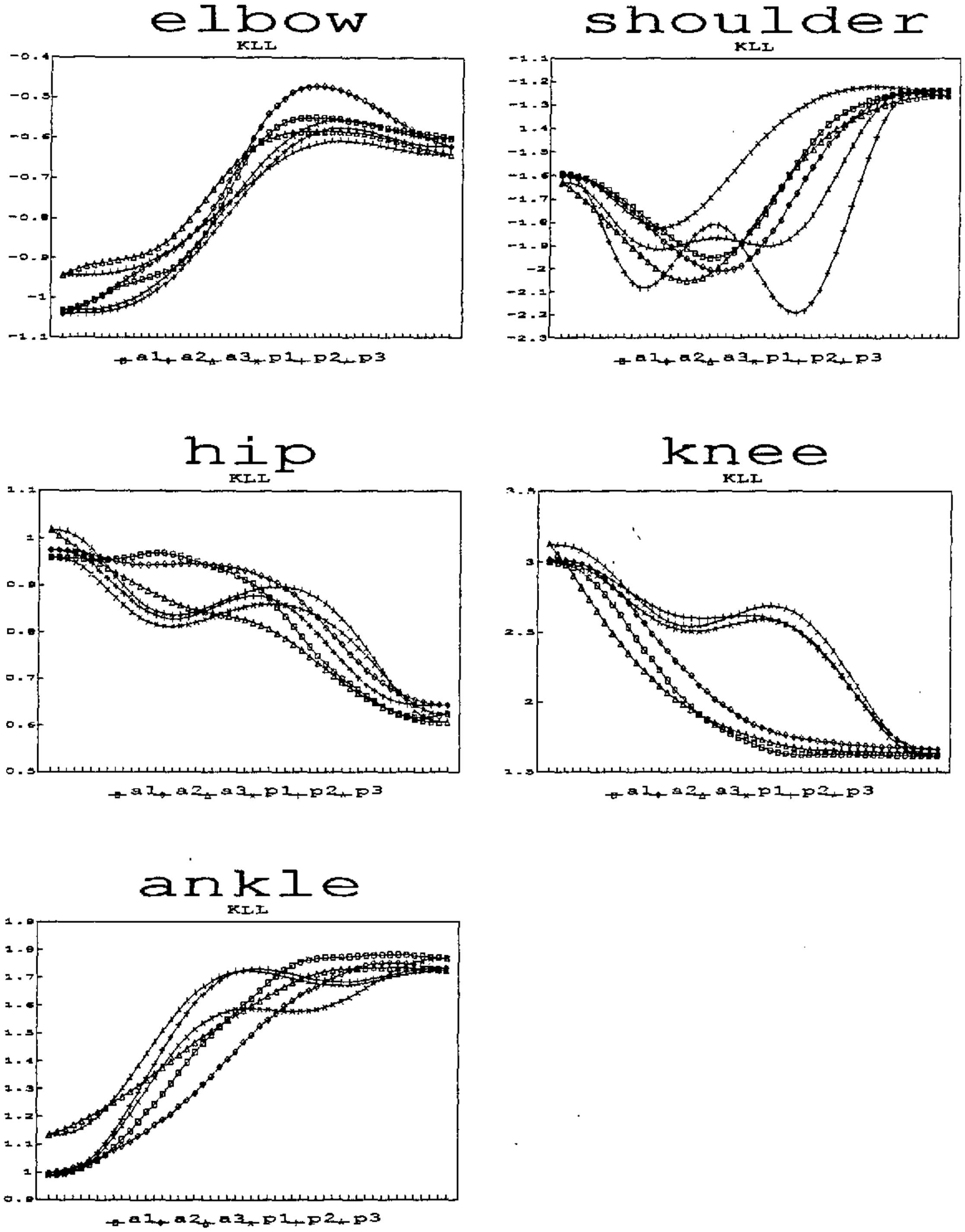

c. KLL

Figure B.8 Continued

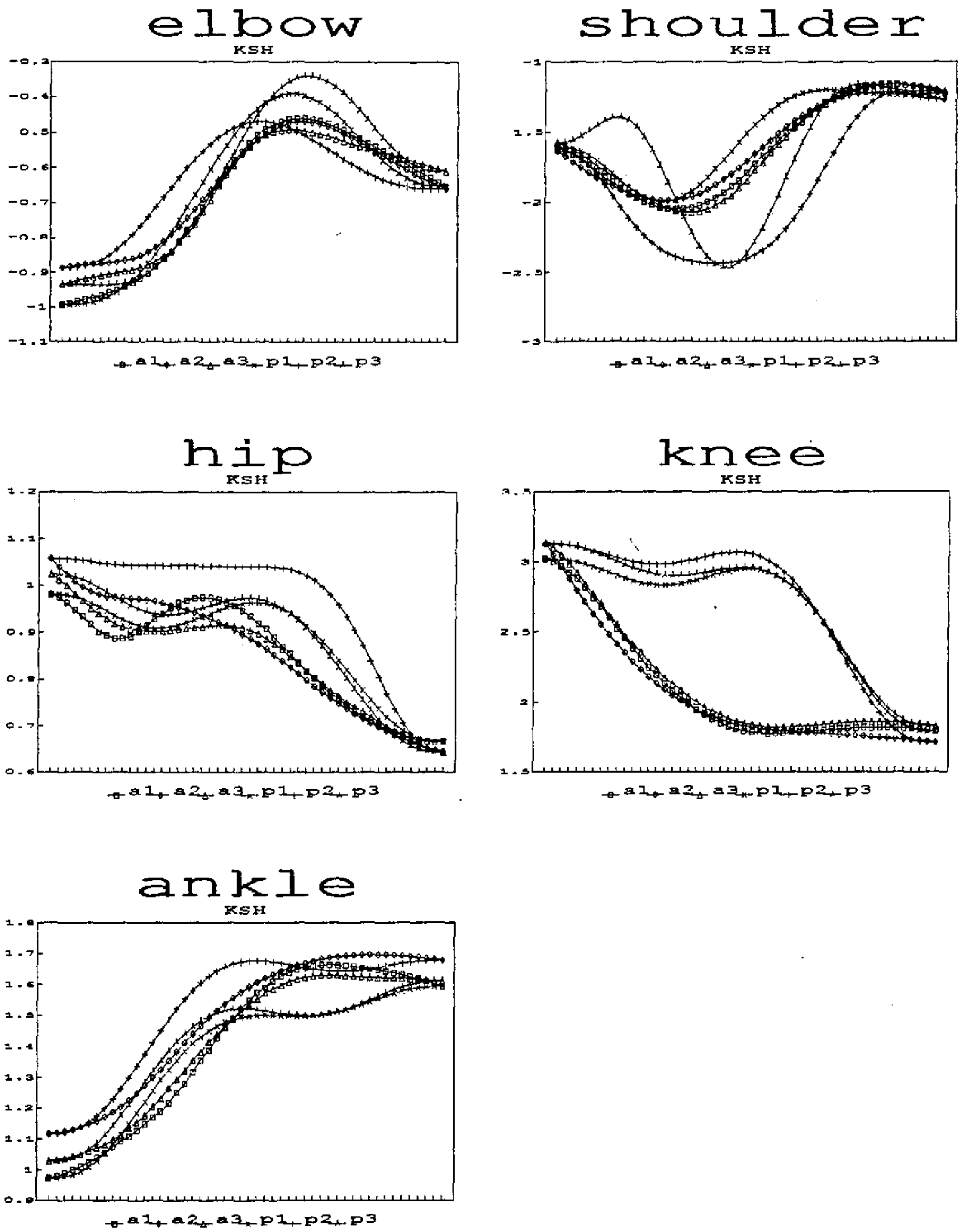

d. KSH

Figure B.8 Continued

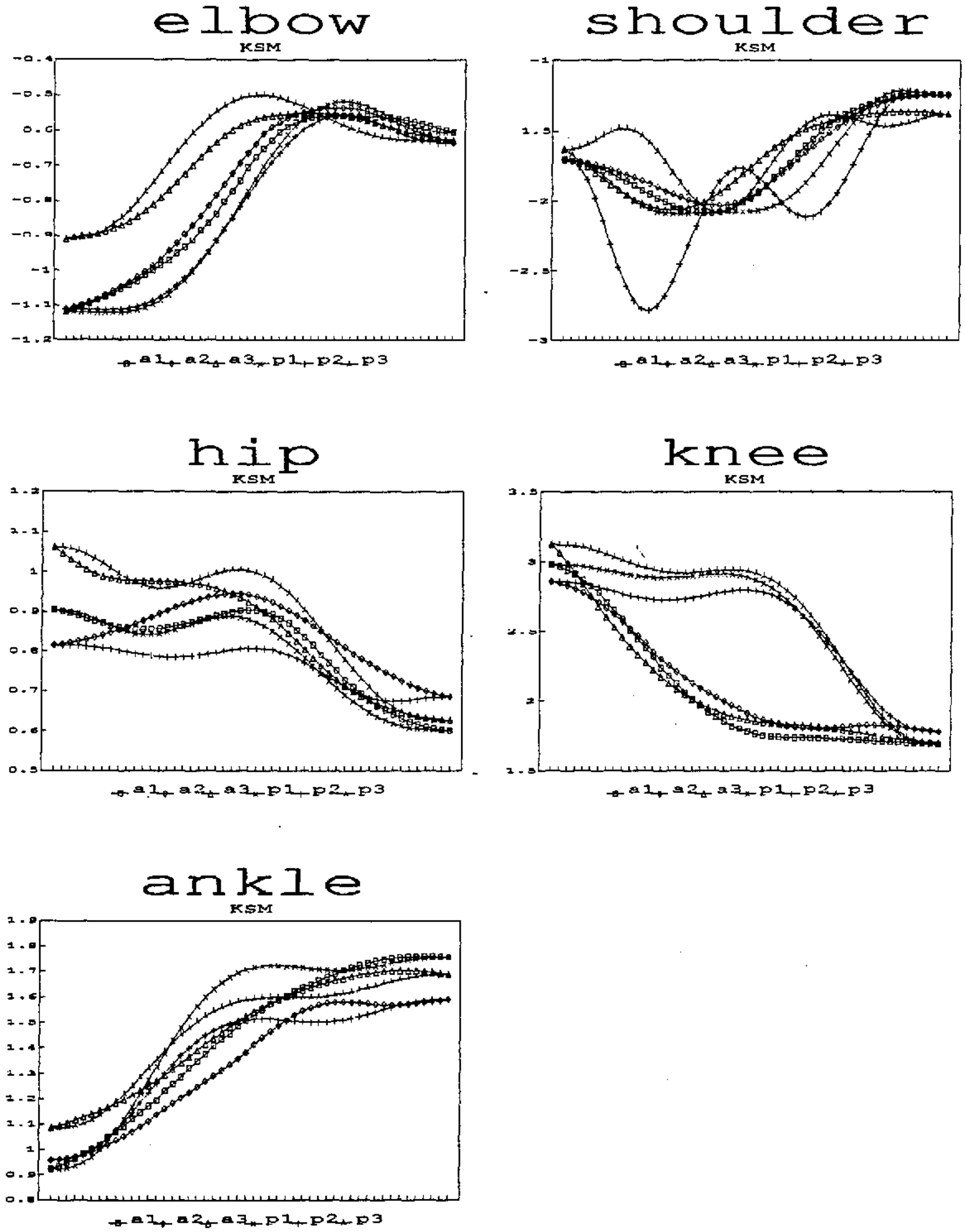

e. KSM

Figure B.8 Continued

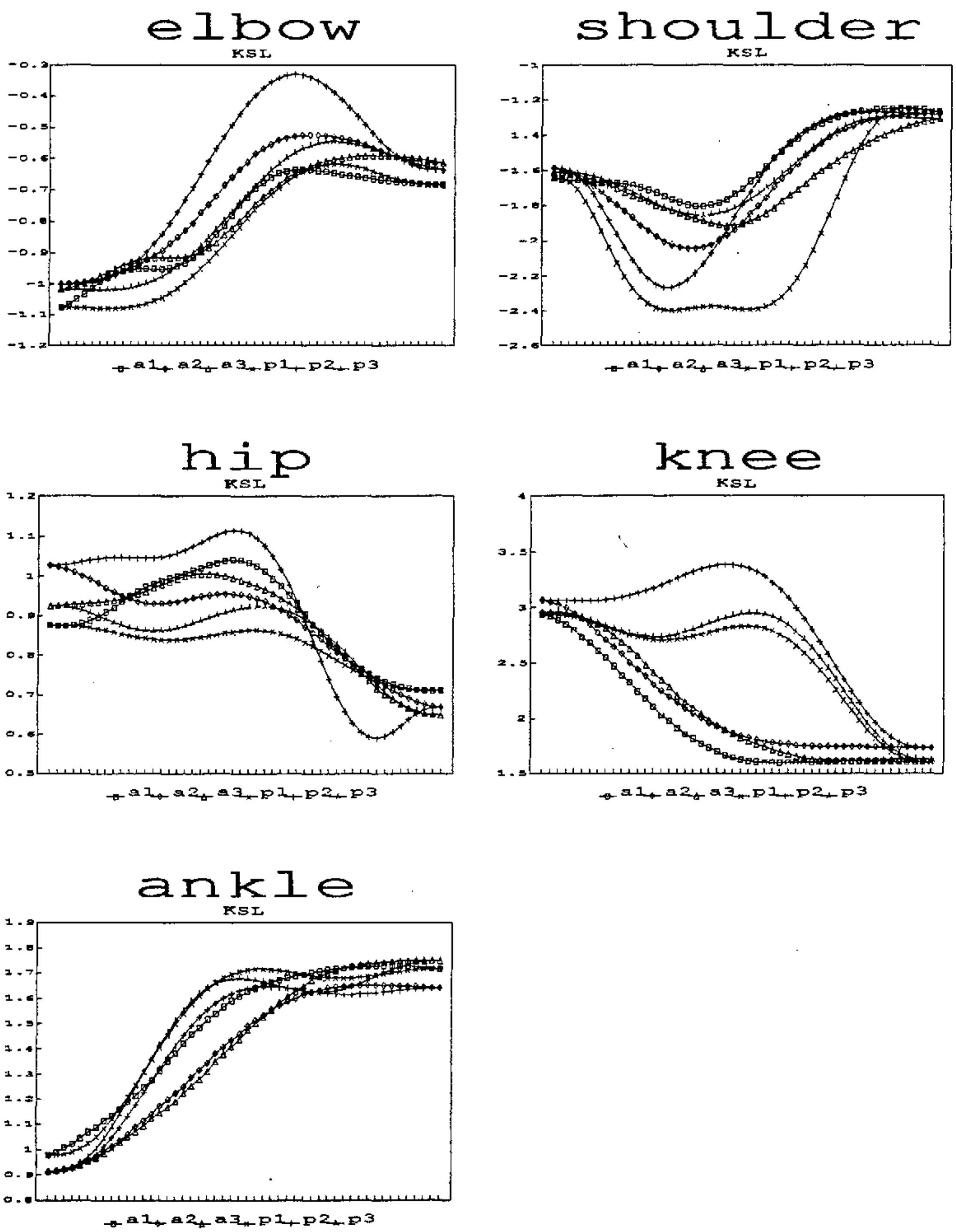

f. KSL

Figure B.8 Continued

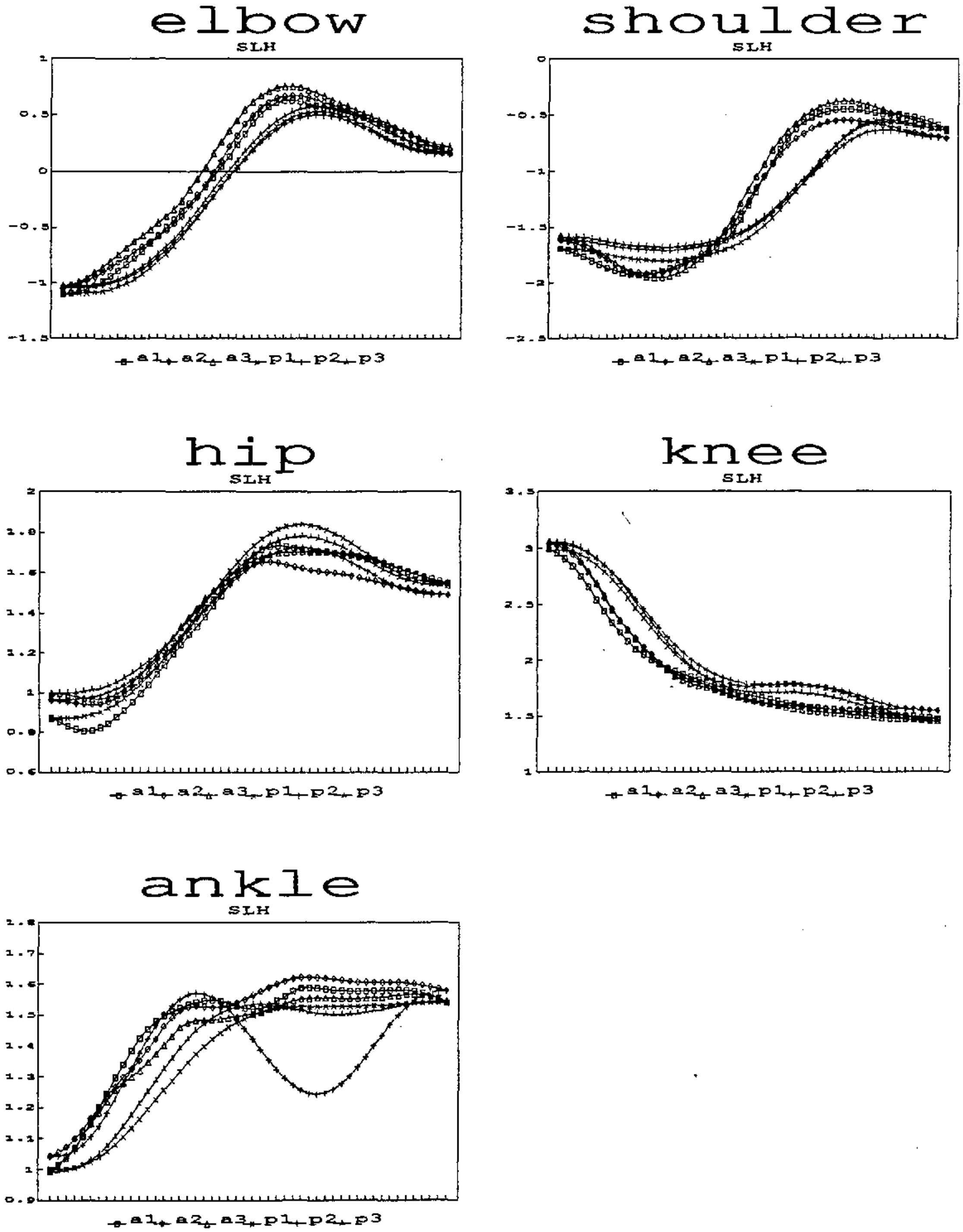

g. SLH

Figure B.8 Continued

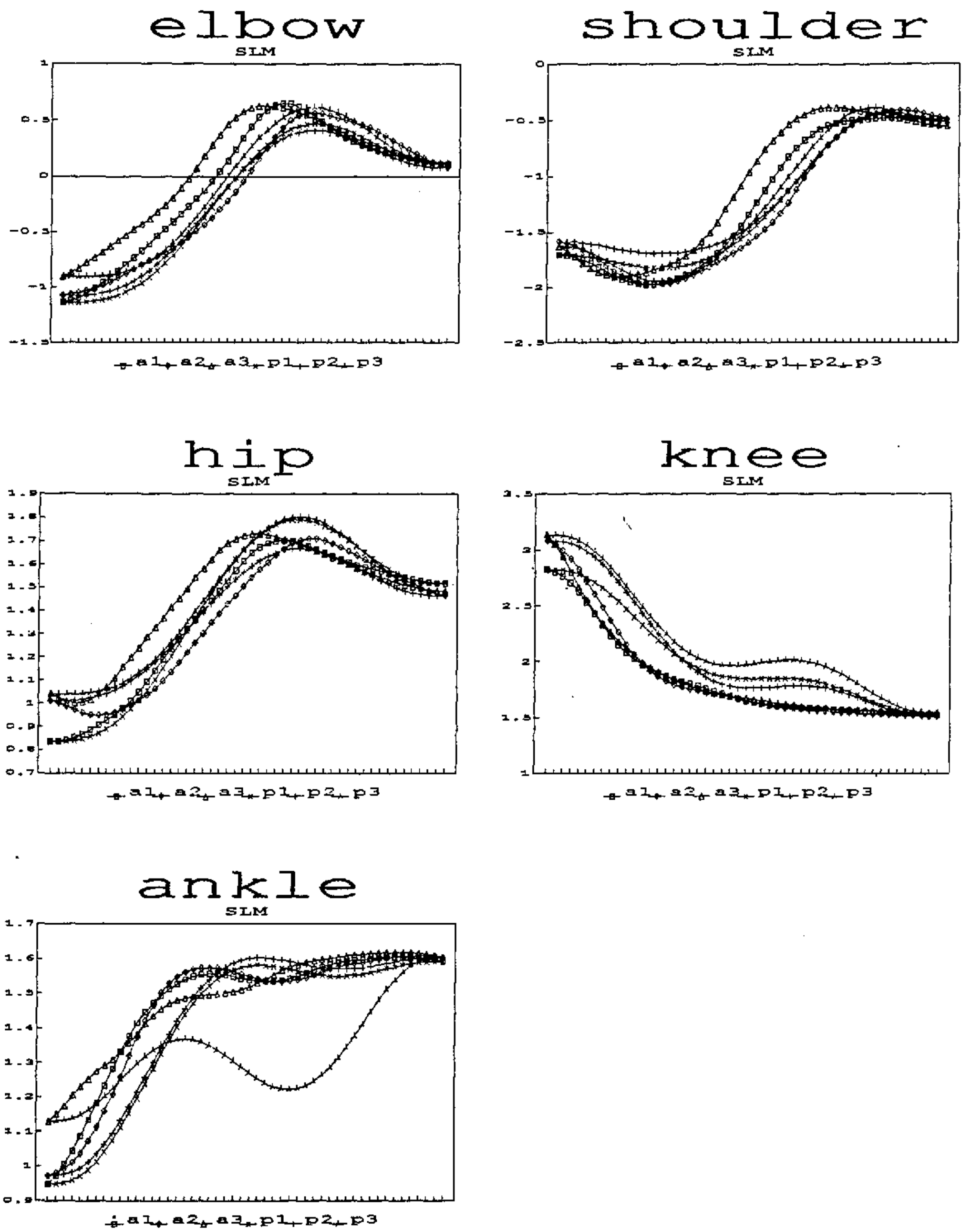

h. SLM

Figure B.8 Continued

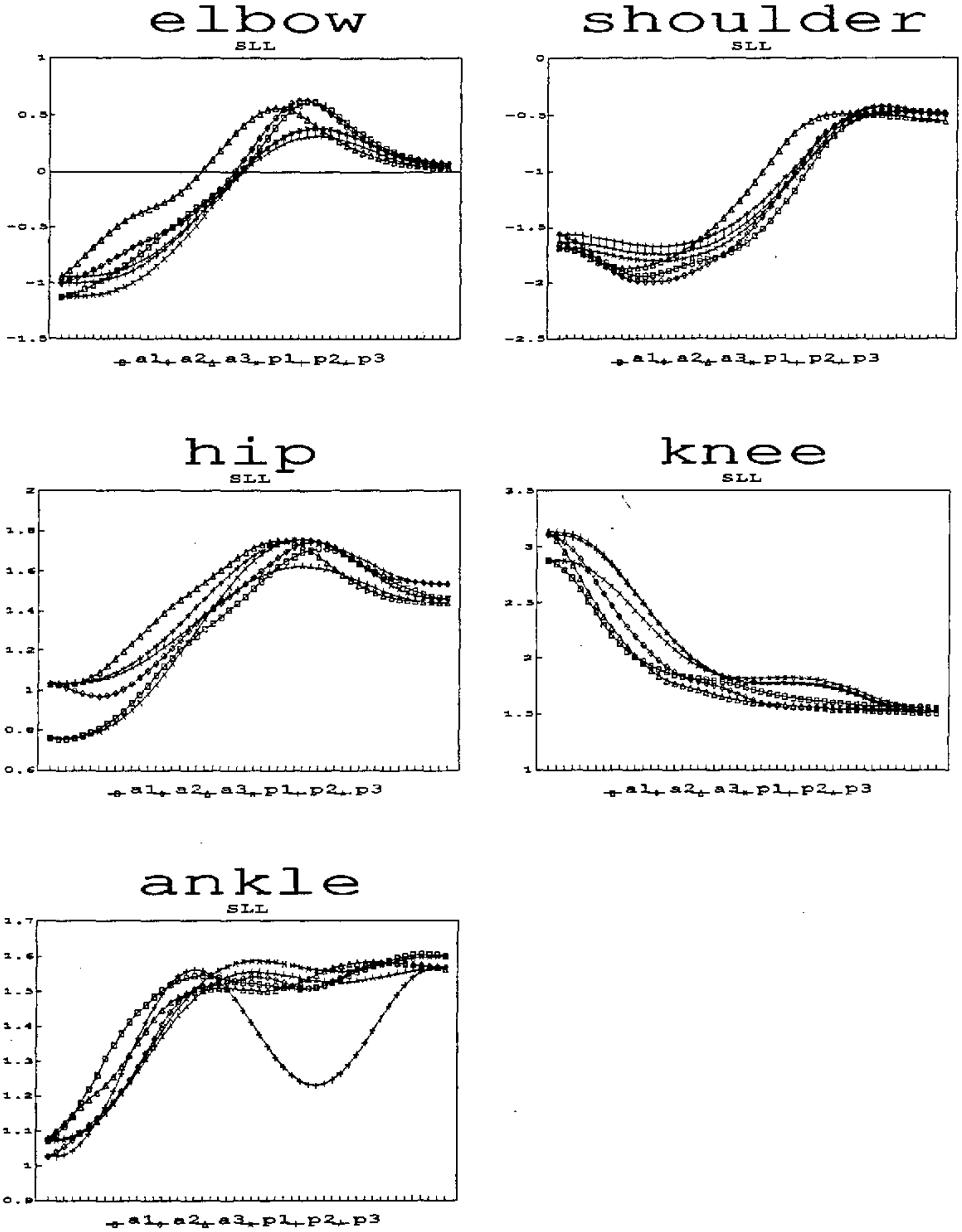

i. SLL

Figure B.8 Continued

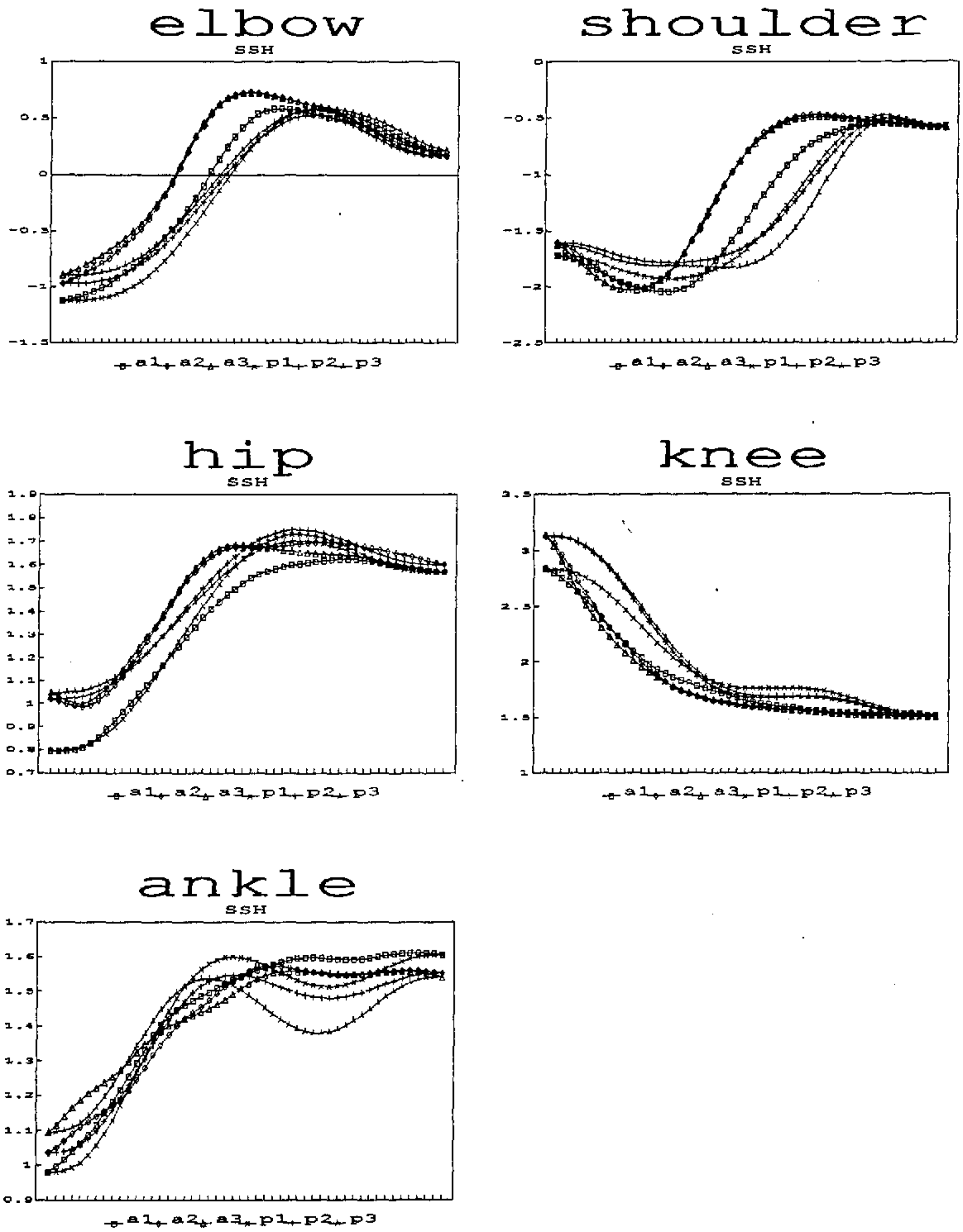

j. SSH

Figure B.8 Continued

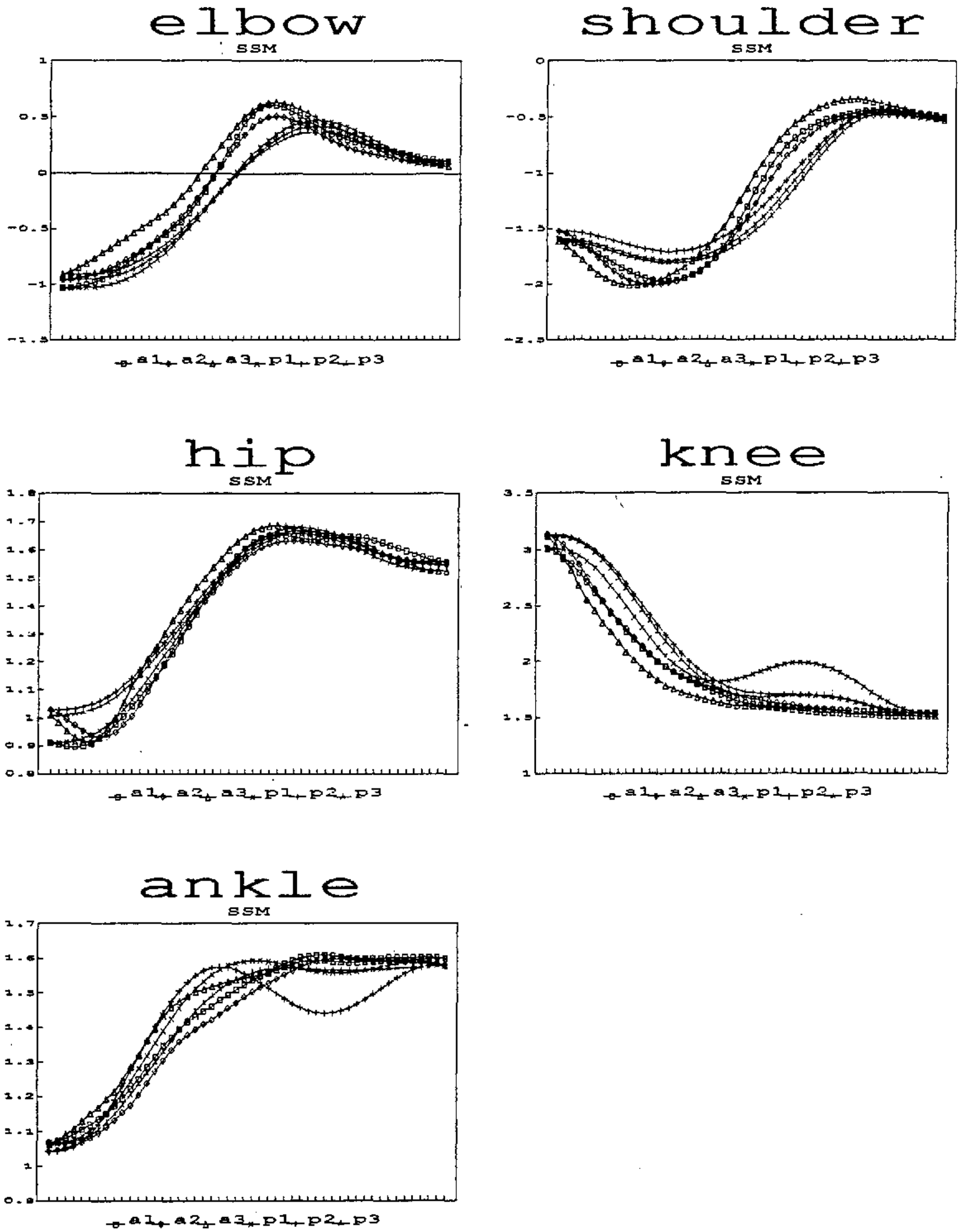

k. SSM

Figure B.8 Continued

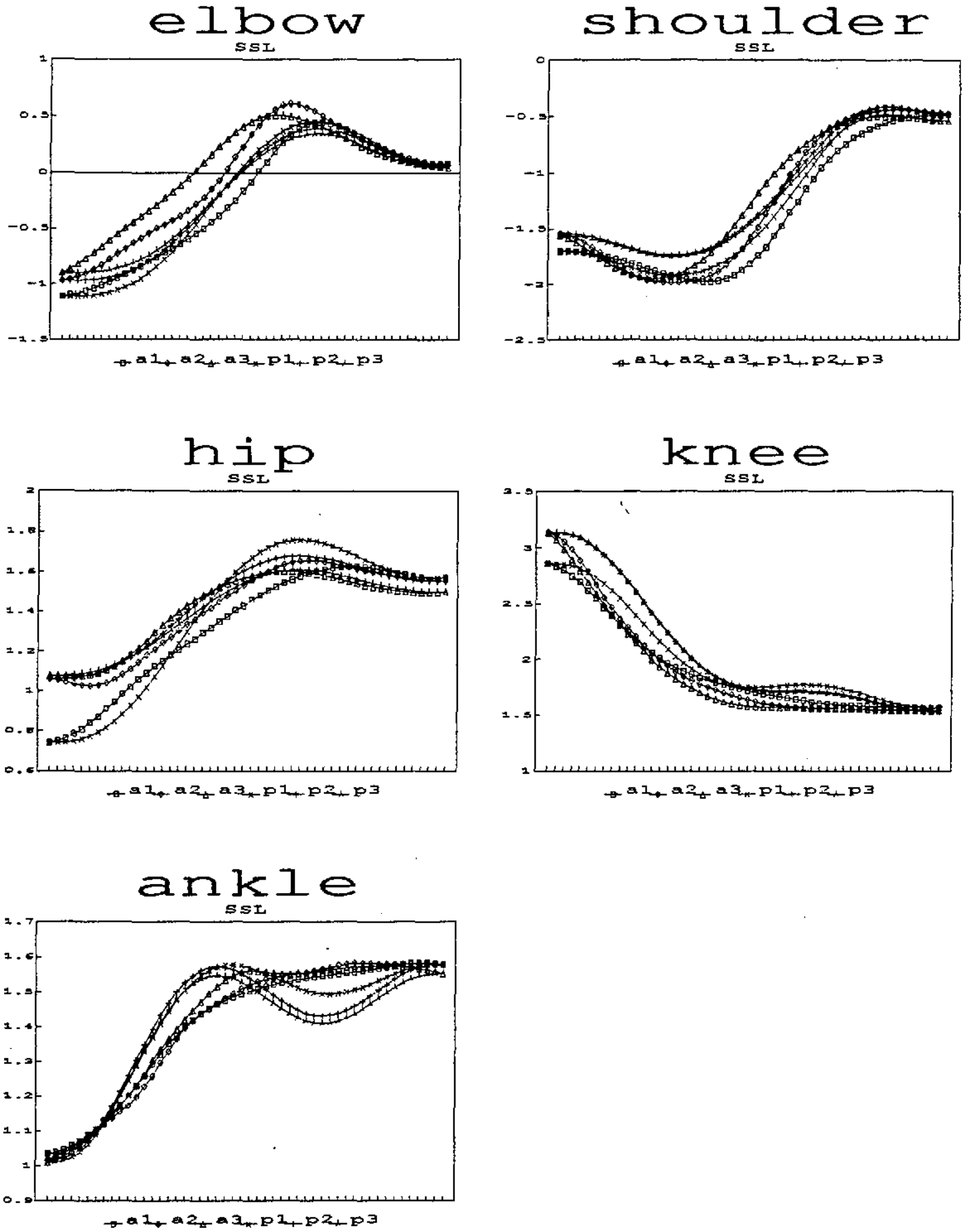

l. SSL

Figure B.8 Continued

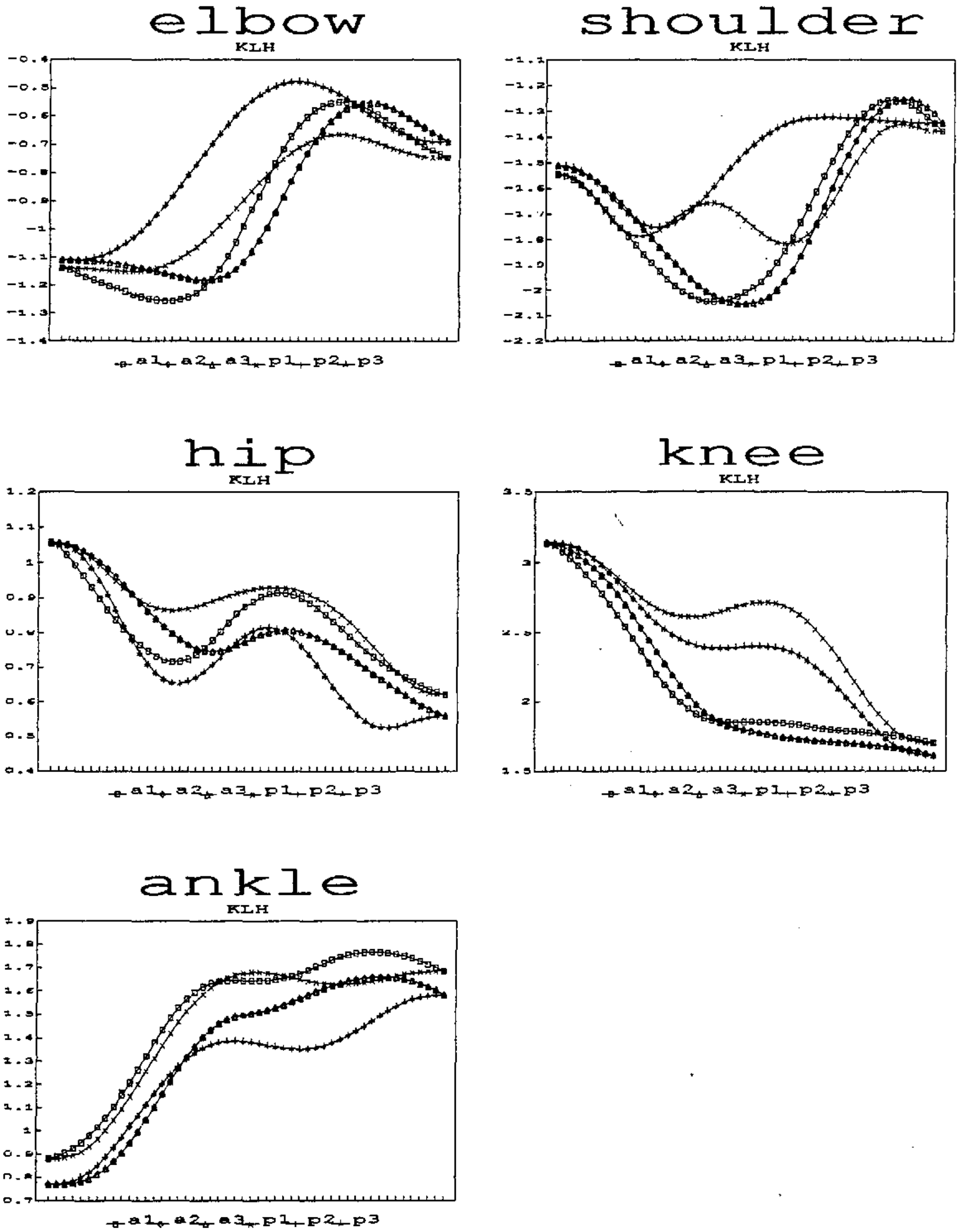

a. KLH

Figure B.9 Actual versus simulated trajectories for subject 10, who performed squat lifts

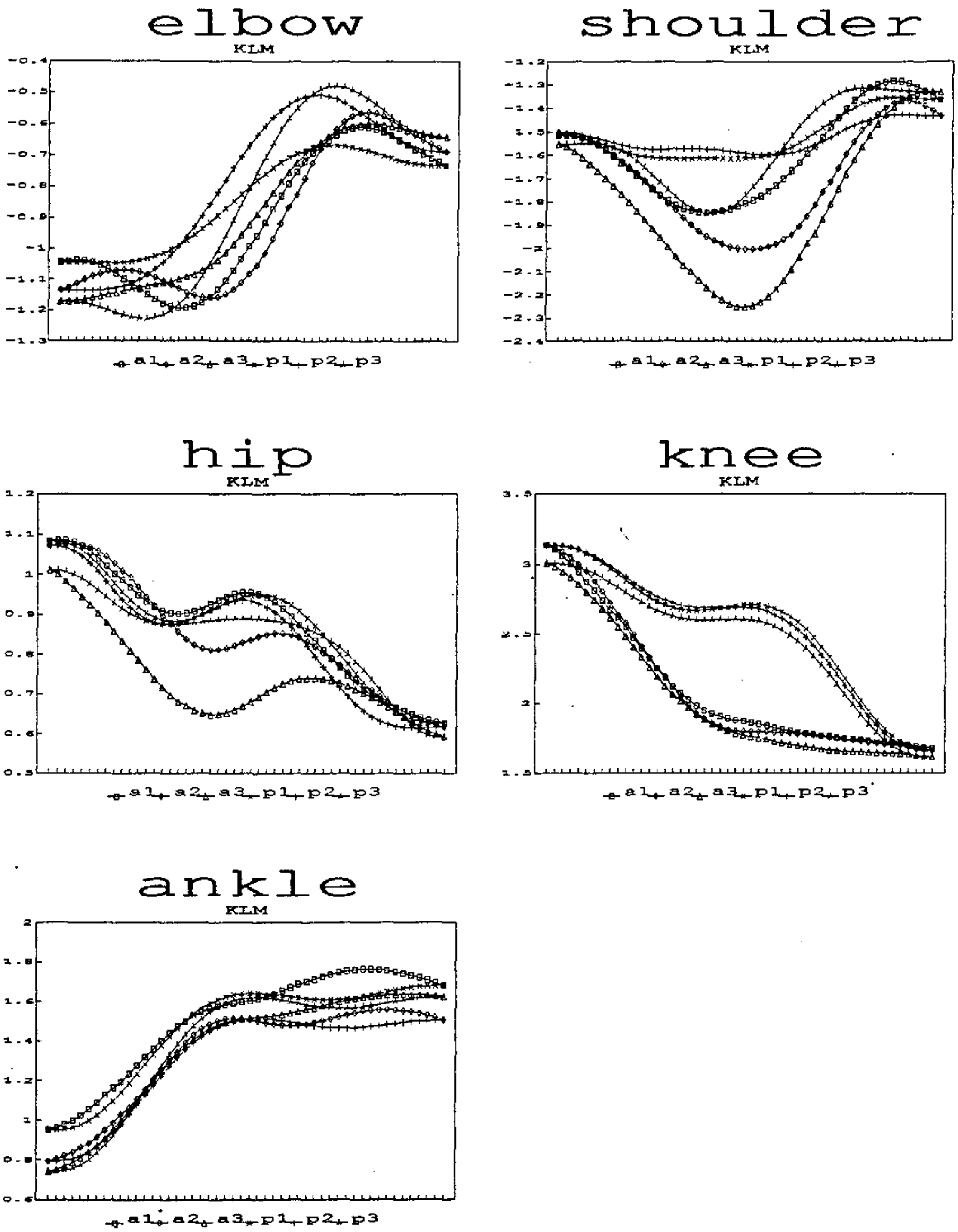

b. KLM

Figure B.9 Continued

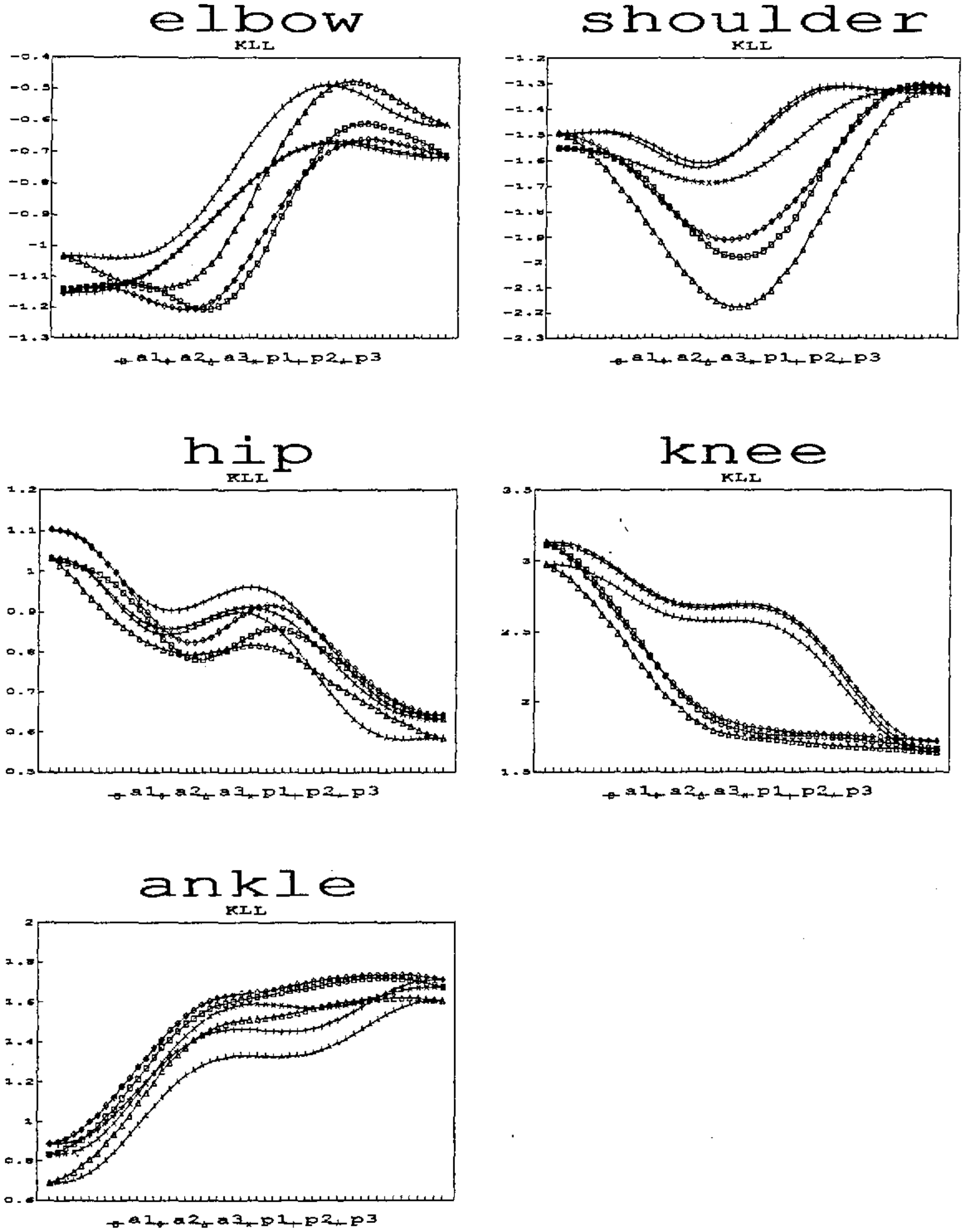

c. KLL

Figure B.9 Continued

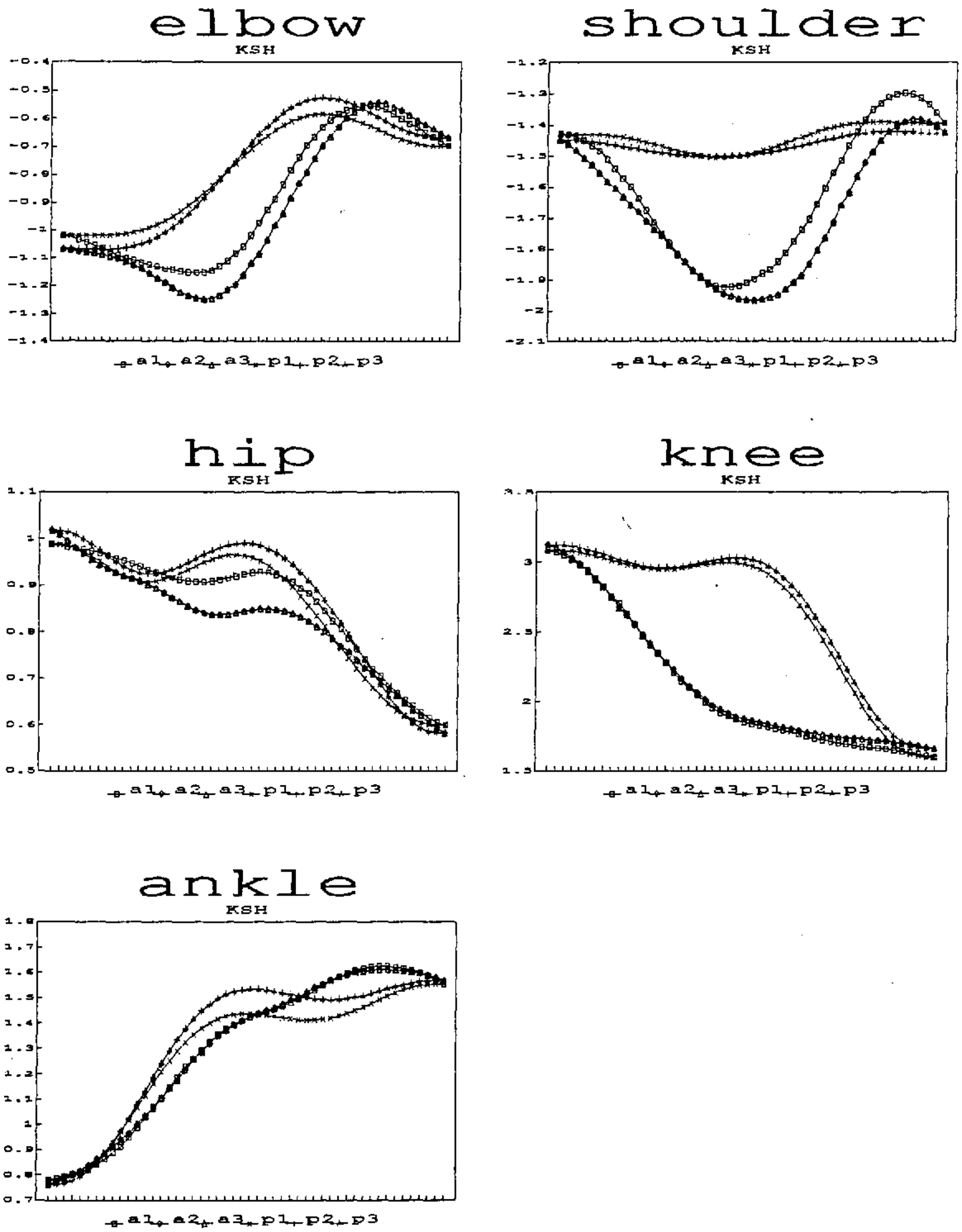

d. KSH

Figure B.9 Continued

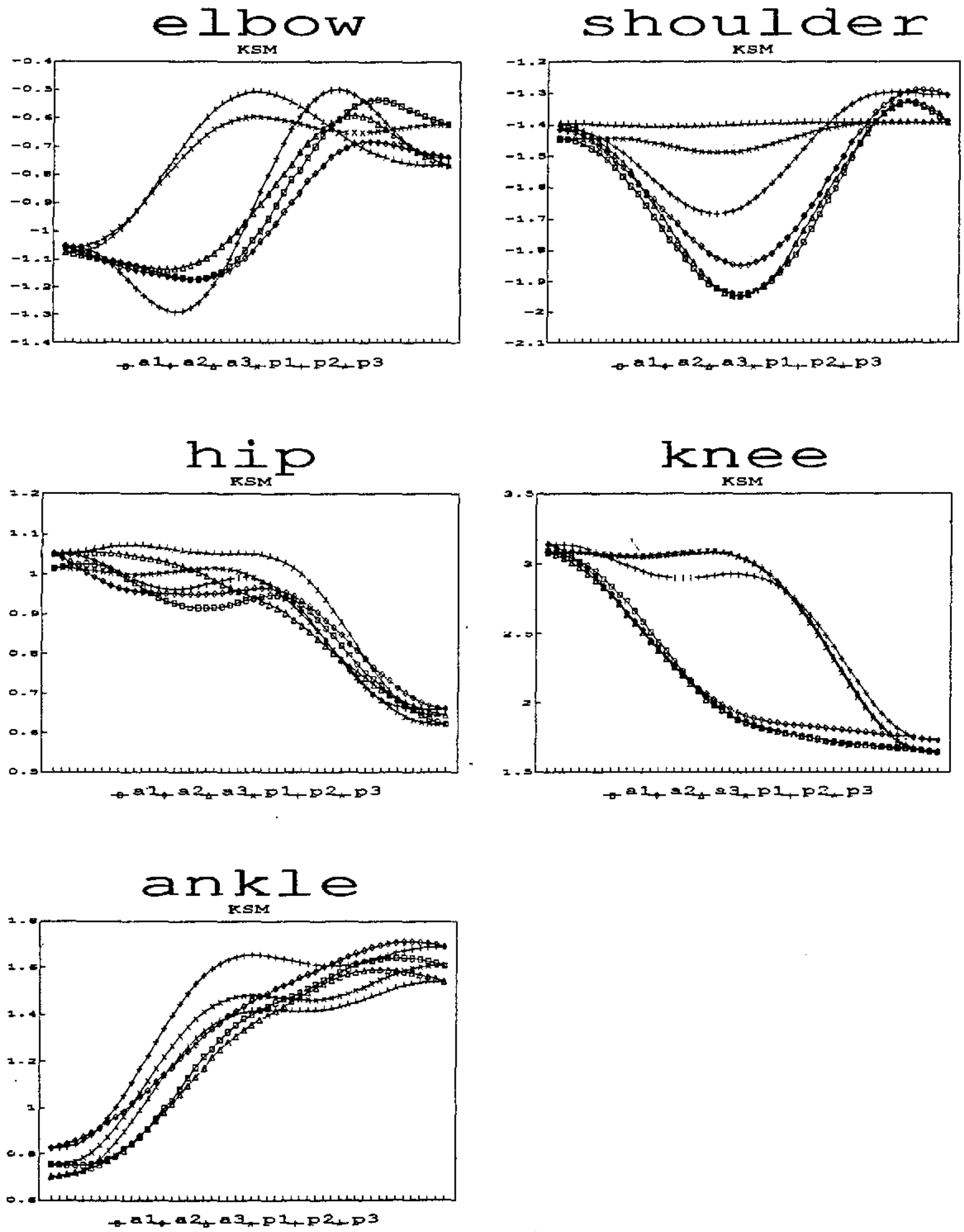

e. KSM

Figure B.9 Continued

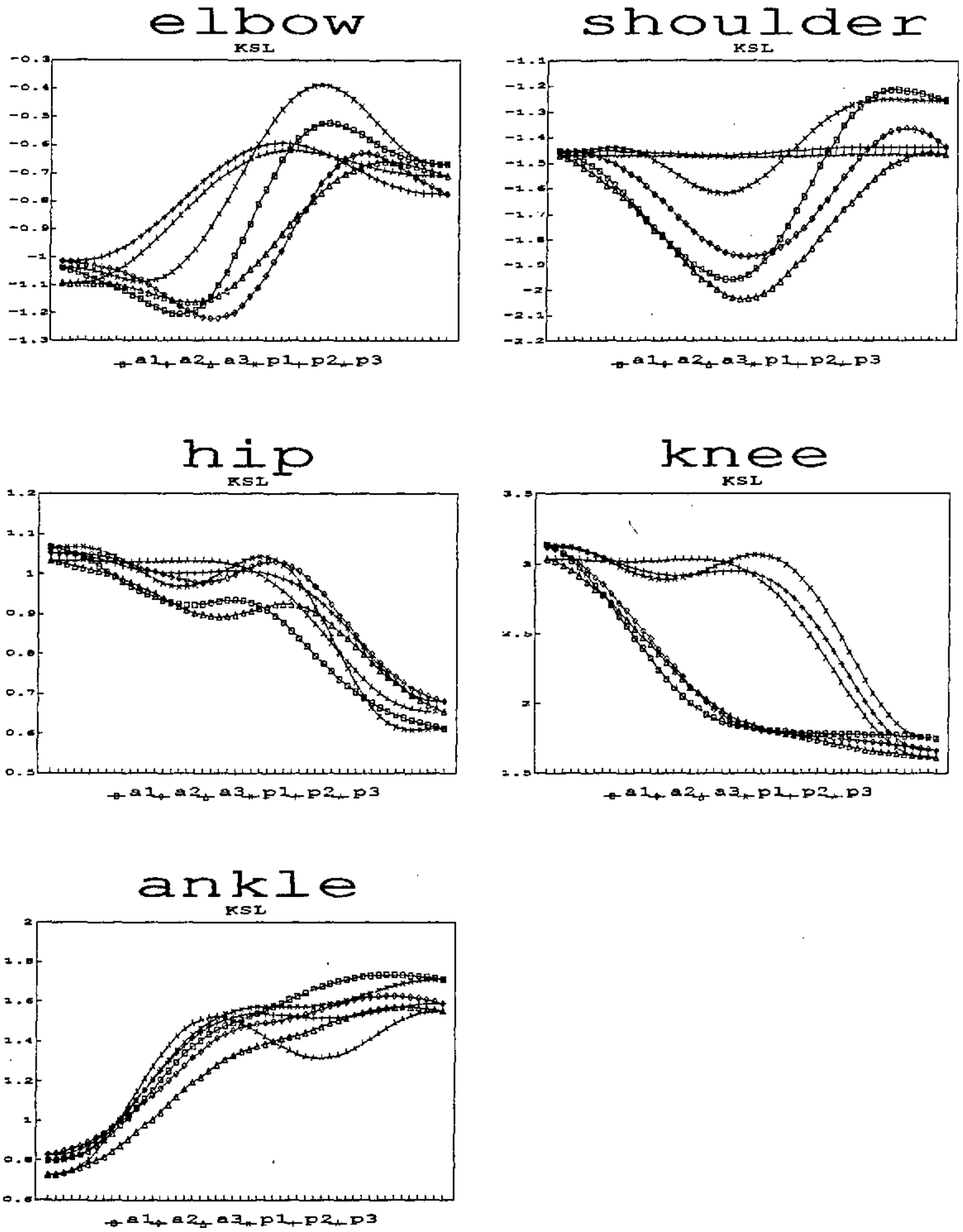

f. KSL

Figure B.9 Continued

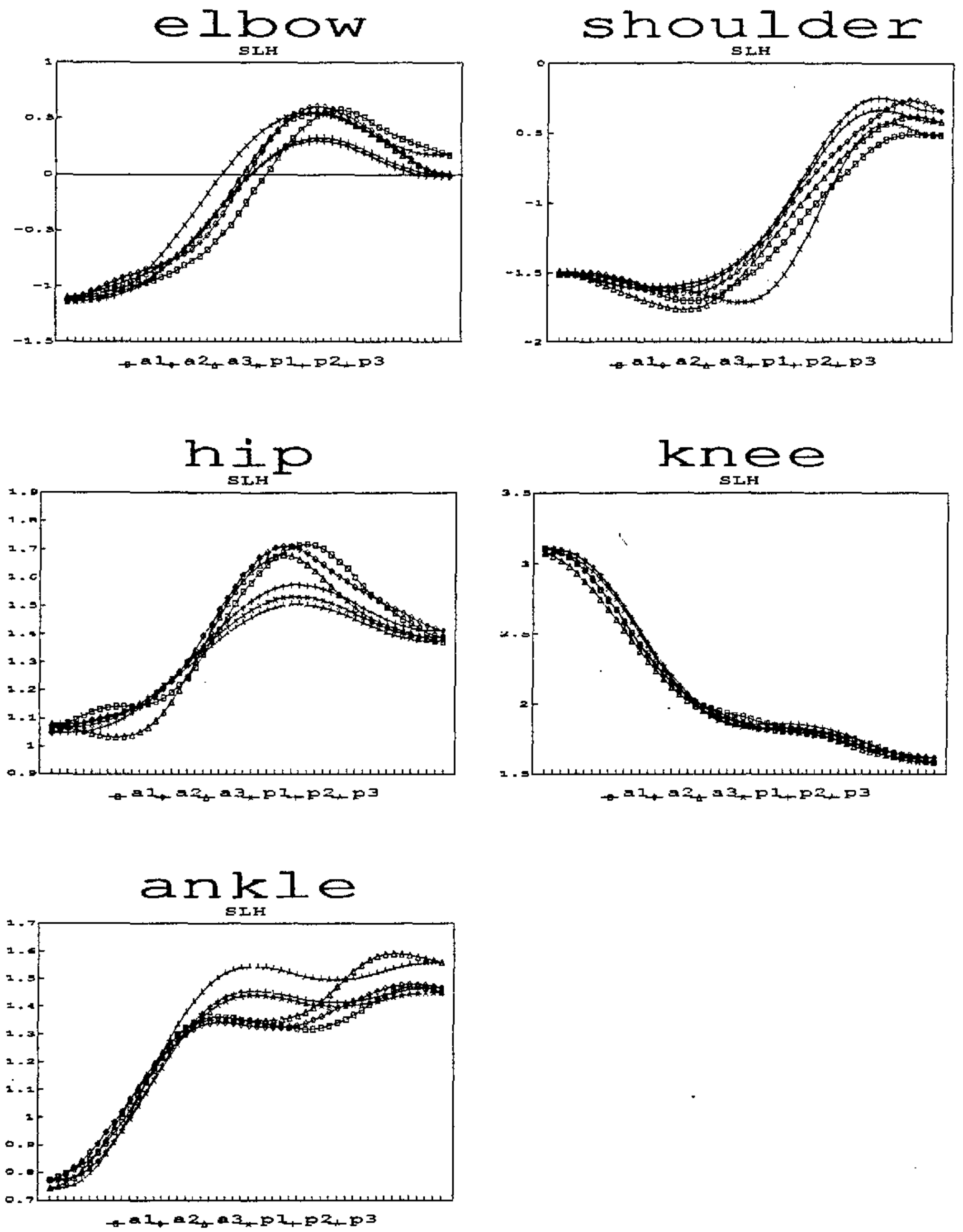

g. SLH

Figure B.9 Continued

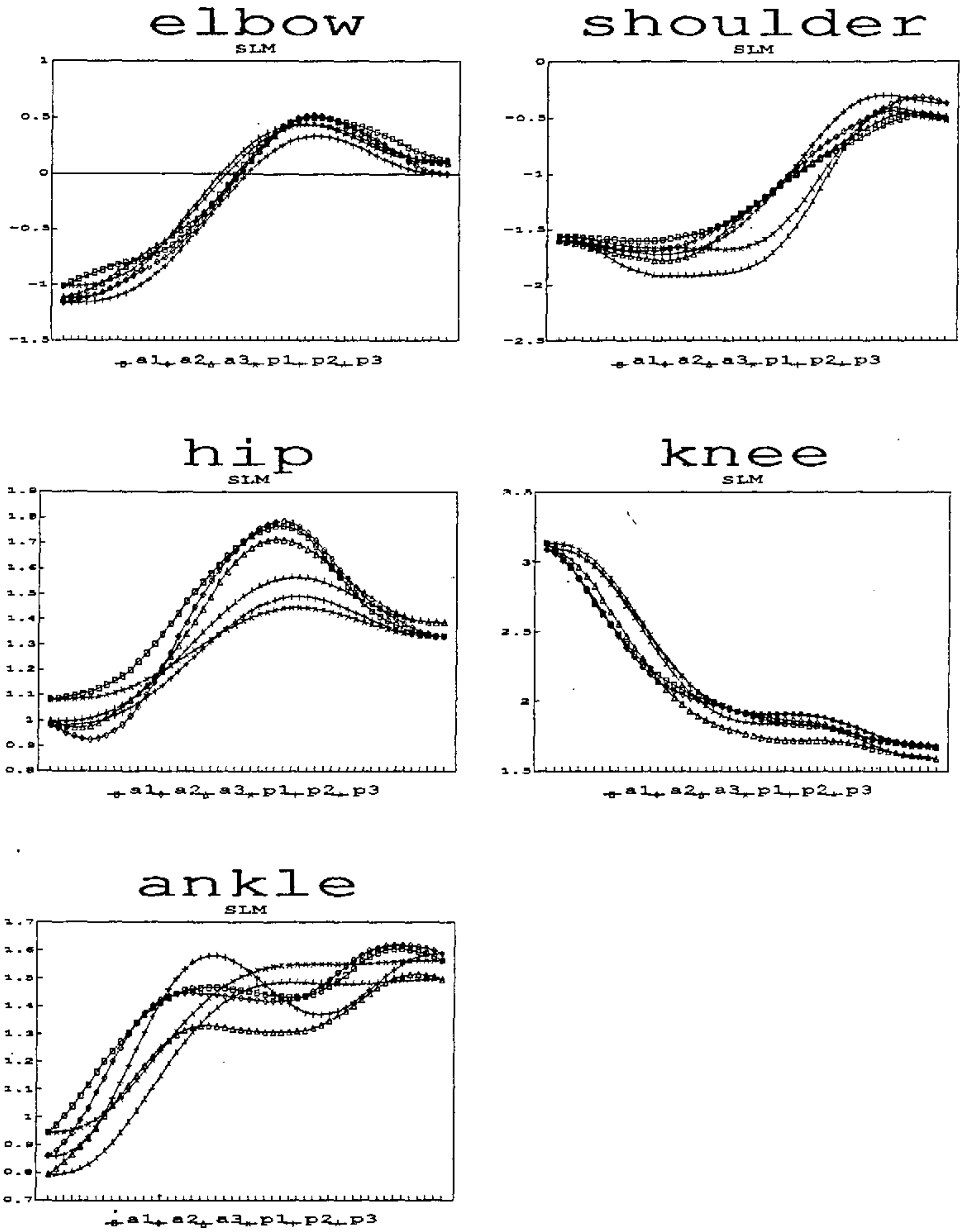

h. SLM

Figure B.9 Continued

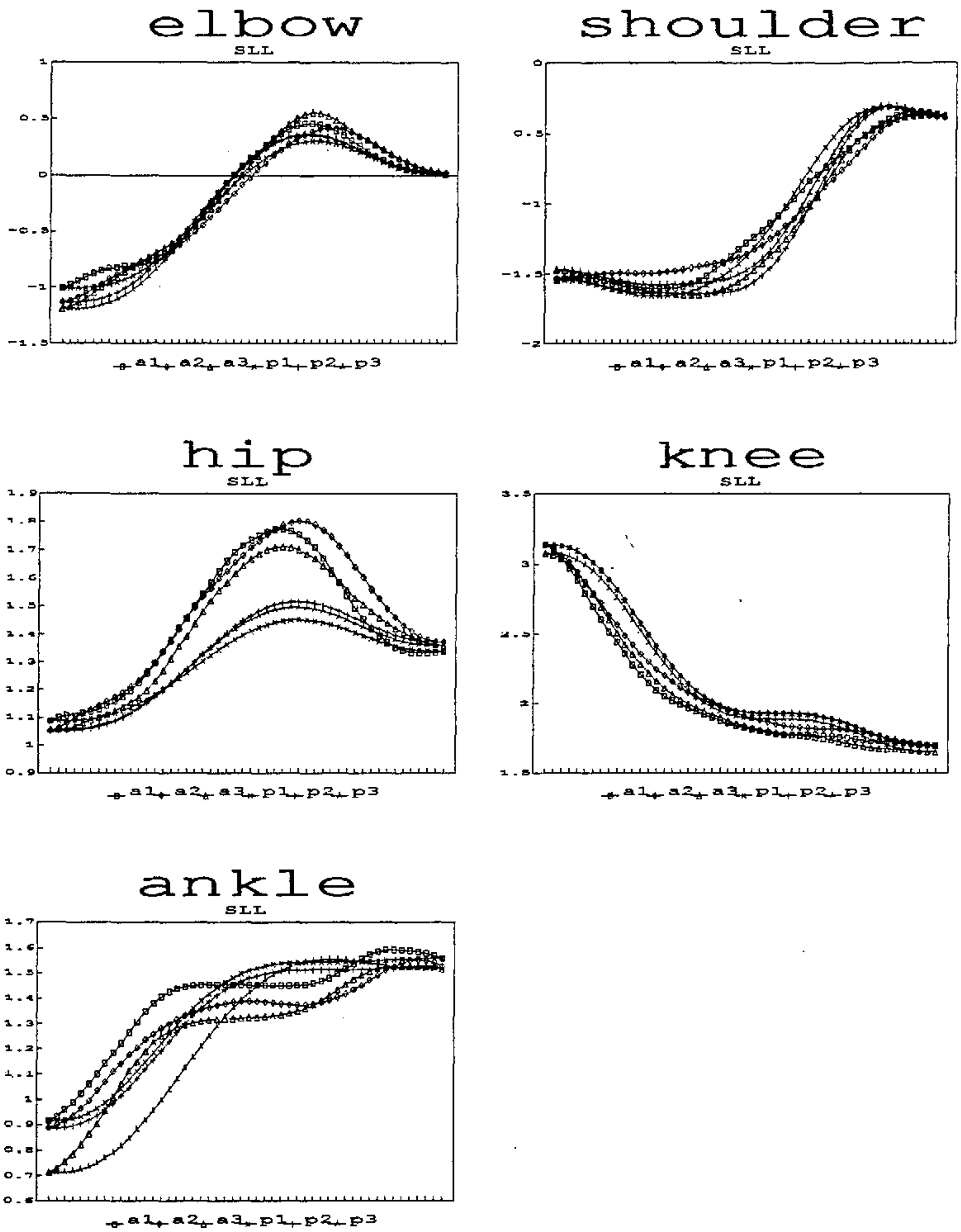

i. SLL

Figure B.9 Continued

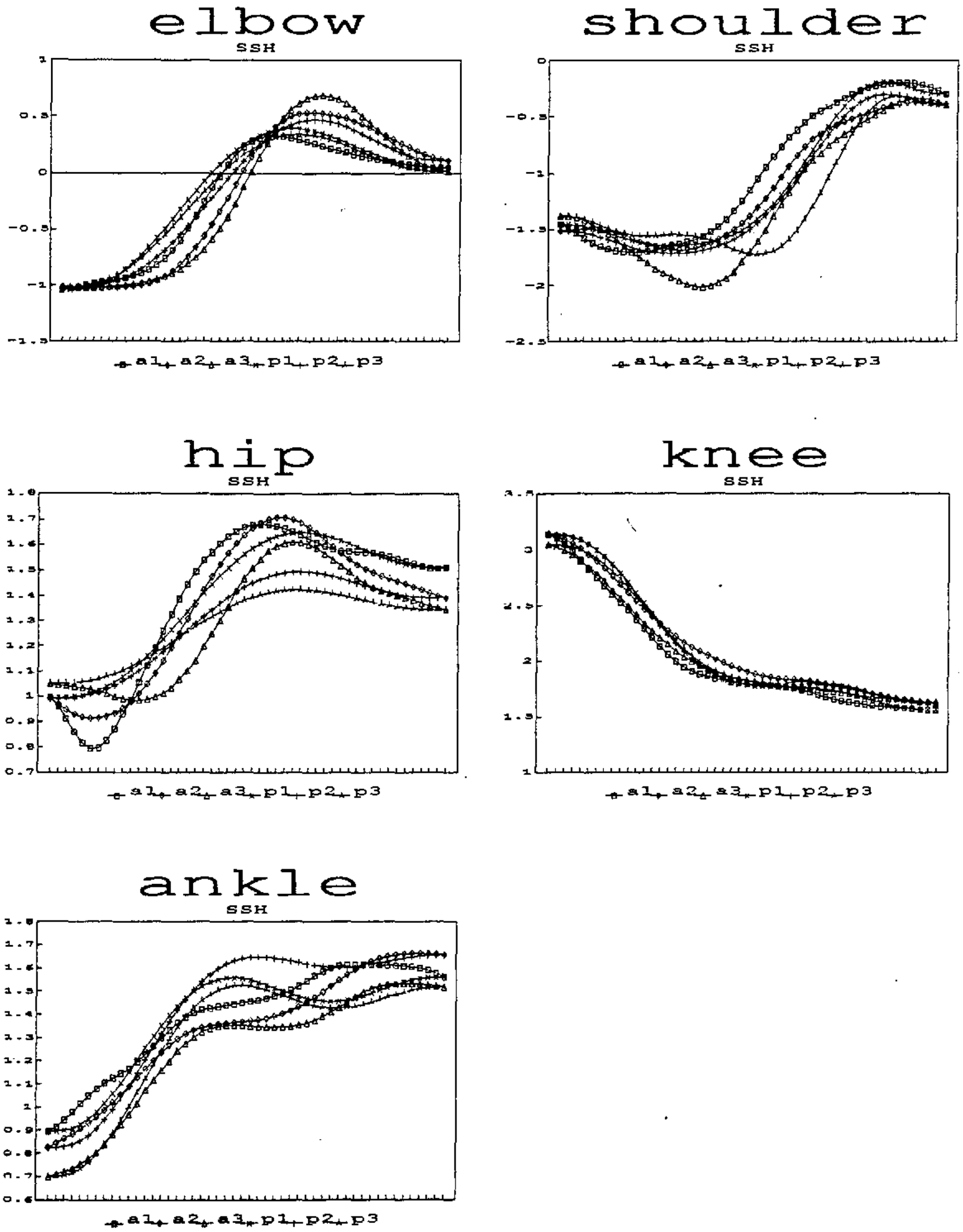

j. SSH

Figure B.9 Continued

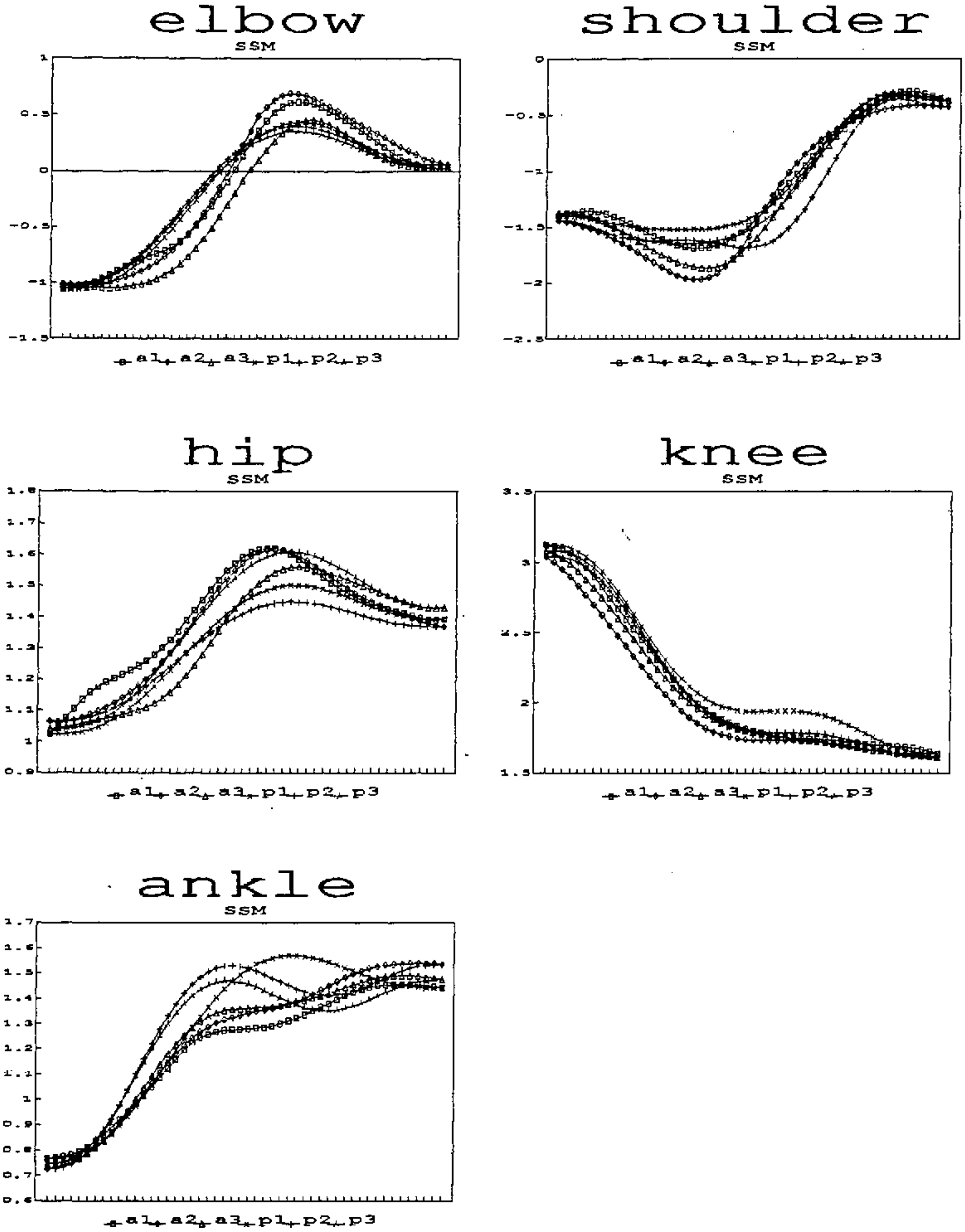

k. SSM

Figure B.9 Continued

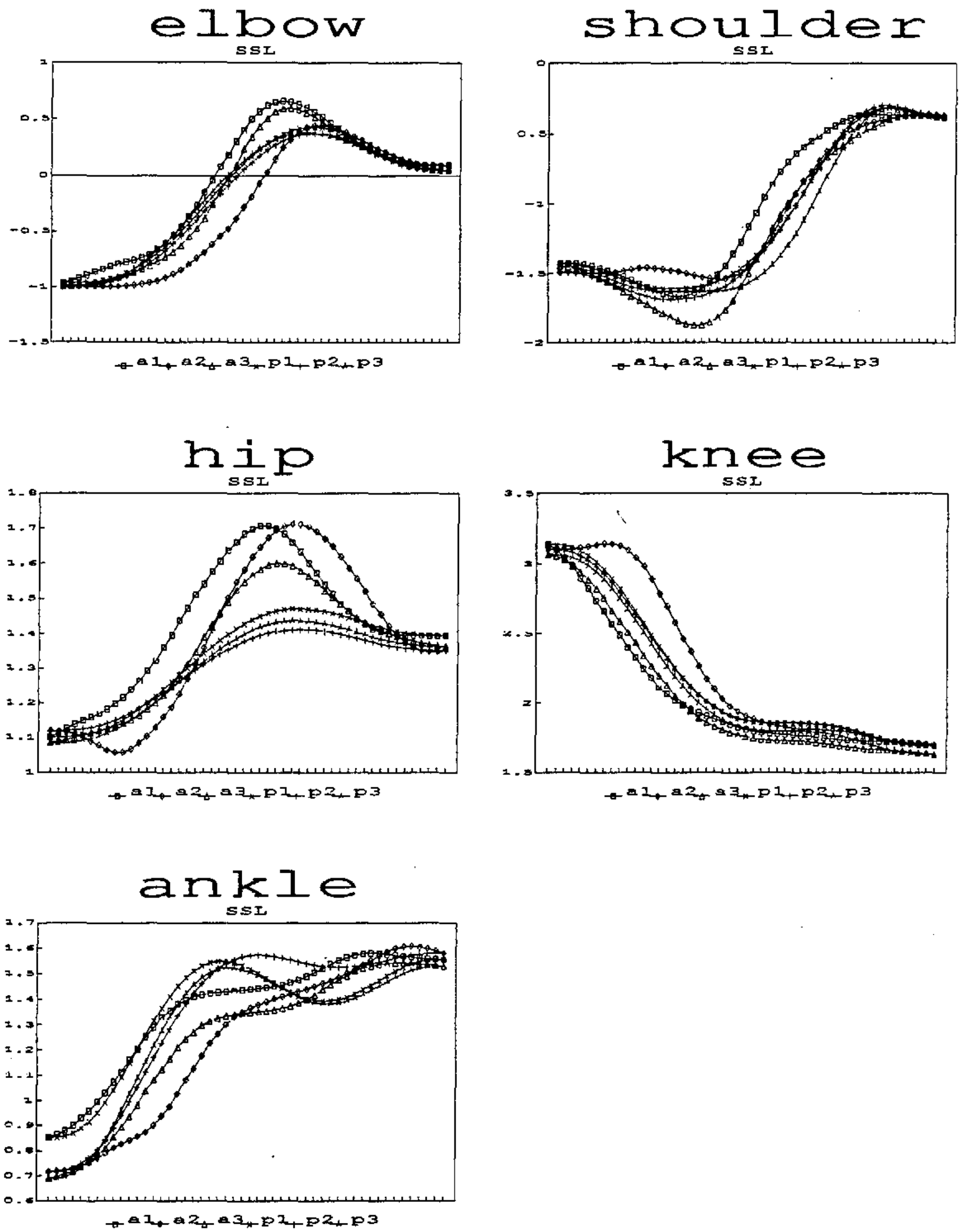

1. SSL

Figure B.9 Continued

APPENDIX C

SUBJECT CHARACTERISTICS

Table C.1 Subject characteristics. The weight is in kilo-grams and length is in meters.

subject	1	2	3	4	5	6	7	8	9	10
sex	f	f	f	m	f	m	m	f	m	m
age	22	28	25	27	21	19	23	29	27	19
height	1.71	1.7	1.62	1.75	1.73	1.83	1.68	1.57	1.76	1.93
weight	59.5	69.1	50.9	69.5	70.4	80.9	79.1	80.9	65	90.9
shoulder height	1.25	1.28	1.18	1.29	1.27	1.35	1.26	1.11	1.29	1.46
knuckle height	0.62	0.63	0.53	0.63	0.61	0.64	0.63	0.51	0.62	0.69
forearm	0.35	0.33	0.34	0.34	0.36	0.39	0.36	0.31	0.35	0.42
upper arm	0.30	0.35	0.31	0.33	0.31	0.33	0.31	0.30	0.32	0.35
trunk	0.51	056	0.45	0.52	0.55	0.56	0.51	0.48	0.47	0.56
thigh	0.40	0.40	0.40	0.38	0.39	0.40	0.42	0.40	0.46	0.45
lower leg	0.41	0.40	0.41	0.43	0.42	0.44	0.42	0.39	0.44	0.48

GENERATED PUBLICATIONS

I. DISSERTATIONS

A. Completed

Hsiang, M.S. (1992). "Simulation of Manual Material Handling." Ph.D. Dissertation, Department of Industrial Engineering, Texas Tech University, Lubbock, TX.

Lee, Y.H.T. (1988). "An Optimization Model to Evaluate Methods of Manual Lifting." Ph.D. Dissertation, Department of Industrial Engineering, Texas Tech University, Lubbock, TX.

Lin, C.J. (1995). "A Computerized Dynamic Biomechanical Simulation Model for Sagittal Plane Lifting Activities." Ph.D. Dissertation, Department of Industrial Engineering, Texas Tech University, Lubbock, TX.

B. In Progress

Bernard, T.M. "Computerized Dynamic Biomechanical Simulation of Lifting Versus Inverse Dynamic Model: Effect of Task Variables." Ph.D. Dissertation, Department of Industrial Engineering, Texas Tech University, Lubbock, TX (to be defended in Fall of 1995).

II. PUBLICATIONS

Ayoub, M.M. (1992). "Problems and Solutions in Manual Materials Handling: The State of the Art," *Ergonomics*, 35(7/8):713-728.

Ayoub, M.M. (1994). "Biomechanics of Manual Material Handling Through Simulation," *Proceedings of The Third Pan-Pacific Conference on Occupational Ergonomics.*

Ayoub, M.M. and Hsiang, M.S. (1992). "Biomechanical Simulation of a Lifting Task," *Advances in Industrial Ergonomics and Safety IV*, Ed. by S. Kumar. Taylor and Francis, pp. 831-838.

Bernard, T.M. (1994). "The Effects of Speed of Lift on Static and Inertial Moments," Unpublished report, Texas Tech University, Lubbock, TX.

Bernard, T.M., Ayoub, M.M., Lin, C.J., and Macedo, J.A. (1994). "Simulation of Optimal Lifting Motions," *Proceedings of the 12th International Ergonomics Association*, Vol. II, pp. 308-310.

Bernard, T.M., Lin, C.J., Ayoub, M.M., and Hsiang, M.S. (1993). "Predicting the Optimal Lifting Motion Through Simulation," *Proceedings of the M.M. Ayoub Occupational Ergonomics Symposium*, pp. 97-100.

Hsiang, S.H. and Ayoub, M.M. (1994). "Development of Methodology in Biomechanical Simulation of Manual Lifting," *International Journal of Industrial Ergonomics*, 13(4):271-288.

Lin, C.J. and Ayoub, M.M. (1995). "Biomechanical Investigation of Lifting Speed," *Proceedings of the Konz/Purswell Occupational Ergonomics Symposium*, pp. 79-85.

Lin, C.J., Bernard, T.M., Ayoub, M.M., and Macedo, J.A. (1994). "Biomechanics of Manual Material Handling Through Simulation," *Advances in Industrial Ergonomics and Safety IV*, Ed. by F. Aghazadeh. London: Taylor and Francis, pp. 635-640.

U.S. DEPARTMENT OF COMMERCE
Technology Administration
National Technical Information Service
Springfield, VA 22161 (703) 487-4650